A global analysis of biomass burning organic aerosol

A thesis submitted to the University of Manchester for the degree of Doctor of Philosophy in the Faculty of Engineering and Physical Sciences

2013

MATTHEW D. JOLLEYS

SCHOOL OF EARTH, ATMOSPHERIC AND

ENVIRONMENTAL SCIENCES

Contents

Abstract 5
Declaration 6
Copyright 7
List of abbreviations 8

1. Introduction **11**
1.1 Motivation 11
1.2 Atmospheric aerosols 13
1.2.1 Background 13
1.2.2 Aerosol properties 14
1.2.2.1 Physical properties 14
1.2.2.2 Chemical composition 16
1.2.3 Aerosol sources 17
1.2.4 Organic aerosols 19
1.2.4.1 Sources and production 21
1.2.4.2 Aging and transformation 22
1.2.5 Hygroscopicity and CCN activity 24
1.2.6 Aerosol sinks 27
1.2.6.1 Dry deposition 27
1.2.6.2 Wet deposition 28
1.3 Aerosols and climate 29
1.3.1 Background 29
1.3.2 Direct effect 31
1.3.3 Indirect effect 36
1.4 Biomass burning aerosols 38
1.4.1 Background 38
1.4.2 Optical properties 40
1.4.3 Combustion conditions 41
1.4.4 Fuel types 43
1.4.5 Aging and SOA production 45

2. Instrumentation and platform **51**
2.1 The Aerosol Mass Spectrometer (AMS) 51
2.2 The Facility for Airborne Atmospheric Measurements (FAAM) 54

3. Papers **57**

3.1 Introduction to papers....57

3.2 Aims and objectives....58

3.3 Overview of experiments....59

3.3.1 Intercontinental Transport of Ozone and Precursors (ITOP)....59

3.3.2 Aerosol and Chemical Transport in Deep Convection (ACTIVE)....60

3.3.3 Dust and Biomass Experiment (DABEX)....61

3.3.4 Megacities Initiative: Local and Global Research Observations (MILAGRO)..62

3.3.5 Quantifying the Impact of Boreal Forest Fires on Tropospheric Oxidants over the Atlantic using Aircraft and Satellites (BORTAS)....63

3.3.6 Fire Lab at Missoula Experiment (FLAME)....64

3.4 Paper 1: Characterizing the aging of biomass burning organic aerosol using mixing ratios - A meta-analysis of four regions....67

Supplementary material....71

3.5 Paper 2: Organic aerosol emission ratios from the laboratory combustion of biomass fuels....73

3.6 Paper 3: Properties and evolution of biomass burning organic aerosol from Canadian boreal forest fires....75

4. Conclusions and further work **77**

5. References **83**

Word count: 56,068

Abstract

Organic aerosols represent one of the main sources of uncertainty affecting attempts to quantify anthropogenic climate change. The diverse physical and chemical properties of organic aerosols and the varied pathways involved in their formation and aging form the basis of this uncertainty, preventing extensive and accurate representation within regional and global scale models. This inability to constrain the radiative forcings produced by organic aerosols within the atmosphere consequently acts as a limitation to the wider objective of providing reliable projections of future climate. Biomass burning constitutes one of the main anthropogenic contributions to the global atmospheric organic aerosol (OA) burden, particularly in tropical regions where the potential for perturbations to the climate system is also enhanced due to higher average levels of solar irradiance.

Emissions from biomass burning have been the subject of an intense research focus in recent years, involving a combination of field campaigns and laboratory studies. These experiments have aimed to improve the limited understanding of the processes involved in the evolution of biomass burning organic aerosol (BBOA) and contribute towards the development of more robust parameterisations for climate and chemical transport models. The main objective of this thesis was to use datasets acquired from several different global regions to perform a broad analysis of the BBOA fraction, with the extensive temporal and spatial scales provided by such measurements enabling investigation of a number of key uncertainties, including regional variability in emissions and the role of secondary organic aerosol (SOA) formation in aging smoke plumes.

Measurements of BBOA mass concentration obtained using Aerodyne Research Inc. Aerosol Mass Spectrometers (AMS) were used to calculate characteristic ΔOA/ΔCO ratios for different environments, accounting for the effects of dilution and contrasting fire sizes to give a proportional representation of OA production. High levels of variability in average ΔOA/ΔCO were observed both between and within different regions. The scale of this variability consistently exceeded any differences between plumes of different ages, while a widespread absence of any sustained increase in ΔOA/ΔCO with aging indicates that SOA formation does not provide a net increase in OA mass. Despite this lack of OA enhancement, increasing proportions of oxygenated OA components in aged plumes highlight the chemical transformations occurring during the evolution of BBOA, and the additional influence of OA loss through evaporation or deposition.

Potential drivers of variability in ΔOA/ΔCO at source, such as changes in fuel types and combustion conditions, were investigated for controlled fires carried out within a combustion chamber. These laboratory experiments revealed a number of complex relationships between BB emissions and source conditions. Although ΔOA/ΔCO was shown to be influenced by both fuel properties and transitions between flaming and smouldering combustion phases, the extent of these effects was limited, while variability between fires exceeded levels observed for ambient measurements. These findings emphasise the complexity of the BBOA lifecycle and the need to address the extensive uncertainties associated with its various constituent processes, in order to improve understanding of eventual climate impacts from biomass burning.

Declaration

No portion of the work referred to in this thesis has been submitted in support of an application for another degree or qualification of this or any other university or other institute of learning.

Copyright

List of abbreviations

ACTIVE	Aerosol and Chemical Transport in Tropical Convection
AMMA	African Monsoon Multidisciplinary Analysis
AMS	Aerosol Mass Spectrometer
ARCTAS	Arctic Research of the Composition of the Troposphere from Aircraft and Satellites
BB	Biomass Burning
BC	Black Carbon
BBOA	Biomass Burning Organic Aerosol
BORTAS	Quantifying the Impact of Boreal Forest Fires on Tropospheric Oxidants over the Atlantic using Aircraft and Satellites
CCN	Cloud Condensation Nucleus
CIMS	Chemical Ionisation Mass Spectrometer
CE	Collection Efficiency
CPC	Condensation Particle Counter
C-ToF-AMS	Compact Time of Flight Aerosol Mass Spectrometer
DABEX	Dust and Biomass Experiment
DODO	Dust Outflow and Deposition to the Ocean
ER	Emission Ratio
EF	Emission Factor
FAAM	Facility for Airborne Atmospheric Measurements
FGGA	Fast Greenhouse Gas Analyser
FLAME	Fire Lab at Missoula Experiment
FSL	Fire Sciences Laboratory
ICARRT	International Consortium for Atmospheric Research on Transport and Transformation
IE	Ionisation Efficiency
ITOP	Intercontinental Transport of Ozone and Precursors
LV-OOA	Low-Volatility Oxygenated Organic Aerosol

MCE	Modified Combustion Efficiency
MCMA	Mexico City Metropolitan Area
MODIS	Moderate Resolution Imaging Spectroradiometer
MILAGRO	Megacities Initiative: Local and Global Research Observations
m/z	Mass to charge ratio
NEMR	Normalised Excess Mixing Ratio
NERC	Natural Environment Research Council
NVOC	Non-Volatile Organic Compound
OA	Organic Aerosol
OC	Organic Carbon
OOA	Oxygenated Organic Aerosol
PAH	Polycyclic Aromatic Hydrocarbon
PCASP	Passive Cavity Aerosol Spectrometer Probe
PILS-IC	Particle-Into-Liquid-Sampler Ion Chromatograph
PM	Particulate Matter
POA	Primary Organic Aerosol
PSAP	Particulate Soot Absorption Photometer
Q-AMS	Quadrupole Aerosol Mass Spectrometer
RH	Relative Humidity
SV-OOA	Semi-Volatile Oxygenated Organic Aerosol
SMPS	Scanning Mobility Particle Sizer
SOA	Secondary Organic Aerosol
SOP	Special Observing Period
SP-2	Single Particle Soot Photometer
STP	Standard Temperature and Pressure
TD-LIF	Thermal Dissociation-Laser Induced Fluorescence
TOOC	Total Observed Organic Carbon
UHSAS	Ultra-High Sensitivity Aerosol Spectrometer Probe
VOC	Volatile Organic Compound

Chapter 1

Introduction

1.1 Motivation

Atmospheric aerosols are suspended solid or liquid particles, with a wide range of sizes and chemical compositions. These properties are influenced by the pathways involved in the formation of particles and their transportation into the atmosphere, and control the impacts of aerosols. Many different processes contribute towards aerosol production, including both natural background sources and anthropogenic activity. Aerosol sources can generally be divided into two main classes; mechanically-driven primary production, where by particles are emitted directly into the atmosphere, and secondary production, involving the emission of precursor gases and subsequent transformation to the particle phase within the atmosphere. Composition is also intrinsically linked with formation, with primary production dominated by suspension of mineral dust and sea salt, while secondary production largely relates to sulphates and organic species (*Penner et al., 2001*). The specific origins of aerosol populations are often difficult to attribute, given the number of potential pathways leading to particle formation and the extent of ensuing processing and transformation. However, it is evident that rises in anthropogenic emissions since the Industrial Revolution have led to increased total atmospheric loadings (*Chung & Seinfeld, 2002*). The large number of sources, together with their broad geographical distribution and variable intensity, cause concentrations to fluctuate significantly on both spatial and temporal scales. Low residence times within the atmosphere, typically on the order of only a few days, further promote highly heterogeneous mixing states.

Elevated aerosol concentrations are widely associated with atmospheric pollution, and as such have implications for air quality, particularly in urban areas. Suspended particles pose a

risk to human health if they are inhaled, with potential risks greatest where particles contain material that is harmful or toxic. The toxicological effects of inhaled particles and their potential for harm are dependent on size, which determines the extent of their progression into various biological systems. Particles less than 10 μm in diameter are able to pass through the throat and enter the respiratory system, while those smaller than 5 μm can enter the alveolar region of the lungs *(Dockery & Pope, 1994*). It is possible for ultrafine particles, smaller than 0.1 μm, to enter the bloodstream through pulmonary alveoli, where they can be transported around the body to different organs, increasing the potential for detrimental effects (*Pöschl, 2005*). However, the most widespread impacts relate to the interactions of aerosols with the climate system, which are driven by the influence upon Earth's radiative budget, through perturbations of the incoming solar radiation flux. These perturbations can act in either direction, creating either positive or negative radiative forcings depending on the optical properties of particles and the extent to which they scatter or absorb solar radiation. The presence of aerosols also affects the formation and lifetime of clouds, which provides an additional radiative effect, as well as influencing the hydrological cycle through alteration of precipitation efficiency.

The complexity and variability of aerosol processes results in a large degree of uncertainty regarding many aspects of the science. Given the importance of aerosols with regards to climate, and the need for full representation of associated forcings in future climate change projections, there is a pressing need for reduction of these uncertainties and better constraint of aerosol effects. Current research activities are ultimately aimed at addressing these requirements across a range of scales, using a number of different approaches. These include working at the process level to gain an improved understanding of aerosol properties, production, transformation and removal processes, and the mechanisms which dictate how aerosols affect climate through interactions with radiative fluxes. The second central aspect of aerosol research targets wider scale effects, with a focus on modelling of regional and global scale trends and impacts. Continued progression of aerosol research is dependent on the

successful amalgamation of these two elements, which provide mutual benefits. Findings from process level studies are used as the basis for aerosol model development, and also provide a point of comparison for evaluation, while models extrapolate these fundamental parameterisations to a wider scale. This provides a transferable end product, enabling understanding of aerosol processes and properties to be implemented in a broader scope.

The need for effective representation of highly complex aerosol cycles within regional or global scale models presents a considerable challenge. It is clearly unrealistic to simulate each component of the aerosol system, together with the wide range of specific processes and pathways they are influenced by throughout their lifetime, explicitly on these scales. Additionally, it is also unfeasible to deliver comprehensive measurement of the complete array of aerosol properties and processes, with experimental analysis instead focusing on certain key species and stages of the lifecycle. As a result, it is necessary to capture the most important aspects of the system and ensure they are represented appropriately. One way of achieving this is through the synthesis of large datasets, whereby extensive measurements of certain parameters are integrated to provide a characteristic overview of more diverse properties. Such work forms an important contribution towards aerosol modelling, as it enables the simplification of multifaceted concepts, and their subsequent parameterisation within models.

1.2 Atmospheric aerosols

1.2.1 Background

The physical and chemical properties of aerosols, such as size, shape and composition, determine their optical properties and subsequent radiative effects. Therefore, understanding of these properties and the ways in which they change is critical in assessing the impacts of aerosols within the atmosphere. While methods of formation control the initial characteristics of newly-formed particles, various processes act to alter these properties throughout the lifetime of aerosols. The recurrent processing of particles by various drivers can cause

considerable changes to their physical and chemical properties, resulting in particles which are significantly different to their initial state. The association and combination of particles of differing compositions is an important aspect of aerosol evolution, with the overall impacts of larger aerosol populations affected by the mixing state of different species. When particles are composed entirely of a single species, but are mixed with separate particles of another species, it is known as an external mixture. In contrast, an internal mixture refers to a population where each particle shares a similar composition, consisting of a combination of different species within each individual particle (*Seinfeld & Pandis, 2006*). The interaction of aerosols with water vapour also forms a fundamental control on their impacts. Aerosols comprised of soluble material will form aqueous solutions at ambient levels of relative humidity (RH). This causes particles to increase in size, altering their radiative effects, as a result of changes to both their optical properties and atmospheric lifetime (*Maßling et al., 2003*). The uptake of water by aerosols also determines their activity as cloud condensation nuclei (CCN) and their role in cloud formation, which ultimately creates an additional radiative forcing.

1.2.2 Aerosol properties

1.2.2.1 Physical properties

Aerosols range in size from approximately 10^{-9} to 10^{-4} m (*Pöschl, 2005*), with particles classified within one of four modes according to their diameter (D_p). These are the nucleation mode (less than 10 nm diameter), Aitken mode (10 to 100 nm), accumulation mode (100 nm to 2 μm) and coarse mode (2 to 50 μm). Particle diameter is a function of source and associated formation pathways, along with subsequent in-situ processing. Aerosols are described more generically as either coarse (larger than 2.5 μm), fine (smaller than 2.5 μm) or ultrafine (smaller than 0.1 μm) particles, with this classification used more in relation to the characteristic effects associated with particles of these sizes. The nucleation mode represents the ultrafine aerosol fraction, formed by secondary production through gas-to-particle conversion in the atmosphere. Fine particles in the Aitken and accumulation modes are

generally produced by the coagulation of smaller particles or condensation of gas-phase species onto pre-existing condensation nuclei (CN), while coarse mode aerosols are predominantly emitted directly as primary particles (*Seinfeld & Pandis, 2006*).

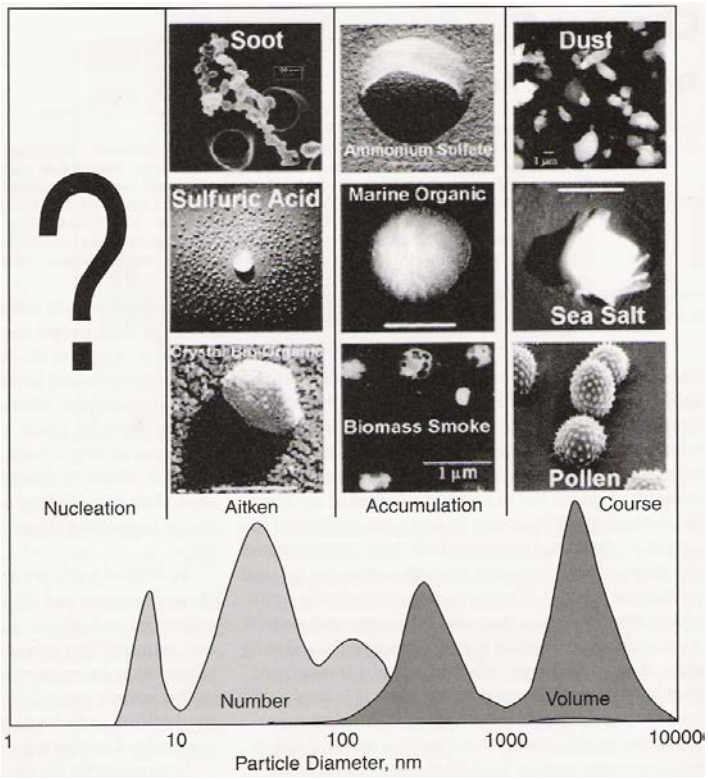

Figure 1: *Typical aerosol size distribution with generic particle shapes and chemical compositions, showing the division of properties between different size modes (Heintzenberg et al., 2003).*

A size distribution describes the variation in particle diameter for an aerosol population, normally given as the number concentration of particles per logarithmic size interval. Typical ambient number size distributions are dominated by the nucleation and Aitken mode, with very little contribution from the accumulation or coarse modes, as shown in Figure 1. However, aerosol distributions can also be expressed in terms of particle surface area, volume or mass. The apportionment of these properties between modes is also not consistent with that of aerosol number. For example, while the nucleation mode accounts for the majority of aerosol number, the small size of the particles results in there being little contribution to the volume, mass or surface area distributions. This reflects the aerosol lifecycle and the effects of atmospheric processing on physical properties (Figure 2).

Coagulation and condensation both act to increase the mass, volume and surface area of aerosols, while simultaneously increasing particle size. As a result, the distribution of these properties is shifted towards the accumulation mode as particles are processed to larger sizes. Although the growth of nucleation particles by coagulation and condensation takes several days under background conditions, the rate increases considerably under polluted conditions, with particles quickly growing to the accumulation mode (*Raes et al., 2000*). The prevalence of the accumulation mode is also highly significant with regard to the radiative impacts of aerosols, as it is particles of this size that are of the greatest importance due to their optical properties and longest atmospheric lifetimes (*Penner et al., 2001*).

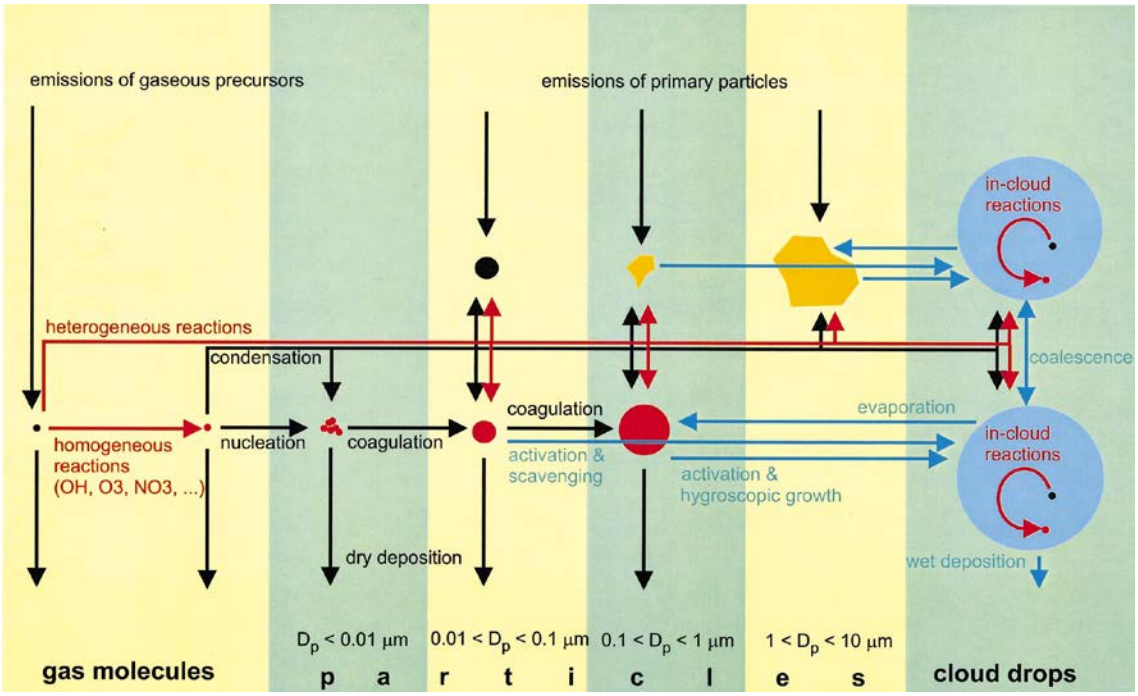

Figure 2: *Major microphysical and chemical processes influencing the size distribution and chemical composition of atmospheric aerosol particles (Raes et al., 2000).*

1.2.2.2 Chemical Composition

The atmospheric aerosol burden consists of several chemical components, which are both natural and anthropogenic in origin. The main constituents are sulphates and other inorganic ions (such as ammonium, nitrates and chloride), carbonaceous material (including both organic and elemental/black carbon), sea salt and mineral dust. Along with particle size,

chemical composition also acts as a control on the optical properties of aerosols, determining the direction of the radiative forcing they produce. The majority of aerosol species primarily scatter incoming solar radiation, producing a negative forcing. In contrast, black carbon (BC) strongly absorbs both solar and terrestrial infrared radiation, and as such represents the main absorbing fraction of atmospheric aerosols (*Koch et al., 2009*). This effect can be intensified when mixed internally with scattering species such as sulphates or organic carbon (OC), potentially doubling the absorption efficiency of BC particles (*Penner et al, 2001*). Other aerosol properties which are dependent on chemical composition, such as solubility and hygroscopicity, can be also be affected in a similar way by changes to their mixing state.

1.2.3 Aerosol sources

Numerous aerosol sources, spread across a wide range of environments, contribute towards the global atmospheric aerosol burden. The diverse nature of these sources and their variability with regard to both magnitude and product are some of the main contributors towards the complexity of aerosol science, and the difficulty faced in providing accurate and reliable quantification of climate impacts. The strengths of many aerosol sources and their subsequent influence on the atmospheric loadings of different species are subject to high levels of uncertainty. This is the result of several factors, including the difficulty in ascribing sources to aerosol populations due to secondary formation from precursor gases at a distance from the initial source; following transformation of particles through mixing, chemical reactions and cloud processing; or because of the differing physical properties of particles from a single source (*Penner et al., 2001*). Isolation of the anthropogenic component of aerosol radiative forcings is also hindered by uncertainties associated with source strengths, limiting the ability to substantiate forcing trends, or to develop projections in response to future changes in emission regimes.

Estimates of aerosol source strengths are derived from a combination of measurement data, including observations of emissions, transformations and removal processes, extrapolated

to a global scale through modelling. The use of different emission parameterisations as the basis for projections, and the inherent uncertainty in measurements from which they are obtained, consequently produces a broad range of emissions estimates. Discrepancies can also arise from the approach taken, with top-down and bottom-up estimates, based on upscaling observed emission rates and inversion of known atmospheric concentrations or removal rates respectively, producing different results. This is most evident in assessments of organic aerosols (OA), which are subject to a high degree of variation. *Hallquist et al.* (*2005*) estimate overall OA production to be between 50 - 90 TgC yr^{-1} using a bottom-up method, while a top-down approach increases this to 60 - 240 TgC yr^{-1}. These estimates account for both primary (POA) and secondary (SOA) organic aerosol from both natural and anthropogenic sources, with the broad range reflecting the limited understanding of many processes involved in OA formation. In contrast, BC is formed solely from the incomplete combustion of fossil fuels, biofuels and biomass. As a result, more concise estimates of 5.8 - 8.0 TgC yr^{-1} are available for BC (*Haywood & Boucher, 2000*), consisting of approximately 4.6 TgC yr^{-1} from fossil fuel and biofuel and 3.3 TgC yr^{-1} from biomass (*Bond et al., 2004*). Sulphate aerosols, which are primarily formed by secondary production from gas-phase SO_2 and dimethylsulphide (DMS) emissions and represent the other main anthropogenic contribution to the atmospheric aerosol burden, are also more narrowly constrained. Estimates are placed at 91.7 - 125.5 TgS yr^{-1}, with an anthropogenic fraction of 66.8 - 92.4 TgS yr^{-1} (*Haywood & Boucher, 2000*). Annual production of nitrate and ammonium is estimated to be 11.6 - 19.8 TgN yr^{-1} and 4.5 - 25.7 TgN yr^{-1} respectively (*Feng & Penner, 2007; Rodriguez & Dabdub, 2004*). Sources for the main natural aerosol components, such as mineral dust and sea salt, are much larger at around 1000 - 3000 Tg yr^{-1} and 1000 - 6000 Tg yr^{-1} respectively (*Penner et al., 2001*). However, as only a small proportion of each source is believed to be of anthropogenic origin, these species are unlikely to create a significant perturbation of the climate system, although they have an important role as CN for the secondary formation of anthropogenic aerosol species.

Size distributions are strongly influenced by aerosol sources, and consequently exhibit considerable variability between different environments due to the dominance of specific formation methods. Proximity to a source is also important, particularly where several different sources, producing characteristically distinctive particles, are present. This is particularly evident in urban areas, where both primary and secondary production is prominent. Number and mass concentrations highlight the influence of urban pollution on aerosol loadings, with respective values of around 10^4 cm^{-3} and 10 $\mu g\ cm^{-3}$ significantly higher than for unpolluted air, where typical concentrations are 100 cm^{-3} and 1 $\mu g\ cm^{-3}$ (*Poschl, 2005*). Close to combustion sources, such as roads experiencing high vehicle emissions, high concentrations of nucleation and Aitken mode particles are observed. However, these concentrations decrease rapidly from the source, as a result of both dilution and coagulation (*Zhu et al., 2002*). The continued effect of these processes, together with the increasing influence of other aerosol sources, causes the size distribution to evolve as distance from the source increases. In environments dominated by a single formation method, such as the production of sea salt in oceans, size distributions tend to be more consistent. The marine number distribution is characterised by Aitken and accumulation modes of a similar magnitude, with a small coarse mode (*Seinfeld & Pandis, 2006*). Although mechanically-generated sea salt accounts for the majority of its aerosol production, the marine environment is also influenced by aerosol populations advected from continental regions, along with localised pollution sources from shipping and sulphates originating from biological emissions of DMS. Furthermore, observations of significant marine organic aerosol concentrations at several sites suggest a global-scale oceanic OC source exists (*Spracklen et al., 2008*).

1.2.4 Organic aerosols

Organic aerosols comprise a significant proportion of tropospheric particulate material, accounting for approximately 10–70% of the total aerosol burden across different environments (*McFiggans et al., 2005*). The organic fraction also represents around 50% on

average of the total submicron aerosol mass (*De Gouw & Jimenez, 2009*), and therefore represent a prominent contributor to the optically-important aerosol burden. Furthermore, OA act as effective CCN given the high proportion of water-soluble compounds present in particles, and as such are highly important with respect to cloud processes and aerosol indirect effects (*Sun & Ariya, 2006*). However, extensive studies of OA properties and processes are a relatively recent development, especially in comparison to other major aerosol fractions such as sulphates, which have been subject to more widespread, comprehensive investigations over a longer period of time (*Jacobson et al., 2000*). Understanding is therefore somewhat inadequate to enable reliable and consistent prediction of any ensuing impacts, with considerable levels of uncertainty associated with many aspects of the organic fraction. This ambiguity is also to some extent a result of the diverse and complex nature of OA chemistry. The number of different compounds which contribute to the overall OA burden could potentially be on the order of millions (*Goldstein & Galbally, 2007*), originating from a wide and highly diverse range of sources. Processing and transformation in the atmosphere, especially that of gas-phase aerosol precursors, promotes a high degree of variability in the chemical and physical properties of organic species. Attempts to constrain these processes and identify their effects on OA characteristics, loadings and impacts at a regional or global scale are based upon the use of chemical transport models (CTMs) and general circulation models (GCMs), which in turn rely on parameterisations derived from process-level measurements and modelling studies. Given the relative infancy of OA research, continued expansion and development of both these approaches is essential in order to more accurately resolve the science of OA and their role in climate perturbation. The scale of these requirements demands a considered focus to provide the most effective and relevant results, with a subsequent emphasis placed on sources or areas where OA production is greatest, or those providing a substantial anthropogenic contribution.

1.2.4.1 Sources and production

The origins of atmospheric OC can be broadly divided between primary and secondary sources. POA accounts for aerosols emitted directly to the atmosphere in the particulate phase, where as SOA undergo a more complex formation pathway, produced in-situ by gas-to-particle conversion of aerosol precursors. Combustion sources account for the majority of POA production, including both natural and anthropogenic biomass burning and combustion of fossil fuels, with additional contributions from suspended soil and road dust, particles from food preparation and biological material such as plant debris, pollen and microbial matter. Estimates for global annual POA sources range from 35 to 81 TgC yr^{-1} (*Bond et al., 2004; Liousse et al., 1996*), although these assessments also differ in their attribution of the major POA sources, highlighting the uncertainty in the contributions of fossil fuel and biomass burning.

Production of SOA precursors in the form of volatile organic compounds (VOCs) is estimated to be approximately 1300 TgC yr^{-1}, with biogenic emissions believed to be around an order of magnitude larger than those from anthropogenic sources (*Goldstein & Galbally, 2007*). A number of mechanisms have been identified for the formation of SOA, involving the processing of initial, highly volatile emission products to form lower volatility compounds. The probable phase of compounds in the atmosphere is essentially determined by their vapour pressure, with compounds typically partitioning to the particle phase at vapour pressures below 10^{-5} atm at ambient temperatures (*Goldstein & Galbally, 2007*). Photochemical oxidation of VOCs and addition of oxygen-containing functional groups increases polarity, and hence reduces vapour pressure, forming semi-volatile organic compounds (SVOCs) (*Seinfeld & Pankow, 2003*). SVOCs are defined as atmospheric constituents with more than 1% of their mass within both the gas and particle phases (*Donahue et al., 2006*), and as such have a greater potential to form aerosols, particularly if involved in further stages of oxidation. This may lead to the formation of low/non-volatile organic compounds (LVOCs/NVOCs) following a progressive reduction in volatility for each generation of products (*Hallquist et al., 2009*), with

critical transformations of SOA precursors often occurring at a later stage of this sequence rather than as a result of the initial oxidation (*Goldstein & Galbally, 2007*). SOA formation can occur through the homogenous nucleation of new particles, or by condensation of VOC oxidation products onto existing aerosols. Gas-phase compounds may also undergo heterogeneous reactions on the surface of, or within, aerosol particles or cloud droplets to form lower volatility products and drive partitioning to the particle phase (*Fuzzi et al., 2006*). The various pathways involved in the formation of SOA from precursors contribute to the uncertainty in the fraction of VOC emissions converted to aerosols. Around 20-40% is expected to be directly oxidised to CO or CO_2, while another 10-20% is removed by dry and wet deposition, with mass balancing of the estimated 1300 TgC yr^{-1} source suggesting a total SOA production from VOC precursors of 510-910 TgC yr^{-1} (*Goldstein & Galbally, 2007*). However, this figure is subject to discrepancies in the assessments of VOC sources and sinks, and would require an SOA yield of up to 70%, the upper limit of which seems unrealistically high based on conversion factors obtained from chamber experiments, which have been shown to generate yields of around 30% (*Hallquist et al., 2009; Ng et al., 2007*). The use of alternative approaches to quantify SOA production also generates highly variable estimates. These include a range of 140-540 TgC yr^{-1} based upon an estimated total sulphate source of 340 Tg yr^{-1} and a typical sulphate to organics ratio of 1:4, and 223-615 TgC yr^{-1} derived from the level of production needed to maintain an estimated atmospheric SOA burden of 6.7 Tg C given an average residence time of 4 to 11 days (*Goldstein & Galbally, 2007*). The considerable difference in these estimates, nearing an order of magnitude between the overall lower and upper limits, emphasises the current inability to accurately constrain the global SOA source, and the need for further refinement of understanding of the various formation processes.

1.2.4.2 Aging and transformation

Uncertainties relating to the different mechanisms involved in OA production make it difficult to reliably determine the relative contributions of POA and SOA, although the distribution of particular sources can be used to infer general geographical trends, such as the

dominance of POA in the tropics as a result of high levels of biomass burning (*Pöschl et al., 2005*). Quantification of the primary and secondary contributions are further complicated by the difficulty in assigning robust classifications to POA and SOA under circumstances where their attributes are altered by the effects of atmospheric processing. POA is considered to be essentially semi-volatile, with effective saturation concentrations, and corresponding vapour pressures, high enough to evaporate under ambient conditions (*Robinson et al., 2007; Cappa & Jimenez, 2010*). This highlights the dynamic nature of the OA system, where by particles can exist as an intermediate phase before re-evaporating to form SVOCs, undergoing further oxidation and ultimately repartitioning to the particle phase to form less volatile aerosols (*Hallquist et al., 2009*). The transformation of aerosols as they age presents an important consideration in assessments of source strengths, particularly regarding the influence of aged POA as an SOA precursor, and the implications of this contribution for conversion yields of primary VOC emissions. Beyond its role in the cycle of aerosol formation, aging is also highly important with respect to the physical and optical properties of OA, which can be altered significantly as a result of processing within the atmosphere (*Fuzzi et al., 2006*).

The complexity of the SOA fraction and level of uncertainty associated with its sources and aging processes presents a considerable challenge for global aerosol models. SOA is typically poorly represented within modelling studies, and in many instances lacking entirely. Of the 16 models included in the Aerosol Model Comparison Project (AeroCom), only one provided full simulation of SOA formation from precursor gases, with the remaining representation limited to incorporation of biogenic SOA within POA emissions (*Textor et al., 2006*). Consequently, significant efforts have been made to provide improved characterisation of SOA properties, focusing upon the effects of aging. *Zhang et al.* (*2007*), and latterly *Jimenez et al.* (*2009*), have proposed a framework for the evolution of SOA, presenting a means of improving parameterisations of SOA in global models through simplification of key processes. This framework is based around the classification of aged OA according to volatility and O:C ratios, with the latter used as an indicator of oxidation. Processing of OA and its precursors

causes an increase in oxidation state and leads to the formation of oxygenated organic aerosols (OOA). Analyses of OOA from a range of urban, urban downwind and remote locations (Figure 3) using an aerosol mass spectrometer (AMS) show their compositions to be distinct from that of hydrocarbon-like OA (HOA), which is more indicative of POA emissions (*Zhang et al., 2005*). These initial oxidation products are denoted as semi-volatile OOA (SV-OOA), and represent fresh OOA originating primarily from SOA. As aging continues, OOA becomes increasingly oxidised and less volatile, forming low-volatility OOA (LV-OOA). Distributions of the various OA fractions relative to their source locations validate this classification, as O:C, total OOA and the LV-OOA fraction are all shown to increase downwind of urban pollution (*Jimenez et al., 2009*). As well as characterising the evolution of OA, this analysis has also emphasised the dominance of OOA in global aerosols, comprising 64%, 83% and 95% of the total OA mass in urban, urban downwind and remote locations respectively, with the influence of HOA restricted to areas that are subject to a high concentration of combustion sources (*Zhang et al., 2007*). Furthermore, this approach illustrates the contribution that can be made towards the potential refinement of aerosol modelling by providing improved wide-scale characterisations of aerosol properties.

1.2.5 Hygroscopicity and CCN activity

Hygroscopicity defines the affinity of aerosols for water vapour in the atmosphere, and subsequent particle growth in response to the uptake of water with increasing RH. Aerosols containing soluble material will form aqueous solutions at a specific RH threshold determined by composition. This process is known as deliquescence, and can occur under sub-saturated conditions with an RH much lower than 100% (*Poschl, 2005*). The corresponding RH is designated the deliquescence relative humidity (DRH), and once this threshold is exceeded, a particle will undergo hygroscopic growth as water is partitioned from the gas-phase and condenses onto particles in accordance with thermodynamic equilibrium. The reverse phase transition, where by a particle is removed from solution as RH decreases and water

evaporates, is known as efflorescence and occurs at the efflorescence relative humidity (ERH) (*Seinfeld & Pandis, 2006*). A particle's response to changing RH is measured as a function of its change in size known as the hygroscopic growth factor, which is given as the ratio of the wet (aqueous) and dry (solid) diameters. While the growth factor is dependent on RH, and is composition-specific, it is also influenced by a range of other factors. These include the initial dry particle diameter, as smaller particles will grow less relative to larger particles of the same composition, as a result of the Kelvin effect (*Swietlicki et al., 2008*).

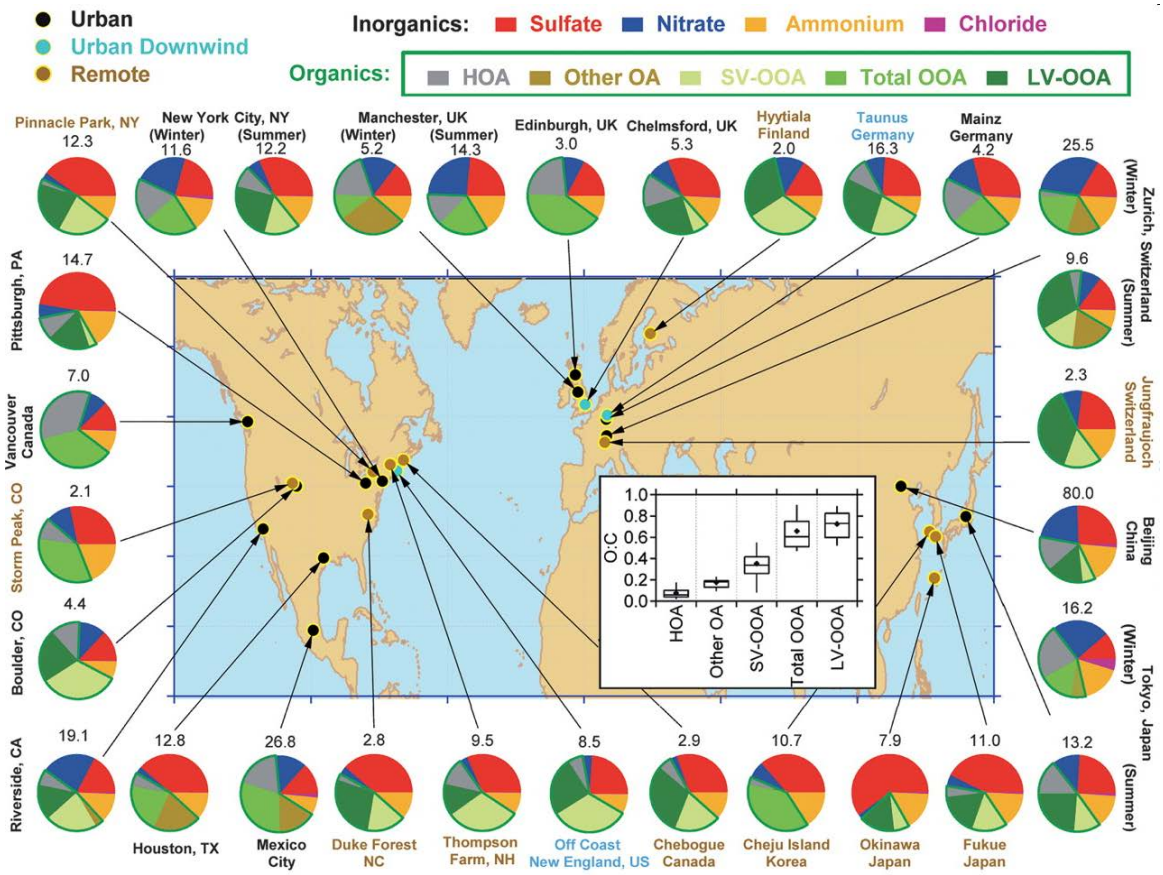

Figure 3: *Total mass concentrations (μg m^{-3}) and mass fractions of inorganic species and organic components measured with the AMS at a range of urban, urban downwind and remote sites. Classification of organic components is based upon oxidation state and volatility, with characteristic O:C ratios for each fraction shown inset (Jimenez et al., 2009).*

Changes in particle size have implications for many of the impacts of atmospheric aerosols. As the scattering effects of aerosols are size dependent, alteration of a size distribution by hygroscopic growth changes the fraction of an aerosol population that is

optically active, affecting its radiative forcing. The extent of a forcing is also influenced by the lifetime of particles, which is also determined by size and hence can be affected by hygroscopicity. Additionally, hygroscopic growth can also influence the effects of aerosols on the respiratory system following particle inhalation. The high RH within the lungs, which can reach 99.5%, results in particle growth, leading to more rapid deposition (*Maßling et al., 2005*). Non-hygroscopic material represents a greater risk, as particles are able to penetrate deeper into the lungs before being deposited (*McFiggans et al., 2005*).

Understanding of the interactions of water vapour with aerosols is critical in order to quantify the indirect radiative forcing associated with cloud effects. However, given the complexity of aerosol and cloud systems, a significant degree of simplification is required in order to include these processes in climate simulations. In this respect, water uptake can be characterised by κ, the hygroscopicity parameter, which can be used to relate the growth rate of aerosols to their role as CCN and activation as cloud droplets (*Petters and Kreidenweis, 2007*). While deliquescence and hygroscopic growth occur under sub-saturated conditions, CCN activation requires an RH greater than 100%. The spontaneous nucleation of water droplets from the gas phase in the absence of CCN would require supersaturations of several hundred percent, where as the presence of CCN in the atmosphere enables the formation of droplets at much lower levels of supersaturation, typically less than 1% (*Poschl, 2005*). Köhler theory (*1936*) provides a model for the formation of cloud droplets, combining the Kelvin and Raoult effects to describe CCN activation and droplet growth. This is shown in Equation 1:-

$$S = a_w \exp\left(\frac{2\nu_w \sigma_{sol/v}}{RTr}\right) \qquad [1]$$

where S is the saturation ratio (vapour pressure of water/saturation vapour pressure of water), a_w is the water activity, ν_w is the partial molar volume of water, $\sigma_{sol/v}$ is the surface tension of the solution, R is the universal gas constant, T is the droplet temperature and r is the particle radius. As with hygroscopicity, CCN activation is highly dependent on aerosol size and composition (*McFiggans et al., 2006*). Activation is effectively a balance between the

competing thermodynamic effects of the Kelvin and Raoult terms, which define the curvature and solute effects associated with particle size and composition respectively. The Kelvin effect causes an increase in equilibrium vapour pressure over a droplet, due to the greater surface tension exerted by curved surfaces. In contrast, equilibrium vapour pressure is reduced by the Raoult effect, as a result of the influence of dissociated ions in solution (*Mochida et al., 2006*). Raoult's law relates the activity of water to the mole fraction of water in solution, with the activity of pure water therefore equal to 1. The dissolution of other species in droplets reduces the fraction of water in solution, and hence the activity (*Petters and Kreidenweis, 2007*). Köhler theory can subsequently be used to determine the critical supersaturation (S_c) of an aerosol. This defines the point at which a particle of a certain size and chemical composition acting as a CCN becomes activated as a cloud droplet, and occurs where the difference between the opposing Kelvin and Raoult effects is greatest (*Andreae & Rosenfeld, 2008*). Once this level of supersaturation is reached, any further condensation will cause the droplet to activate and grow exponentially, independent of any further increase in supersaturation. Alternatively, the activation of cloud droplets can be described by the critical radius (r_c) or diameter (D_c); the particle size at which, for a specific composition at a given supersaturation, a droplet will undergo spontaneous growth (*McFiggans et al., 2006*).

1.2.6 Aerosol sinks

1.2.6.1 Dry deposition

The aerosol cycle is completed by the removal of particles from the atmosphere through deposition. This occurs via two processes, which are controlled by aerosol physical and chemical properties, together with local atmospheric conditions. The first of these is dry deposition, where by particles undergo aerodynamic transport through the atmosphere before being taken up by a receptor at the surface. Particle size and mass density determine the type of transport that occurs, and the resulting deposition velocity, which can be used in conjunction with the local aerosol concentration to calculate the overall dry deposition flux

(*Seinfeld & Pandis, 2006*). Small, light particles (D_p < 100 nm) undergo turbulent transport and Brownian diffusion, where as larger particles (D_p > 5 μm) are subject to gravitational settling due to their greater mass. Accumulation mode particles are not significantly affected by either of these mechanisms, and are removed by less effective interception and impaction processes, contributing to their extended lifetime and sustained radiative effects (*Fowler et al., 2009*). Deposition velocity is also affected by resistant forces, comprising the aerodynamic resistance, quasi-laminar resistance and surface resistance, effective at different stages in the depositional process, as shown in equation 2:-

$$v_d = \left(r_a + r_b + r_a r_b v_g\right)^{-1} + v_g \qquad [2]$$

where v_d is the deposition velocity, v_g is the gravitational settling velocity, r_a is the aerodynamic resistance and r_b is the quasi-laminar resistance, while the surface resistance (r_c) is assumed to be zero (*Seinfeld & Pandis, 2006*). This parameterisation is subsequently used in aerosol and climate models to quantify dry depositional fluxes. However, the limited understanding of many of the processes involved and a lack of observational data lead to a considerable degree of uncertainty in simulated deposition rates.

1.2.6.2 Wet deposition

Wet deposition refers to the scavenging of aerosols by precipitation, both within and below clouds. Several mechanisms exist for the inclusion of aerosols within cloud droplets. During convective cloud formation, aerosols surrounding clouds are entrained by updrafts and incorporated within droplets. Within wide-scale/synoptic cloud systems, aerosols acting as CCN are activated as cloud droplets which eventually precipitate out, where as particles below the cloud base are removed through interception by raindrops (*Guelle et al., 1998*). Wet deposition is dominated by droplet formation with CCN, in part due to the greater prominence of large-scale clouds in comparison to those formed by convection (*Kanakidou et al., 2005; Fowler et al., 2009*). The rate of wet deposition is therefore highly dependent on

aerosol physical and hygroscopic properties, which control the propensity for particles to form cloud droplets, in addition to the influence of local meteorological conditions, such as RH and cloud formation processes. Composition is also important given its effects on hygroscopicity and CCN activation, with deposition rate generally increasing with the solubility of components (*Textor et al., 2006*). Insoluble species are not affected by in-cloud processes, as a result of their inability to form cloud droplets, but are removed by precipitation below clouds (*Chung & Seinfeld, 2002*). However, the factors which determine the efficiency of rainfall scavenging are subject to much uncertainty. Aerosol and raindrop sizes, along with rainfall intensity, have been proposed as controls on particle washout rates, although contradictory evidence exists regarding the effects of each property (*Jurado et al., 2008; Koch et al., 1999*). Wet deposition is also further constrained by the evaporation of falling droplets, which leads to the formation of new aerosols (*Seinfeld & Pandis, 2006*).

Despite the uncertainty relating to both the controls on wet deposition and the processes involved, it is clearly a highly effective mechanism for the removal of atmospheric aerosols, with rainfall events able to largely purge the boundary layer of particles. This is most prominent in areas with high rainfall frequency, such as within the tropics and at high latitudes (*Jurado et al., 2008*). Wet deposition is also most effective with respect to accumulation mode particles (*Kanakidou et al., 2005*), particularly those composed of OC, BC or sulphate, for which it forms the primary sink (*Textor et al., 2006*). Accurate and reliable simulation of the key aerosol radiative impacts is therefore dependent on improved parameterisation of wet deposition processes in global models.

1.3 Aerosols and Climate

1.3.1 Background

Atmospheric aerosols have a significant influence upon Earth's radiative balance, with the potential to produce sizeable climate modifications. Given the variable nature of aerosol

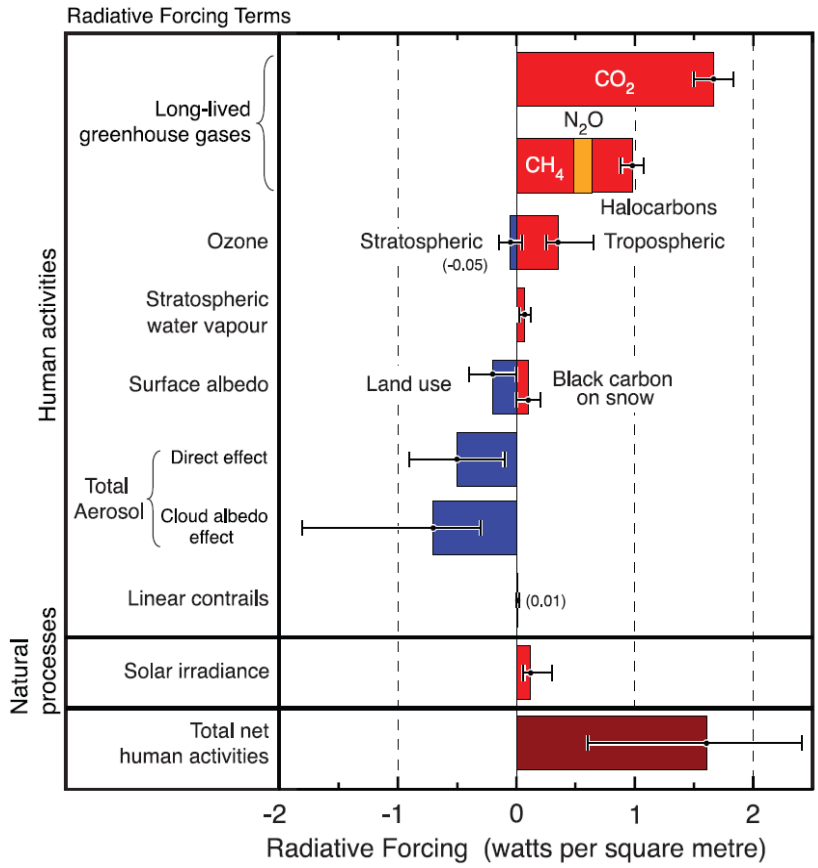

Figure 4: *Radiative forcings produced by the principal components of climate change relative to the pre-industrial era, with associated uncertainties (Forster et al., 2007).*

optical properties, these can involve both warming and cooling effects, depending on the way particles interact with incoming solar radiation. Alterations to this flux are the combined result of direct and indirect effects, which together comprise the overall aerosol radiative perturbation, although the man-made origins of many aerosol species mean that these effects also form a fundamental contribution to anthropogenic forcing of the climate system. Estimates for the possible magnitude of these impacts are largely derived from climate model simulations, and as such are dependent on the parameterisations used to drive models. Knowledge of the processes involved, their controls and sources of variability is therefore essential to develop a greater understanding of the causes and effects of climate change, improving the potential for successful mitigation. However, the latest assessments of constituent radiative forcings from the Intergovernmental Panel on Climate Change (IPCC) reveal that the greatest levels of uncertainty are associated with the contributions from

aerosols, and in particular the indirect effect, as indicated in Figure 4. Consequently, the reduction of these uncertainties represents a critical aim of aerosol research, and could ultimately present significant ramifications within the wider scope of climate science.

1.3.2 Direct effect

The aerosol direct radiative effect relates to the perturbation of the Earth's radiative budget from scattering and absorption of incoming solar shortwave and infrared radiation by particles in the atmosphere. This can lead to a net warming or cooling effect within the atmosphere, depending on the relative intensity of each process as determined by the optical properties of aerosols, together with their abundance, distribution and mixing state. Scattering species produce a cooling effect both within the atmosphere and at the surface, as radiation is removed from the Earth system and prevented from reaching the surface. However, while absorbing species cause radiation to be retained within the atmosphere creating a warming effect, the flux of incident radiation is also reduced, leading to a reduction in temperature at the surface (*Schult et al., 1997*). Several key optical properties determine the direction and intensity of aerosol radiative effects, and are used to define the aerosol optical depth (τ), which characterises the extinction of a direct solar beam as a result of aerosol effects along a given path within the atmosphere. These properties are the single scattering albedo (ω_0), which defines the fraction of light extinction by scattering; the mass extinction efficiency (α_e), which gives a measure of how effectively a particle attenuates light per unit mass; and the asymmetry parameter (g), describing the predominant direction of scattering relative to the path of light (*Penner et al., 2001; Seinfeld & Pandis, 2006*). Each of these parameters operates as a function of radiation wavelength and particle size, while RH is also important as a result of both hygroscopic growth effects and its direct influence on scattering efficiency, which is known as the humidification factor, *f(RH)*, and defines the ratio of scattering with a changing RH relative to a baseline level (*Clarke et al., 2002*). It is the dependence on particle size which forms the basis for the importance of accumulation mode aerosols, as certain parameters are at a

maximum for sub-micron particles. The intensity of both mass extinction efficiency and single scattering albedo is greatest when particle diameter is between approximately 0.2 – 2 μm, peaking at around 0.6 μm as shown in Figure 5 (*Penner et al., 2001*).

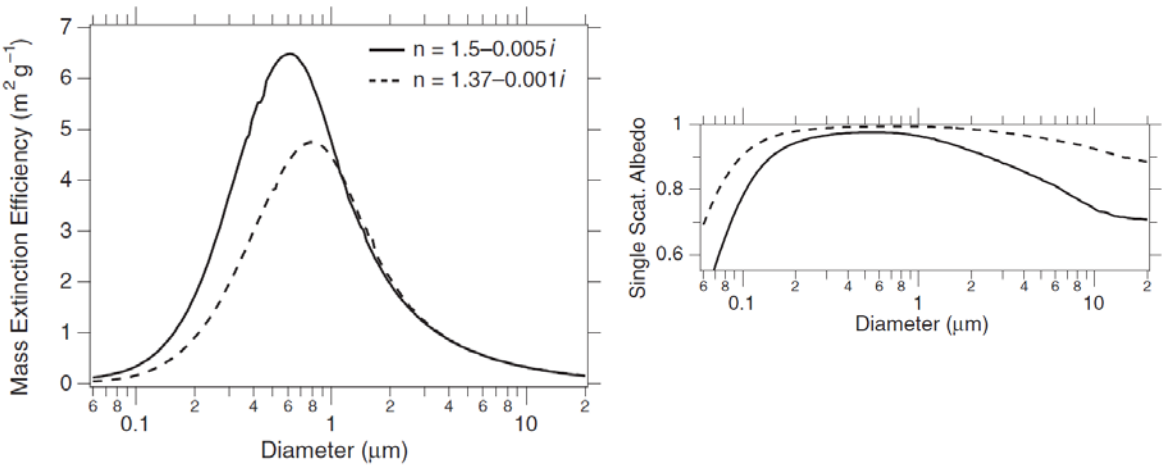

Figure 5: *Mass extinction efficiency and single scattering albedo of aerosols, integrated over a typical solar spectrum for two different refractive indices (Penner et al., 2001).*

ω_0 is given as the ratio of the light scattering (σ_s) and extinction (σ_e) coefficients, which are the effective cross-sections of attenuation by scattering and overall optical effects, respectively, as created by a particle of a given size (*Seinfeld & Pandis, 2006*). σ_e is represented by the sum of the scattering and absorption (σ_a) coefficients, such that:-

$$\omega_0 = \frac{\sigma_s}{\sigma_s + \sigma_a} \qquad [3]$$

The bulk optical effect of an aerosol population can be determined by relating σ_s and σ_a to the aerosol loading to give the mass scattering (α_s) and absorption (α_a) efficiencies, where by:-

$$\sigma_a \cong \alpha_a c_m \qquad [4]$$

and:

$$\sigma_s \cong \alpha_s c_m f(RH) \qquad [5]$$

where c_m is the aerosol mass concentration (*Reid & Hobbs, 1998*). These parameters can then be combined to derive the net radiative effect for an aerosol layer, in the form of the change in mean planetary albedo ($\Delta\alpha_p$):-

$$\Delta\alpha_p = [T_a^2(1 - A_c)]\left[2(1 - R_s)^2\bar{\beta}\tau_s - 4R_s\tau_a\right] \quad [6]$$

where T_a^2 is the transmissivity of the atmosphere above the aerosol layer, A_c is the cloud fraction, R_s is the reflectivity of the underlying surface and $\bar{\beta}$ is the average fraction of incident radiation scattered in a backwards direction across a range of sun angles. τ_s and τ_a are the optical depths for light scattering and absorption, which represent the products of the total column aerosol burden and σ_s and σ_a, respectively (*Hobbs et al., 1997*). Ultimately, the overall direct radiative forcing for an aerosol layer can be calculated by accounting for the intensity of incident solar radiation (S_0) such that:-

$$DRF = \Delta\alpha_p S_0/4 \quad [7]$$

Optical parameters can be calculated in accordance with Mie theory for scattering by spherical particles, although this requires explicit understanding of the aerosol size distribution and chemical composition. The difficulty in accurately constraining key parameters represents the first of several contributors to the overall uncertainty associated with model projections of direct radiative forcings. Further sources of uncertainty include the complexity and variability of the global aerosol burden, and the additional factors affecting the integration of optical parameters and aerosol properties to derive forcings (*Ramaswamy et al., 2001*). Examples of this include the representation of external influences and feedbacks which affect the forcing exerted by aerosols. The distribution of aerosols and the reflectivity of underlying surfaces are a vital consideration, and can have a significant effect on the overall albedo of the combined system, potentially altering the magnitude or even direction of forcing (*Chylek & Wong, 1995; Schult et al., 1997, Haywood & Boucher, 2000).* The level of contrast in albedo between the aerosol and surface components determine the apparent brightness of the system, with dark

surfaces such as the ocean increasing reflectivity, while light surfaces such as clouds or snow promote absorption. This is particularly relevant with respect to BC, for which the forcing varies considerably depending on vertical distribution and positioning relative to clouds, increasing when particles are located above or within clouds rather than below (*Haywood & Shine, 1997*). Absorption by BC particles can also affect cloud processes through warming of the atmosphere. This is known as the semi-direct effect, and can both suppress cloud formation and reduce existing cloud cover by altering RH and atmospheric stability (*Hansen et al., 1997; Ackerman et al., 2000; Lohmann & Feichter, 2001*). Deposition of BC on snow and ice produces a similar response by lowering the surface albedo, leading to increased melting and the formation of a feedback loop with a potentially significant global radiative impact, estimated at +0.3 W m^{-2} for the Northern Hemisphere (*Hansen & Nazarenko, 2004*). The additional effects attributed to these processes must also be accounted for in assessments of aerosol forcings, increasing the complexity of simulations and providing further sources of uncertainty.

Satellite observations provide an alternative method for calculating the aerosol direct effect, with increasing viability and accuracy as a result of continuing development within the field, involving new instruments and improved retrieval techniques. The advantages of satellite retrievals over ground-based measurements include the potential for global-scale observations and the high degree of flexibility offered by variable spatial, temporal and spectral resolution data products. However, the reliability of satellite data is limited to a certain extent by the various stages of processing that must be undertaken and the inherent uncertainties they entail, together with the difficulties faced in separating natural and anthropogenic radiative effects to derive the aerosol direct forcing. Consequently, estimates more frequently detail the combined aerosol direct effect, with the compilation in the IPCC Fourth Assessment Report (AR4) and *Yu et al.* (*2006*) providing a range of -3.8 to -6.8 W m^{-2}, with an average of -5.4 ± 0.9 W m^{-2}. Attempts have been made to constrain the aerosol direct forcing from satellite observations, with *Kaufman et al.* (*2005*) and *Christopher et al.* (*2006*) using data acquired from the MODIS (Moderate-resolution Imaging Spectroradiometer) and CERES

(Clouds and the Earth's Radiant Energy System) instruments to provide respective estimates of -1.4 ± 0.4 W m^{-2} and -1.4 ± 0.9 W m^{-2} for the clear sky top-of-atmosphere (TOA) forcing over oceans (*Forster et al., 2007*). Limited estimates are also available for globally-averaged clear sky TOA forcings, although the requirement for the use of multiple data sources and their subsequent assimilation contribute further uncertainties. *Bellouin et al.* (2005) and *Yu et al.* (*2006*) combined satellite observations with modelling and measurement data for certain optical parameters to give estimates of -1.9 ± 0.3 W m^{-2} and -1.3 ± 0.8 W m^{-2}, respectively. In comparison, estimates from global models range from -0.53 W m^{-2} to -0.89 W m^{-2}, with an average of -0.73 ± 0.18 W m^{-2}. The simulations included in AeroCom provide estimates of -0.29 W m^{-2} to -0.94 W m^{-2}, with an average of -0.68 ± 0.24 W m^{-2}. However, a greater degree of variation is observed in estimates of the all sky aerosol direct forcing, which accounts for the contribution from cloudy regions as well as clear skies, even including the suggestion of an overall positive forcing with a range of +0.01 W m^{-2} to -0.63 W m^{-2} from models included in the IPCC AR4 assessments (Figure 6). For the AeroCom models the estimated range is +0.04 W m^{-2} to -0.41 W m^{-2}, although the averages for the two datasets correlate closely at -0.23 ± 0.21 W m^{-2} (IPCC) and -0.22 ± 0.16 W m^{-2} (AeroCom).

Attempts have been made to isolate the individual contributions from the main anthropogenic aerosol species towards the overall direct forcing, although these are again subject to significant levels of variability and uncertainty. Across the full series of models used in the AR4, the forcing attributed to sulphate aerosol is estimated to range from -0.16 W m^{-2} to -0.96 W m^{-2}. Estimates for carbonaceous species exhibit slightly less divergence, with ranges of -0.06 W m^{-2} to -0.34 W m^{-2} for OC, and 0.08 W m^{-2} to 0.61 W m^{-2} for BC. As the majority of the simulations used in the comparison do not account for contributions from nitrates or anthropogenic mineral dust, consideration of these effects and inclusion of observational estimates are required to give an overall global average direct forcing, which is subsequently estimated to be 0.5 ± 0.4 W m^{-2} (*Forster et al., 2007*). However, the inconsistencies in estimates derived from different sources and the high levels of associated

uncertainties highlight the need for a greater availability of aerosol measurement data, particularly in a form that can be beneficial to modelling studies, focusing on areas that are poorly represented or understood at present. These improvements will ultimately enable more accurate and consistent parameterisation of aerosol properties, providing more reliable assessments of the climate impacts of anthropogenic aerosols.

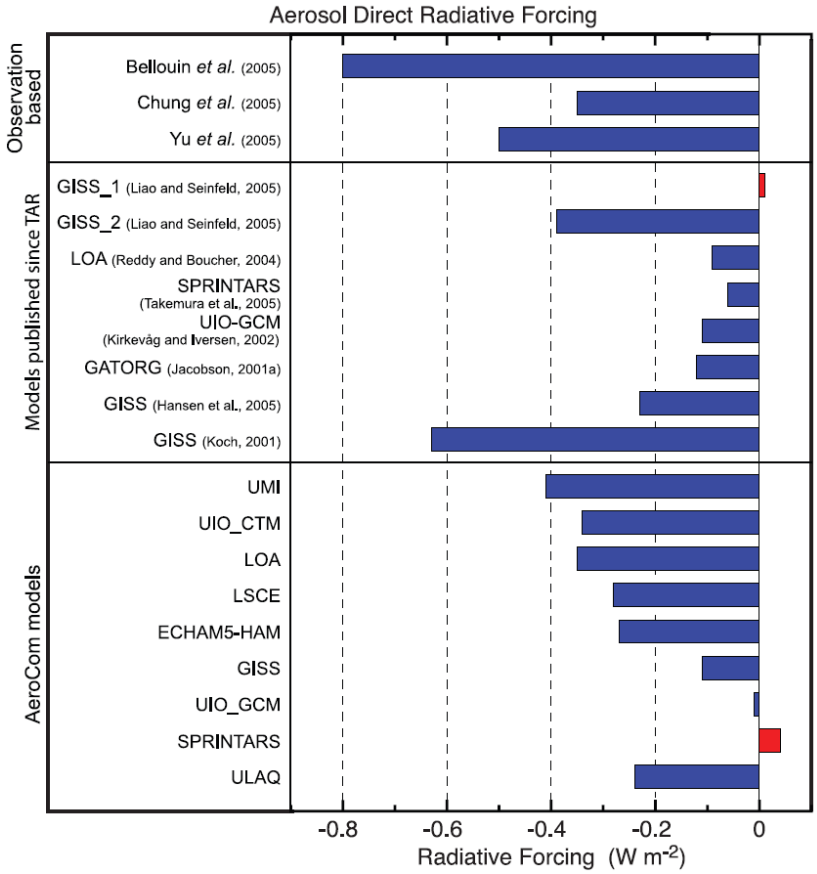

Figure 6: *Estimates of aerosol direct radiative forcing derived from observational studies, independent modelling studies and models included in the AeroCom experiment, showing the high degree of variability in current model projections (Forster et al., 2007).*

1.3.3 Indirect effect

Aerosols generate a further influence upon the climate system through their ability to act as CCN. Changes to aerosol burdens affect the availability of CCN, with subsequent implications for a range of cloud processes. Elevated aerosol emissions provide a greater number of CCN, promoting cloud droplet formation. The resulting increase in cloud droplet number concentrations causes an increase in albedo, due to greater scattering of solar

radiation by droplets. While the liquid water content of a cloud remains fixed, an increase in droplet number will also result in a reduction of droplet size, further enhancing the scattering efficiency, and ultimately the albedo, of the cloud (*Seinfeld & Pandis, 2006; Forster et al. 2007*). These modifications of albedo brought about by changes to droplet number and size represent the first set of perturbations associated with cloud-aerosol interactions, and are known as the cloud albedo effect or Twomey effect (*Twomey, 1977*). The magnitude of this perturbation is strongly influenced by aerosol properties, particularly those which affect hygroscopicity and cloud droplet activation, such as particle size, chemical composition and mixing state. Although fundamental relationships between aerosol and cloud microphysical properties have been identified, with aerosol number concentrations shown to be consistently important, the specific effects of particle size and composition on droplet size distributions are highly variable (*McFiggans et al., 2006*). Furthermore, there is a high level of uncertainty regarding the eventual implications for cloud optical properties and subsequent effects on radiative forcing (*Haywood & Boucher, 2000*). These uncertainties are reflected in the modelling studies documented in the AR4, which estimate forcings from -0.3 W m^{-2} to -1.85 W m^{-2}, although an additional caveat is placed on this range given that the representation of different aerosol species and cloud types is not consistent across the full series of models (*Forster et al., 2007*).

The aerosol indirect effect also accounts for the wider influences of atmospheric particles on cloud processes. Reduced droplet sizes can suppress the onset of precipitation, as it takes longer for smaller droplets to reach a size which is large enough to rain out. As a result, the lifetime of a cloud is extended, increasing the liquid water content and maintaining radiative effects for a longer period of time, subsequently enhancing the overall forcing. This alteration of rainfall regimes affects the cycling of aerosols within the atmosphere through a reduction in wet deposition, while also creating a perturbation of the local hydrological cycle. The collective impacts of these processes comprise the cloud lifetime effect or Albrecht effect (*Albrecht, 1989*). However, the overall forcing is difficult to constrain, given the disparate and varied nature of the constituent effects. This results in considerable uncertainty regarding the

magnitude of the forcing and its importance relative to the cloud albedo effect. *Lohmann & Feichter* (*2005*) show that several simulations estimate the cloud lifetime effect to be equivalent to only a small fraction of the cloud albedo effect, while others suggest it is actually more important. The overall range from the included models is -0.3 W m^{-2} to -1.4 W m^{-2}, with an average of -1.0 ± 0.4 W m^{-2}, comparing to a range of -0.5 W m^{-2} to -1.9 W m^{-2} and an average of -1.2 ± 0.3 W m^{-2} for the cloud albedo effect.

Limited understanding of many aspects of cloud-aerosol interactions mean assessments of the indirect aerosol effect should essentially be considered as guidelines for probable impacts. Significant reduction of prevalent uncertainties is necessary in order to more accurately constrain the importance of these processes in anthropogenic climate change. This also extends to the role of feedbacks, such as the effect of cloud forcings on the rate of evaporation and subsequent implications for the hydrological cycle and precipitation (*Rosenfeld et al., 2008*). As current considerations are largely restricted to aerosol effects on warm (liquid-phase) clouds, an increased focus on mixed-phase and ice clouds is also needed, as knowledge of these processes requires even greater refinement.

1.4 Biomass burning aerosols

1.4.1 Background

Biomass burning acts as a prominent source of atmospheric gases and particulates, involving a wide range of combustion processes across an extensive geographical distribution. Significant contributors to biomass burning emissions include vegetation fires, combustion of biofuels and incineration of biomass waste material. While naturally occurring wildfires are widespread in a number of vegetated ecosystems around the world, anthropogenic activity accounts for an increasing proportion of emissions. This is largely due to accelerating rates of deforestation and the conversion of land for agricultural use or development, particularly in tropical regions, from which 80% of total biomass burning emissions originate (*Hobbs et al.,*

1997). Emissions are dominated by carbonaceous species, and although the majority of this mass is made up of gaseous combustion products such as CO_2, CO and CH_4, which can account for up to 95% of the total emitted carbon mass (*Langmann et al., 2009*), the remaining fraction includes a contribution from particulate matter. Biomass burning aerosols consist of both OC and BC, representing 50-60% and 5-10% of the overall smoke particle composition respectively (*Reid et al., 2005*), along with a number of inorganic species including sulphates, nitrates and potassium. The overall size of the biomass burning aerosol burden is difficult to quantify, given the large number of different sources and their extensive geographical spread. Several attempts have been made to quantify emissions of the various species produced from biomass burning. Assessments of BC production include the closely correlated estimates of 4.8 and 4.9 Tg yr^{-1} (*Andreae & Merlet, 2001; Bond et al., 2004*), while estimates of POA emissions range from 22 to 54 Tg yr^{-1} (*Iinuma et al., 2007*). Overall biomass burning organic aerosol (BBOA) production is estimated to be between 45 and 80 Tg yr^{-1} (*Penner et al., 2001*), although a high level of uncertainty exists regarding SOA formation in biomass burning plumes.

The large anthropogenic contribution to biomass burning sources means resulting particles are expected to provide a significant radiative forcing, despite comprising only a small proportion of overall emissions. However, the diversity of combustion products and their properties mean that both the magnitude and direction of this forcing are poorly constrained (*Forster et al., 2007*). The dominance of primarily scattering OC species contributed to previous studies ascribing a net cooling effect to biomass burning aerosols (*Liousse et al., 1996; Ramaswamy et al., 2001*). In contrast, more recent assessments have highlighted the importance of absorbing components, with particular emphasis on the implications of surface reflectivity and the enhancement of absorption above clouds. The IPCC AR4 estimates an overall warming effect from biomass burning aerosol, placing the mean radiative forcing derived from a series of studies as +0.03 W m^{-2} ± 0.12 W m^{-2} (*Forster et al., 2007*). The wide range in proposed forcings, from -0.05 to +0.22 W m^{-2} throughout the AR4 and AeroCom

models, provides an indication of the uncertainty associated with the radiative impacts of biomass burning aerosols and the need for improved characterisation of their properties.

1.4.2 Optical properties

Approximately 80-90% of the biomass burning aerosol volume is in the accumulation mode (*Reid et al., 2005*), while 40-80% of the OC content is water soluble (*Janhall et al., 2010*), meaning particles can be considered to be optically important with regard to both their direct scattering and absorption effects and their role as CCN. The concurrent presence of both OC and BC and their contrasting optical effects forms the basis for highly variable radiative impacts from biomass burning plumes. Given that the overall forcing of an aerosol layer is dependent on the column burden of radiation-attenuating aerosol species along with their specific optical parameters, the processes which act to alter these properties must be well constrained and understood in order to accurately infer the resultant radiative effects. Observed biomass burning aerosol optical properties are subject to considerable deviation across a range of scales and between different environments. For example, typical single scattering albedos for particles from tropical fires are around 0.82 – 0.84, which are comparable to reported values for mid-latitude fires (0.80 – 0.85), but lower than boreal fires which stand at 0.85 – 0.90 (*Hobbs et al., 1997*). These variations have been attributed to a number of causes, including the distinct chemical compositions and size distributions associated with different fires, and the influence of RH on aerosol plumes and potential cloud formation, which are all affected by differences in production pathways and the lifecycle of particles once present in the atmosphere. The relationships between these drivers, and the implications for their subsequent effects on optical properties, are typically complex, making it difficult to confidently prescribe the reasons for the observed variability (*Wong & Li, 2002*).

1.4.3 Combustion conditions

The chemical composition of biomass burning aerosols, and more specifically the ratio of black carbon to organic carbon (BC/OC), are highly dependent upon the combustion conditions of the fires from which they originate. The development of biomass fires involves a series of critical stages, beginning with the dehydration, pyrolysis and volatilisation of fuels, where by the thermal cracking of fuel molecules produces a mixture of tar and gas products (*Andreae & Merlet, 2001*; *Weimer et al., 2008*). These products are then mixed with air to form a flammable mixture, initiating flaming combustion (*Andreae & Merlet, 2001*). As combustion is more efficient during the flaming-phase of a fire, CO_2 provides a greater proportion of emissions, as oxidation is able to progress to completion. Production of BC is also greatest during the flaming-phase, as a result of the increased abundance of polycylic aromatic hydrocarbon (PAH) precursors, which form at higher temperatures (1300-1600 K) and act as CN for other pyrolised species (*Reid & Hobbs, 1998; Richter & Howard, 2000*). In regions of fires where fuel concentrations are high, mixing of combustion products with air can be restricted, with the lack of available oxygen enabling newly-formed particles to avoid complete oxidation and remain as BC (*McMeeking, 2008; Reid & Hobbs, 1998*). Smouldering combustion occurs at lower temperatures (< 850 K) and primarily involves surface reactions of oxygen and the solid, high carbon content products derived from the initial stages of fuel pyrolysis, due to decreasing availability of flammable volatile compounds as fuels become depleted (*Andreae & Merlet, 2001; Reid et al., 2005*). The reduced temperatures decrease the rate at which the processes involved in the oxidation of emission products occur, promoting the release of partially oxidised species such as CO (*Andreae & Merlet, 2001*). However, the fraction of BC in emissions from smouldering fires is severely reduced, due to the lack of PAH formation. The BC/OC ratio is subsequently lower, with an increasing dominance of OC in particulate emissions (*Reid et al., 2005*).

Combustion conditions are characterised using the modified combustion efficiency (MCE), based on the fraction of emitted carbon in the form of CO_2, as follows:-

$$MCE = \frac{\Delta[C]_{CO_2}}{\Delta[C]_{CO_2} + \Delta[C]_{CO}} \quad [8]$$

where $\Delta[C]_{CO}$ and $\Delta[C]_{CO2}$ are the excess concentrations above the ambient background for carbon in CO and CO_2, respectively. A high proportion of CO_2, and hence a high MCE, are indicative of the flaming-phase, with an MCE greater than 0.9 taken to represent the occurrence of flaming combustion for more than 50% of the duration of the fire, while an MCE lower than 0.9 indicates a dominance of smouldering combustion (*Hobbs et al., 2003*). MCE can therefore be used to characterise combustion conditions and the typical chemical compositions of their emission products, with the size of the BC fraction of particular interest. Laboratory studies involving a range of biomass types have shown that overall bulk aerosol optical properties are more dependent on BC/OC than on variations in the key optical parameters of OC components (*McMeeking, 2008*). This highlights the potential for using inventories of emission ratios, in conjunction with established measurements of optical properties, to infer expected radiative impacts from biomass burning aerosols. Existing studies provide parameterisations of emissions from different vegetation or ecosystem types, but these are typically independent of geographical location and based on limited observations (*Janhall et al., 2010*). Large aerosol datasets from extensive field campaigns could therefore be exploited to develop upon existing studies and provide parameterisations across wider regional and continental scales, whilst examining potential links between BC/OC measurements and observed variations in biomass burning aerosol optical properties across different source regions. However, any such parameterisations would also need to account for the additional factors which influence the composition of biomass burning emissions. MCE does not provide an accurate representation of combustion temperature, which can vary considerably, irrespective of combustion phase. Such variations are highly relevant to the temperature-dependent processes involved in different stages of the fire process, the reduction or enhancement of which may significantly alter the eventual composition of any aerosol products. In the absence of accompanying direct measurements, the lack of accurate

temperature data should be considered a caveat to the use of MCE as a means of justifying observed aerosol properties.

The relationship between aerosol size distributions and MCE is highly uncertain, with results from different biomass burning experiments providing polarised assessments. In their compilation of size distributions from a number of vegetation fire field surveys, focusing largely on southern Africa and the Amazon region of South America, *Janhall et al.* (*2010*) propose that particle geometric mean diameters typically exhibit a positive correlation with MCE, with flaming combustion producing larger particles. In contrast, the review of biomass burning aerosol physical properties by *Reid et al.* (*2005*) states the opposite, suggesting that larger particle sizes are generally associated with smouldering combustion. The numerous factors which influence aerosol production in biomass fires are presented as potential contributors to this ambiguity. These include the overall size and intensity of fires, and their specific dynamics, which determine oxygen cycling, the progression of oxidation and subsequent abundance and properties of intermediate emission products. In turn, this affects particle formation pathways, altering the rate of coagulation and condensation (*Reid & Hobbs, 1998; Reid et al., 2005*). Although these effects must be considered, and understanding of the exact nature and importance of their roles improved, analysis of a broader range of experimental studies may help to resolve the relationships between size distributions and fire properties.

1.4.4 Fuel types

The direct relationships between fuel types and the physical, chemical and optical properties of emission products form the basis of attempts to parameterise global biomass burning aerosols. Emission factors are an important tool in analysing these links, giving an indication of the magnitude of aerosol production from the initial biomass source. These are based upon the concentration of a particular species relative to the amount of fuel burned, although as the latter is difficult to infer from field studies, the total concentration of

carbonaceous species in a plume is typically used, with emission factors therefore defined as such:-

$$EF_x = \frac{[x]}{\Sigma[C]_{products}}[C]_{biomass} \quad [9]$$

where *[x]* is the concentration of species *x*, $\Sigma[C]_{products}$ is the sum of the concentrations of all carbonaceous species and $[C]_{biomass}$ is the concentration of carbon in the biomass burned, which in the absence of precise measurements is usually taken as 45% (*Ferek et al., 1998*; *Andreae & Merlet, 2001*). Emission factors are calculated in terms of both particle mass and number, with both parameters relevant to the radiative impacts of aerosol populations. Major syntheses of biomass burning data typically use broad fuel types to characterise emissions, rather than focusing on specific geographical regions (*Andreae & Merlet, 2001; Reid et al., 2005; Janhall et al., 2010*). However, it may be the case that emissions from different locations, sharing similar dominant vegetation types, exhibit a significant degree of variability (*Capes, 2009*). Parameterisations using these general classifications may consequently fail to fully represent any such disparity, which could be an important consideration with regard to emissions inventories for modelling studies. Analysis of any such trends and postulation of the factors responsible would also require a clear understanding of the specific vegetation distribution for each source region, which would be difficult to ascertain from aircraft-based surveys without the availability of additional observations. Furthermore, consideration must be taken of the role of fire characteristics and the additional influences on emission properties beyond differing fuel types. These include combustion efficiency, comparison to which can help constrain the relative importance of the various controls on biomass burning aerosols. However, to a certain extent MCE itself is a function of fuel type, along with fire intensity, oxidation rate and fuel-air ratio (*Reid & Hobbs, 1998*), emphasising the complexity of the relationships between different controls.

While MCE can be used to rationalise observed aerosol compositions as a function of the proportion of flaming and smouldering combustion, experimental results have also revealed divergences from the general trends identified, with fires dominated by flaming combustion producing little BC (*McMeeking, 2008*). The reasons for these anomalies are unclear, but may be due to perturbations of the processes involved in BC formation as a result of variations in the characteristics of biomass burning events. Formation of BC precursors such as PAH requires high temperatures which may not always be reached, regardless of the length of time for which the flaming phase is active. The presence of certain inorganic species is also believed to inhibit production of PAH and other precursors, as Cl, Na and K ions react competitively with the radicals involved in the initial polymerisation processes which lead to the formation of PAH (*McMeeking, 2008; Richter & Howard, 2000*). Inorganic fractions in biomass burning emissions are a function of fuel type and the chemical composition of the vegetation in question. Given the huge potential plant species diversity, even within a particular ecosystem or geographical location, possible links between fuel type and BC fraction are likely to be highly complex.

1.4.5 Aging and SOA production

While measurements of aerosol properties and overall production from vegetation fires form an essential part of efforts to improve the understanding of key atmospheric constituents, these initial observations alone are not sufficient to fully resolve the radiative impacts of these species. Physical and chemical evolution over time can bring about changes in optical behaviour, altering particles significantly from their initial conditions at source. The formation of SOA is a critical aspect of this process due to its effects on both optical properties and overall aerosol loadings. Observations from biomass burning plumes in Southern Africa show an increase in single scattering albedo with age. Over a period of 5 hours, ω_0 increased from 0.84 at source to 0.90 in the far-field (*Abel et al., 2003*). This change is attributed primarily to an elevated abundance of scattering material, and in effect a reduction

in BC/OC, resulting from the condensation of gas-phase OC species onto existing CN. Alteration of aerosol size distributions can also affect optical properties, with aged particles in biomass burning-dominated regional hazes around the Amazonian tropical forests of Brazil showing an increase in mass scattering efficiency (α_s) with volume median diameter (*Reid et al., 1998*). Increasing particle sizes are likely to be the result of a combination of chemical and physical aging processes, as both condensation and coagulation act to increase particle diameter. The contribution of coagulation to particle aging can be inferred from changes in particle number concentrations, although these must be compared to the variation in excess concentration of a reference species such as CO, which is used as an indicator for plume aging to account for the reduction in concentrations resulting from the dilution of plumes as they mix with ambient air (*Hobbs et al., 2003*). While aging has been shown to increase scattering in aerosols, the processes responsible can also enhance absorption by BC particles. The condensation of OC or other volatile species onto BC nuclei produces a lensing effect, focusing light onto the BC core and subsequently increasing the mass absorption efficiency (α_a) (*Pósfai et al., 2003*). However, given the widely observed increases in ω_0, it is likely that the overall impact of this effect is limited by the greater influence of changes to α_s.

Numerous field campaigns provide evidence of significant SOA formation involving emission products from vegetation fires. These include measurements taken across a range of environments, encompassing a variety of ecosystems and different fuel types. *Reid et al.* (*1998*) report increases in particle loadings from fires in the Brazilian rainforest during the Smoke, Clouds and Radiation-Brazil project (SCAR-B). Particle mass concentrations increased by around 20-45% over a period of four days, with OC condensation believed to account for around a quarter of this increase. Results from the Tropical Forest and Fire Emissions Experiment (TROFFEE) within the same region show a similar trend, suggesting that around 5% of total VOC emissions were converted to SOA within 1 to 3 days of emission (*Yokelson et al, 2008*). This would also include a contribution from biogenic VOCs, although such species are not expected to be highly concentrated in biomass burning plumes, despite their

prevalence at global and regional scales. Pyrogenic OA tend to be characterised by the presence of the carbohydrate levoglucosan, which is subsequently used as a tracer for biomass burning aerosols. Levoglucosan represents an important SOA constituent, and is shown to increase in concentration by an order of magnitude only 40 minutes after emission from savanna fires during the Southern African Regional Science Initiative (SAFARI 2000). SOA production involving other species was also highly active during SAFARI, with the total aerosol mass concentration increasing by more than a factor of 3 over the same period (*Gao et al., 2003*).

Observations from SAFARI also highlight the photochemical mechanisms responsible for aging in biomass burning plumes, and the pathways involved in SOA production. *Trentmann et al.* (*2005*) report an increase in O_3 mixing ratio of approximately 90 ppb within 60 minutes of emission, while the emission ratio normalised to CO to account for the effects of dispersion (O_3/CO) increases by around 8.5%. The observations of *Hobbs et al.* (*2003*) are consistent with this trend, showing a rise of around 9% in O_3/CO over an even shorter period of 30 minutes. The increased abundance of O_3 is the result of photochemical production following the oxidation of VOC precursors by oxidising agents such as OH and NO_3 radicals (*Mason et al., 2001*). Measured mixing ratios for a range of hydrocarbons (HC/CO) within the aging plume support this mechanism, decreasing rapidly as the precursor species are consumed in photochemical reactions (*Hobbs et al., 2003; Trentmann et al., 2005*). Further corroboration is provided by *Yokelson et al.* (*2009*) from the Megacity Initiative Local and Global Research Observations (MILAGRO) project in the Yucatan region of Mexico, where an increase in O_3/CO of around 15% was observed over less than 1 hour of aging, in conjunction with a doubling of $PM_{2.5}$/CO within 2 hours in response to SOA formation. However, it is also suggested that SOA formation in biomass burning plumes is affected by VOC precursors from other sources, following discrepancies in the balance between the loss of known precursors emitted from vegetation fires and overall SOA loadings. This effect appears particularly evident with regard to organic acids, for which the observed secondary formation was much

larger than the expected availability of precursors (*Yokelson et al., 2009*). While enhanced production may be the result of high concentrations of previously unidentified precursors, it also highlights the potential complexity of contributions to SOA formation in biomass burning plumes, particularly in areas influenced by a number of different major VOC sources, as is the case in the Yucatan given the proximity to the large urban area of Mexico City. The mixing of different air masses and the supply of precursors from alternative sources could therefore form an important constraint on the rate of secondary formation and resulting properties of biomass burning aerosols. As such, this scenario should form a consideration for any analysis of aerosol evolution in areas likely to be subject to several different emissions sources, in order to more accurately resolve the key transformations and their main drivers.

Chamber studies provide an additional means of examining the evolution of biomass burning aerosols, using controlled laboratory conditions to enable analysis of the dominant processes and mechanisms for specific prescribed combustion scenarios. Photochemical aging is promoted by developing a conducive environment, initiating photo-oxidation by exposing fresh smoke from vegetation fires to UV light, and diluting emissions with clean air to simulate conditions in real plumes. *Grieshop et al.* (*2009a*) performed such a series of experiments, showing consistency with results derived from earlier field studies. Total OA mass concentrations were observed to increase by a factor of 1.3 within the first hour of UV exposure, and by an average factor of 1.5 – 2.8 throughout the duration of the experiments, in conjunction with a 220 ppb increase in O_3 concentration. Analysis of aerosol volatility also provides potential reasoning for the production of SOA far in excess of that expected from measurements of known precursors. It is proposed that initial POA emissions are in fact semi-volatile, and will evaporate under ambient conditions. Photo-oxidation of these vapours reduces their volatility, producing LVOCs which readily partition to the particle phase. This mechanism identifies a possible source for the high levels of SOA produced, whilst also indicating that photochemical aging reduces the volatility of OA from vegetation fires, a point which opposes the current consensus and as such should be the focus of further clarification.

Results from the chamber studies performed by *Grieshop et al.* (*2009a*) also highlight certain aspects of the uncertainties associated with SOA production in biomass burning plumes. The rate of production showed a decline beyond 1 hour, suggesting that the majority of SOA forms within the first hour of aging, although the extent to which this trend is replicated in real plumes is unclear. Furthermore, analysis of plumes across a wider range of environments has shown a distinct variability in photo-oxidation rates. Increases in O_3/CO are typically slower at higher latitudes in comparison to the tropics, while photolysis rate constants for certain species have been shown to vary within single plumes (*Yokelson et al., 2009*). This uncertainty is accentuated by measurements of aerosol composition during the Dust and Biomass Burning Experiment (DABEX) and Dust Outflow and Deposition to the Ocean (DODO) projects in West Africa. Results from *Capes et al.* (*2008*) show that OC/CO remains constant within aging plumes, despite evidence of photochemical activity from increasing O_3 concentrations. The lack of an increasing OC mass over time implies an absence of SOA formation, at least to an extent whereby there is no net rise in OC, with OA losses balancing secondary production. Given an observed increase in O:C ratio within the plume OA mass, which indicates that OC species become increasingly oxidised with age, and the additional evidence for photochemical activity, it is suggested that OA is lost through evaporation following volatility changes as a result of aging. This is consistent with *Grieshop et al.* (*2009a*), and the evolution framework proposed by *Donahue et al.* (*2006*), identifying a sink for OA that would support an increase of O:C concurrent with stable OC/CO. However, the reasons for the increased magnitude of this effect and its bearing on OA concentrations in comparison to other locations are uncertain, but could be of great importance to understanding SOA processes at regional and global levels.

The uncertainty regarding SOA production in biomass burning plumes makes it difficult to reliably constrain the effects of aerosol aging. Chamber studies enable exhaustive investigation of aging processes, with precise regulation of fire properties such as the types and amounts of fuel used during each event, which in turn influence the condition and overall

intensity of the fire. In order to develop a better understanding of the implications of these processes for aerosol loadings and their radiative effects, it is also necessary to determine the temporal and spatial resolutions at which they operate. The timescales associated with aging form an important control on aerosol lifetimes and their subsequent impacts, while knowledge of spatial resolution is vital as a means of providing accurate representation within aerosol modelling, with suggestions that transformations occur at finer scales than those employed by current models (*Yokelson et al., 2009*). Although chamber studies can be used to infer temporal variations in aerosol properties, they cannot represent the spatial scales involved in aerosol evolution. This analysis is therefore primarily dependent on in-situ measurements, the examination of which may help to resolve uncertainties regarding the nature of aging in biomass burning plumes. The ability of chamber experiments to accurately reproduce the chemistry of aerosols in real plumes also acts as a potential caveat to their results (*Kroll & Seinfeld, 2008*), given the inherent regulation of fuel components and combustion conditions. However, some studies have shown a strong correlation between the mass spectra of aged SOA derived from ambient and laboratory measurements, with the limited variation produced by altering experimental conditions suggesting that the eventual composition of SOA is largely independent of fuel, combustion and aging conditions (*Grieshop et al., 2009b*). In order to confidently substantiate this relationship and determine whether it is observed consistently throughout different plumes, a broader analysis of biomass burning aerosol properties is required. Extensive measurement datasets can be used as the basis for comprehensive analysis of trends in SOA composition, along with further chemical and physical properties, and the main factors which influence these characteristics. Syntheses of these datasets from a wide range of environments hold the potential to provide improved parameterisation of these major aerosol components, and ultimately clarify their role in regional and global scale climate forcing.

Chapter 2

Instrumentation and platform

2.1 The Aerosol Mass Spectrometer (AMS)

The Aerodyne Research Inc. Aerosol Mass Spectrometer (AMS; *Jayne et al., 2000*) represents the primary source of data used in the range of analyses which comprise this thesis. Although several other sources of data have been employed extensively, including measurements of multiple gas phase species and additional particulate properties, AMS measurements form the basis for the characterisation of BBOA. The AMS provides high time resolution, size-resolved mass concentrations and chemical speciations for non-refractory, sub-micron particulate matter. Its deployment within a wide range of different environments and across a number of different measurement platforms highlight the versatility of the instrument, and its scope to deliver comprehensive, quantitative assessments of atmospheric aerosol populations.

Several different versions of the AMS have been developed, although the majority of components and basic layout remain the same across all versions, only differing in the type of mass spectrometer used. Extensive descriptions of the instrument, including variants, and methods for the derivation of data products are available (*Jayne et al., 2000; Allan et al., 2003; Jimenez et al., 2003; Drewnick et al., 2005; DeCarlo et al., 2006; Canagaratna et al., 2007*), with an overview of key elements given here. Operation of the AMS consists of three main stages, beginning with the formation of a particle beam. Sample flow into the instrument is focused by an aerodynamic lens system comprising a critical orifice and a series of apertures, transmitting particles with aerodynamic diameters between 70 and 600 nm at near 100% efficiency (*Allan et al., 2003*). While particles between 30 and 70 nm, and up to 2.5 μm, in diameter are also able to progress through the aerodynamic lens, transmission efficiency is reduced (*Canagaratna et*

al., 2007). The focused particle beam then enters a vacuum chamber, wherein particles are aerodynamically sized by their time of flight. A mechanical chopper wheel, comprising a rotating disc with two radial slits, modulates the particle beam and allows discrete packets of particles to pass through the sizing region, with the time taken to traverse the chamber used to infer particle diameter according to size-dependent velocity. These measurements of particle diameter ultimately enable chemically speciated size distributions to be developed following detection and resolution of composition.

When the chopper wheel is left in an open position, particles are able to pass freely to the detection region of the AMS. The first stage of detection involves the vaporisation of particles by impaction upon a heated tungsten plate, typically held at a temperature of 600°C. The gaseous molecules resulting from vaporisation then undergo ionisation through electron impact, involving 70 eV electrons emitted by a tungsten filament source, to give positively charged ions. These ions are then passed through an electric field to the mass spectrometer. The original version of the instrument (Q-AMS; Figure 7) that was used throughout the majority of experiments contributing to this analysis employed a quadrupole mass spectrometer (*Jayne et al., 2000*). More recent iterations of the AMS incorporate time-of-flight (ToF) mass spectrometers, with the compact (C-ToF-AMS; *Drewnick et al., 2005*) and high resolution (HR-ToF-AMS; *DeCarlo et al., 2006*) versions providing improved sensitivity and time resolution. The quadrupole selects ions according to their mass-to-charge ratios (m/z), as varying the applied voltage allows only ions of a specific m/z to pass through to be detected by an electron multiplier. As the quadrupole is only able to transmit ions of a single m/z to the electron multiplier at any given time, it is not possible to provide a complete mass spectrum of a single particle. However, a composite mass spectrum of an aerosol ensemble can be derived by scanning over an m/z range of 0-300. This is achieved by varying the voltage applied to the quadrupole through the complete mass resolution range of the instrument, and subtracting the average spectrum obtained when the chopper is placed in the closed position, which blocks

the particle beam to prevent vaporisation and ensure only signals from background gases are detected (*Allan et al., 2003*).

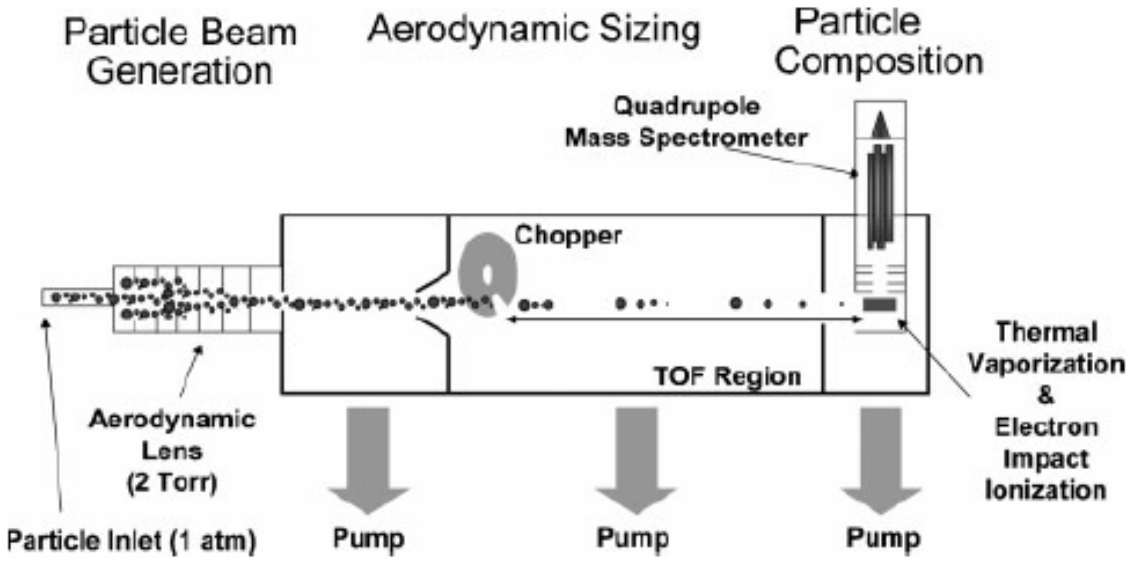

Figure 7: *Schematic of an Aerodyne Quadrupole Aerosol Mass Spectrometer (Canagaratna et al., 2007).*

Calculation of quantitative aerosol mass concentrations from detected ion signals requires a number of conversion steps to be applied. Firstly, the limited ionisation efficiency (IE) achieved by electron impact must be accounted for, as only a small proportion of the potential ion source from vaporised molecules will be successfully ionised and detected. Furthermore, variability in IE provides a source of uncertainty in derived concentrations, manifested as detection limits which define the minimum concentrations which can be reliably measured. Detection limits are dependent on the sampling time of the instrument, and can be reduced by sampling over longer time periods. While longer averaging provides a greater level of precision, it is not always a viable approach, particularly when measurements are required at a high time resolution, such as under ambient conditions. As vaporised molecules fragment into several different constituent ions upon impact by electrons, it is also necessary to perform a summation of each component in order to derive a mass concentration for a given species. However, interferences within mass spectra make this process difficult for the majority of species, requiring the use of known fragmentation patterns to extract mass spectra for

individual species from the overall ensemble (*Allan et al., 2004*). Finally, a further correction factor is applied to account for the incomplete detection of all particles sampled by the instrument. Collection efficiency (CE) is used to define the proportion of particles which are successfully vaporised, with particle losses largely attributed to deflection off the heated surface (*Quinn et al., 2006*). CEs can be evaluated through comparison with concurrent measurements from additional instrumentation, with typical values around 0.5 (*Canagaratna et al., 2007*).

2.2 The Facility for Airborne Atmospheric Measurements (FAAM)

While a number of different measurement platforms were employed throughout the range of campaigns contributing towards this analysis, the majority involved the Facility for Airborne Atmospheric Measurement (FAAM) atmospheric research aircraft. FAAM represents a collaboration between the UK Met Office and Natural Environment Research Council (NERC), which jointly fund the operation of a modified BAe-146-301 regional airliner to perform a wide range of in-situ atmospheric observations. Research flights undertaken by the BAe-146 are able to provide a wide geographical coverage, with a maximum cruising speed of just under 800 km h^{-1} and science speed of approximately 100 m s^{-1} giving a maximum flight time of around 5.5 hours and a range of up to 3000 km with a full scientific payload of 4200 kg. The BAe-146 can operate between heights of 50 and 35000 ft, enabling vertical profiling over a considerable altitudinal range. The extensive ranges obtainable by the BAe-146 subsequently provide an optimal platform for observing BB plumes, facilitating measurements at highly variable distances from source and over long time periods, such that aging processes can be explicitly examined.

The substantial payload of the BAe-146 allows for the installation of a wide range of instrumentation. While the specific complement of instrumentation is determined by the

scientific objectives of each deployment, a number of core instruments are included on all research flights, although not necessarily always operated. This ensemble includes several instruments for monitoring atmospheric chemistry, with the data provided used extensively throughout this analysis. CO is measured using an Aerolaser AL5002 UV fluorescence analyser, which determines the concentration of CO from the proportional relationship to fluorescence under UV light at 150 nm. A Thermo Scientific TEi49C UV photometric analyser was used to derive concentrations of O_3 from UV absorption at a wavelength of 254 nm, while NO_x and its constituents (NO and NO_2) are measured by an Air Quality Design Inc. chemiluminescence NO_x analyser, based upon the intensity of light emitted by the reaction of NO with O_3. TSI Inc. condensation particle counters are frequently installed on the BAe-146 to measure total particle number concentration within a size range of approximately 3 nm to 3 μm. Particles are detected optically following activation as condensation nuclei under supersaturated conditions. Different condensing agents are used in different models of the CPC, with a water filled model 3786 replacing a butanol-based model 3025 on the BAe-146.

Several variants of the AMS have been operated on the BAe-146 since its first deployment in 2004. Samples of ambient air are drawn through a Rosemount inlet (*Foltescu et al., 1995*), with negligible losses within the sub-micron particle size range measured by the AMS (*Haywood et al., 2003*). Heating of sample air due to the elevation of cabin temperatures above ambient levels also dries aerosol prior to detection (*Crosier et al., 2007*). The original Q-AMS has been superseded by newer C-ToF-AMS and HR-ToF-AMS versions, providing improved signal-to-noise ratios and alleviating a common problem affecting Q-AMS measurements, particularly for high altitude operation (*Bahreini et al., 2003*; *Morgan et al., 2009*). The reduction in sampling flow rate with decreasing pressure at higher altitudes increases species detection limits for the Q-AMS. *Crosier et al.* (*2007*) report a detection limit of 1.69 μg m^{-3} for organics based on three standard deviations in 30-second Q-AMS measurements at a height of approximately 1000 m, while *Capes et al.* (*2008*) calculated a typical instrument noise of 3.3 μg m^{-3} for a 30-second sample at 600 m. *Drewnick et al.* (*2009*)

report an improvement in collection efficiency of more than an order of magnitude relative to the Q-AMS for organics measured by the C-ToF-AMS. Degradation of the internal air beam standard, which is used as a correction factor for all other measured fragments (*Allan et al., 2003*), due to changing ambient pressure is also accounted for during aircraft operations (*Bahreini et al., 2003*).

Chapter 3

Papers

3.1 Introduction to papers

The analysis presented here utilises a number of datasets acquired from field campaigns and laboratory experiments undertaken by members of the Centre for Atmospheric Science and collaborators at other institutions. These field campaigns generally form part of major international collaborative research programs, aimed at improving understanding of various aspects of atmospheric processes and composition. In some instances the study of BB emissions represented the main focus of the research activity, while in others measurements were performed within the wider scope of more extensive investigations. The diverse objectives of these campaigns has provided an inventory of BB observations across a broad range of environments and different stages of plume evolution, further augmented by measurements of emissions directly at source under controlled conditions during laboratory experiments. As a consequence of the range of geographical locations and contrasting ages of emissions sampled, it has been possible to perform an extensive, multi-faceted analysis aimed at addressing a number of the major uncertainties relating to the lifecycle of BBOA in the atmosphere. However, due to the requirements of wider research interests in some instances, and restrictions emplaced by the availability of instrumentation and prevailing technological capabilities, these datasets are by no means exhaustive. Subsequent analysis has revealed areas of ongoing uncertainty, and the potential to address these through future research efforts.

3.2 Aims and objectives

The main body of original research within this thesis comprises three papers focusing on different aspects of the production and evolution of BBOA. The first paper, now published in *Environmental Science & Technology*, addresses the variability in BBOA emission ratios between different geographical regions and amongst different fires within the same locality. The overall impact of SOA formation on aerosol loadings in aging BB plumes is also examined through comparison of normalised OA mixing ratios close to source and several days after emission, and evaluated against wider observations amongst the literature base. Factors potentially affecting the magnitude and nature of BBOA emissions are examined in Paper 2, through analysis of prescribed fires carried out within a combustion chamber. A number of different vegetation types from several distinct ecosystem types associated with the southern and western U.S. were used as fuels, enabling assessment of the implications of changes in fuel types and properties, and ensuing impacts on combustion conditions, for emissions from BB events. Characteristic burn-averaged values were calculated for various parameters and compared with ambient measurements from field campaigns. Variability throughout the duration of fires in response to changing combustion phases was also investigated, focusing upon changes in composition by using contributions of key mass fragments as tracers for the oxygenation of OA constituents. The characterisation of contrasting OA composition in the near and far-field with mass fragment tracers formed a key aspect of Paper 3, based upon aircraft observations of Canadian boreal forest fires. Measurements of BB plumes at a wide range of distances from source enabled the progression of OA composition with aging to be determined and combined with findings from previous studies to provide a representation of the evolution of BBOA. A clear shift in dominant combustion phase throughout the period of fire activity also provided a means of determining the effects of combustion conditions on the distribution of BB emissions throughout the atmosphere, and the subsequent implications for the processing of plumes.

3.3 Overview of experiments

The various field campaigns contributing towards this analysis comprised both airborne and ground-based measurements carried out between 2004 and 2011. While locations were largely determined according to their wider appropriateness with regard to a range of research aims, this diversity represents a valuable asset for the analysis of BB and the inherent variability associated with contrasting conditions in different global regions. An overview of each campaign, presented in chronological order, is given here, along with a description of additional laboratory measurements.

3.3.1 Intercontinental Transport of Ozone and Precursors (ITOP)

ITOP formed part of the International Consortium for Atmospheric Research on Transport and Transformation (ICARTT), a multi-agency research program undertaken in the summer of 2004. ICARTT consisted of a number of separate campaigns focusing on the study of regional air quality and the transport of pollutants around the North Atlantic (*Fehsenfeld et al., 2006*). The primary objectives of the ITOP component were to observe the intercontinental transport and transformation of aerosols, ozone and their associated precursors from North America to western Europe. Measurements were performed from the FAAM BAe-146, with research flights originating from Faial Island in the Azores. A total of 12 flights were carried out, including transits between the UK and the Azores, operating at an altitudinal range of 50-9000 m. During several flights BB plumes from boreal forest fires in Alaska and northern Canada were encountered within the upper troposphere between 4500 and 6500 m (*Lewis et al., 2007*). Together with observations of extensive burning within prescribed source regions (*Real et al., 2007*), the high altitudes of these plumes suggest that fires were of a sufficient size and intensity to generate significantly elevated injection heights. Interception of these plumes at distances of several thousand kilometres from source also indicates that emissions would have been subject to considerable aging and dilution during

transportation. This uniform extensive aging is in contrast to the remaining field campaigns included here, where sampled air masses corresponded to a range of ages, from directly at source to in excess of five days transport downwind. As such, measurements from ITOP provide a representation of properties typical of the latter stages of BBOA evolution, contrasting with the source profiles obtained from measurements of active fires.

3.3.2 Aerosol and Chemical Transport in Deep Convection (ACTIVE)

The ACTIVE campaign took place in northern Australia in two phases during late autumn 2005 and early 2006, with each phase timed to coincide with the end of the local dry season and the onset of the monsoon period, respectively. A number of aircraft operated by different agencies were deployed throughout the extent of the campaign period, providing a range of measurements pertaining to atmospheric chemistry, cloud microphysics and meteorology (*Vaughan et al., 2008*). Aerosol measurements were carried out on the NERC Dornier-228 across 11 science flights from Darwin, sampling a combination of fresh and aged BB emissions throughout the local region. The altitudinal range of the Dornier is less than that of the BAe-146, with a maximum operating altitude of around 5000 m. Active fires were most widespread within the eucalypt forests located upon the Tiwi Islands to the north, which subsequently formed the focus of the majority of research flights, although several fires were also surveyed in areas of grassland directly to the east of Darwin. Throughout the dry season fires were particularly widespread in areas further to the east, including Arnhem Land and the Cape York peninsula in northern Queensland. Aged emissions from these fires and others across the wider region were frequently encountered during ACTIVE following transportation for periods of up to five days (*Allen et al., 2008*). In contrast to ITOP, it was therefore possible to perform a comparison of BB plumes of significantly different ages, and to assess the impact of aging on BBOA concentrations and composition.

3.3.3 Dust and Biomass Experiment (DABEX)

DABEX and the accompanying Dust Outflow and Deposition to the Ocean (DODO) experiment took place in January and February 2006 as part of the wider African Monsoon Multidisciplinary Analysis (AMMA) project (*Redelsperger et al., 2006*). AMMA was an extensive international research program aimed at improving understanding of the west African monsoon and its implications on atmospheric dynamics, the continental water cycle and atmospheric chemistry. Measurements were performed across a number of platforms and time scales, ranging from a number of short term special observing periods (SOP), of which aircraft observations formed an integral component, to long term ground-based measurements taking place over several years. DABEX and DODO comprised the first SOP during the local dry season, although a second phase of DODO flights took place during the wet season. Scientific objectives differed for each of the BAe-146 deployments. While the aims of DABEX were to observe the properties of BB and mineral dust in the region adjacent to the Gulf of Guinea, flying from Niamey in Niger to survey areas of Nigeria and Benin, DODO focused on the transport of dust from the Sahara to the Atlantic ocean, with operations based at Dakar, Senegal. Wildfires are exceptionally prevalent throughout the dry season in sub-Saharan Africa, forming an almost continuous band across the full breadth of the continent, as shown in Figure 8 (*Haywood et al., 2008*). Plumes from such fires, along with widespread agricultural burning, were frequently encountered during DABEX flights. Measurements were carried out within as little as 300 m from some sources (*Johnson et al., 2008*), enabling characterisation of very fresh emissions. In contrast, layers of more aged, transported BB emissions were sampled during DODO, following advection from the DABEX source region. These aged plumes were often extensively mixed with dust from the Sahara, and were typically found at higher altitudes than fresh plumes, as air masses became increasingly lofted with transport to the Atlantic (*Capes et al., 2008*).

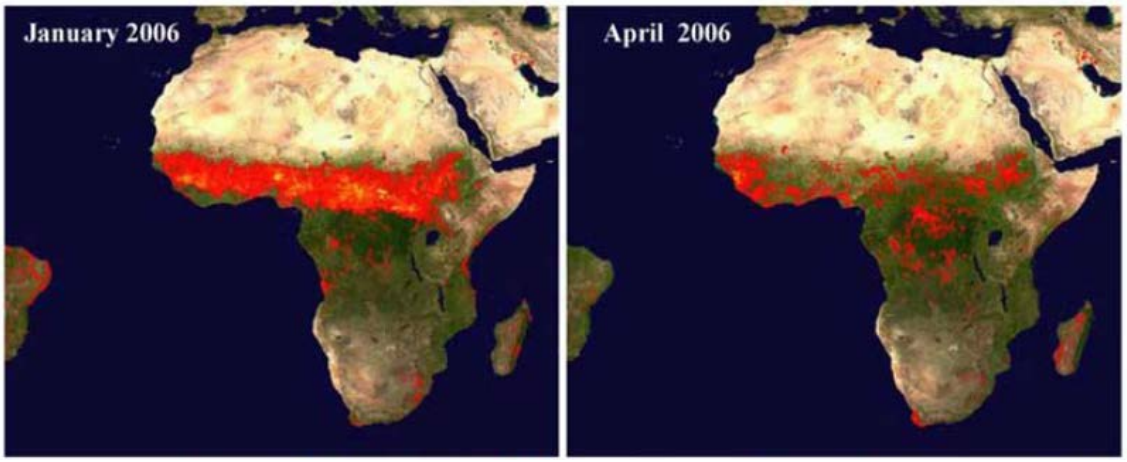

Figure 8: *MODIS fire retrievals showing the seasonality of biomass burning over the African continent during 2006 (Haywood et al., 2008).*

3.3.4 Megacities Iniative: Local and Global Research Observations (MILAGRO)

The extensive research activities performed as part of MILAGRO provided a comprehensive characterisation of gas and particulate emissions from the Mexico City Metropolitan Area (MCMA). Mexico City is one of the world's largest megacities, and the largest population centre in North America, with a population exceeding 20 million. The MCMA is affected by persistent air quality issues associated with atmospheric pollutants, exacerbated by its location within a basin upon the central Mexican plateau, surrounded by mountain ranges on three sides. A wide range of instrumentation across a number of different measurement platforms was deployed throughout the duration of March 2006, in order to study the sources and processing of emissions within the MCMA (*Molina et al, 2010*). Three ground supersites were established to provide continuous measurements of an array of pollutants. The first of these sites was located within the extent of the MCMA, with further sites situated at 30 km intervals away from the urban area, enabling the evolution of plumes transported throughout the wider region to be traced. Geographical coverage was further increased through the deployment of seven research aircraft to survey the MCMA and surrounding regions, along with a series mobile laboratories operating across the urban centre, and continuous observations from a number of satellite platforms.

In addition to ubiquitous urban pollution sources, the MCMA is influenced by BB emissions from wildfires and agricultural activity in the surrounding region (*Molina et al., 2007*). An additional MILAGRO ground site at Altzomoni, located near the Paso de Cortes around 60 km southwest of Mexico City, provided measurements of numerous BB plumes throughout the campaign (*Baumgardner et al., 2009*). Fresh plumes originating from pine forest and grassland fires on the slopes surrounding the Paso de Cortes were detected at Altzomoni, along with more aged plumes transported from wider regions. Fire activity in the mountains surrounding Mexixo City during MILAGRO was above the average level for the time of year, and was expected to represent a significant contribution to levels of fine particulate mass in the MCMA (*Yokelson et al., 2007*). Aged emissions sampled at Altzomoni are expected to have originated from a number of sources, including savanna fires on the Pacific coast and deforestation and burning of crop residues on the Yucatan peninsula (*Baumgardner et al., 2009; Yokelson et al., 2011*).

3.3.5 Quantifying the Impact of Boreal Forest Fires on Tropospheric Oxidants over the Atlantic using Aircraft and Satellites (BORTAS)

The FAAM BAe-146 again provided a platform for airborne measurements of BB emissions during the BORTAS campaign in eastern Canada throughout July and August 2011. Deployment of the aircraft actually constituted the second phase of research activity (BORTAS-B), with the first phase (BORTAS-A) carried out a year previously and restricted solely to ground-based measurements. While the main objective of the experiment was to improve understanding of the chemical aging of emissions from boreal forest fires, focusing primarily on ozone and its impacts on regional air quality following transportation (*Palmer et al., 2013*), sampling of BBOA over a broad range of distances from source facilitated analysis of aging processes within the organic particulate fraction. Boreal forests have a significant influence on atmospheric composition, with fires in North American alone accounting for around 10% of global carbonaceous emissions (*van der Werf et al., 2006*). Research flights

largely targeted locations around the eastern coast of Canada, within range of the base of aircraft operations at Halifax, Nova Scotia. Aged plumes originating from a period of intense fire activity in the forests of northwestern Ontario during the early stages of the campaign (Figure 9) were widely intercepted in these regions, following downwind transportation for up to ten days, covering distances of several thousand kilometres. Fires within the source region were surveyed directly at source during a single flight later in the campaign, by which time fire activity had significantly reduced, bringing about a substantial change in dominant combustion conditions. Measurements at source sampled predominantly smouldering fires, with plumes intercepted at altitudes of around 1000 m. Earlier fires appear to be more characteristic of strongly flaming combustion, as indicated by the injection of plumes into the upper troposphere, and subsequent downwind interception at altitudes of up to 6000 m.

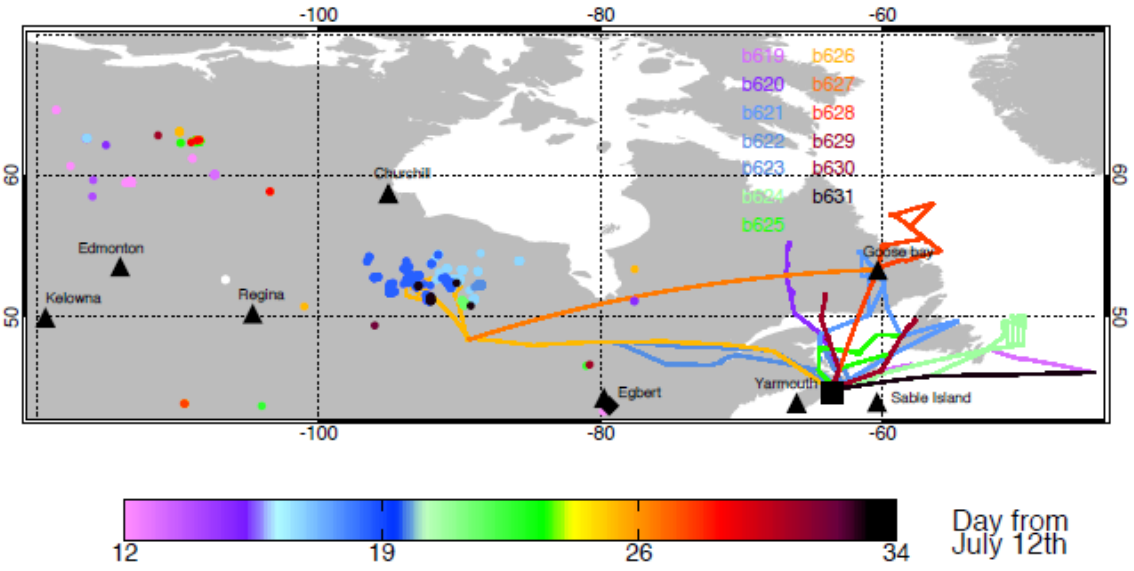

Figure 9: *Flight tracks for BORTAS, with solid upward triangles denoting ozonesonde launch sites, and the solid square denoting the Dalhousie ground station. Coloured circles denote active burning throughout the BORTAS period, with flights using a common colour scale to denote date (Palmer et al., 2013).*

3.3.6 Fire Lab at Missoula Experiment (FLAME II)

The U.S. Forest Service's Fire Sciences Laboratory (FSL) has hosted a number of experiments examining fire behaviour and emissions of trace gases and aerosols from biomass combustion (e.g. *Yokelson et al., 1996; Christian et al., 2003; Chen et al., 2007; Freeborn et al.,*

2008). Laboratory experiments have the advantage of enabling source conditions to be carefully controlled, allowing emissions from specific fuels with defined properties to be investigated in detail. The ability to control fuel and combustion conditions in chamber burns is offset against the fundamental differences with real vegetation fires. Combustion under ambient conditions cannot be replicated within a laboratory setting, and while it is possible to simulate aging of emissions, conditions are not entirely analogous to atmospheric processing. However, chamber experiments also provide a valuable opportunity to investigate the influence of different fuel types and combustion conditions, which represent major sources of uncertainty within observations of BB emissions, and prove difficult to reliably assess under ambient conditions.

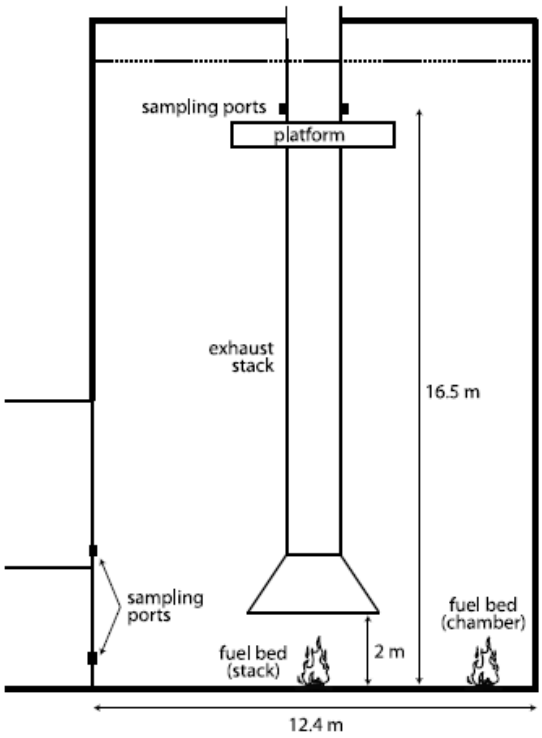

Figure 10: *Schematic of the U.S. Forest Service Fire Sciences Laboratory combustion facility, located in Missoula, Montana (McMeeking et al., 2009).*

FLAME II took place at the FSL in 2007, with the aim of characterising emissions from fires in the US. Fuels used throughout the experiment are associated with environments across the western and southern US which are subject to significant fire activity, and were selected according to their frequency of consumption in BB events (*McMeeking et al., 2009*). A

total of 33 different species representing 6 different fuel types were investigated during the first two FLAME experiments. Fuel components, properties and combinations of different species were varied between burns in order to examine the effect of changing source conditions on resulting emissions. Burns were carried out within the main combustion chamber at the FSL (Figure 10), with the fuel bed positioned below a central exhaust stack through which emissions were drawn. Instruments were located on a platform suspended below the chamber ceiling, sampling through ports in the side of the exhaust stack. External laboratories adjacent to the combustion chamber contained additional instruments, with sample lines running between the exhaust sampling ports and laboratories. While FLAME I did not involve any online measurement of aerosols, the inclusion of an AMS amongst the array of instrumentation used during FLAME II provided real-time measurements of BBOA mass and composition.

3.4 Paper 1: Characterizing the aging of biomass burning organic aerosol using mixing ratios – A meta-analysis of four regions

Status:

Submitted to Environmental Science & Technology, 14th June 2012

Revised 6th November 2012

Accepted and published 19th November 2012

Environmental Science & Technology, *46*(24), 13093-13102, doi:10.1021/es302386v

Overview:

This paper provides an intercomparison of BBOA mixing ratios from four field campaigns undertaken in a range of locations, representing different ecosystems and fuel types. Average △OA/△CO was shown to vary considerably between campaigns, while segregating fresh and aged emissions revealed an overall trend of decreasing △OA/△CO with aging. This absence of net SOA formation coincided with consistent increases in the oxygenation of BBOA, suggesting the loss of OA in aging plumes is more significant than any secondary additions. However, in all cases the magnitude of variability in △OA/△CO amongst fresh emissions exceeded any changes occurring with aging. These findings are also compared to wider observations, revealing discrepancies with previous studies and highlighting the extensive uncertainties associated with the BBOA fraction.

Contributions from co-authors:

G. Capes, J. Allan, J. Crosier, P. Williams, G. Allen, K. Bower and M. Grutter participated in fieldwork and performed initial data processing. L. Russell and D. Baumgardner supplied instrumentation. H. Coe, G. McFiggans and J. L. Jimenez assisted with preparation of the manuscript.

Characterizing the aging of biomass burning organic aerosol using mixing ratios – a meta-analysis of four regions

Matthew D. Jolleys[1], Hugh Coe[1], Gordon McFiggans[1], Gerard Capes[1], James D. Allan[1,2], Jonathan Crosier[1,2], Paul I. Williams[1,2], Grant Allen[1], Keith N. Bower[1], Jose L. Jimenez[3], Lynn M. Russell[4], Michel Grutter[5], Darrel Baumgardner[5]*

* Corresponding author email: matthew.jolleys@postgrad.manchester.ac.uk

[1] Centre for Atmospheric Science, School of Earth, Atmospheric and Environmental Science, University of Manchester, UK

[2] National Centre for Atmospheric Science, University of Manchester, UK

[3] Cooperative Institute of Research in the Environmental Sciences and Department of Chemistry and Biochemistry, University of Colorado, Boulder, Colorado, USA

[4] Scripps Institution of Oceanography, University of California San Diego, La Jolla, California, USA

[5] Centro de Ciencias de la Atmósfera, Universidad Nacional Autónoma de México, Mexico City, Mexico

Environmental Science & Technology

Article

pubs.acs.org/est

Characterizing the Aging of Biomass Burning Organic Aerosol by Use of Mixing Ratios: A Meta-analysis of Four Regions

Matthew D. Jolleys,*[,†] Hugh Coe,[†] Gordon McFiggans,[†] Gerard Capes,[†] James D. Allan,[†,‡] Jonathan Crosier,[†,‡] Paul I. Williams,[†,‡] Grant Allen,[†] Keith N. Bower,[†] Jose L. Jimenez,[§] Lynn M. Russell,[∥] Michel Grutter,[⊥] and Darrel Baumgardner[⊥]

[†]Centre for Atmospheric Science, School of Earth, Atmospheric and Environmental Science, and [‡]National Centre for Atmospheric Science, University of Manchester, Manchester, United Kingdom

[§]Cooperative Institute of Research in the Environmental Sciences and Department of Chemistry and Biochemistry, University of Colorado, Boulder, Colorado, United States

[∥]Scripps Institution of Oceanography, University of California San Diego, La Jolla, California, United States

[⊥]Centro de Ciencias de la Atmósfera, Universidad Nacional Autónoma de México, Mexico City, Mexico

Supporting Information

ABSTRACT: Characteristic organic aerosol (OA) emission ratios (ERs) and normalized excess mixing ratios (NEMRs) for biomass burning (BB) events have been calculated from ambient measurements recorded during four field campaigns. Normalized OA mass concentrations measured using Aerodyne Research Inc. quadrupole aerosol mass spectrometers (Q-AMS) reveal a systematic variation in average values between different geographical regions. For each region, a consistent, characteristic ratio is seemingly established when measurements are collated from plumes of all ages and origins. However, there is evidence of strong regional and local-scale variability between separate measurement periods throughout the tropical, subtropical, and boreal environments studied. ERs close to source typically exceed NEMRs in the far-field, despite apparent compositional change and increasing oxidation with age. The absence of any significant downwind mass enhancement suggests no regional net source of secondary organic aerosol (SOA) from atmospheric aging of BB sources, in contrast with the substantial levels of net SOA formation associated with urban sources. A consistent trend of moderately reduced ΔOA/ΔCO ratios with aging indicates a small net loss of OA, likely as a result of the evaporation of organic material from initial fire emissions. Variability in ERs close to source is shown to substantially exceed the magnitude of any changes between fresh and aged OA, emphasizing the importance of fuel and combustion conditions in determining OA loadings from biomass burning.

1. INTRODUCTION

Biomass burning represents a significant source of organic aerosol (OA) on a global scale, forming an important influence on climate through perturbations to Earth's solar radiation balance. Around 90% of total global primary organic aerosol (POA) is derived from wildfires, prescribed burns, and biofuel combustion, which contribute toward the overall biomass burning (BB) emissions source.[1] The physical and chemical properties of biomass burning organic aerosol (BBOA) and the geographical distribution of fires act to increase the potential for radiative forcing. Sources in tropical regions account for 80% of global BBOA emissions,[2] providing a significant potential radiative forcing given the elevated levels of solar irradiance in the tropics. Eighty to ninety percent of BBOA is in the optically active accumulation mode,[3] a significant fraction of which (45−75%) is highly water-soluble and hence important in promoting cloud droplet formation through increased cloud condensation nuclei (CCN) availability.[4] While efforts have been made to quantify overall source inventories,[5] the fundamental difficulty of prediction of biomass burning emissions exacerbates the uncertainty in these assessments. A critical element of this uncertainty relates to the evolution of aerosol loadings within the atmosphere. In addition to an increase in overall aerosol loadings, secondary formation also acts to increase the single scattering albedo for BB aerosols,[6−8] potentially changing the sign of the resulting climate forcing and presenting a significant uncertainty with regard to the direct radiative effect. While secondary organic aerosol (SOA) formation leading to significant additional OA mass has been widely observed in anthropogenic urban emissions, its net contribution in aging biomass burning plumes remains unclear.[9,10]

Several parameters can be used to characterize biomass burning emissions with respect to source conditions. Emission ratios (ERs) and normalized excess mixing ratios (NEMRs) represent the concentration of an emitted species relative to that of a coemitted reference species,[11,12] with the two definitions applied separately to measurements in the near and far field,

Received: June 14, 2012
Revised: November 6, 2012
Accepted: November 19, 2012
Published: November 19, 2012

respectively. This reference species is typically a nonreactive, conserved gas such as CO or CO_2, expressed as an excess concentration above atmospheric background levels. The ER and NEMR for OA are defined as follows:

$$ER_{OA} = \frac{\Delta OA_{source}}{\Delta CO_{source}} \quad (1)$$

$$NEMR_{OA} = \frac{\Delta OA_{farfield}}{\Delta CO_{farfield}} \quad (2)$$

where ΔOA and ΔCO are the excess OA and CO concentrations, with the latter used in preference to CO_2 due to the greater relative difference with respect to background concentrations. Given that the atmospheric CO lifetime of around 1 month[13] exceeds that of OA (of the order of days to weeks), any reduction in CO concentration over the time scales of several days relevant to the study of BB plumes is primarily limited to the effects of dispersion. The concurrent effect of dispersion on OA concentrations means that any changes in the ΔOA/ΔCO ratio with aging are expected to be dominated by changes to OA in the absence of extensive secondary sources or sinks of CO. The ΔOA/ΔCO ratio can therefore be used as an indicator of OA processing, and specifically SOA formation, which would cause the ratio to increase as OA mass is added in the absence of any coincident enhancement of CO. Throughout this paper, ERs and NEMRs are expressed as dimensionless mass ratios, with both ΔOA and ΔCO concentrations given in units of micrograms per cubic meter at standard temperature and pressure (STP; 273 K, 1 atm). This gives a lower value than ratios expressed in the alternative form of micrograms per cubic meter of OA/parts per million (ppm) of CO. Where necessary, conversion of literature values for comparison was performed in accordance with the ideal gas law at STP.

Emission factors (EFs) provide an alternative means of characterizing biomass burning emissions, relating the amount of a given combustion product to the mass of dry fuel consumed, such that:

$$EF_{OA} = \frac{m_{OA}}{m_{biomass}} = \frac{m_{OA}}{\Delta CO + \Delta CO_2 + \Delta CH_4 + \Delta NMHC + \Delta PM_C} x_c \quad (3)$$

where ΔCO_2, ΔCH_4, ΔNMHC, and ΔPM_C are the masses of C in CO_2, CH_4, all remaining gaseous nonmethane hydrocarbons, and particulate matter, respectively, and x_c is the fuel carbon mass fraction.[14,15] Where the mass of fuel burnt in a fire is not accurately known, fuel consumption can be approximated to the total emitted mass of carbonaceous species. Conversely, in areas where emissions have not been explicitly measured but fire budgets are well-known, a combination of representative EFs and fuel consumption can be used to estimate OA production.

The prevalence of SOA in areas influenced by anthropogenic emissions is well-documented.[9,16] Compiling data from an array of campaigns based in and around urban environments, Zhang et al.[17] showed that SOA constitutes an increasing proportion of total organic particulate mass with increasing distance from source for the urban, urban downwind, and remote sites studied. De Gouw and Jimenez[9] also demonstrate the use of NEMRs to reflect OA aging in urban plumes, highlighting the elevation in ΔOA/ΔCO for measurements of combined POA and SOA above those of POA alone. Initial primary ERs are invariably shown to increase by up to an order of magnitude following addition of SOA. However, no such trend is observed consistently for aging biomass burning emissions. Previous assessments of ambient BBOA have identified both increasing[6,18,19] and decreasing[20] ΔOA/ΔCO with aging, while other studies suggest little or no net change in ΔOA/ΔCO during aging regardless of physical and chemical changes to OA.[21,22] Cubison et al.[22] recently summarized published field measurements of the evolution of ΔOA/ΔCO from BB with aging and reported the potential for a net source of SOA equivalent to 5% of the total global source, albeit with significant statistical uncertainty, encompassing scenarios of no net SOA formation.

This uncertainty in the extent of SOA formation from biomass burning undermines attempts to parametrize the overall effect of aging on aerosol loadings, therefore limiting model prediction of the effects of OA from biomass burning on the climate system. This paper aims to assess the extent of SOA formation in biomass burning plumes by bringing together ERs and NEMRs derived from several different field observations in a range of different biomass burning environments and placing these findings in the context of wider assessments of BBOA emissions and evolution, providing a broader characterization of biomass burning as an aerosol source.

2. DATA SELECTION

A screening procedure was applied to all data in order to isolate those time periods subject to a biomass burning influence, as identifying individual plumes manually would have led to an element of subjectivity in the analysis. Minimum thresholds of ΔCO, number concentration, and f_{60} [ratio of the mass fragment at m/z (mass-to-charge ratio) 60 to the total OA signal] were used to define biomass burning influence, as outlined by Capes et al.[21] The m/z 60 fragment is used as a marker for biomass burning because it is associated with anhydrous sugars such as levoglucosan and related species[23−25] produced by the pyrolysis of plant material, particularly cellulose.[26] An f_{60} threshold of 0.3% was applied, in accordance with background f_{60} levels widely identified in ambient ΔOA measurements,[22] together with minimum ΔCO and number concentrations of 20 ppb and 1000 cm^{-3}, respectively. Minimum observed concentrations for relevant species throughout each individual measurement period were taken as the background values used to determine excess concentrations, with a single background used for the duration of each period. Average ΔOA/ΔCO values were then determined from the fit coefficients for ΔOA versus ΔCO plots for data conforming to these screening criteria from each day or flight (Figure S1, Supporting Information), by use of linear regressions given the larger uncertainties in ΔOA compared to ΔCO. Data were also collated to provide a campaign-wide, regional characteristic ΔOA/ΔCO, while the range of daily/flight average values gave an indication of the extent of variability in ΔOA/ΔCO.

In order to investigate changes in ΔOA/ΔCO with age, data were segregated into fresh and aged fractions. Fresh BB plumes were isolated by identifying peaks in ΔOA concentrations in all time series, where ΔOA concentrations throughout a peak were at least 50% higher than the mean value calculated across the full extent of the given flight or day. Peak selections were then checked for agreement with corresponding reductions of 50% below the mean value in $\Delta O_3/\Delta CO$ time series; this ratio was used as an indicator of aerosol aging, given that the production of O_3 is strongly associated with the photochemical activity that may be expected to be involved in the processing of OA in the

Table 1. ΔOA/ΔCO Coefficients[a]

	ΔOA/ΔCO				
	campaign avg	lowest flight/daily avg	highest flight/daily avg	range	max/min ratio
		ACTIVE			
all data	0.293 ± 0.006	0.203 ± 0.016 (AD09)	0.489 ± 0.013 (SD06)	0.286	2.41
fresh OA	0.329 ± 0.023	0.238 ± 0.013 (SD07)	0.520 ± 0.030 (SD06)	0.282	2.18
aged OA	0.251 ± 0.005	0.203 ± 0.016 (AD09)	0.290 ± 0.008 (AD03)	0.087	1.43
		MILAGRO			
all data	0.049 ± 0.001	0.022 ± 0.003 (01/03/06)	0.090 ± 0.006 (17/03/06)	0.068	4.08
fresh OA	0.051 ± 0.001	0.035 ± 0.010 (10/03/06)	0.070 ± 0.014 (08/03/06)	0.035	1.98
aged OA	0.041 ± 0.001	0.022 ± 0.003 (01/03/06)	0.090 ± 0.003 (17/03/06)	0.068	4.08
		DABEX			
all data	0.056 ± 0.001	0.022 ± 0.002 (B168)	0.071 ± 0.003 (B166)	0.049	3.18
fresh OA	0.065 ± 0.002	0.052 ± 0.003 (B157)	0.080 ± 0.008 (B162)	0.028	1.54
aged OA	0.043 ± 0.001	0.022 ± 0.002 (B168)	0.054 ± 0.001 (B158)	0.031	2.41
		ITOP			
all data	0.019 ± 0.002	0.015 ± 0.002 (B032)	0.054 ± 0.005 (B038)	0.039	2.91

[a]Derived from linear regressions for full campaign data sets, along with segregated fresh and aged OA fractions, with standard deviations of 1σ. Entries in parentheses denote flight numbers and dates corresponding to stated maximum and minimum values.

atmosphere.[27,28] These classifications were further corroborated against concurrent increases in ΔCO and number concentrations, with data fulfilling all criteria designated as fresh OA. While the use of additional aging tracers would have further refined the classification of aerosol ages, wider gas-phase measurements were not consistently performed across all campaigns, preventing intercomparison of this approach between regions and therefore compromising the main aim of this analysis.

3. RESULTS AND DISCUSSION

A series of four ambient biomass burning data sets were included within this meta-analysis, with the aim of characterizing OA emissions and transformations across a number of different regions representing boreal and tropical forests and subtropical grasslands. These data sets are derived from deployments carried out between 2004 and 2006, involving aircraft and ground-based measurements. During the ACTIVE (Aerosol and Chemical Transport in Tropical Convection) campaign, measurements were performed onboard the NERC Dornier-228 aircraft in northern Australia. Other airborne data sets included within this analysis were obtained from two campaigns involving the FAAM (Facility for Airborne Atmospheric Measurements) BAe-146. DABEX (Dust and Biomass Experiment) took place in western Africa, targeting wildfires throughout the region, while ITOP (Intercontinental Transport of Ozone and Precursors) involved the study of highly aged boreal forest fire plumes around the Azores. As part of the wider MILAGRO (Megacities Initiative: Local and Global Research Observations) project, emissions from biomass fires were measured at a ground site at Altzomoni, to the southeast of Mexico City. In each case, total OA mass concentrations were obtained by use of an Aerodyne quadrupole aerosol mass spectrometer (Q-AMS). CO mixing ratios were measured by an Aerolaser AL5002 UV fluorescence CO analyzer on all aircraft campaigns, with both CO and CO_2 measured by a long-path Fourier transform infrared spectrometer at the MILAGRO ground site. Further descriptions of campaigns and instrumentation are provided in the Supporting Information.

A high degree of variability exists in both ERs and NEMRs from biomass burning events. Analysis of ambient aerosol populations influenced by biomass fires from a number of environments demonstrates these differences over a range of temporal and spatial scales, showing significant contrasts in ΔOA/ΔCO both between different regions and between separate fires within a region. Instantaneous ΔOA/ΔCO values cover a range exceeding 2 orders of magnitude, with an overall mean and standard deviation across all campaigns of 0.079 ± 0.078. Representative campaign-averaged ΔOA/ΔCO ratios were calculated by use of regressions incorporating all data points meeting the outlined selection procedure. While the characteristic ratios derived for MILAGRO (0.049 ± 0.001, where the statistical uncertainty associated with fit coefficients is ±1σ) and DABEX (0.056 ± 0.001) are similar, the ratio from ACTIVE (0.293 ± 0.006) is higher by around a factor of 5, illustrating the contrasting nature of emissions originating from different fire locations and mixing of fresh and aged BB airmasses (Table 1). Flight-averaged ΔOA/ΔCO ratios throughout ACTIVE consistently exceeded average ratios from MILAGRO and DABEX by at least a factor of 3 and in some instances by up to an order of magnitude. The lowest flight-averaged ratio derived from the eight ACTIVE flights targeting biomass burning emissions remained more than double the highest examples from any other campaign.

Observed ranges between minimum and maximum flight-averaged, or daily-averaged, values are used to give an indication of the levels of variability in ΔOA/ΔCO between separate sampling periods within each region. A range of 0.286 was identified throughout ACTIVE, exceeding those from MILAGRO (0.068) and DABEX (0.049) by a considerable margin. However, reporting each range as a percentage of its corresponding overall campaign average also accounts for the large contrasts between campaigns and the greater potential for variability where ΔOA/ΔCO ratios are significantly elevated. These proportional values show that the ranges in average values are comparable for DABEX and ACTIVE, at 88% and 98%, respectively, while a higher value of 139% was derived for MILAGRO. The wider variability identified throughout MILAGRO may in part be the result of the longer campaign duration, comprising 23 days of measurements. During this time the site at Paso de Cortes was influenced by air masses of differing origins and is therefore likely to have been subject to emissions from a range of different fire types.

Although there are widespread differences in the average ΔOA/ΔCO identified for different periods throughout each campaign, strong linear relationships are maintained across

aerosol of all ages. The variability within campaigns reflects the potential effects of source conditions and processing in perturbing ΔOA/ΔCO ratios for BB events. However, when all data sets are considered in their entirety, it appears that these effects average out and any differences are compensated, giving a consistent, characteristic ratio for each region. This consistency indicates that while these various factors are capable of propagating localized changes in ΔOA/ΔCO, any such changes are not widespread or uniform enough to create a significant alteration of the overriding ratio established for a given region. The differences in these characteristic ΔOA/ΔCO levels between regions suggest either that a dominant condition or process underpins BB emissions or that potential sources of variability are effectively balanced overall in all locations examined here. The majority of the potential drivers are not characterized extensively enough throughout these campaigns to provide any definitive parametrizations, but they give an indication as to where key uncertainties remain.

3.1. Drivers of Variability. The differences in average ΔOA/ΔCO between separate sampling periods within each campaign are expected to be the manifestation of highly variable properties of individual fire events. However, this analysis shows no evidence for any conclusive relationships with potential drivers, such as geographical influences on fuel types. The maximum (0.520) and minimum (0.238) flight-averaged fresh ΔOA/ΔCO ratios for ACTIVE were actually derived from flights occurring on consecutive days (SD06 and SD07; 23 and 24 November 2005), sampling a fire in a similar location at approximately 12.375° S, 131.592° E. As such, the dominant vegetation and overall range of fuel types contributing to the sampled fire plume are unlikely to have changed significantly given the constrained area, with MODIS Rapid Response hotspot images of the area suggesting that this may indeed have been the same fire or group of fires. It is not possible to provide any further assessment of these effects given the lack of direct observations of source conditions resulting from aircraft measurements, but it would appear that different species typical to a common ecosystem and within a localized environment are potentially capable of producing highly contrasting ERs. Conversely, wider fuel properties such as moisture content, and the implications of these factors for burn conditions, could equally contribute toward the extensive range observed during ACTIVE.

Throughout MILAGRO, there appears to be no correlation between ERs for fresh OA and any specific back trajectory origins (Figure S2, Supporting Information). Although urban emissions are likely to influence the site at Altzomoni given the close proximity to Mexico City,[29] the extent of any effect on overall ΔOA/ΔCO is limited given the much greater magnitude of BB emissions. Several large-scale events in close proximity to the measurement site were observed, most notably between 5 and 6 March, where respective peak ΔOA and ΔCO concentrations exceeded 250 $\mu g \cdot m^{-3}$ and 4000 ppb. In contrast, peak concentrations from urban sources are reported as approximately 60 $\mu g \cdot m^{-3}$ and 550 ppb, respectively, suggesting BB emissions dominate the derived ΔOA/ΔCO ratios. The availability of CO_2 measurements throughout MILAGRO also enabled calculation of modified combustion efficiencies (MCEs), which represent the ratio of excess CO_2 mixing ratios to excess CO_2 and CO combined and give an indication of the dominant combustion phase in associated fires, with MCEs either above or below the threshold of 0.9 indicating a dominance of flaming or smoldering combustion phases, respectively.[7] Changes in combustion conditions are widely purported as one of the main drivers affecting variability in biomass burning emissions.[30,31] However, MCEs calculated for fresh plumes during MILAGRO show no strong correlations with ΔOA/ΔCO beyond the overriding dominance of high MCEs, consistent with the comparatively lower ERs identified throughout the campaign, which are likely to be influenced by reduced total particulate and OA mass fractions from flaming combustion.[3,14]

Although this analysis cannot provide any further clarification of the causes of observed ΔOA/ΔCO variability, the strong regional differences are likely to affect assessments of the global atmospheric aerosol burden. The dominance of OA in PM_1 budgets for these regions implies that the PM_1/ΔCO ratio changes from region to region in response to changing BB emissions. However, if these regional differences prove to be more widespread, then this variability may have significant implications for future BB emission estimates based on remote sensing methods.

3.2. Changes with Age. ΔOA/ΔCO ratios appear to be influenced by the residence time of OA within the atmosphere, in response to levels of physical and chemical processing. ITOP provides the lower extent of the observed range of average ΔOA/ΔCO across the different campaigns included in this analysis, representing the most heavily aged emissions, with measurements taken at the greatest distance from source. The average ratio of 0.019 is equivalent to just 6% of the levels observed during ACTIVE, where both fresh local fire plumes and aged transported air masses were encountered. This lower ratio is likely to be influenced by the long-range transport of air masses sampled during ITOP and the potential for OA removal through precipitation as air is lifted to higher altitudes during convection, along with potential further wet deposition during transportation. Cubison et al.[22] and Hecobian et al.[32] show significantly elevated ΔOA/ΔCO (~0.140) for Canadian boreal forest fires during the Arctic Research of the Composition of the Troposphere from Aircraft and Satellites (ARCTAS) campaign, which involved sampling very close to source. Peltier et al.[33] also identified a lower ΔOA/ΔCO than the values reported by Cubison et al.[22] and Hecobian et al.,[32] reporting ratios from the NEAQS campaign of ~0.050 for the same aged boreal forest fire plumes from Alaska and the Yukon as encountered during ITOP. Despite these consistently lower ΔOA/ΔCO ratios for aged plumes, Petzold et al.[34] suggest there is little evidence for the removal of black carbon (BC) throughout the full duration of transportation, based on the comparison of BC/ΔCO ratios for plumes measured by the DLR Falcon over central Europe with source ERs, although these source profiles are based on the range of EFs reported by Andreae and Merlet[12] rather than specific measurements of Canadian or Alaskan boreal plumes at source. Real et al.[35] also refute the possibility of wet deposition during transportation due to the absence of clouds along the plume path based on European Centre for Medium-range Weather Forecast cloud fields, suggesting that the effect of wet deposition during transportation remains highly uncertain.

Distinguishing between fresh and aged OA in ACTIVE, DABEX, and MILAGRO gives an indication of how processing influences the atmospheric loadings of OA, showing consistently lower ΔOA/ΔCO for the aged fraction in all cases (Figure 1). The greatest relative disparity between fresh and aged fractions was observed during DABEX, where there was a difference of 0.022 between the averages for fresh OA (0.065 ± 0.002) and aged OA (0.043 ± 0.001), equivalent to a change of 34% from the ER near to source. In comparison, smaller differences of 24% and 20%, respectively, were observed during ACTIVE (0.329 ± 0.023 to 0.251 ± 0.005) and MILAGRO (0.051 ± 0.001 to 0.041 ± 0.001).

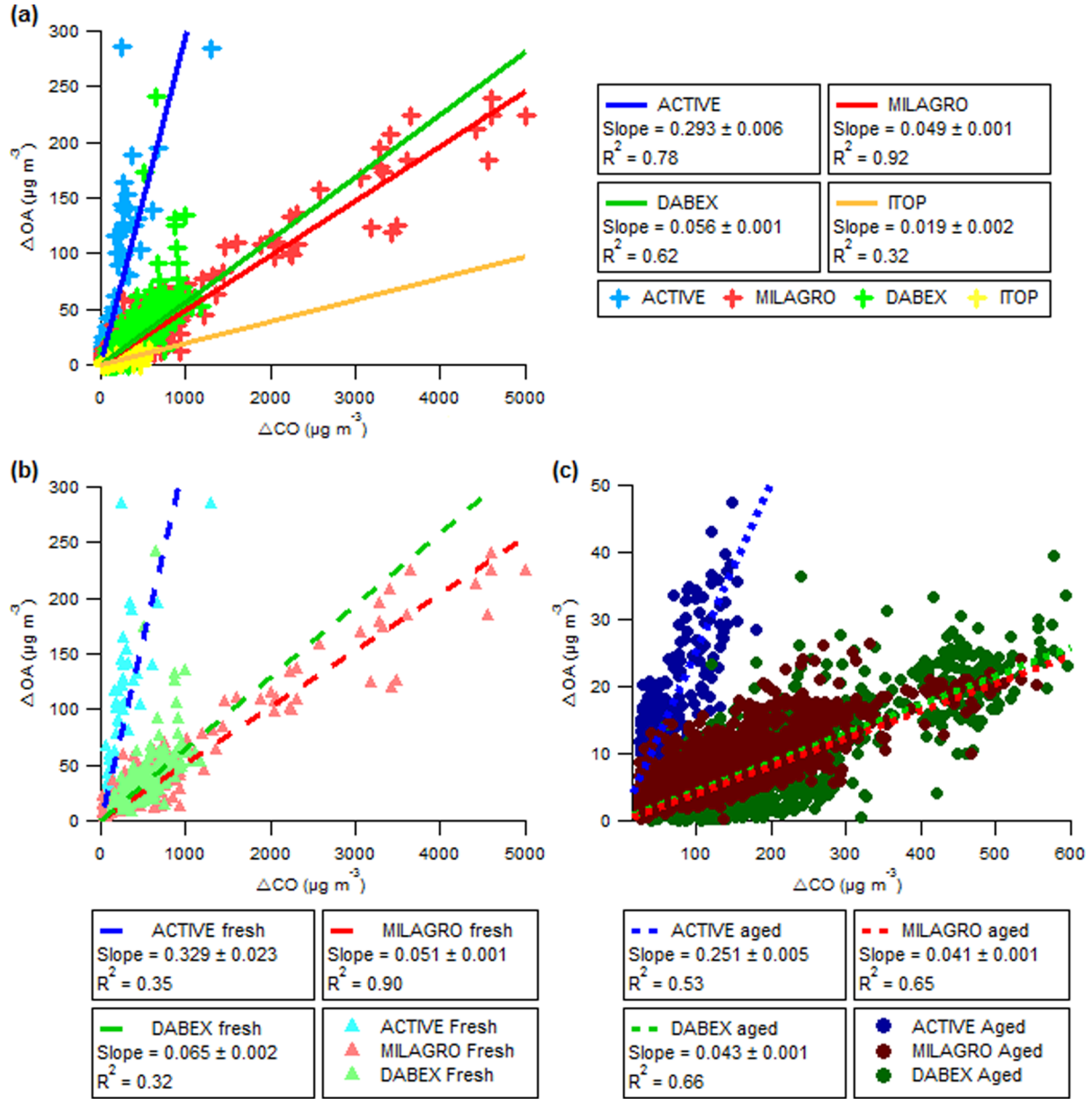

Figure 1. (a) Excess organic aerosol mass concentration versus excess CO for all campaigns. Coefficients are for linear regressions with uncertainties of $\pm 1\sigma$. Average $\Delta OA/\Delta CO$, derived from line slopes, is substantially elevated for ACTIVE above average values from all other campaigns. Fit lines for DABEX and ITOP have been extrapolated using line equations for greater clarity. (b) ΔOA versus ΔCO for segregated fresh and (c) aged OA fractions from ACTIVE, MILAGRO and DABEX. Average $\Delta OA/\Delta CO$ is shown to be consistently higher for fresh OA in comparison to aged OA.

The reduction in $\Delta OA/\Delta CO$ with age throughout DABEX is further substantiated by the concurrent increase in $\Delta O_3/\Delta CO$, where $\Delta O_3/\Delta CO$ is used as a continuous indicator for aging to provide further verification beyond the basic discrete classification of OA as either fresh or aged.

The greater contrast in average $\Delta OA/\Delta CO$ between fresh and aged fractions during DABEX may demonstrate the implications of a changing balance between OA enhancement through secondary formation and OA loss through deposition or physical and chemical transformations during aging, relative to the comparable effects throughout other campaigns. While concentrations of OA and inert marker species such as CO are primarily reduced by dilution as smoke plumes disperse into the ambient atmosphere, OA is also removed through wet deposition and by the evaporation of semivolatile compounds, reducing aerosol concentrations to a greater degree than would be expected from dispersion alone.[36,37] Conversely, the extent to which secondary formation compensates the loss of primary OA may vary, affecting the moderation of $\Delta OA/\Delta CO$ differently between regions. The large contributions of coarse mode aerosol during some DABEX flights provide a potential mechanism for the loss of organic carbon (OC) through preferential secondary condensation to dust particles, reducing the submicrometer OC mass measured by the Q-AMS. Hand et al.[38] provide circumstantial evidence to indicate there may have been condensation of OC onto dust particles, such as the reduced presence of tar balls in mixed dust/biomass burning samples, while Johnson et al.[39] also show an increase in absorption by biomass burning particles downwind from source, indicative of a reduction in highly scattering OC. However, environmental scanning electron microscope analysis showed no discernible differences in particle structure between dust-dominated samples and mixed

Table 2. Mean Values for Composition and Aging Indicators Associated with Segregated Fresh and Aged OA Fractions Throughout Each Campaign[a]

	f_{43}		f_{44}		f_{57}	
	fresh	aged	fresh	aged	fresh	aged
ACTIVE	0.051 ± 0.018	0.057 ± 0.035	0.078 ± 0.043	0.152 ± 0.050	0.011 ± 0.004	0.015 ± 0.012
MILAGRO	0.065 ± 0.006	0.061 ± 0.010	0.099 ± 0.030	0.169 ± 0.028	0.021 ± 0.005	0.013 ± 0.004
DABEX	0.079 ± 0.035	0.104 ± 0.096	0.079 ± 0.030	0.147 ± 0.127	0.023 ± 0.014	0.030 ± 0.054
ITOP		0.109 ± 0.097		0.176 ± 0.137		0.037 ± 0.052
	f_{60}		f_{44}/f_{57}		$\Delta O_3/\Delta CO$	
	fresh	aged	fresh	aged	fresh	aged
ACTIVE	0.006 ± 0.003	0.005 ± 0.003	8.9 ± 7.9	27.4 ± 43.1	0.277 ± 0.147	0.486 ± 0.165
MILAGRO	0.018 ± 0.006	0.006 ± 0.003	5.6 ±3. 7	15.2 ± 7.4	0.382 ± 0.218	0.698 ± 0.201
DABEX	0.011 ± 0.009	0.040 ± 0.072	4.1 ± 2.1	22.3 ± 126.9	0.213 ± 0.052	0.370 ± 0.101
ITOP		0.029 ± 0.049		13.1 ± 16.8		0.837 ± 0.337

[a]With standard deviations of 1σ.

dust/biomass burning particles. As such, the partitioning of processed OC to dust as a potential cause of reduced ΔOA/ΔCO remains highly uncertain. This process is also unlikely to be of significance as a possible fate for SOA throughout either ACTIVE or MILAGRO, where no significant coarse mode was identified.[29,40] Heterogeneous oxidation of OA may also lead to some loss of OA for very long aging times,[41] which may contribute to the lower ΔOA/ΔCO observed for ITOP.

There is little evidence from these data sets to support significant net SOA formation, to the point of a positive impact on ΔOA/ΔCO exceeding other losses. Capes et al.[21] showed that OA became increasingly oxidized with age during DABEX, with an increase in oxygen/carbon ratio (O/C) providing an overall offset for any loss of carbon mass. A stable ΔOA/ΔCO level was therefore maintained, when aerosol of all ages was considered, with a similar result also reported by Cubison et al.[22] for boreal forest fire smoke. However, the shift in the balance of these processes becomes more apparent when older and fresher aerosol are segregated. A number of key OA mass fragments measured by the Q-AMS can be used to infer changes in composition as a result of transformations relating to aging. The m/z 44 fragment is associated with the CO_2^+ ion derived from organic acid species, which form a significant contribution (5−15%) to the overall oxygenated OA mass,[42,43] and is therefore expected to be less prevalent in fresh OA emissions. The ratio of m/z 44 to the total OA concentration (f_{44}) is used as a simplified proxy for the O/C ratio in OA and hence an indicator of aerosol age.[44,45] Although elevated f_{44} levels have been observed in fresh emissions from domestic wood burners,[46] such a trend is not widely apparent for ambient measurements. This is likely to be an effect of the contrasting conditions and behavior of wildfires and controlled burners, with Weimer et al.[46] identifying an increase in f_{44} to dominate the organic mass spectrum for more efficient automatic furnaces where combustion is more complete. Consistency has also been observed between the O/C for laboratory and ambient measurements of open biomass fires, while organic mass (OM)/OC ratios for both are shown to be lower than values for fireplace combustion.[43] Higher mean f_{44} values were observed for the aged OA fraction across all campaigns (Table 2), providing evidence for consistent secondary processing of OA in aging biomass plumes. Mean f_{44}/f_{57} values (where m/z 57 is indicative of fresh primary OA emissions) were also consistently elevated for aged OA compared to fresh OA. However, there are substantial uncertainties associated with the values derived for both age fractions, which must be considered as a major caveat to the identified contrasts in composition. These uncertainties are exacerbated by the reduced signal-to-noise ratio attained by the Q-AMS under aircraft operation, particularly at greater altitudes.[47]

Measurements of both fresh and aged plumes during MILAGRO show a progression toward higher f_{44} and lower f_{60} values with increasing aging (Figure S3, Supporting Information). This trend, characterized by Cubison et al.[21] using measurements from MILAGRO and ARCTAS, alludes to a greater contribution of oxygenated OA and concurrent reduction in primary BB-derived species as plumes age. However, such trends are not observed within measurements from any of the other campaigns included here, most likely as a result of the high levels of noise associated with certain Q-AMS measurements. These issues are particularly evident throughout DABEX and ITOP, where sampling occurred at altitudes of up to 7000 and 10 000 m, respectively, and are also reflected in the large standard deviations quoted in Table 2. The stronger relationships between age and composition apparent throughout MILAGRO are likely to result from an improved signal-to-noise ratio given the longer averaging period applied during data processing.

Hawkins and Russell[10] observed a similar increase in the fraction of oxygenated OA species for progressively more aged emissions from wildfires in California. This increasing level of oxidation, again in the absence of an increase in total OA mass, was attributed to particle phase transformations of OA functional groups as opposed to additional SOA formation. The potential influence of this process on the trends in composition identified throughout this analysis represents a further source of uncertainty regarding the role of SOA formation in BB emissions. As a result, the use of these markers is not able to fully reconcile distributions of ΔOA/ΔCO with the aging processes but gives an indication of the relative influences of OA addition and removal in aging biomass burning plumes, with losses through evaporation, heterogeneous chemistry, and/or deposition persistently matching or exceeding SOA formation.

While there is a consistent reduction in average ΔOA/ΔCO between the fresh and aged OA fractions in all regions, the scales of these changes are always smaller than the associated variability in average fresh ΔOA/ΔCO within each campaign. Throughout ACTIVE, the difference between minimum and maximum flight-averaged values for fresh OA of around 0.28 is

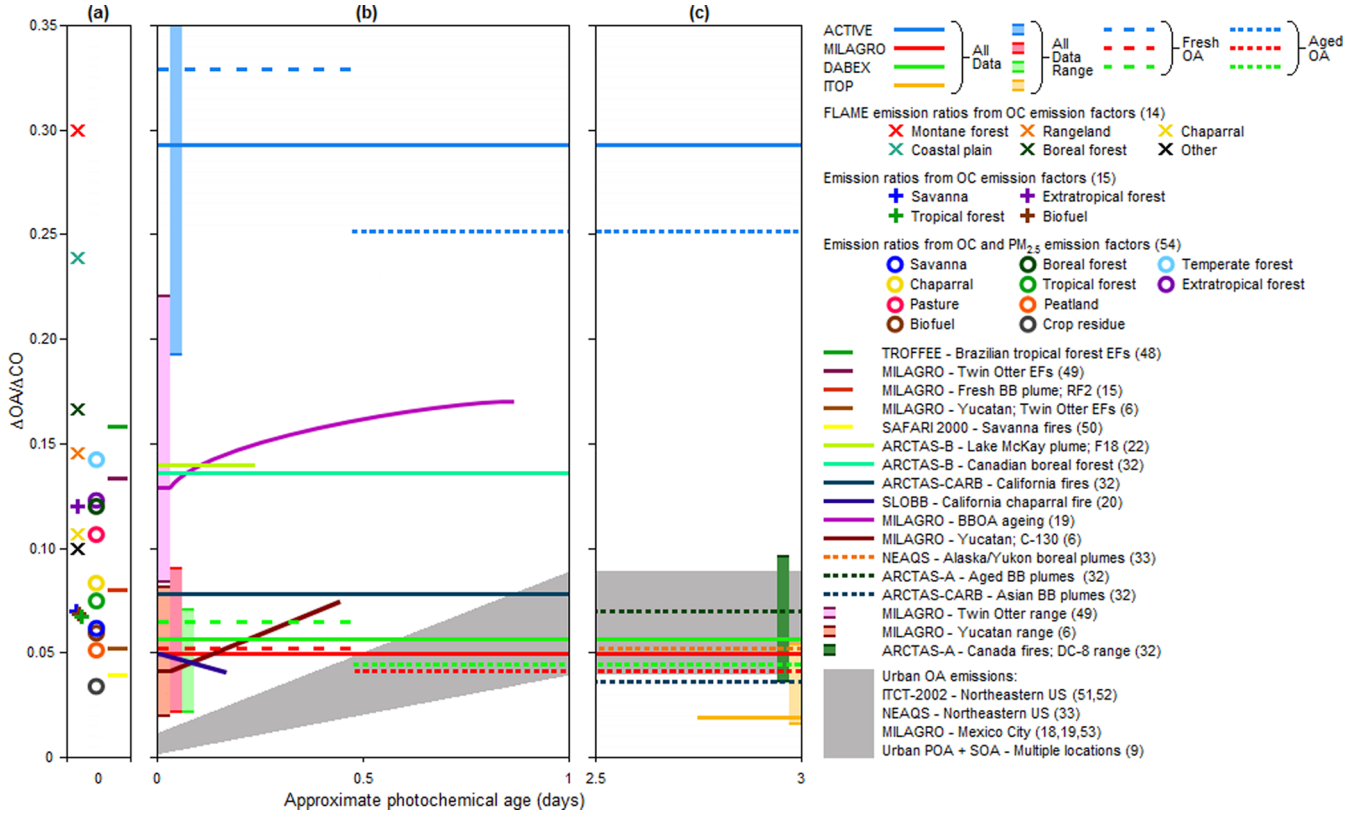

Figure 2. Schematic diagram showing changes in ΔOA/ΔCO with photochemical age in emissions from biomass burning and urban sources. (a) Source emission ratios derived from emission factors calculated during chamber studies[15] or from an ensemble of literature sources.[12,54] (b) Evolution of ΔOA/ΔCO during ~1 day of aging throughout different studies. Tall, narrow bands next to vertical axes show ranges in average ΔOA/ΔCO ratios across separate measurement periods within certain campaigns. (c) Eventual ΔOA/ΔCO after several days aging. *x*-axis values are approximate, given widespread lack of accurate aging constraints. Figure adapted from DeCarlo et al.[19]

nearly 4 times larger than the difference of 0.078 between age fractions, with a similar contrast observed for MILAGRO (0.035 to 0.01). The values from DABEX for flight-to-flight variability (0.028) and change with age (0.022) are more closely comparable, although the variability remains larger. These results emphasize that the effects of BBOA processing appear to be much less significant than initial conditions as a source of uncertainty in emissions. Given the lack of continuous plume sampling throughout these four studies, it is not possible to completely rule out that emissions may have been subject to rapid addition of SOA, as documented by Yokelson et al.[6] Unfortunately, it has not been possible to provide a more rigorous assessment of aerosol composition, or more accurate segregation of POA and SOA, throughout these campaigns. The use of techniques such as positive matrix factorization was not possible for the given data sets due to the insufficient signal-to-noise ratio attainable by the Q-AMS during aircraft deployment. However, with regard to the resolution of regional and global models, the apparent lack of increase in ΔOA/ΔCO for emissions sampled away from source would suggest that any chemical processing is occurring at a subgrid scale. As such, the distinction between POA and combined POA and rapidly formed SOA becomes less significant, as any transformations are occurring on much shorter time scales. Any wider-scale aerosol impacts, such as radiative forcing effects, can be considered to be dominated by what are effectively "primary" emissions with respect to global model resolution. It is therefore increasingly important that consideration of the variability at source is appropriately integrated into model simulations in order to deliver an accurate and appropriate representation of the BBOA fraction.

3.3. Comparisons with BBOA from Other Studies.

Analysis of these four ambient data sets has revealed a number of significant differences in the properties and evolution of BBOA emissions across a range of different environments and atmospheric regimes. Comparison of these results with examples from literature highlights the extent of the variability in average biomass burning ΔOA/ΔCO at source, with a range of more than an order of magnitude across all studies represented here (Figure 2). The large variability in ΔOA/ΔCO between and within the different experiments presented in this study is consistent with the overall variability of ΔOA/ΔCO presented within the literature, as ratios for all four campaigns fall well within the observed spread for biomass burning assessments, including both laboratory and ambient measurements across a range of ages. ACTIVE represents an outlier to the typical range of ΔOA/ΔCO for both fresh and aged fractions, although similarities can be drawn with ERs derived from EFs for controlled burns during the Fire Lab at Missoula Experiment (FLAME; ref 15). The range of EFs reported by McMeeking et al.[15] represents the combustion of plant species that form a significant contribution to the annual wildfire budget in the western and southeastern United States. The highest ER from FLAME was identified for montane forest samples, comprising pine and fir species. Such species are not comparable to the eucalypt forests that dominate the regions studied during ACTIVE (see Supporting Information). However, the coastal plain classification used during FLAME,

comprising myrtle, shrub, and grass species, also produced a similar level of ΔOA/ΔCO as observed during ACTIVE, with potential similarities to vegetation types in areas to the east of Darwin where fires were also sampled. The factor of 3 difference between minimum and maximum ERs is indicative of the high potential variability across different ecosystems and their associated biomass fuels. In contrast, a fairly good level of consistency exists between assessments of boreal forest ERs. Agreement within 40% is observed for all ΔOA/ΔCO ratios close to source in boreal regions, for values taken from both chamber experiments and field campaigns.[22,32,54] Greater divergence is evident among aged ΔOA/ΔCO from boreal fires, although the ratios for heavily aged OA during ITOP increase this spread.

While a net reduction in ΔOA/ΔCO for aged fractions was identified across all projects within this study for which near- and far-field measurements were available, some previous biomass burning studies have shown ΔOA/ΔCO to increase with age close to source in some instances.[6,19] Further evidence exists for the formation of SOA within aging biomass burning plumes across a number of studies, both within the first hour after emission[31] and over a period of several days.[7] Findings from chamber experiments also support substantial SOA formation due to photo-oxidation of wood smoke, with both Grieshop et al.[55] and Hennigan et al.[56] reporting an enhancement in OA mass by up to a factor of 3 over a period of several hours. However, wood burning in closed stoves may be significantly different from open burning, and the dilution conditions in chamber experiments are different from those in the field. These contrasting cases of OA evolution are likely to arise from a shift in the complex balance of various conditions and processes that control OA loss and secondary formation in biomass burning plumes, the full extent of which cannot be elucidated from currently available data sets.

A notable contrast can be identified between biomass burning and urban emission regimes (Figure 2). Numerous studies of anthropogenic urban aerosol emissions consistently show ΔOA/ΔCO to increase with age as a result of SOA formation.[19] These trends with aging have been constrained explicitly where photochemical tracers have been used to determine the age of emissions,[51−53] with further evidence provided by the recurrent increase in ΔOA/ΔCO between POA emissions and combined POA and SOA in urban areas.[9] The absence of similar behavior in biomass burning emissions across a diverse range of locations may be related to the much larger POA emissions of BBOA, at about an order of magnitude larger than urban POA/ΔCO,[9] so that any SOA formation in BB plumes cannot overwhelm the very large POA emissions. As a result, BB emissions may be more susceptible to the greater variability of source conditions. Such differences are evidenced by the observed changes in the nature of ΔOA/ΔCO evolution for BB between regions, in contrast to the greater uniformity identified among urban OA emissions.

The time scales involved in SOA formation, and the stage at which plumes are intercepted, may also affect the ability to observe any increase in ΔOA/ΔCO. During chamber experiments, Grieshop et al.[55] observed a dependence on the VOC/NO_x ratio for OA enhancement in aging wood smoke. The fast rate of OA production identified in that study is consistent with some field observations, which show significant increases in OA mass over periods of less than half a day.[6,19,31] For cases where measurements of aged air masses are performed after a longer period of time, it is possible that any initial increase in ΔOA/ΔCO from SOA formation will have been masked by the aggregate effects of progressive OA loss. In contrast, other studies, including some measuring fresh OA very close to source, show a lack of OA increase over time scales of less than 1 day (refs 20 and 22 and references therein). Given a daytime average atmospheric OH concentration of ∼5 × 10^6 molecules·cm^3, typical in-plume values of (1−1.7) × 10^7 molecules·cm^3 [6,13] represent only around 2−3 times typical concentrations. Therefore, these changes are not likely to cause aging to occur on such a rapid time scale that it cannot be observed through aircraft measurements. With the exception of ITOP, where only highly aged plumes were encountered, each campaign included measurements of active fires very close to source and within a time scale of less than 1 hour since emission (see Supporting Information). Conversely to the possibility of unobserved, very rapid SOA formation, the absence of any sustained increase in ΔOA/ΔCO with aging throughout these regions may be a result of greater losses of POA through evaporation of more volatile aerosol, to such an extent that the addition of SOA simply maintains ΔOA/ΔCO at a stable level rather than presenting any identifiable enhancement. The causes of these observed discrepancies between studies therefore remain unclear, with a range of different factors potentially affecting the apparent evolution of ΔOA/ΔCO with aging. However, the regional differences in biomass burning ΔOA/ΔCO ratios, together with the inherent chaotic and unpredictable nature of biomass fires driving variability near to source, underlie the variability in the atmospheric burden of BBOA. As such, these uncertainties are likely to contribute toward reported discrepancies between measurements and model estimates,[57] restricting reliable global-scale prediction of biomass burning aerosol loadings and their climate effects. Improved parametrization of BBOA in global models is therefore dependent on continued advances in the characterization of aerosol properties and their evolution to understand the causes and implications of this variability, through integration of laboratory measurements and field studies.

■ ASSOCIATED CONTENT

Ⓢ Supporting Information

Additional text, describing campaign backgrounds, instrumentation, fire types and plume ages, and MILAGRO back trajectories and ΔOA/ΔCO variability; and three figures, showing ΔOA and ΔCO time series for all campaigns; a satellite image of the region surrounding the MILAGRO study site, detailing back trajectories throughout the measurement period; and ΔOA vs ΔCO plots for fresh and aged OA fractions with color scales denoting various compositional parameters. This material is available free of charge via the Internet at http://pubs.acs.org/.

■ AUTHOR INFORMATION

Corresponding Author

*E-mail: matthew.jolleys@postgrad.manchester.ac.uk.

Notes

The authors declare no competing financial interest.

■ ACKNOWLEDGMENTS

We acknowledge financial support from the United Kingdom Natural Environment Research Council (NERC). NERC provided funding for several of the projects included in this study, including ACTIVE (NE/C512688/1), ITOP (NER/T/S/2002/00579), and DABEX-DODO, as part of AMMA-UK (NE/B505562/1 and NE/C517292/1). The deployment of the Q-AMS at Paso de Cortez during MILAGRO was funded by NSF (ATM 05-11772)

and DOE (W/GEC05-010 and MPC35TA-A5) grants, with participation supported by the Royal Society International Joint Projects scheme. Additional thanks goes to the NERC Airborne Research and Survey Facility (ASRF) for operational support of the Dornier-228 aircraft, and the Facility for Airborne Atmospheric Measurements (FAAM), together with DirectFlight, Avalon, the Met Office and the BAe-146 air and ground crews. M.D.J. was supported by a NERC studentship NE/H525162/1. J.L.J. was supported by DOE (BER, ASR) DE-SC0006035 and DE-FG02-11ER65293 and NASA NNX12AC03G.

REFERENCES

(1) Bond, T. C. A technology-based global inventory of black and organic carbon emissions from combustion. *J. Geophys. Res., [Atmos.]* **2004**, *109*, No. D14203.
(2) Hobbs, P. V.; et al. Direct radiative forcing by smoke from biomass burning. *Science* **1997**, *275* (5307), 1776−1778.
(3) Reid, J. S.; et al. A review of biomass burning emissions part II: Intensive physical properties of biomass burning particles. *Atmos. Chem. Phys.* **2005**, *5*, 799−825.
(4) Asa-Awuku, A.; et al. Investigation of molar volume and surfactant characteristics of water-soluble organic compounds in biomass burning aerosol. *Atmos. Chem. Phys.* **2008**, *8* (4), 799−812.
(5) Penner, J. E., et al. Aerosols, their direct and indirect effects. In *Climate Change 2001: The Scientific Basis. Contribution of Working Group I to the Third Assessment Report of the Intergovernmental Panel on Climate Change*; Houghton, J. T., et al., Eds.; Cambridge University Press: Cambridge, U.K., and New York, 2001; pp 289−348.
(6) Yokelson, R. J.; et al. Emissions from biomass burning in the Yucatan. *Atmos. Chem. Phys.* **2009**, *9* (15), 5785−5812.
(7) Reid, J. S.; et al. Physical, chemical, and optical properties of regional hazes dominated by smoke in Brazil. *J. Geophys. Res., [Atmos.]* **1998**, *103* (D24), 32059−32080.
(8) Abel, S. J.; et al., Evolution of biomass burning aerosol properties from an agricultural fire in southern Africa. *Geophys. Res. Lett.* **2003**, *30*, (15).
(9) De Gouw, J.; Jimenez, J. L. Organic aerosols in the Earth's atmosphere. *Environ. Sci. Technol.* **2009**, *43* (20), 7614−7618.
(10) Hawkins, L. N.; Russell, L. M. Oxidation of ketone groups in transported biomass burning aerosol from the 2008 Northern California Lightning Series fires. *Atmos. Environ.* **2010**, *44* (34), 4142−4154.
(11) LeCanut, P.; et al. Airborne studies of emissions from savanna fires in southern Africa. 1. Aerosol emissions measured with a laser optical particle counter. *J. Geophys. Res., [Atmos.]* **1996**, *101* (D19), 23615−23630.
(12) Andreae, M. O.; Merlet, P. Emission of trace gases and aerosols from biomass burning. *Glob. Biogeochem. Cycles* **2001**, *15* (4), 955−966.
(13) Hobbs, P. V.; et al. Evolution of gases and particles from a savanna fire in South Africa. *J. Geophys. Res.* **2003**, *108* (D13), 8485.
(14) Ferek, R. J.; et al. Emission factors of hydrocarbons, halocarbons, trace gases and particles from biomass burning in Brazil. *J. Geophys. Res., [Atmos.]* **1998**, *103* (D24), 32107−32118.
(15) McMeeking, G. R. Emissions of trace gases and aerosols during the open combustion of biomass in the laboratory. *J. Geophys. Res., [Atmos.]* **2009**, *114*, No. D19210.
(16) Volkamer, R. Secondary organic aerosol formation from anthropogenic air pollution: Rapid and higher than expected. *Geophys. Res. Lett.* **2006**, *33*, No. L17811.
(17) Zhang, Q.; et al. Understanding atmospheric organic aerosols via factor analysis of aerosol mass spectrometry: a review. *Anal. Bioanal. Chem.* **2011**, *401* (10), 3045−3067.
(18) DeCarlo, P. F.; et al. Fast airborne aerosol size and chemistry measurements above Mexico City and Central Mexico during the MILAGRO campaign. *Atmos. Chem. Phys.* **2008**, *8* (14), 4027−4048.
(19) DeCarlo, P. F.; et al. Investigation of the sources and processing of organic aerosol over the Central Mexican Plateau from aircraft measurements during MILAGRO. *Atmos. Chem. Phys.* **2010**, *10* (12), 5257−5280.
(20) Akagi, S. K.; et al. Evolution of trace gases and particles emitted by a chaparral fire in California. *Atmos. Chem. Phys.* **2012**, *12* (3), 1397−1421.
(21) Capes, G. Aging of biomass burning aerosols over West Africa: Aircraft measurements of chemical composition, microphysical properties, and emission ratios. *J. Geophys. Res., [Atmos.]* **2008**, *113*, No. D00C15.
(22) Cubison, M. J.; et al. Effects of aging on organic aerosol from open biomass burning smoke in aircraft and laboratory studies. *Atmos. Chem. Phys.* **2011**, *11* (23), 12049−12064.
(23) Schneider, J.; et al. Mass spectrometric analysis and aerodynamic properties of various types of combustion-related aerosol particles. *Int. J. Mass Spectrom.* **2006**, *258* (1−3), 37−49.
(24) Alfarra, M. R.; et al. Identification of the mass spectral signature of organic aerosols from wood burning emissions. *Environ. Sci. Technol.* **2007**, *41* (16), 5770−5777.
(25) Aiken, A. C.; et al. Mexico City aerosol analysis during MILAGRO using high resolution aerosol mass spectrometry at the urban supersite (T0) - Part 1: Fine particle composition and organic source apportionment. *Atmos. Chem. Phys.* **2009**, *9* (17), 6633−6653.
(26) Andreae, M. O.; Rosenfeld, D. Aerosol-cloud-precipitation interactions. Part 1. The nature and sources of cloud-active aerosols. *Earth-Sci. Rev.* **2008**, *89* (1−2), 13−41.
(27) Mason, S. A.; et al. Complex effects arising in smoke plume simulations due to inclusion of direct emissions of oxygenated organic species from biomass combustion. *J. Geophys. Res., [Atmos.]* **2001**, *106* (D12), 12527−12539.
(28) Herndon, S. C. Correlation of secondary organic aerosol with odd oxygen in Mexico City. *Geophys. Res. Lett.* **2008**, *35*, No. L15804.
(29) Baumgardner, D.; et al. Physical and chemical properties of the regional mixed layer of Mexico's Megapolis. *Atmos. Chem. Phys.* **2009**, *9* (15), 5711−5727.
(30) Yokelson, R. J.; et al. Trace gas and particle emissions from open biomass burning in Mexico. *Atmos. Chem. Phys.* **2011**, *11* (14), 6787−6808.
(31) Gao, S. Water-soluble organic components in aerosols associated with savanna fires in southern Africa: Identification, evolution, and distribution. *J. Geophys. Res., [Atmos.]* **2003**, *108* (D13), 8941.
(32) Hecobian, A.; et al. Comparison of chemical characteristics of 495 biomass burning plumes intercepted by the NASA DC-8 aircraft during the ARCTAS/CARB-2008 field campaign. *Atmos. Chem. Phys.* **2011**, *11* (24), 13325−13337.
(33) Peltier, R. E.; et al. Fine aerosol bulk composition measured on WP-3D research aircraft in vicinity of the Northeastern United States - results from NEAQS. *Atmos. Chem. Phys.* **2007**, *7* (12), 3231−3247.
(34) Petzold, A.; et al. Perturbation of the European free troposphere aerosol by North American forest fire plumes during the ICARTT-ITOP experiment in summer 2004. *Atmos. Chem. Phys.* **2007**, *7* (19), 5105−5127.
(35) Real, E. Processes influencing ozone levels in Alaskan forest fire plumes during long-range transport over the North Atlantic. *J. Geophys. Res., [Atmos.]* **2007**, *112*, No. D10S41.
(36) Robinson, A. L.; et al. Rethinking organic aerosols: Semivolatile emissions and photochemical aging. *Science* **2007**, *315* (5816), 1259−1262.
(37) Shrivastava, M. K.; et al. Modeling semivolatile organic aerosol mass emissions from combustion systems. *Environ. Sci. Technol.* **2006**, *40* (8), 2671−2677.
(38) Hand, V. L. Evidence of internal mixing of African dust and biomass burning particles by individual particle analysis using electron beam techniques. *J. Geophys. Res., [Atmos.]* **2010**, *115*, No. D13301.
(39) Johnson, B. T. Aircraft measurements of biomass burning aerosol over West Africa during DABEX. *J. Geophys. Res., [Atmos.]* **2008**, *113*, No. D00C06.

(40) Allen, G. Aerosol and trace-gas measurements in the Darwin area during the wet season. *J. Geophys. Res., [tmos.* **2008**, *113*, No. D06306.
(41) George, I. J. Chemical aging of ambient organic aerosol from heterogeneous reaction with hydroxyl radicals. *Geophys. Res. Lett.* **2008**, *35*, No. L13811.
(42) Alfarra, M. R.; et al. Characterization of urban and rural organic particulate in the lower Fraser valley using two aerodyne aerosol mass spectrometers. *Atmos. Environ.* **2004**, *38* (34), 5745−5758.
(43) Aiken, A. C.; et al. O/C and OM/OC ratios of primary, secondary, and ambient organic aerosols with high-resolution time-of-flight aerosol mass spectrometry. *Environ. Sci. Technol.* **2008**, *42* (12), 4478−4485.
(44) Ng, N. L.; et al. Changes in organic aerosol composition with aging inferred from aerosol mass spectra. *Atmos. Chem. Phys.* **2011**, *11* (13), 6465−6474.
(45) Morgan, W. T.; et al. Airborne measurements of the spatial distribution of aerosol chemical composition across Europe and evolution of the organic fraction. *Atmos. Chem. Phys.* **2010**, *10* (8), 4065−4083.
(46) Weimer, S. Organic aerosol mass spectral signatures from wood-burning emissions: Influence of burning conditions and wood type. *J. Geophys. Res., [Atmos.]* **2008**, *113*, No. D10304.
(47) Morgan, W. T.; et al. Vertical distribution of sub-micron aerosol chemical composition from North-Western Europe and the North-East Atlantic. *Atmos. Chem. Phys.* **2009**, *9* (15), 5389−5401.
(48) Yokelson, R. J.; et al. The Tropical Forest and Fire Emissions Experiment: overview and airborne fire emission factor measurements. *Atmos. Chem. Phys.* **2007**, *7* (19), 5175−5196.
(49) Yokelson, R. J.; et al. Emissions from forest fires near Mexico City. *Atmos. Chem. Phys.* **2007**, *7* (21), 5569−5584.
(50) Sinha, P.; et al. Emissions of trace gases and particles from savanna fires in southern Africa. *J. Geophys. Res., [Atmos.]* **2003**, *108* (D13), 8487.
(51) de Gouw, J. A. Budget of organic carbon in a polluted atmosphere: Results from the New England Air Quality Study in 2002. *J. Geophys. Res., [Atmos.]* **2005**, *110*, No. D16305.
(52) Kleinman, L. I. Aircraft observations of aerosol composition and ageing in New England and Mid-Atlantic States during the summer 2002 New England Air Quality Study field campaign. *J. Geophys. Res., [Atmos.]* **2007**, *112*, No. D09310.
(53) Dzepina, K.; et al. Evaluation of recently-proposed secondary organic aerosol models for a case study in Mexico City. *Atmos. Chem. Phys.* **2009**, *9* (15), 5681−5709.
(54) Akagi, S. K.; et al. Emission factors for open and domestic biomass burning for use in atmospheric models. *Atmos. Chem. Phys.* **2011**, *11* (9), 4039−4072.
(55) Grieshop, A. P.; et al. Laboratory investigation of photochemical oxidation of organic aerosol from wood fires 1: measurement and simulation of organic aerosol evolution. *Atmos. Chem. Phys.* **2009**, *9* (4), 1263−1277.
(56) Hennigan, C. J.; et al. Chemical and physical transformations of organic aerosol from the photo-oxidation of open biomass burning emissions in an environmental chamber. *Atmos. Chem. Phys.* **2011**, *11* (15), 7669−7686.
(57) Kaiser, J. W.; et al. Biomass burning emissions estimated with a global fire assimilation system based on observed fire radiative power. *Biogeosciences* **2012**, *9*, 527−554.

Characterizing the aging of biomass burning organic aerosol using mixing ratios – a meta-analysis of four regions

Supplementary material for the manuscript submitted to Environmental Science & Technology

Contents:

10 pages

Text ST1 – ST4

3 figures

References

ST1. Campaign backgrounds

The ACTIVE experiment was carried out between November 2005 and February 2006 around the Darwin region of northern Australia (*S1, S2*). Measurements of BBOA were most widespread during the 2005 part of the campaign, coinciding with the biomass burning season within the region, prior to the onset of the monsoon period. Biomass burning influences within the region included both local fires and more aged, transported emissions from fires to the east in Queensland. All data considered here were obtained from flights performed by the NERC Dornier-228 aircraft, covering the local Darwin area and the Tiwi Islands to the north, where several active fires were surveyed.

DABEX and DODO (Dust Outflow and Deposition to the Ocean, hereafter referred to singularly as DABEX) formed part of the wider AMMA (African Monsoon Multidisciplinary Analyses) program, with the FAAM BAe-146 aircraft deployed in a series of flights across West Africa throughout February 2006 (*S3, S4*). DABEX flights originated from Niamey in Niger, and targeted fresh biomass burning emissions from widespread fires to the south over Benin and Nigeria, along with more aged emissions at higher altitudes. Layers of lofted aged biomass burning aerosol were also encountered during DODO flights, flying from Dakar in Senegal, further to the west and downwind from the region surveyed throughout DABEX.

The final aircraft dataset included in this analysis came from further FAAM flights during the ITOP campaign in July and August 2004 (*S5*), as part of the International Consortium for Atmospheric Research on Transport and Transformation (ICARTT; *S6*). The wider scope of ICARTT included measurements of emissions from boreal forest fires in North America. Highly aged plumes from these fires were sampled by the BAe-146 around the Azores, following advection across the North Atlantic. Data selection throughout ITOP followed the direction of *Lewis et al.* (*S5*), where biomass burning influences were inferred from back trajectory cluster analysis, showing repeated transport from Alaska and Northern Canada.

A further ground-based dataset was acquired from a site at Altzomoni (19.117° N, 98.654° W), located near the Paso de Cortez to the southeast of Mexico City (*S7*). Continuous measurements were performed throughout the duration of March 2006, in parallel with the broader MILAGRO series of atmospheric measurements (*S8*), which involved a number of intensive studies at ground-based supersites within the Mexico City Metropolitan Area (MCMA). While the main objectives of MILAGRO focused on the assessment of anthropogenic emissions from the MCMA, the site at Altzomoni was strongly influenced by biomass burning, with contributions from both local mountain forest fires and savanna fires to the southeast of the city region (*S9*).

ST2. Instrumentation

The Q-AMS provides high time resolution (30 seconds), size-resolved measurement of sub-micron aerosol mass and composition (*S10*). Concentrations of all major non-refractory aerosol species are retrieved from sampled mass spectra, for *m*/*z* ratios from 0 to 300 at unit mass resolution. Peaks associated with certain ions can therefore be related to specific organic components, and used to infer the component contributions to the overall OA mass. Total particle number concentrations were measured with TSI Inc. condensation particle counters (CPCs) in each campaign, with a model 3010 CPC used during ACTIVE and MILAGRO, and a model 3025 Ultrafine CPC for all flights on the BAe-146. In each instance, concentrations of gaseous species and aerosol number concentrations, along with positional data, were averaged to the Q-AMS timebase, given the lower temporal resolution of the Q-AMS relative to the other instruments used (typically 1 second).

Accuracy of Q-AMS measurements under laboratory conditions were evaluated by *Drewnick et al.* (*S11*), with a reported minimum detection limit for the organic fraction of 0.5 μg m^{-3}. *Crosier et al.* (*S12*) observed a detection limit of 1.69 ug m^{-3} for 30-second aircraft measurements of OA at an altitude of 1000 m. However, this figure is expected to increase with altitude, as indicated by airborne measurements of vertical aerosol distribution in

northern Europe, which show an increasing variability about the mean OA concentration by around a factor of 11 for 500m altitude bins between 500 m and 11 km (*S13*). The precision of Q-AMS measurements in response to instrument noise was estimated to be approximately 3.3 ug m^{-3} by *Capes et al.* (*S14*) for 30-second aircraft measurements at an altitude of 600 m.

All Q-AMS measurements were corrected for collection efficiency (CE) as part of the initial data processing. *Allen et al.* (*S1*) report ratios of between 0.4 and 0.7 for the comparison of UHSAS particulate volume to accumulated AMS and PSAP volume during ACTIVE, resulting in a derived CE of 0.5. *Baumgardner et al.* (*S7*) demonstrated the closure between AMS and BC mass and volume derived from SMPS size distributions for MILAGRO. A lower CE of 0.34 was calculated by *Capes et al.* (*S3*) for DABEX, indicating that the AMS may provide a lower measure of mass compared to estimates derived from PCASP size distributions given the contributions of BC and mineral dust within the study region. A collection efficiency of 0.5 was also calculated for ITOP through comparison of AMS data with measurements of aerosol composition by PILS-IC.

ST3. Fire types and plume ages

Given the predominance of aircraft measurements throughout these campaigns, it has not been widely possible to obtain accurate classifications of fires within each region. Similarly, the lack of an extensive range of photochemical measurements limits the ability to accurately constrain plume ages. However, these details can be inferred to an extent from wider sources, in order to provide an overview of the nature of sampled emissions. Detailed vegetation maps covering the regions subject to widespread fires during ACTIVE are available from the Territory Natural Resource Management/Charles Darwin University Cooperative Research Centre for Tropical Savannas Management's Northern Land Manager service (*S15-S18*). These maps indicate that the region surveyed during ACTIVE was generally dominated by eucalypt forests and woodlands, characterized by the species *Eucalyptus tetrodonta* and *Eucalyptus miniata*. The Tiwi Islands also contain smaller pockets of acacia shrubland and

mangrove swamps, while the region immediately to the east of Darwin where several active fires were also sampled features areas of grassland, wetland and tea tree swamps. During the ACTIVE study period large scale land clearance was taking place across both Arnhem Land and the Cape York Peninsula in northern Queensland, as evidenced by MODIS fire maps (*S1*). Arnhem Land consists of fairly extensive heathlands and areas of tea tree woodlands and wetlands, with tea tree woodlands also widespread along the eastern and western fringes of Cape York, along with areas of wet heath, grassland and rainforest. Observations of active fires indicate that some plumes were sampled directly at source, while aged emissions from fires in Arnhem Land and Cape York were transported over a period of up to five days (*S1*).

Measurements of BB plumes during DABEX took place at a wide range of distances from source. *Johnson et al.* (*S19*) report sampling active fires at a height of 300 m, while layers of more aged emissions and regional hazes were encountered downwind from the source region, up to several days after emission. Small agricultural fires were widespread across the region throughout the duration of the campaign, with grasses, scrub vegetation and agricultural residues expected to constitute the dominant fuel types. Observations indicate that both flaming and smoldering combustion phases were occurring throughout these fires. Grass fires were also prevalent during MILAGRO, while many small shrub and agricultural fires were observed across the wider Mexico City region (*S20*). Back trajectory analysis suggests aged emissions had been transported for between three and five days prior to measurement, as inferred from the locations of potential BB source regions beyond the local area.

Aged plumes sampled during ITOP were also encountered at other positions across their transit as part of further aircraft studies within the wider ICARTT program. Both the NASA DC8 and the DLR Falcon performed measurements of the plumes, over Newfoundland and continental Europe respectively. Using a combination of these observations and back trajectory simulations, *Real et al.* (*S21*) and *Petzold et al.* (*S22*) suggest that the plumes had been transported for between three and six days before being sampled around the Azores. Furthermore, model simulations of plume evolution have shown high levels of photochemical

activity, with strong O_3 production during transportation towards Europe. Mixing and dilution of plumes with surrounding air also appears to have a significant effect, as indicated by the large observed decrease in CO concentrations with increasing distance from source (*S21*).

ST4. MILAGRO back trajectories and ΔOA/ΔCO variability

Daily distributions of individual fresh ΔOA/ΔCO values throughout MILAGRO appear to be characterised by two distinct modes. Between the 5th and 9th March, the peak frequency occurs between 0.03 and 0.07, followed by a rapid decrease in frequency above this threshold. Between the 10th and 17th March there is a pronounced change in ΔOA/ΔCO distribution, as peaks tend to occur at a higher position and frequencies do not decrease as consistently above 0.07. Distributions are most substantially shifted towards higher values on the 10th, 15th and 17th, with ΔOA/ΔCO greater than 0.1 for 31%, 46% and 77% of datapoints on each of these dates respectively. There is also no consistent relationship between the two ΔOA/ΔCO modes and back trajectory origins. Between the 15th and 17th March, when the most significant enhancements in ΔOA/ΔCO distribution were identified, with more than 60% of values above 0.07 on each day, sampled air masses had originated from the northeast and north five days prior to detection at the measurement site, switching to an easterly approach in the final 24 hours before arrival. A comparable change in ΔOA/ΔCO was observed on the 10th and 12th, when back trajectories indicated a shift in origin to the west and southwest. Although this back trajectory pattern was also identified on the 9th and 11th, ΔOA/ΔCO distributions for these dates show better agreement with the low ΔOA/ΔCO mode observed earlier in the month. ΔOA/ΔCO values from the 23rd also conform to this initial trend, again peaking between 0.04 and 0.06, despite a further change in back trajectories towards the northwest.

The elevated ΔOA/ΔCO distributions identified on the 12th and 15th-17th March coincided with an enhancement in the $\Delta O_3/\Delta CO$ distribution, suggesting an increase in photochemical processing within these plumes and possible influence by SOA formation.

However, there is no such shift in $\Delta O_3/\Delta CO$ distribution on the 10th March, when $\Delta OA/\Delta CO$ was also higher. Furthermore, these trends show poor consistency with aerosol composition. While f_{44} and f_{57} distributions generally show reconciliatory correlations with $\Delta OA/\Delta CO$ for the days on which the latter is increased, these trends are also repeated on days when $\Delta OA/\Delta CO$ is low. These discrepancies highlight the limitations in attributing more finite $\Delta OA/\Delta CO$ variability to compositional changes.

Figure S1: ΔOA and ΔCO time series for (a) ACTIVE, (b) MILAGRO, (c) DABEX and (d) ITOP. Data is shown for all flights or dates where sufficient data were available to contribute to overall campaign datasets following screening by f_{60}, ΔCO and number concentration thresholds. Grey sections represent data removed by screening and subsequently omitted from analysis.

Figure S2: MODIS satellite image of central Mexico, showing one and five day back trajectories from Altzomoni (19.117° N, 98.654° W) initiated at 650 mb at 1800 UTC (1200 local time), as provided by the BADC Web Trajectory service (http://badc.nerc.ac.uk/community/trajectory/). Back trajectories are shown for all days on which fresh OA plumes were identified. *Inset:* (a) ΔOA/ΔCO and (b) $\Delta O_3/\Delta CO$ distributions for fresh OA during MILAGRO. Grey sections show percentage values averaged across corresponding bins for each day, while black sections represent the distribution of counts as a percentage of total counts.

Figure S3: ΔOA vs. ΔCO plots for (a) ACTIVE, (b) MILAGRO, (c) DABEX and (d) ITOP, segregated into (i) fresh and (ii) aged OA fractions, coloured by (left to right) f_{44}/f_{57}, f_{44}, f_{57} and f_{60} respectively. Distinctions in the composition of BBOA between age fractions are most evident during MILAGRO. Several moderate trends can also be identified within the aged OA fraction for MILAGRO which consistently indicate a decrease in ΔOA/ΔCO with progressive ageing. Both f_{44}/f_{57} and f_{44}, as indicators for ageing, are generally negatively correlated with ΔOA/ΔCO. In contrast, f_{57} and f_{60}, which represent the proportional abundances of characteristic fresh OA components, show overall positive trends with ΔOA/ΔCO. Evidence for similar relationships within the fresh OA fraction is limited.

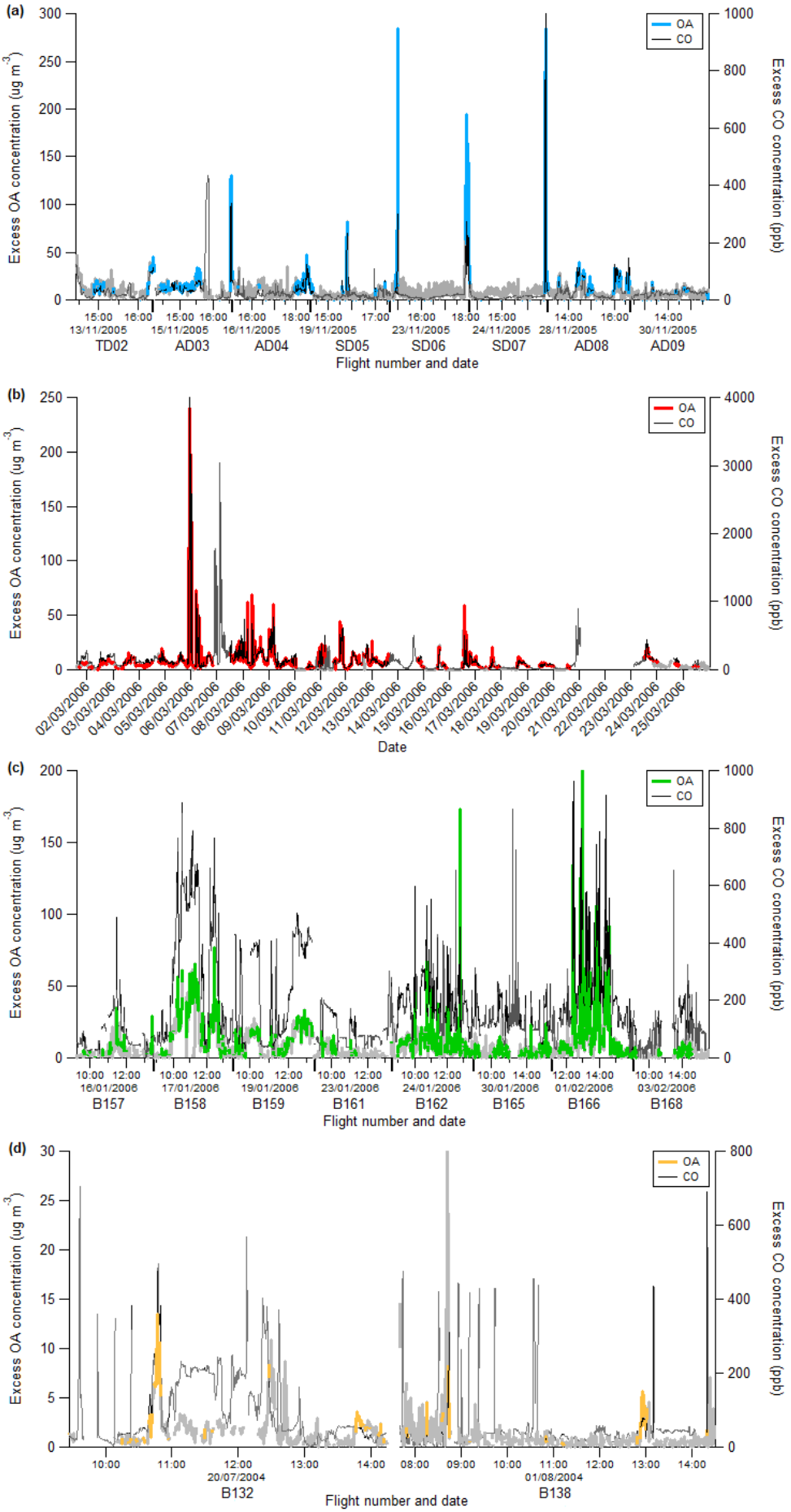
(a)
Excess OA concentration (ug m-3)
Excess CO concentration (ppb)
OA
CO
13/11/2005 TD02
15/11/2005 AD03
16/11/2005 AD04
19/11/2005 SD05
23/11/2005 SD06
24/11/2005 SD07
28/11/2005 AD08
30/11/2005 AD09
Flight number and date
(b)
Excess OA concentration (ug m-3)
Excess CO concentration (ppb)
OA
CO
Date
(c)
Excess OA concentration (ug m-3)
Excess CO concentration (ppb)
OA
CO
16/01/2006 B157
17/01/2006 B158
19/01/2006 B159
23/01/2006 B161
24/01/2006 B162
30/01/2006 B165
01/02/2006 B166
03/02/2006 B168
Flight number and date
(d)
Excess OA concentration (ug m-3)
Excess CO concentration (ppb)
OA
CO
20/07/2004 B132
01/08/2004 B138
Flight number and date

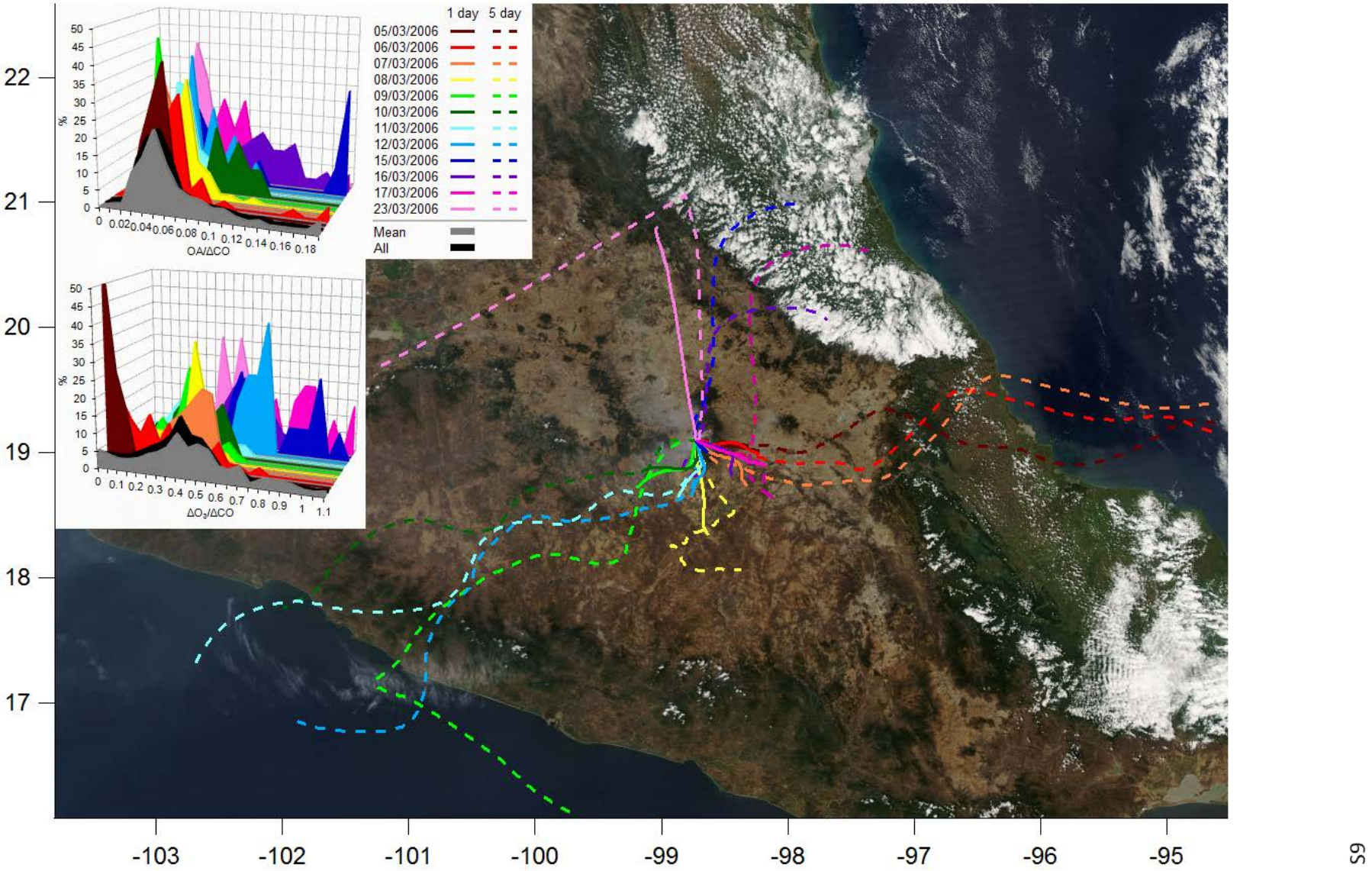
1 day
5 day
05/03/2006
06/03/2006
07/03/2006
08/03/2006
09/03/2006
10/03/2006
11/03/2006
12/03/2006
15/03/2006
16/03/2006
17/03/2006
23/03/2006
Mean
All
%
OA/ΔCO
ΔO3/ΔCO
22
21
20
19
18
17
-103
-102
-101
-100
-99
-98
-97
-96
-95

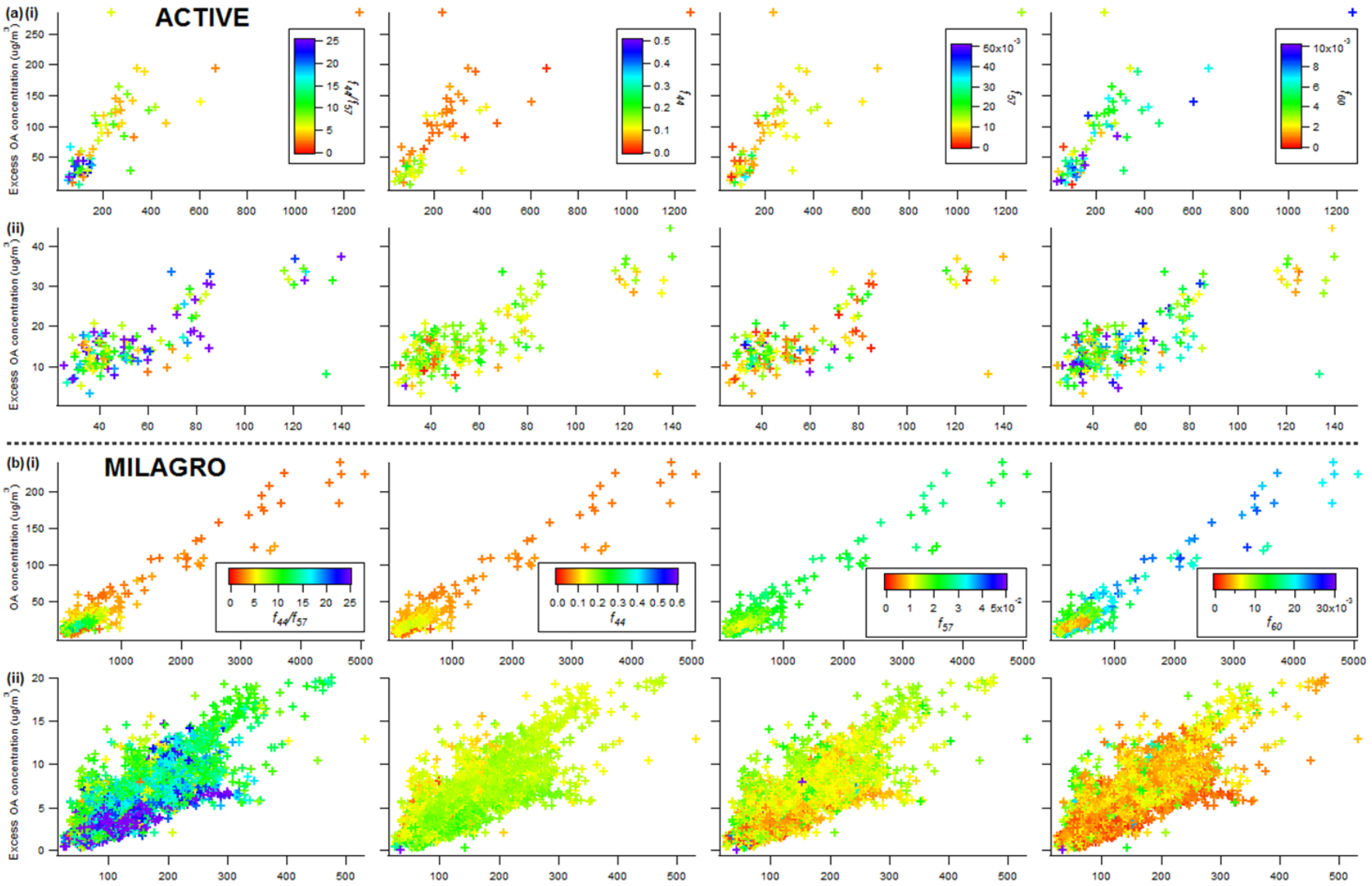
(a) (i)
ACTIVE
Excess OA concentration (ug/m3)
f44/f57
f44
f57
f60
(ii)
(b) (i)
MILAGRO
OA concentration (ug/m3)
(ii)

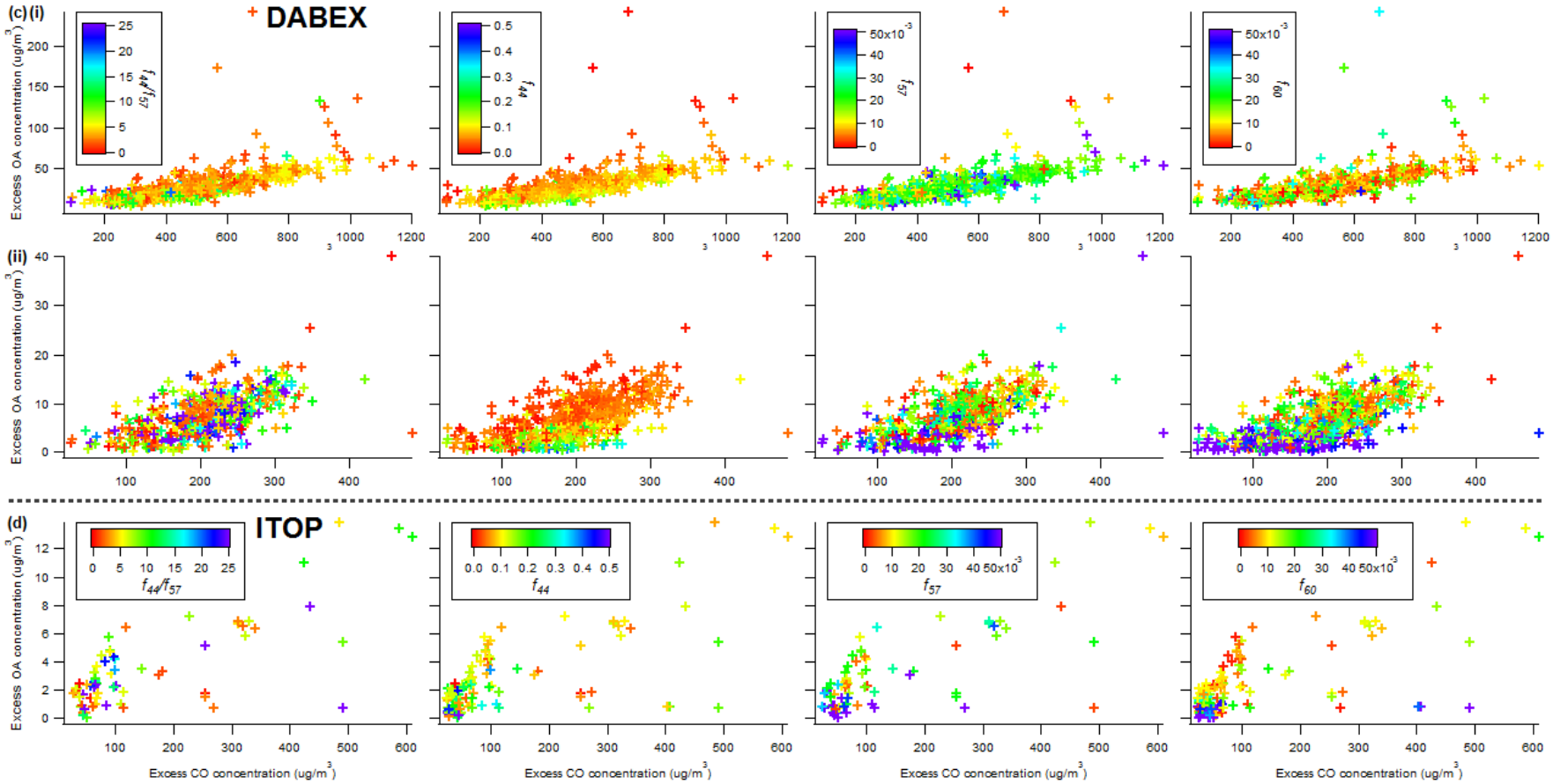
(c) (i)
DABEX
Excess OA concentration (ug/m3)
f44/f57
f44
f57
f60
(ii)
(d)
ITOP
Excess CO concentration (ug/m3)

Supplementary references

(S1) Allen, G.; et al. Aerosol and trace-gas measurements in the Darwin area during the wet season. *J. Geophys. Res.-Atmos.* 2008, *113*, (D6).

(S2) Vaughan, G.; et al. SCOUT-03/ACTIVE - High-altitude aircraft measurements around deep tropical convection. *B. Am. Meteorol. Soc.* 2008, *89*, (5), 647-662.

(S3) Capes, G.; et al. Aging of biomass burning aerosols over West Africa: Aircraft measurements of chemical composition, microphysical properties, and emission ratios. *J. Geophys. Res.-Atmos.* 2008, *113*, (D20).

(S4) Haywood, J. M.; et al. Overview of the Dust and Biomass-burning Experiment and African Monsoon Multidisciplinary Analysis Special Observing Period-0. *J. Geophys. Res.-Atmos.* 2008, *113*.

(S5) Lewis, A. C.; et al. Chemical composition observed over the mid-Atlantic and the detection of pollution signatures far from source regions. *J. Geophys. Res.-Atmos.* 2007, *112*, (D10).

(S6) Fehsenfeld, F. C.; et al. International Consortium for Atmospheric Research on Transport and Transformation (ICARTT): North America to Europe - Overview of the 2004 summer field study. *J. Geophys. Res.-Atmos.* 2006, *111*, (D23).

(S7) Baumgardner, D.; et al. Physical and chemical properties of the regional mixed layer of Mexico's Megapolis. *Atmos. Chem. Phys.* 2009, *9*, (15), 5711-5727.

(S8) Molina, L. T.; et al. An overview of the MILAGRO 2006 Campaign: Mexico City emissions and their transport and transformation. *Atmos. Chem. Phys.* 2010, *10*, (18), 8697-8760.

(S9) Yokelson, R. J.; et al. Trace gas and particle emissions from open biomass burning in Mexico. *Atmos. Chem. Phys.* 2011, *11*, (14), 6787-6808.

(S10) Canagaratna, M. R.; et al. Chemical and microphysical characterization of ambient aerosols with the aerodyne aerosol mass spectrometer. *Mass Spectrom. Rev.* 2007, *26*, (2), 185-222.

(S11) Drewnick, F.; et al. Aerosol quantification with the Aerodyne Aerosol Mass Spectrometer: detection limits and ionizer background effects. *Atmos. Meas. Tech.* 2009, *2*, (1), 33–46.

(S12) Crosier, J.; et al. Chemical composition of summertime aerosol in the Po Valley (Italy), northern Adriatic and Black Sea. *Q. J. R. Meteorol. Soc.* 2007, *133*, (S1) 61–75.

(S13) Morgan, W. T.; et al. Vertical distribution of sub-micron aerosol chemical composition from North-Western Europe and the North-East Atlantic. *Atmos. Chem. Phys.* 2009, *9*, (15), 5389-5401.

(S14) Capes, G.; et al. Secondary organic aerosol from biogenic VOCs over West Africa during AMMA. *Atmos. Chem. Phys.* 2009, *9*, (12), 3841–3850.

(S15) Territory Natural Resource Management (TNRM) & Charles Darwin University Cooperative Research Centre for Tropical Savannas Management (CDU Tropical Savannas CRC). Northern Land Manager Tiwi Islands vegetation map, http://www.landmanager.org.au/land_manager/downloads/Map-of-the-Vegetation-of-the-Tiwi-Islands-Region.pdf, September 2012.

(S16) TNRM & CDU Tropical Savannas CRC. Northern Land Manager Tiwi Islands vegetation map, http://www.landmanager.org.au/land_manager/downloads/Map-of-the-Vegetation-of-the-Darwin-Daly-Region.pdf, September 2012.

(S17) TNRM & CDU Tropical Savannas CRC. Northern Land Manager Tiwi Islands vegetation map, http://www.landmanager.org.au/land_manager/downloads/Map-of-the-Vegetation-of-the-Arnhem-Land.pdf, September 2012.

(S18) TNRM & CDU Tropical Savannas CRC. Northern Land Manager Tiwi Islands vegetation map, http://www.landmanager.org.au/land_manager/downloads/Map-of-the-Vegetation-of-the-Cape-York-Peninsula.pdf, September 2012.

(S19) Johnson, B. T.; et al. Aircraft measurements of biomass burning aerosol over West Africa during DABEX. *J. Geophys. Res.-Atmos.* 2008, *113*, (D17).

(S20) Fast, J. D.; et al. A meteorological overview of the MILAGRO field campaigns. *Atmos. Chem. Phys.* 2007, *7*, (9), 2233-2257.

(S21) Real, E.; et al. Processes influencing ozone levels in Alaskan forest fire plumes during long-range transport over the North Atlantic. *J. Geophys. Res.-Atmos.* 2007, *112*, (D10).

(S22) Petzold, A.; et al. Perturbation of the European free troposphere aerosol by North American forest fire plumes during the ICARTT-ITOP experiment in summer 2004. *Atmos. Chem. Phys.* 2007, *7*, (19), 5105-5127.

3.5 Paper 2: Organic aerosol emission ratios from the laboratory combustion of biomass fuels

Status:

To be submitted to Atmospheric Chemistry & Physics

Overview:

This paper presents an inventory of BBOA ERs from the FLAME II experiment, during which plant species commonly involved in US wildfires and prescribed fires were burned under laboratory conditions. Variability in burn-averaged △OA/△CO was shown to exceed levels identified from ambient measurements, even amongst single fuel types and species. The influence of several potential drivers of variability in △OA/△CO, including fuel type, fuel properties and combustion conditions, were investigated. These relationships were shown to be highly complex, with a lack of overriding controls on BBOA emissions. Changes in fuel moisture content, particularly in certain fuel components, had a significant effect on △OA/△CO levels for coniferous species, which also exhibited a greater dependency on MCE than other fuels. Consistent trends of decreasing △OA/△CO with increasing oxygenation of OA suggest that the availability of oxygen during combustion strongly influences the magnitude of particulate formation in biomass fires.

Contributions from co-authors:

G. McMeeking, T. Lee and A. Sullivan participated in experiments and performed initial data processing. S. Kreidenweis and J. Collett initiated the project. H. Coe and G. McFiggans assisted with preparation of the manuscript.

Organic aerosol emission ratios from the laboratory combustion of biomass fuels

Matthew D. Jolleys[*1], *Hugh Coe*[1], *Gordon McFiggans*[1], *Gavin R. McMeeking*[2,3], *Taehyoung Lee*[2,4], *Amy P. Sullivan*[2], *Sonia M. Kreidenweis*[2], *Jeffrey L. Collett Jr.*[2]

* Corresponding author email: matthew.jolleys@postgrad.manchester.ac.uk

[1] Centre for Atmospheric Science, School of Earth, Atmospheric and Environmental Science, University of Manchester, Manchester, UK

[2] Department of Atmospheric Science, Colorado State University, Fort Collins, Colorado, USA

[3] Now at Droplet Measurement Technologies, Boulder, Colorado, USA

[4] Now at Department of Environmental Science, Hankuk University of Foreign Studies, Yongin-si, Gyeonggi-do, Korea

Abstract

Organic aerosol (OA) emission ratios (ER) have been characterised for 67 burns during the second Fire Laboratory at Missoula Experiment (FLAME II). These fires involved 19 different species representing 6 major fuels, each of which forms an important contribution to the US biomass burning (BB) inventory. Average normalised △OA/△CO ratios show a high degree of variability, both between and within different fuel types and species, typically exceeding variability between separate plumes in ambient measurements. Significant contrasts were also identified between combustion emissions from different components of several species. No strong correlation across all fires was observed between △OA/△CO and modified combustion efficiency (MCE), which is used as an indicator of the proportional contributions of flaming and smouldering combustion phases throughout each burn. However, a negative correlation exists between △OA/△CO and MCE for some coniferous species, most notably Douglas fir, for which there is also an apparent influence from fuel moisture content. Changes in fire efficiency were also shown to dramatically alter emissions for fires with very similar initial conditions. Although the relationship with MCE is variable between species, there is greater consistency with the level of oxygenation in OA. The ratio of the *m*/*z* 44 fragment to total OA mass concentration (f_{44}) as measured by aerosol mass spectrometer (AMS) provides an indication of oxygenation as influenced by combustion processes at source, with △OA/△CO decreasing with increasing f_{44} for all fuel types. Inconsistencies in the magnitude of the effects associated with each potential influence on △OA/△CO emphasise the lack of a single dominant control on fire emissions, and a dependency on both fuel properties and combustion conditions.

1. Introduction

Biomass burning (BB) comprises a significant contribution to the global atmospheric organic aerosol (OA) burden (*Crutzen & Andreae, 1990; Bond et al., 2004*), and as such has an important influence on local and regional air quality and climate impacts (*Andreae & Merlet, 2001; Langmann et al., 2009*). The unpredictable nature of biomass burning events, in relation to both the characteristics of fires and resulting emissions inventories, represents a major source of uncertainty associated with attempts to provide reliable assessments of the role of such events as a contributor to global climate change. In-situ measurements of OA emissions from wildfires have been undertaken throughout a number of field campaigns across a wide range of locations and environments. These studies have revealed widespread inconsistencies regarding the production of OA from biomass burning, identifying highly contrasting emissions regimes across different spatial and temporal scales (*Akagi et al., 2011; Jolleys et al., 2012*). Contributions from secondary organic aerosol (SOA) formation in aging biomass burning plumes have been shown to vary considerably for different events, with evidence supporting both a net enhancement and loss of OA with aging (*Capes et al., 2008; DeCarlo et al., 2008; Yokelson et al., 2009; Akagi et al., 2012*). Furthermore, the extent of variability within emissions close to source can frequently exceed any changes occurring as a result of the physical and chemical processes affecting aging plumes, indicating that source conditions may represent a determining factor for biomass burning organic aerosol (BBOA) emissions regimes (*Jolleys et al., 2012*). However, the importance of different source conditions and their specific implications for OA emissions is currently poorly understood. Modified combustion efficiency (MCE) represents the molar ratio of CO_2 to the sum of combined CO_2 and CO emissions ($MCE = \triangle CO_2/(\triangle CO_2+\triangle CO)$, where $\triangle$ signifies excess concentrations above background levels) and is used as a measure of the predominance of flaming and smouldering combustion phases in fires (*Yokelson et al., 1996; Ferek et al., 1998*). MCE is expected to form one of the main controls on OA production given the more favourable conditions associated with smouldering fires. Lower temperatures and reducing conditions in smouldering fires promote formation of

OA and CO, with higher temperatures and increased turbulent mixing with oxygen required to form soot precursors or fully oxidise combustion products to CO_2 (*Ward, 1990; Reid et al., 2005*).

The influence of MCE as a control on BB emissions has been examined throughout a number of experimental studies under both ambient and laboratory settings (*Ferek et al., 1998; Yokelson et al., 2007; Grieshop et al., 2009; Janhall et al., 2010; Burling et al., 2011; Akagi et al., 2011; Yokelson et al., 2011*). The majority of existing studies have focused upon the calculation of emission factors (EF), where by the mass of an emitted species is related to the mass of fuel consumed in a fire ($EF_x = M_x(g)/M_{fuel}(kg)$). While EFs provide a valuable tool for assessing the OA contributions from fires in different environments involving different fuel types, and are particularly useful for modelling studies of fire emissions through integration with biomass consumption databases, they are also limited to representation of average conditions across the duration of a burn. Significant and dynamic transitions in combustion phase have been widely observed in biomass fires, along with changes in associated emission profiles (*Chen et al., 2007; Lee et al., 2010*). Highly time-resolved measurements of aerosol mass and composition can be obtained by use of aerosol mass spectrometers (AMS; *Canagaratna et al., 2007*), enabling the continuous observation of OA from biomass burning, including the response to changes in combustion conditions throughout the duration of a fire. The second Fire Laboratory at Missoula Experiment (FLAME II) provided extensive highly time-resolved measurements of burns involving six fuel types representing the major contributors to wildfire budgets in the western and southeastern United States. These experiments allow the effects of differing combustion conditions and fuel types as drivers of variability in source emissions to be comprehensively examined, providing a potential insight to the factors affecting observed contrasts in ambient BBOA. Emissions properties are presented both as burn averages and real-time measurements in order assess the typical behaviour of a range of fires and the extent of changes occurring throughout the different stages of combustion. The effects of drivers affecting variability in emissions are then evaluated, focusing on the roles of combustion

processes, source conditions such as fuel type and morphology, and oxygenation levels of resulting OA. The consistency of these influences across multiple fires are also examined, before comparing observations from FLAME II with those from past field campaigns.

2. Background

The FLAME II experiment was carried out at the U.S. Forest Service's Fire Sciences Laboratory (FSL) in Missoula, Montana in 2007. Previous publications relating to the FLAME experiments have primarily focused on the analysis of filter samples and subsequent evaluation of burn-averaged EFs. The analysis of AMS data presented here retains the capacity to present characteristic assessments of average burn properties as a means of intercomparison, while also enabling investigation of dynamic changes in emissions. For this purpose, OA measurements are presented as dimensionless mass-based emission ratios (ERs) normalised to CO, where $ER_{OA} = \triangle OA/\triangle CO$. Presenting OA concentrations in this normalised manner accounts for any difference in fire intensity or size between burns in order to represent the relative OA emissions for different biomass fuels. Furthermore, this approach enables comparison with findings from field campaigns, albeit with the caveat of contrasting conditions between laboratory and field settings and potential differences in fire behaviour and emissions (*Yokelson et al., 2008*).

The experimental specifications of the FSL facility are discussed in detail in existing publications (*Christian et al., 2003; McMeeking et al., 2009*), with a brief overview given here. The combustion chamber has a floor plate of 12.5 x 12.5 m and a height of 22 m, giving a total volume of approximately 3000 m^3. An exhaust stack with an internal diameter of 1.6 m is located in the centre of the chamber, extending from approximately 2 m above the chamber floor through the ceiling of the facility. All data included within this study are derived from 'stack' burns, where by the fuel bed is located directly below the exhaust stack in the centre of the chamber and emissions drawn up the stack through a 3.6 m diameter inverted funnel. Gas

phase instrumentation included a Li-Cor Model 6262 nondispersive infrared gas analyser for CO_2, a Thermo Environmental Model 48C variable-range gas filter correlation analyser for CO and Thermo Environmental Model 42 chemiluminescence analyser for NO_x (NO and NO_2). These instruments were located on a platform at a height of 17 m above the chamber floor, drawing samples through ports in the wall of the exhaust stack. The AMS was located in a laboratory adjacent to the combustion chamber, with a sample line running from the platform-level exhaust stack port down to ground level. This increased distance between the sampling port and instrument resulted in an offset of approximately 30 seconds between the AMS and gas phase instrument time series (*Lee et al., 2010*), which was corrected during data processing.

In total, data from 67 burns performed during FLAME were included in this analysis. Fuels involved in the burns included 19 species across 6 fuel types, comprising a number of fuel components as summarised in Table 1. The 6 fuel types represent key environments forming a major contribution to biomass burning within the U.S., namely montane forests, rangeland, chaparral, coastal plains and boreal forests. A more extensive description of the fuels used during FLAME is provided by *McMeeking et al.* (*2009*). Montane forest fuels comprised a range of ponderosa pine (*Pinus ponderosa*) and Douglas fir (*Pseudotsuga menziesii*) components, including needles, branches and sticks in both fresh and dry states. These species are widespread across the Sierra Nevada, Cascade and Rocky mountain ranges across the west and northewestern U.S., although samples used during FLAME were obtained from rural locations close to the FSL in Missoula, Montana. Rangeland ecosystems dominated by sagebrush (*Artemisia tridentata*) are common across the arid and semi-arid habitats of the inter-mountain west, with samples taken from urban sites near Salt Lake City, Utah, and rural areas near Missoula. Chaparral represents a further shrubland ecosystem widespread throughout the western U.S., ranging from Baja California in the south to southern Oregon at the northern extent. Characteristic species include Eastwood's manzanita (*Arctostaphylos glandulosa*), hoaryleaf ceanothus (*Ceanothus crassifolius*) and chamise (*Adenstoma fasciculatum*).

Samples were collected from the San Jacinto Mountains, and exhibited highly variable properties, with chamise in particular exhibiting the widest range of moisture content for a single species within all fuels used throughout the experiment (11.2 – 57.4 %). Several species common to the varied ecosystems of the coastal plain regions of the southeastern U.S. were collected from sites in Florida, Mississippi, Georgia and North Carolina. Shrubs including palmetto (*Serenoa repens*), gallberry (*Ilex coriacea*), and wax myrtle (*Myrica cerifera*) were burned either independently or combined with samples from other species. These included trees, such as longleaf pine (*Pinus palustris*), hickory (*Carya nutt*) and turkey oak (*Quercus laevis*), grass species including wiregrass (*Aristida beyrichiana*) and saw grass (*Cladium mariscus*), along with black needlerush (*Juncus roemerianus*) and the invasive vine species kudzu (*Pueraria montana*). In addition to the range of fuels representing U.S. ecosystems, samples of rice straw (*Oryza sativa*), an agricultural waste product widely burned across southeast Asia, were obtained from a site near Douliou City, Taiwan.

During all stack burns throughout FLAME II, fuels were positioned on a 46 x 61 cm metal tray below the exhaust stack. A selection of fuels that had not dried sufficiently after collection were dried at a temperature of 35 – 40˚C for a period of 2 to 3 days prior to combustion, while others received no additional treatment in order to maintain fuels as close as possible to fresh condition. Despite this lack of additional drying, water will have been lost from fuels during transport and storage to give lower moisture contents than would be expected under natural conditions. Although these fuels remain closer to their fresh state, they cannot be considered entirely representative of fuel properties in the wild. Similarly, the use of fuel samples from a number of different locations may also introduce further variability, given possible differences in plant morphology or composition due to changing environmental or growing conditions. As such, resulting combustion behaviour is likely to differ somewhat from that of wildfires. However, contrasting fuel properties constitute only part of the broader discrepancy between ambient and laboratory fires, with additional factors such as fuel

mass, fire size and meteorological conditions also affecting resultant emissions, providing an intrinsic caveat to any comparison between experiment types.

In order to give uniform ignition across the fuel bed, burns were initiated by a lattice of ethanol-soaked heating tape upon which the fuels were laid, with the exception of Alaskan duff samples, which required continuous application of a propane torch to maintain combustion. Fuel mass was measured throughout the duration of each burn, with the fuel bed situated on a Mettler-Toledo PM34 balance. However, the balance was likely to have been affected by convection and resulting positive buoyancy during fires, giving unreliable measurements. As a result additional measurements of the initial fuel mass prior to combustion and the final residual mass at the end of each burn were performed using a Mettler-Toledo PM34-K balance.

Initial processing of gas phase and AMS data from FLAME II involved the calculation of excess concentrations with regard to background concentrations within the chamber. These excess concentrations were then used to calculate instantaneous $\triangle OA/\triangle CO$ values, along with time series of MCE and key AMS mass fragment ratios. Burn average values for all parameters were calculated using the trapezoidal average for the duration of the burn from ignition to end, in accordance with the timings at which filter sampler pumps were switched off based on visual observations. Where multiple burns of a single species were performed, the calculated single burn values were averaged across all burns to give species averaged values.

3. Results and discussion

3.1 Overview of $\triangle OA/\triangle CO$ during FLAME II

Burn-averaged $\triangle OA/\triangle CO$ throughout FLAME II exhibited a high level of variability, ranging from 0.004 to 0.850 from 67 fires. A summary of $\triangle OA/\triangle CO$ for each fuel type and species is given in Table 2. Significant contrasts in emissions were identified both between separate burns of the same fuel type and between different fuel types, as shown in Figure 1.

The lowest average △OA/△CO was observed for a gallbery burn, and the highest for fresh Douglas fir needles. The high values observed for Douglas fir burns provided the only instances of average △OA/△CO greater than 0.5, resulting in the largest range between maximum and minimum values (0.837) occurring for montane forest fuels, for which several particularly low values were also derived from ponderosa pine needle burns. The smallest range in burn-averaged △OA/△CO was identified for chaparral fires, at just 0.066. Average values for fuel types ranged from 0.232 (montane forest) to 0.037 (chaparral). This range is comparable to the difference identified between ambient measurements of fresh OA across a number of environments (*Jolleys et al., 2012*).

Figure 2 shows that flaming combustion is more frequently associated with low △OA/△CO, with 24 of 32 burns for which the average MCE was 0.9 or above yielding △OA/△CO values less than 0.1. For burns where smouldering combustion dominates (average MCE < 0.9), average △OA/△CO was less than 0.1 for only 12 of 35 burns. Average △OA/△CO values exceeding 0.3 were also observed only for smouldering-dominated fires. However, there is no strong overriding relationship between burn averaged △OA/△CO and MCE across all FLAME II experiments. The correlation coefficient for the linear regression between △OA/△CO and MCE is just 0.075, reflecting the inconsistency of △OA/△CO under both combustion phases. There is also little correlation between the observed variabilities for △OA/△CO and MCE (Figure 2). The widest ranges between highest and lowest average MCE occur for montane forest (0.141) and coastal plain (0.136) fuels, where as the respective ranges of △OA/△CO (0.837 and 0.460) show greater disparity. Rangeland and chaparral fuels also show highly contrasting levels of variability in △OA/△CO (0.325 and 0.066) despite similar ranges in average MCE (0.072 and 0.064). Variability in △OA/△CO appears to ultimately depend more on differences in OA emissions than those of CO. A fairly strong linear relationship exists between △OA/△CO and △OA (R^2 = 0.578). In contrast, there is no correlation between △OA/△CO and △CO, with an R^2 of less than 0.001. These

contrasting relationships indicate that variability in △OA/△CO is driven more by changes in △OA, and as such by the fuel properties and burn conditions which influence OA production.

Total OA concentrations measured during FLAME II are a function of partitioning of organic species between the gas and particle phase (*McMeeking, 2008*). As partitioning of semi-volatile organic compounds (SVOCs) is strongly dependent on dilution (*Donahue et al., 2006*), concentrations from laboratory fires consistently exceed those from ambient measurements, as a result of limited mixing with background air. However, emissions of SVOCs from BB may represent a substantial source of OA following partitioning in aging plumes, but are currently unaccounted for in assessments of OA contributions using △OA/△CO. The proportions of total organic emissions which are emitted in the gas and particle phase for different fuels may therefore have a significant influence on observed △OA/△CO variability. Total observed organic carbon (TOOC) is used as a measure of overall emissions of organic species which can be quantified with current measurement capabilities (*Heald et al., 2008*). Although measurements of gas phase species were performed during FLAME II, these were limited to C_{1-4} hydrocarbons, and subsequently do not provide a full representation of SVOC emissions (*McMeeking, 2008*). Measurements of a wider range of SVOCs would improve the representation of TOOC, which could in turn be used to calculate ERs providing a more comprehensive measure of potential OA emissions from biomass fires.

3.2 Drivers of △OA/△CO variability

3.2.1 Influence of combustion processes

The main advantage provided by AMS data over previously analysed filter samples is the ability to examine changes in emissions and their response to changing combustion conditions throughout experiments. Both flaming and smouldering phases were observed for the majority of burns, often driving a significant shift in emissions. Changing emissions regimes would also be expected to be directly affected by both the fundamental differences in

morphology and composition between different species, and the ways in which fuel samples had been prepared. In some instances, changing the mass or moisture content of a fuel, even for samples of the same species, had an appreciable effect on resultant △OA/△CO levels. However, other examples show greatly contrasting △OA/△CO despite near identical initial conditions. Burns 205 and 206 both used dry ponderosa pine needles with a moisture content of 8.7%, with respective consumed masses of 205 and 211 g and burn durations of approximately 8 minutes. The average △OA/△CO for burn 205 was 0.488 ± 0.498, while for burn 206 the value was just 0.031 ± 0.036. Respective average MCEs were 0.863 ± 0.084 and 0.926 ± 0.059, indicating a shift in the dominant combustion phase. Time series for the two burns are shown in Figure 3, revealing that the timing of the transition between flaming and smouldering phases may have been a critical factor in determining the two conflicting ratios. Both burns begin with a strongly flaming phase, with MCE values close to 1. After approximately 2 minutes, the MCE for burn 205 rapidly declined, marking an abrupt transition to smouldering combustion. This transition coincides with a dramatic increase in OA concentration, rising from around 3000 to over 17000 μg m^{-3} within 30 seconds. During this time △OA/△CO increases from 0.309 to 1.587. In contrast, MCE during burn 206 remained above 0.95 for nearly 4 minutes. The transitions in each burn occurred at a point when a similar proportion of the initial fuel mass, 33 and 34% respectively, had been consumed. Given the shorter flaming phase, the similar levels of fuel consumption suggest that burn 205 was more intense, consuming the same amount of fuel in roughly half the time. This apparent contrast in fire intensity is likely to have been the main cause of the exceptional difference in average △OA/△CO. Previous studies indicate that increased fire intensity during the flaming phase can lead to oxygen deprivation in the interior of a fire, increasing particle production (*Reid et al., 2005*). As particle formation during the smouldering phase primarily involves condensation of volatile compounds onto existing particles (*Ward, 1990*), elevated production during the flaming phase would provide a greater abundance of available condensation nuclei,

and may therefore provide the basis for the rapid and substantial rise in OA concentrations as identified during burn 205.

The previous cases illustrate the potential magnitude of the influence that MCE can have on △OA/△CO. However, such dramatic effects were not typical throughout FLAME II as a whole. Figure 4 shows real-time △OA/△CO values plotted against MCE for all fuel types, revealing an absence of any consistent relationships between the two parameters. Despite this overriding variability, some underlying trends can be identified between △OA/△CO, MCE and other potential drivers affecting fire emissions. Clear discrepancies are apparent in the relationships between △OA/△CO and MCE for different fuel types, species and components. Both ponderosa pine and Douglas fir show highly variable △OA/△CO values across a similarly broad range of MCEs between around 0.6 and 1. However, there are also several significant differences between the two montane forest fuels. There are very few instances of △OA/△CO values greater than 0.5 from ponderosa pine fires, while higher ratios are more frequently observed for Douglas fir fires. This disparity is reflected in the respective averages and standard deviations across all burns, which stand at 0.139 ± 0.190 for ponderosa pine and 0.395 ± 0.336 for Douglas fir. The greater variability for Douglas fir emissions coincides with a reduced variability in MCE, with a mean of 0.907 ± 0.069, compared to ponderosa pine (0.894 ± 0.099). Segregating flaming and smouldering phases also reveals contrasting offsets in △OA/△CO between phases for each species. Mean △OA/△CO values for periods of flaming and smouldering combustion were 0.047 ± 0.089 and 0.170 ± 0.238 respectively for ponderosa pine, while averages for Douglas fir were closer at 0.417 ± 0.349 and 0.514 ± 0.441. Although emphasising a general enhancement in △OA/△CO during smouldering combustion in both cases, these differences highlight the consistently greater variability associated with emissions from the laboratory Douglas fir fires, particularly when compared to the level of consistency observed for the flaming phase of the laboratory ponderosa pine fires. △OA/△CO for both species generally remained below 0.5 when MCE was less than 0.8, suggesting that production of OA eventually becomes less favourable for

increasingly smouldering-dominated combustion, which is possibly linked to a reduction in fire intensity.

3.2.2 Influence of fuel properties

Contrasts in emissions properties between combustion phases also extend to different components of the same species and, moreover, to the different physical properties of these components. Figure 5 shows the relationships between burn averaged △OA/△CO and MCE for each plant component used during FLAME II. Trends in △OA/△CO vary between fuel types and species, and are more apparent for certain fuels. Coniferous fuels, from both montane and boreal forests, generally show a more linear decrease in △OA/△CO with increasing MCE, although the gradient of this trend varies between species and components. Fires involving only woody material rather than needles are dominated by flaming combustion, with average MCEs uniformly above 0.9, yielding consistently low △OA/△CO. Average ratios were below 0.03 for all burns involving ponderosa pine sticks, and below 0.11 for Douglas fir branches. Far greater variability is evident when burning needles of either species. Average △OA/△CO ratios for two smouldering-dominated fires (MCE = 0.862 ± 0.131 and 0.886 ± 0.061) involving fresh Douglas fir needles (moisture content = 42.1%) were 0.850 ± 0.446 and 0.766 ± 0.304, while for dry needles under more strongly flaming combustion (moisture content = 20.9%, MCE = 0.911 ± 0.046) the average was just 0.062 ± 0.086. A similar trend was also observed for combinations of needles and branches, for which the maximum average △OA/△CO and minimum MCE resulted from a fire involving fresh components (burn 170; △OA/△CO = 0.738 ± 0.282, MCE = 0.895 ± 0.034). This relationship with fuel moisture content is consistent with the larger variability in △OA/△CO observed for Douglas fir fuels. Moisture content ranged from 20.7 - 51.2%, where as for ponderosa pine fuels the range was just 6.9 - 9.2%, contributing to a much reduced level of variability. However, average values for the one other fresh needle/branch fire (burn 171; 0.298 ± 0.239/0.918 ± 0.036) were more closely comparable to those for dry fuel (burn 169; 0.279 ± 0.158/0.937 ± 0.23). Despite the similarity in ERs for burns 169 and 171, the former was characterised almost entirely by

flaming combustion, while the latter was subject to equal flaming and smouldering phases. Mean △OA/△CO throughout the two phases is markedly different, at 0.443 ± 0.228 and 0.081 ± 0.048 respectively. Contrary to the observed trend for burn averages, higher mean △OA/△CO, and associated standard deviations, for the flaming phase are a common feature of all Douglas fir fires. This disparity between trends in fire behaviour for single burns in isolation and the aggregation of multiple burns highlights how smaller scale properties can be masked when viewed across a broader scale, and may be considered analogous to aircraft observations and their relationship to the contributions from numerous separate fires.

The extensive variability present throughout montane forest burns is not replicated across all fuel types. Although such contrasting behaviour may in part be a result of the smaller number of samples available for some fuels, and subsequent reduced variation of source conditions and repeat burns, some systematic differences between fuel types are evident. Chaparral fuels exhibited highly consistent average △OA/△CO across three different species, with a range of only 0.066 far lower than that identified for any other fuel type. Leaf and grass samples from coastal plain species also always yielded average values below 0.1, with the exception of two turkey oak fires, for which anomalously high averages of 0.320 ± 0.253 and 0.464 ± 0.371 were observed. Despite this limited variability in △OA/△CO, chaparral and coastal plain fires are characterised by a broad range of average MCEs. The range of MCEs for chaparral burns (0.849 – 0.913) is comparable to that of rangeland burns (0.832 – 0.905), for which △OA/△CO was far more variable, with a difference of 0.325 between minimum and maximum average values. This greater variability for rangeland fires also stemmed from the use of a single species, sagebrush, in contrast to the three chaparral species of manzanita, ceanothus and chamise. While the moisture content of montane forest fuels, and in particular needles, seemed to have a significant effect on resulting emissions profiles, it appears to have little bearing on either chaparral or rangeland fuels. Chaparral samples exhibited a wider range of moisture contents than rangeland samples,

confounding the observed distributions of △OA/△CO, with no overriding relationship between △OA/△CO and moisture content identified for either fuel type.

3.2.3 Oxygenation of OA

Although the inconsistencies identified in the effects of potential drivers of △OA/△CO variability are likely to be influenced to an extent by the inherent unpredictability of fires, there is evidence to suggest additional processes during combustion may also be a significant factor. The *m/z* 44 fragment measured by the AMS is strongly associated with the CO_2^+ ion derived from oxygenated organic compounds (*Alfarra et al., 2004; Aiken et al., 2008*). When expressed relative to the total OA mass concentration, this ratio (f_{44}) can be used as an indicator of the extent to which OA is oxidised. While primarily used as a tracer for secondary OA, *m/z* 44 has also been shown to form a significant component of primary OA from wood burning (*Alfarra et al., 2007; Weimer et al., 2008*). For measurements of OA composition directly at source, as were performed during FLAME II, changes in f_{44} are more likely to reflect the influence of combustion processes rather than subsequent heterogeneous oxidation given the short ageing times involved. For all burns where comparison between phases was possible, mean f_{44} was higher for flaming combustion in 40 burns, and for smouldering combustion in 21 burns. This greater frequency of increased f_{44} during flaming combustion is in contrast to the findings of *Weimer et al.* (*2008*), who showed f_{44} to be consistently higher for smouldering combustion, attributing this trend to the dominance during the flaming phase of primary hydrocarbon fragments, prior to the biopolymers from which they derive becoming progressively depleted. The correlation between f_{44} and MCE appears to be highly dependent on fuel type, with any relationship between the two only evident for coniferous species from montane and boreal forests, and also for the few rice straw burns included here (Figure 6). Real-time measurements also indicate that this relationship of increasing f_{44} with MCE may be further restricted to fires involving needles, given that no trend is maintained where only sticks or branches from montane forest species were burned. It is difficult to assess the significance of fuel composition with regard to relationships with

coniferous species, as an extensive characterisation of fuel constituents was not performed. Only total carbon and nitrogen contents were determined, which remained fairly consistent across different fuel types and did not show any strong correlation with emissions properties. Fuel composition has been shown to be an influential factor in determining emissions of inorganic gas-phase and particulate emissions from BB events (*Keene et al., 2006; McMeeking et al., 2009; Burling et al., 2010*). A dependence on fuel composition has previously been reported for organic compounds emitted from combustion of a range of biofuel pellets (*Olsson, 2006*), with concentrations of methoxyphenols, derived from lignin, and anhydroglucose and furan-related compounds originating from fuel polysaccharides varying between different fuel types. However, wider implications for OA emissions, including the overall magnitude and oxygenation of emissions, are not well defined.

Despite the limited dependence on combustion behaviour, f_{44} appears to be strongly correlated with $\triangle$OA/$\triangle$CO across all fuel types. Figure 7 shows a near exponential decrease in $\triangle$OA/$\triangle$CO with f_{44} over a range of 0.017 to 0.101. The highest average $\triangle$OA/$\triangle$CO values all coincide with an average f_{44} of less than 0.03, while $\triangle$OA/$\triangle$CO does not exceed 0.15 when f_{44} is greater than 0.05. Distributions of real-time f_{44} values are also in agreement with the $\triangle$OA/$\triangle$CO profiles of certain fuel types and components. f_{44} nearly always exceeds 0.04 for chaparral fires, along with those involving woody coniferous components. In contrast, the vast majority of f_{44} values for high-$\triangle$OA/$\triangle$CO ponderosa pine and Douglas fir fires fall below this threshold. Variations in f_{44} also show good agreement with the differences in emission profiles for separate burns of the same species or component. All ponderosa pine burns with an average $\triangle$OA/$\triangle$CO above 0.1 also had an average f_{44} of less than 0.03, while all lower $\triangle$OA/$\triangle$CO averages coincide with higher f_{44}. The same inverse correlation exists for Douglas fir burns, with burns 165, 166 and 170 exhibiting the highest $\triangle$OA/$\triangle$CO and lowest f_{44}, although f_{44} is uniformly higher than for ponderosa pine across all burns and never falls below 0.024. Further concordance can be seen for rangeland and boreal forest fuels, for which average $\triangle$OA/$\triangle$CO consistently lies above respective thresholds of 0.2 and 0.1 when

average f_{44} is below 0.04 and 0.035. These repeated trends between levels of oxygenation and the proportional magnitude of OA production further emphasise the importance of fire efficiency, such that as completeness of combustion and the capacity to fully oxidise combustion products increases, yields of OA decrease accordingly. It would therefore appear that OA formation is highly sensitive to the availability of oxygen during a burn, which is largely determined by the level of turbulent mixing occurring (*Ward, 1990*), and hence influenced by wider combustion conditions such as fire phase and intensity. However, the relationship between $\triangle$OA/$\triangle$CO and f_{44} does show some inconsistency, including the contrasting thresholds between regimes of high and low OA production between different species. This deviation is particularly evident for coastal plain fuels, which involved the largest number of species. As a consequence of this diversity, no apparent trends are observed, indicating that any relationship is likely to be influenced also by both fuel composition and morphology, as well as oxygen availability and fire dynamics.

3.3 Typical fire behaviour for multiple burns

The considerable variability associated with $\triangle$OA/$\triangle$CO and the various drivers influencing it are complicated by the chaotic nature of fires, and any attempts to provide a characterisation of OA emissions from biomass burning emissions are underpinned by this uncertainty. However, assessing broader trends for similar burns can give an indication of the more typical behaviour of different fuels. Figure 8 shows the contrasts in $\triangle$OA/$\triangle$CO under differing conditions when averaged across multiple burns. The ability to trace changes in $\triangle$OA/$\triangle$CO across a full range of conditions is limited by the number of fires included in the study and the incomplete distribution of different behaviours. Nevertheless, a number of trends are evident for certain fuel types, which are generally consistent with previous observations. When averaging $\triangle$OA/$\triangle$CO by moisture content bins, there is a positive correlation for Douglas fir needles and needles/branches, with the former increasing from 0.062 ± 0.086 to 0.808 ± 0.350 and latter from 0.279 ± 0.158 to 0.518 ± 0.314. Sagebrush

fires also show a similar relationship, although △OA/△CO begins to decline when moisture content increases beyond 30%. In contrast, an inverse correlation is observed with both f_{44} and MCE. Bin-averaged △OA/△CO decreases with f_{44} for ponderosa pine needles and sticks, Douglas fir needles/branches, sagebrush, chamise, palmetto, gallberry and sawgrass. The same trend exists with MCE for Douglas fir needles and needles/branches, longleaf pine and black spruce. Ponderosa pine needle fires show decreasing △OA/△CO with MCE for bins of 0.8 and above, although △OA/△CO is lower when MCE is below 0.8, possibly indicating a minimum threshold below which fire efficiency is reduced to an extent that OA production is eventually inhibited. Sagebrush fires show a trend of increasing average △OA/△CO with MCE, although the magnitude of change is considerably smaller than those associated with coniferous species. There is little evidence to support any relationships between △OA/△CO and fire duration, consumed mass or mass consumption rate, with conflicting trends observed for different components of the same fuel type and an overall lack of consistency between species. Although similar discrepancies are evident to some extent with moisture content, f_{44} and MCE, overall trends are generally more uniform with respect to these conditions. This increased consistency is particularly notable for the relationship with f_{44}, where △OA/△CO was shown to progressively decrease for all species for which ratios could be calculated across multiple bins.

3.4 Comparison of laboratory and ambient observations

Average values calculated across multiple laboratory burns represent a more appropriate comparison with field observations, as the identified contrasts in emission properties are likely to reflect the different sampling conditions involved in each set of experiments, and more specifically the aggregation of multiple plumes from different fires for ambient measurements. While the scale of the range in average △OA/△CO between fuel types is comparable to that from ambient measurements, differences between burns throughout FLAME II far exceed those between separate measurement periods during four

field campaigns (Figure 1). Using the plume classification described by *Jolleys et al.* (*2012*), ranges in average △OA/△CO for fresh emissions during the Megacities Initiative: Local and Global Research Observations (MILAGRO) campaign (0.035) and the Dust and Biomass Experiment (DABEX; 0.028) were shown to be lower than that occurring for chaparral burns, which represented the smallest variability for a single fuel type. Although a wider range was observed during the Aerosol and Chemical Transport in Tropical Convection (ACTIVE) campaign (0.282), this was enhanced by a single exceptional value and remained well below the variabilities exhibited by montane forest, coastal plain and rangeland fuels. Part of this discrepancy may be attributable to the contrasting conditions between laboratory and ambient fires, and the implications for fire behaviour and emissions. However, it may also be the case that such variability in emissions does occur for real fires, but that ambient sampling is unable to adequately capture its full extent, or that sampled plumes represent an aggregation of different fires and conditions, which when taken in isolation may provide a similar level of variability as that identified for chamber burns.

Despite the differing conditions, relating to both combustion and sampling processes, several comparisons can be drawn between observations from laboratory and ambient fires. Potential behaviours associated with certain plant types identified from analysis of FLAME II experiments may also be pertinent to wildfire emissions. The mountain slopes below the Paso de Cortes are dominated by Hartweg's pine (*Pinus hartwegii*), and as such the △OA/△CO levels observed for fresh OA emissions during MILAGRO may have been expected to be of a similar magnitude to those identified for montane forest species. However, the average △OA/△CO for fresh OA during MILAGRO (0.051 ± 0.001) is consistent with only the lower end of burn average values for montane forest fuels, typically associated with dry woody materials, and is significantly lower than the elevated △OA/△CO values identified for other montane fuel components. The treeline at Paso de Cortes is located below the Altzomoni measurement site (4010m; *Baumgardner et al., 2009*) at around 3700 m, with higher sections dominated by subalpine zacaton grasses such as *Festuca tolucensis* and *Muhlenbergia*

quadridentata (*Beaman, 1962*), which are well correlated with the occurrence of wildfires (*Rodríguez-Franco, 2002*). Grasses burned during FLAME II typically yielded very low △OA/△CO values (<0.1). The potential inclusion of similar fuels in wildfires during MILAGRO may therefore have contributed to the relatively low average ER. Maximum ambient △OA/△CO was associated with fires in the eucalyptus forests of northern Australia during ACTIVE, and as such the vegetation types involved were not directly comparable to the montane forest species providing the highest ratios during FLAME II.

The comparably low average △OA/△CO of 0.065 ± 0.002 for fresh OA during DABEX would also appear to reflect the influence of grassland fires. Fresh BB plumes were encountered during research flights covering an area from approximately 8 - 13.5°N and 1.5 - 6°E. This region of West Africa encompasses a number of different ecosystems, from forest-savanna mosaic in the south, through the southern and northern Guinea zones to the Sudan zone in the north, fringing the Sahel. Dominant plant species, together with overall ecosystem structure and physiognomy, vary considerably between each zone. However, continuous layers of tussocky grasses below trees are a common feature, leading to widespread fires during the dry season between December and February (*Sanford & Isichei, 1986*). The open and dry vegetation found throughout the savanna provides the optimal conditions for wildfires throughout the region, with more dense forests less conducive to fires (*Sowunmi, 1986*).

Forest-savanna mosaics are derived from the more extensive lowland rainforests in the south of the region, where human activity has caused the opening of the forest canopy, allowing grasses to colonise the forest floor resulting in areas of savanna forming between the remaining forest stands (*Lawson, 1986*). Forests located close to the forest-savanna boundary are typically drier than those further to the south and are characterised by varieties of mulberry (*Moraceae* spp.), mallow (*Malvaceae* spp.) and trema (*Ulmaceae* spp.) (*Hopkins, 1965*). The southern Guinea zone marks the transition between forest and savanna systems, comprising open savanna woodland and long grasses, typically between 1.5 and 3 m tall (*Sanford & Isichei, 1986*). Characteristic tree species include African mahogany (*Afzelia*

africana), red heart (*Hymenocardia acida*), black plum (*Vitex doniana*), red oak (*Lophira lanceolata*) and Ilorin balsam (*Daniellia oliveri*), with thorny staff (*Maytenus senegalensis*) and Christmas berry (*Psorospermum febrifugum*) common shrubs.

Distribution of trees in the southern Guinea zone is typically more mixed than in the northern zone, where stands are more widely found to consist of a single species. Isoberlinia woodlands (*Isoberlinia doka* and *I. tomentosa*) dominate, while sweet detar (*Detarium microcarpum*), wild seringa (*Burkea africana*), *Monotes kerstingii, Uapaca togoensis, Terminalia avicennioides* and *Parinari polyandra* are also widespread, along with the shrubs *Grewia mollis*, *Protea elliotti*, African custard-apple (*Annona senegalensis*), bush willows (*Combretum* sp.) and yellow plum (*Ximenia americana*). Grasses are typically shorter in the northern zone, but maintain a minimum height of around 1.2 m (*Sanford & Isichei, 1986*). Wild oatgrass (*Monocymbium ceresiiform*), gamba grass (*Andropogon gayanus*), beard grass (*Andropogon pseudapricus*), thatching grass (*Hyparrhenia* spp.), fountain grass (*Pennisetum* spp.), bluestem grass (*Schizachyrium* spp.) and *Beckeropsis uniseta* represent the dominant grasses throughout the Guinean savanna, while the trees *Cassonia barteri*, mupundu (*Parinari curatellifolia*), bushwillows (*Combretum* spp.), *Caesalpinioideae* spp. and *Terminalia* spp., and shrubs wild bauhinia (*Piliostigma thonningii*), pink jacaranda (*Stereospermum kunthianum*) and *Gardenia* spp. are also equally common throughout both zones (*Hopkins, 1965*).

The northernmost savanna surveyed by DABEX flights was the Sudanian zone, which is dominated by *Isoberlinia* and *Acacia* spp. Trees are more widely spaced than in the Guinean zone, and grasses are usually shorter than 1.2 m (*Sanford & Isichei, 1986*). The Sudanian zone is also more heavily populated than other zones to the south, and as a result has been much more extensively farmed. Valued species have been widely introduced or preferentially retained, including shea (*Vitellaria paradoxa*), locust bean (*Parkia clappertoniana*) and baobab (*Adansonia* sp.) (*Lawson, 1986; Sanford & Isichei, 1986*). The majority of fresh plumes encountered during DABEX were located within a region between 9 – 11˚N, 3 - 6˚E (*Johnson et al., 2008*) within the extent of the Sudanian zone (*Kamara et al., 2009*). *Johnson et al.* (*2008*)

reported the prevalence of agricultural fires throughout the region, of which grasses were expected to be a significant component. The presence of a continuous herbaceous layer throughout the wider ecosystem further increases the likelihood that grasses were a common fuel in the DABEX fires, which may have contributed to the lower average △OA/△CO consistent with grass burns during FLAME II.

4. Conclusions

Highly variable burn-averaged △OA/△CO have been calculated for 67 fires carried out during the FLAME II experiment, involving a number of fuel types which comprise a major contribution to annual US biomass burning. Plant species representing montane forest, rangeland, chaparral, coastal plain and boreal forest environments, as well samples of agricultural residues, yielded respective averages of 0.232, 0.214, 0.037, 0.090, 0.112 and 0.199. The extent of this variability in △OA/△CO far exceeds the levels identified from measurements of BB plumes close to source during field campaigns, particularly for coniferous montane forest fuels, for which the widest range of average values was observed. In some instances fires involving similar fuels and initial conditions were found to produce highly contrasting emissions, with this disparity attributed to the effects of differing fire evolution and the subsequent changing influence of combustion processes on OA formation. While such changes in fire intensity and efficiency have the potential to significantly alter △OA/△CO levels, even for the same species and fuel components, examples of such behaviour are limited and would appear to be an extreme example. Different components of the same species were more commonly found to provide a greater contrast in △OA/△CO, as widely identified between fires involving needles and more woody materials for montane forest fuels. No overriding relationships between △OA/△CO and MCE across all burns were identified, while there is little consistency in the observed variabilities in each property amongst single fuel types. However, underlying trends were identified for specific vegetation types or plant components. A dependence on MCE was more apparent for coniferous species, and most

notably Douglas fir samples, with an indication that this relationship is further influenced by differences in fuel moisture content. In contrast chaparral fuels showed little variation in average △OA/△CO, despite fires exhibiting average MCEs over a wide range. The extent of this range was comparable to those observed for rangeland and boreal forest fuels, for which variability in △OA/△CO was significantly increased.

Processes affecting the oxygenation of OA appear to be closely linked to △OA/△CO levels from fires. Real-time measurements during FLAME II show a consistent decrease in △OA/△CO with increasing f_{44}, while f_{44} is also more frequently elevated during periods of flaming combustion. As f_{44} is likely to be a function of fire intensity and the availability of oxygen, this relationship provides a further indication of the influence of combustion processes in determining △OA/△CO. However, the inconsistencies in relationships with various potential drivers emphasise the inherent variability associated with fire emissions. In the absence of evidence to support any overriding control on OA production, it would appear that emissions from biomass burning are highly sensitive to both what is being burned and how combustion occurs. These influences are expected to remain consistent for fires under ambient conditions, although the full extent of their influence is likely to be masked by the contribution of multiple fires to sampled plumes, resulting in the lower magnitude of variability in △OA/△CO identified for field campaigns relative to laboratory fires.

More widespread study of a broader range of fire types, under both laboratory and ambient conditions, is required in order to more accurately constrain the influence of fuel types and combustion processes in controlling fire emissions. Underlying causes of the variability in BB emissions remain highly uncertain, and while results from the FLAME II experiment give an indication of potential drivers, understanding of specific relationships is limited. For example, the timing of the transition between flaming and smouldering phases during fires has been shown to be a critical influence on OA emissions, producing hugely variable ERs for near-identical fuel samples, but the processes affecting this transition under similar fuel conditions are unclear. These influences could be examined more extensively

within future research efforts by applying stricter controls to source conditions throughout laboratory experiments, in order that variation of a single desired property can be more closely scrutinised. It has not been possible to provide an exhaustive characterisation of the composition of fuels used throughout FLAME II, yet this is likely to have a significant effect on resulting OA emissions. Similarly, an influence of oxygen availability on OA production is apparent from these experiments, but any such effect is not well quantified. Processing fuels to a uniform state with consistent mass, morphology and moisture content would remove any variability associated with these properties, while performing burns at a fixed fuel:air ratio within a controlled combustor would ensure combustion conditions remained comparable across different fuel types. If such an approach were to yield similar ERs, fuel and combustion properties could then be altered to determine the implications of changing these parameters for $\triangle OA/\triangle CO$ variability. As experiments of this type are solely concerned with analysis of fundamental combustion processes and their determining factors, there is only limited applicability to ambient fire emissions. Further investigation of biomass fires under laboratory conditions could therefore also contribute towards improving understanding of variability in BB emissions from open burning. With regard to the specific limitations of the FLAME II experiment, more extensive replication of burns with similar initial conditions would enable the influence of combustion processes to be examined in greater depth, while widening the range and variation of fuel properties would enable further analysis of the variability within single fuel types.

Acknowledgments

The authors would like to acknowledge financial support from the United Kingdom Natural Environment Research Council (NERC). M. D. Jolleys was supported by a NERC studentship NE/H525162/1. We also thank the USFS Fire Science Laboratory staff for their assistance during the FLAME II campaign and to a large number of individuals for providing fuels. J. L. Collett, T. Lee, G. R. McMeeking and S. M. Kreidenweis gratefully acknowledge support for this work from the National Park Service under NPS CA2380-99001 TO0356, the US Joint Fire Science Program under JFSP 05-3-1-06, and the US Environmental Protection Agency STAR program through the National Center for Environmental Research (NCER) under grant R833747. Although the research described in this article has been funded in part by the United States Environmental Protection Agency, it has not been subjected to the Agency's required peer and policy review and therefore does not necessarily reflect the views of the Agency and no official endorsement should be inferred.

References

Aiken, A. C., et al. (2008), O/C and OM/OC ratios of primary, secondary, and ambient organic aerosols with high-resolution time-of-flight aerosol mass spectrometry, *Environmental Science & Technology*, *42*(12), 4478-4485, doi:10.1021/es703009q.

Akagi, S. K., et al. (2012), Evolution of trace gases and particles emitted by a chaparral fire in California, *Atmospheric Chemistry and Physics*, *12*(3), 1397-1421, doi:10.5194/acp-12-1397-2012.

Akagi, S. K., R. J. Yokelson, C. Wiedinmyer, M. J. Alvarado, J. S. Reid, T. Karl, J. D. Crounse, and P. O. Wennberg (2011), Emission factors for open and domestic biomass burning for use in atmospheric models, *Atmospheric Chemistry and Physics*, *11*(9), 4039-4072, doi:10.5194/acp-11-4039-2011.

Alfarra, M. R., et al. (2004), Characterization of urban and rural organic particulate in the lower Fraser valley using two aerodyne aerosol mass spectrometers, *Atmospheric Environment*, *38*(34), 5745-5758, doi:10.1016/j.atmosenv.2004.01.054.

Alfarra, M. R., A. S. H. Prevot, S. Szidat, J. Sandradewi, S. Weimer, V. A. Lanz, D. Schreiber, M. Mohr, and U. Baltensperger (2007), Identification of the mass spectral signature of organic aerosols from wood burning emissions, *Environmental Science & Technology*, *41*(16), 5770-5777, doi:10.1021/es062289b.

Andreae, M. O., and P. Merlet (2001), Emission of trace gases and aerosols from biomass burning, *Global Biogeochemical Cycles*, *15*(4), 955-966.

Baumgardner, D., M. Grutter, J. Allan, C. Ochoa, B. Rappenglueck, L. M. Russell, and P. Arnott (2009), Physical and chemical properties of the regional mixed layer of Mexico's Megapolis, *Atmospheric Chemistry and Physics*, *9*(15), 5711-5727.

Beaman, J. H. (1962), Timberlines of Iztaccihuatl and Popocatepetl, Mexico, *Ecology*, *43*(3), 377-&, doi:10.2307/1933367.

Bond, T. C., D. G. Streets, K. F. Yarber, S. M. Nelson, J. H. Woo, and Z. Klimont (2004), A technology-based global inventory of black and organic carbon emissions from combustion, *Journal of Geophysical Research-Atmospheres*, *109*(D14), doi:10.1029/2003jd003697.

Burling, I. R., et al. (2010), Laboratory measurements of trace gas emissions from biomass burning of fuel types from the southeastern and southwestern United States, *Atmospheric Chemistry and Physics*, *10*(22), 11115-11130, doi:10.5194/acp-10-11115-2010

Burling, I. R., R. J. Yokelson, S. K. Akagi, S. P. Urbanski, C. E. Wold, D. W. T. Griffith, T. J. Johnson, J. Reardon, and D. R. Weise (2011), Airborne and ground-based measurements of the trace gases and particles emitted by prescribed fires in the United States, *Atmospheric Chemistry and Physics*, *11*(23), 12197-12216, doi:10.5194/acp-11-12197-2011.

Canagaratna, M. R., et al. (2007), Chemical and microphysical characterization of ambient aerosols with the aerodyne aerosol mass spectrometer, *Mass Spectrometry Reviews*, *26*(2), 185-222, doi:10.1002/mas.20115.

Capes, G., B. Johnson, G. McFiggans, P. I. Williams, J. Haywood, and H. Coe (2008), Aging of biomass burning aerosols over West Africa: Aircraft measurements of chemical composition, microphysical properties, and emission ratios, *Journal of Geophysical Research-Atmospheres*, *113*(D20), doi:10.1029/2008jd009845.

Chen, L. W. A., H. Moosmuller, W. P. Arnott, J. C. Chow, J. G. Watson, R. A. Susott, R. E. Babbitt, C. E. Wold, E. N. Lincoln, and W. M. Hao (2007), Emissions from laboratory combustion of wildland fuels: Emission factors and source profiles, *Environmental Science & Technology*, *41*(12), 4317-4325, doi:10.1021/es062364i.

Christian, T. J., B. Kleiss, R. J. Yokelson, R. Holzinger, P. J. Crutzen, W. M. Hao, B. H. Saharjo, and D. E. Ward (2003), Comprehensive laboratory measurements of biomass-burning emissions: 1. Emissions from Indonesian, African, and other fuels, *Journal of Geophysical Research-Atmospheres*, *108*(D23), doi:10.1029/2003jd003704.

Crutzen, P. J., and M. O. Andreae (1990), Biomass Burning in the Tropics - Impact on Atmospheric Chemistry and Biogeochemical Cycles, *Science*, *250*(4988), 1669-1678, doi:10.1126/science.250.4988.1669.

DeCarlo, P. F., et al. (2008), Fast airborne aerosol size and chemistry measurements above Mexico City and Central Mexico during the MILAGRO campaign, *Atmospheric Chemistry and Physics*, *8*(14), 4027-4048.

Donahue, N. M., A. L. Robinson, C. O. Stanier, and S. N. Pandis (2006), Coupled partitioning, dilution, and chemical aging of semivolatile organics, *Environmental Science & Technology*, *40*(8), 02635-02643, doi:10.1021/es052297c.

Ferek, R. J., J. S. Reid, P. V. Hobbs, D. R. Blake, and C. Liousse (1998), Emission factors of hydrocarbons, halocarbons, trace gases and particles from biomass burning in Brazil, *Journal of Geophysical Research-Atmospheres*, *103*(D24), 32107-32118.

Grieshop, A. P., J. M. Logue, N. M. Donahue, and A. L. Robinson (2009), Laboratory investigation of photochemical oxidation of organic aerosol from wood fires 1: measurement and simulation of organic aerosol evolution, *Atmospheric Chemistry and Physics*, *9*(4), 1263-1277.

Heald, C. L., et al. (2008), Total observed organic carbon (TOOC) in the atmosphere: a synthesis of North American observations, *Atmospheric Chemistry and Physics*, *8*(7), 2007-2025, doi:10.5194/acp-8-2007-2008.

Hopkins, B. (1965), Forest and Savanna: An Introduction to Tropical Plant Ecology with Special Reference to West Africa, Heinemann, London.

Janhall, S., M. O. Andreae, and U. Poschl (2010), Biomass burning aerosol emissions from vegetation fires: particle number and mass emission factors and size distributions, *Atmospheric Chemistry and Physics*, *10*(3), 1427-1439.

Johnson, B. T., S. R. Osborne, J. M. Haywood, and M. A. J. Harrison (2008), Aircraft measurements of biomass burning aerosol over West Africa during DABEX, *Journal of Geophysical Research-Atmospheres*, *113*, doi:10.1029/2007jd009451.

Jolleys, M. D., et al. (2012), Characterizing the Aging of Biomass Burning Organic Aerosol by Use of Mixing Ratios: A Meta-analysis of Four Regions, *Environmental Science & Technology*, *46*(24), 13093-13102, doi:10.1021/es302386v.

Kamara, A. Y., F. Ekeleme, D. Chikoye, and L. O. Omoigui (2009), Planting Date and Cultivar Effects on Grain Yield in Dryland Corn Production, *Agronomy Journal*, *101*(1), 91-98, doi:10.2134/agronj2008.0090.

Keene, W. C., R. M. Lobert, P. J. Crutzen, J. R. Maben, D. H. Scharffe, T. Landmann, C. Hely, and C. Brain (2006), Emissions of major gaseous and particulate species during experimental burns of southern African biomass, *Journal of Geophysical Research-Atmospheres*, *111*(D4), doi:10.1029/2005jd006319.

Langmann, B., B. Duncan, C. Textor, J. Trentmann, and G. R. van der Werf (2009), Vegetation fire emissions and their impact on air pollution and climate, *Atmospheric Environment*, *43*(1), 107-116, doi:10.1016/j.atmosenv.2008.09.047.

Lawson, G. W. (1986), Vegetation and environment in West Africa, in: Lawson, G. W., *Plant Ecology in West Africa: Systems and Processes*, p 273-308, John Wiley & Sons, Chichester.

Lee, T., et al. (2010), Chemical Smoke Marker Emissions During Flaming and Smoldering Phases of Laboratory Open Burning of Wildland Fuels, *Aerosol Science and Technology*, *44*(9), I-V, doi:10.1080/02786826.2010.499884.

McMeeking, G. R. (2008), The Optical, Chemical, and Physical Properties of Aerosols and Gases Emitted by the Laboratory Combustion of Wildland Fuels, PhD Thesis, Department of Atmospheric Science, Colorado State University.

McMeeking, G. R., et al. (2009), Emissions of trace gases and aerosols during the open combustion of biomass in the laboratory, *Journal of Geophysical Research-Atmospheres*, *114*, doi:10.1029/2009jd011836.

Olsson, M. (2006), Wheat straw and peat for fuel pellets - organic compounds from combustion, *Biomass & Bioenergy*, *30*(6), 555-564, doi:10.1016/j.biombioe.2006.01.005.

Reid, J. S., R. Koppmann, T. F. Eck, and D. P. Eleuterio (2005), A review of biomass burning emissions part II: intensive physical properties of biomass burning particles, *Atmospheric Chemistry and Physics*, *5*, 799-825.

Rodriguez-Franco, C. (2002), Forests in the Basin of Mexico: types, geographic Distribution, and Condition, in: Fenn, M. E. et al., *Ecological Studies*, *156*, Urban Air Pollution and Forests: Resources at Risk in the Mexico City Air Basin, p 68-85, Springer-Verlag, New York.

Sanford, W. W. & Isichei, A. O. (1986), Savanna, in: Lawson, G. W., *Plant Ecology in West Africa: Systems and Processes*, p 95-150, John Wiley & Sons, Chichester.

Sowunmi, M. A. (1986), Change of vegetation with time, in: Lawson, G. W., *Plant Ecology in West Africa: Systems and Processes*, p 273-308, John Wiley & Sons, Chichester.

Ward, D. E. (1990), Factors Influencing the Emissions of Gases and Particulate Matter from Biomass Burning, in: Goldammer, G. W., *Ecological Studies*, *84*, Fire in the Tropical Biota: Ecosystem Processes and Global Challenges, p 418-436, Springer-Verlag, New York.

Weimer, S., M. R. Alfarra, D. Schreiber, M. Mohr, A. S. H. Prevot, and U. Baltensperger (2008), Organic aerosol mass spectral signatures from wood-burning emissions: Influence of burning conditions and wood type, *Journal of Geophysical Research-Atmospheres*, *113*(D10), doi:10.1029/2007jd009309.

Yokelson, R. J., D. W. T. Griffith, and D. E. Ward (1996), Open-path Fourier transform infrared studies of large-scale laboratory biomass fires, *Journal of Geophysical Research-Atmospheres*, *101*(D15), 21067-21080, doi:10.1029/96jd01800.

Yokelson, R. J., T. Karl, P. Artaxo, D. R. Blake, T. J. Christian, D. W. T. Griffith, A. Guenther, and W. M. Hao (2007), The Tropical Forest and Fire Emissions Experiment: overview and airborne fire emission factor measurements, *Atmospheric Chemistry and Physics*, *7*(19), 5175-5196.

Yokelson, R. J., T. J. Christian, T. G. Karl, and A. Guenther (2008), The tropical forest and fire emissions experiment: laboratory fire measurements and synthesis of campaign data, *Atmospheric Chemistry and Physics*, *8*(13), 3509-3527.

Yokelson, R. J., et al. (2009), Emissions from biomass burning in the Yucatan, *Atmospheric Chemistry and Physics*, *9*(15), 5785-5812.

Yokelson, R. J., I. R. Burling, S. P. Urbanski, E. L. Atlas, K. Adachi, P. R. Buseck, C. Wiedinmyer, S. K. Akagi, D. W. Toohey, and C. E. Wold (2011), Trace gas and particle emissions from open biomass burning in Mexico, *Atmospheric Chemistry and Physics*, *11*(14), 6787-6808, doi:10.5194/acp-11-6787-2011.

Tables

Table 1: Fuel properties for burns during FLAME II (Adapted from *McMeeking et al.* (*2009*)).

Fuel type	Species	Scientific name	Number of burns	Components	Moisture content (%)	Carbon content (%)	Nitrogen content (%)
Montane forest	Ponderosa pine	*Pinus ponderosa*	14	Needles (8), sticks (6)	6.9 – 9.2	46 - 49	0.04 – 1.3
	Douglas fir	*Pseudotsuga menziesii*	8	Needles (3), needles/branches (3), branches (2)	20.7 – 51.2	54	0.5 – 0.9
Rangeland	Sagebrush	*Artemisia tridentata*	8	Leaves/branches	9.4 – 33.3	47 - 51	1.5 – 2.1
Chaparral	Manzanita	*Arctostaphylos glandulosa*	1	Leaves/branches	28.3	48	0.8
	Ceanothus	*Ceanothus crassifolius*	2	Leaves/branches	15.4	48	1.3
	Chamise	*Adenstoma fasciculatum*	5	Leaves/branches	11.2 – 57.4	49	1.0
Coastal plain	Palmetto	*Serenoa repens*	3 (+1)	Leaves	5 – 7.1	51	1.0
	Gallberry	*Ilex coriacea*	2 (+2)	Leaves/branches	6	56	0.8
	Longleaf pine	*Pinus palustris*	2 (+2)	Needles	6.4	52	1.1
	Hickory	*Carya nutt*	1	Leaves	7.8	48	2.1
	Wiregrass	*Aristida beyrichiana*	1 (+1)	Grass	5.4	48	0.5
	Wax myrtle	*Myrica cerifera*	1	Leaves/branches	13.3	48 - 53	1.1 – 1.4
	Kudzu	*Pueraria montana*	2	Vine	99.2	47	3.6
	Turkey oak	*Quercus laevis*	2	Leaves	8.5	53	1.3
	Black needle rush	*Juncus roemerianus*	1	Rush	32.7	49	0.9
	Saw grass	*Cladium mariscus*	2	Grass	14.9	42	3.0
Boreal forest	Black spruce	*Picea mariana*	4	Needles/branches	12.8 – 22.5	49	1.1
	Alaskan duff	-	2	Duff	10.9	31	0.5
Other	Rice straw	*Oryza sativa*	2	Straw	8	39 - 46	0.6 – 0.9

Table 2: Average △OA/△CO for individual fuel types, species and components during FLAME II[a].

Fuel type	Species	Component	Class average △OA/△CO	Minimum burn average △OA/△CO	Maximum burn average △OA/△CO	Range
Montane forest	Ponderosa pine	Needles	0.227 ±0.231	0.031 ±0.036	0.488 ±0.498	0.457
		Sticks	0.021 ±0.036	0.013 ±0.017	0.029 ±0.028	0.016
		All	0.139 ±0.190	0.013 ±0.017	0.488 ±0.498	0.475
	Douglas fir	Needles	0.559 ±0.433	0.062 ±0.086	0.850 ±0.446	0.788
		Needles/ branches	0.438 ±0.251	0.279 ±0.158	0.738 ±0.313	0.459
		Branches	0.083 ±0.036	0.058 ±0.022	0.109 ±0.029	0.051
		All	0.395 ±0.336	0.058 ±0.022	0.850 ±0.446	0.792
	All	-	**0.232** ±0.257	**0.013** ±0.017	**0.850** ±0.446	**0.837**
Rangeland	Sagebrush	Leaves/ branches	**0.214** ±0.104	**0.118** ±0.076	**0.443** ±0.236	**0.325**
Chaparral	Manzanita	Leaves/ branches	0.087 ±0.044	-	-	-
	Ceanothus	Leaves/ branches	0.031 ±0.042	0.021 ±0.018	0.041 ±0.057	0.020
	Chamise	Leaves/ branches	0.030 ±0.064	0.021 ±0.013	0.058 ±0.057	0.037
	All	Leaves/ branches	**0.037** ±0.059	**0.021** ±0.013	**0.087** ±0.044	**0.066**
Coastal plain	Palmetto	Leaves	0.017 ±0.026	0.006 ±0.008	0.034 ±0.043	0.028
	Gallberry	Leaves/ branches	0.014 ±0.020	0.004 ±0.005	0.024 ±0.026	0.020
	Longleaf pine	Needles	0.069 ±0.055	0.056 ±0.061	0.082 ±0.048	0.026
	Hickory	Leaves	0.029 ±0.048	-	-	-
	Wiregrass	Grass	0.004 ±0.040	-	-	-
	Wax myrtle	Leaves/ branches	0.057 ±0.035	-	-	-
	Kudzu	Vine	0.114 ±0.071	0.105 ±0.057	0.124 ±0.083	0.019
	Turkey oak	Leaves	0.392 ±0.315	0.320 ±0.264	0.464 ±0.364	0.144
	Black needle rush	Rush	0.192 ±0.134	-	-	-
	Saw grass	Grass	0.041 ±0.046	0.015 ±0.013	0.066 ±0.049	0.051
	All	-	**0.090** ±0.170	**0.004** ±0.005	**0.464** ±0.364	**0.460**

Boreal forest	Black spruce	Needles/ branches	0.115 ±0.158	0.034 ±0.028	0.211 ±0.178	0.177
	Alaskan duff	Duff	0.107 ±0.062	0.086 ±0.054	0.127 ±0.073	0.041
	All	-	**0.112** ±0.133	**0.034** ±0.028	**0.211** ±0.178	**0.177**
Other	Rice straw	Straw	**0.199** ±0.174	**0.127** ±0.133	**0.270** ±0.187	**0.143**

[a] With standard deviations of 1σ.

Figures

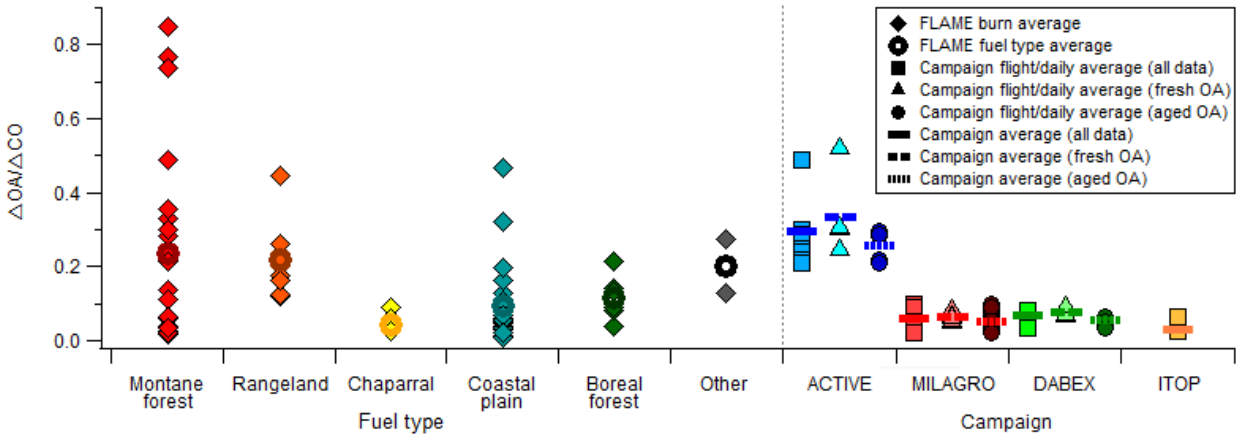

Figure 1: Distributions of burn-averaged △OA/△CO for different fuel types during FLAME II, in comparison to averages for individual measurement periods and campaigns as a whole for four ambient datasets.

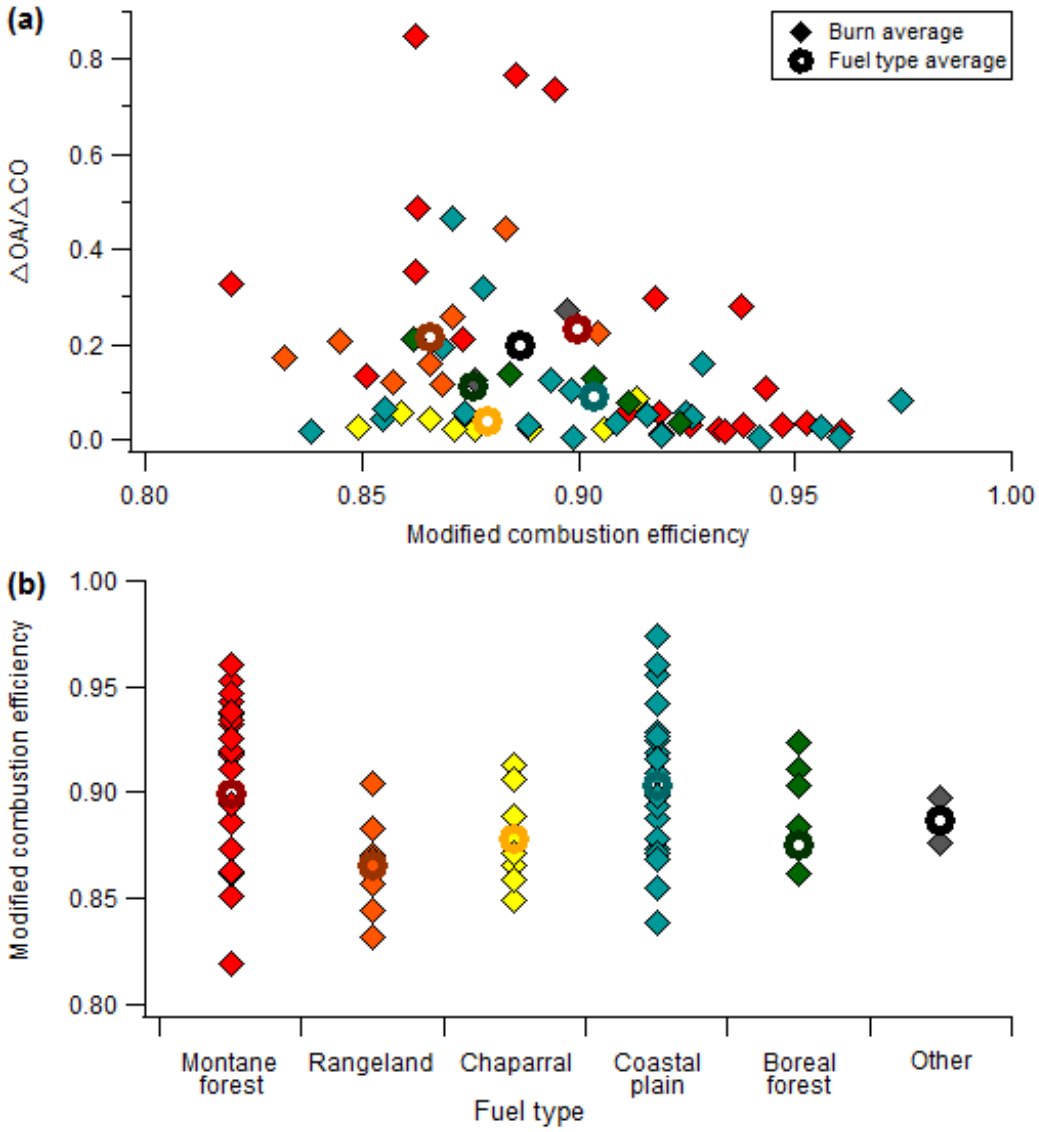

Figure 2: (a) Burn-averaged △OA/△CO versus MCE for all FLAME II burns. (b) Distribution of burn-averaged MCE for different fuel types.

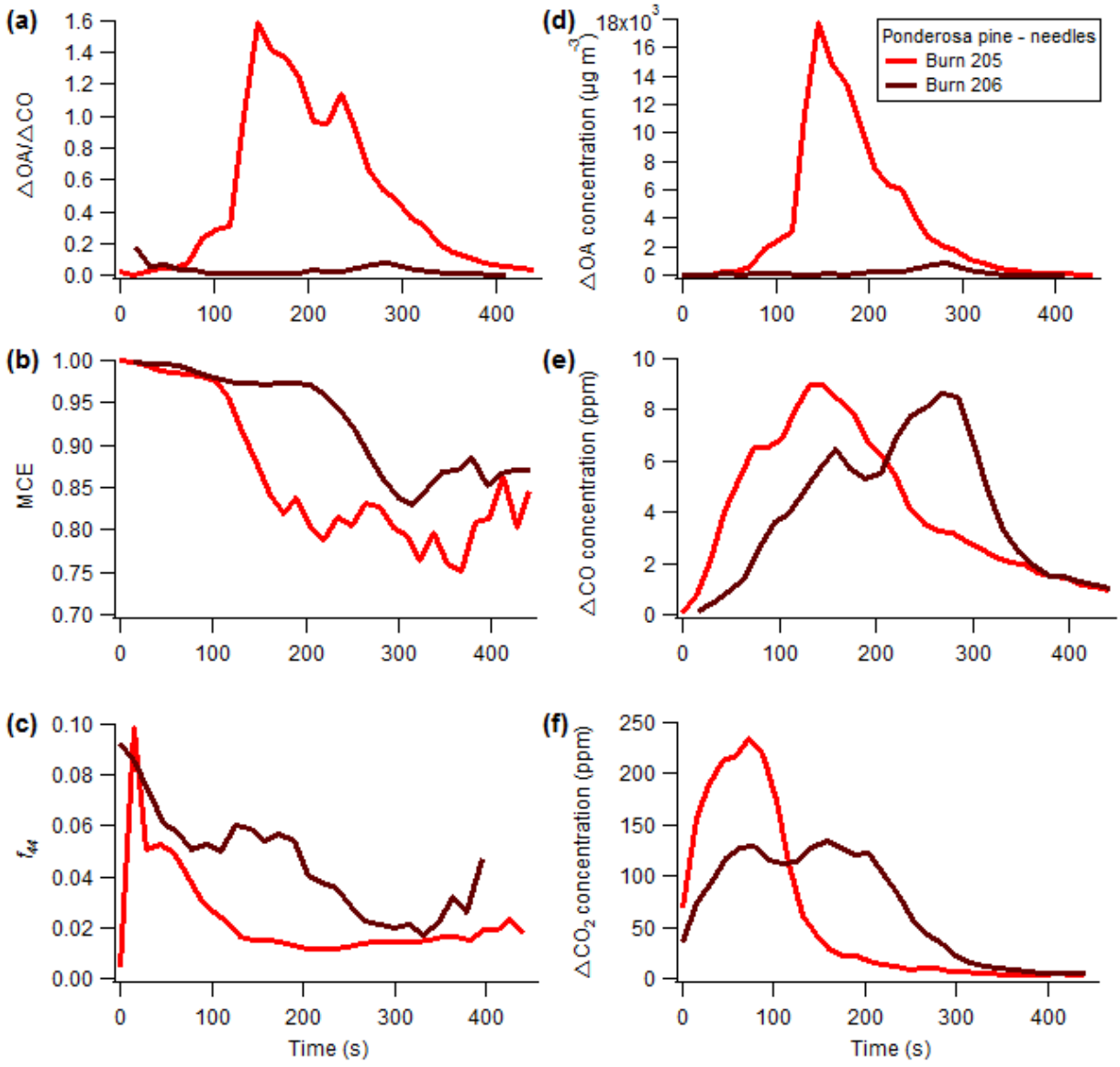

Figure 3: Time series for (a) △OA/△CO, (b) MCE, (c) f_{44}, (d) △OA, (e) △CO and (f) △CO_2 for two ponderosa pine needle fires with similar fuel and burn properties (moisture content = 8.7%, consumed fuel mass = 205 g/211 g, burn duration = ~8 minutes).

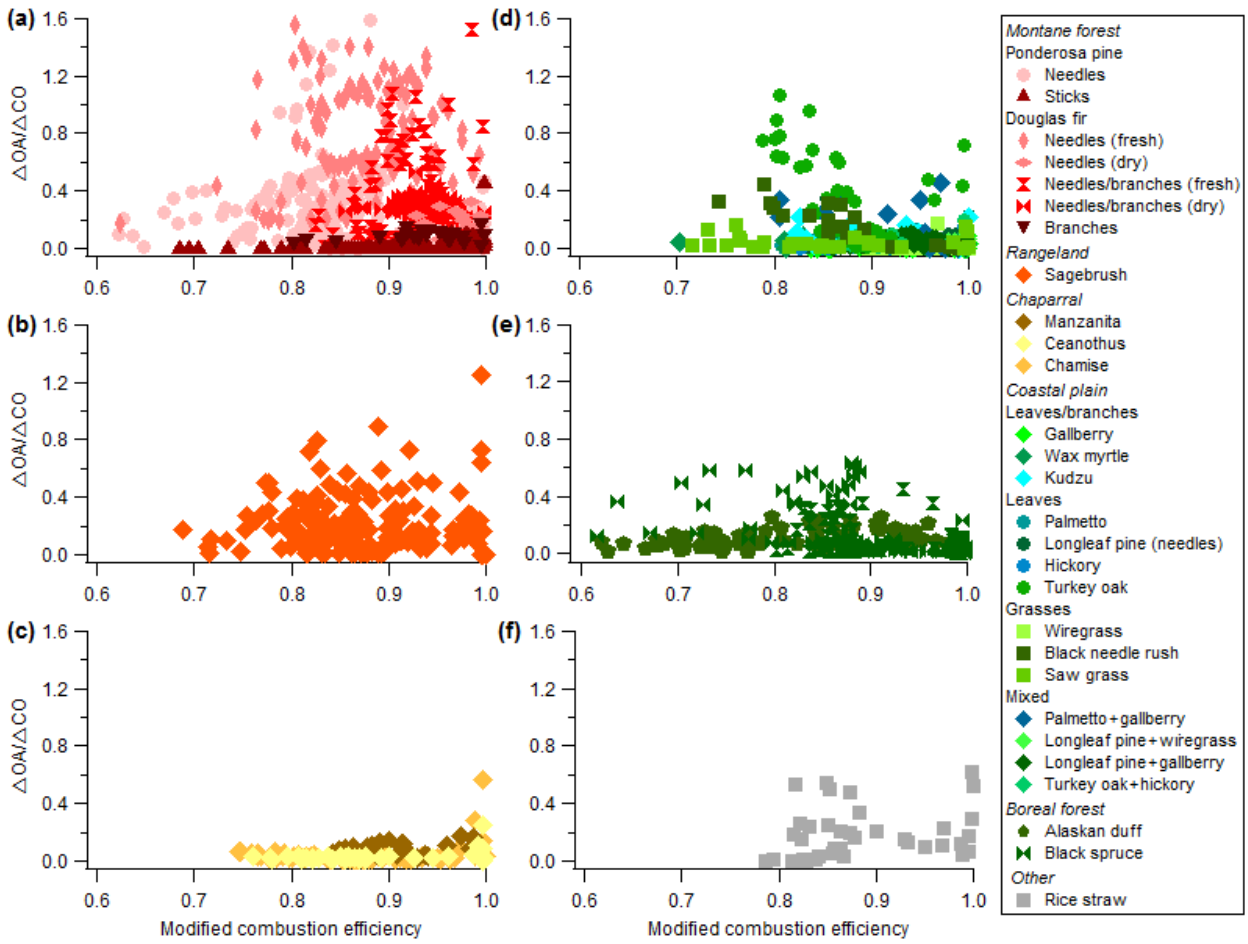

Figure 4: Instantaneous △OA/△CO versus MCE for fires involving (a) montane forest, (b) rangeland, (c) chaparral, (d) coastal plain, (e) boreal forest and (f) rice straw fuels. Fuel types are sub-divided into constituent species and fuel components.

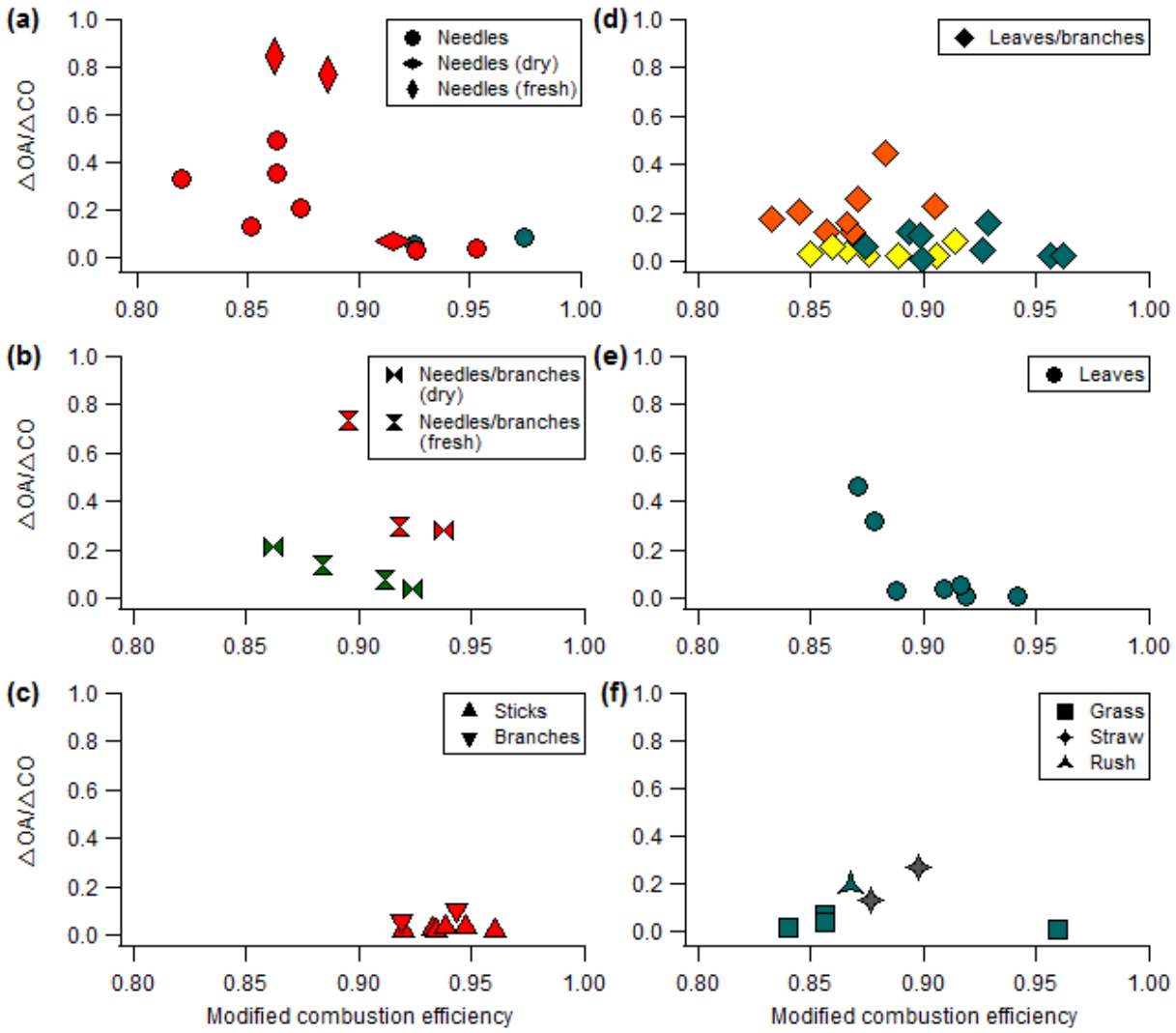

Figure 5: Burn-averaged △OA/△CO versus MCE for fires involving (a) needles, (b) needles/branches, (c) sticks/branches, (d) leaves/branches, (e) leaves and (f) grass and straw. Fuel components are sub-divided into individual fuel types.

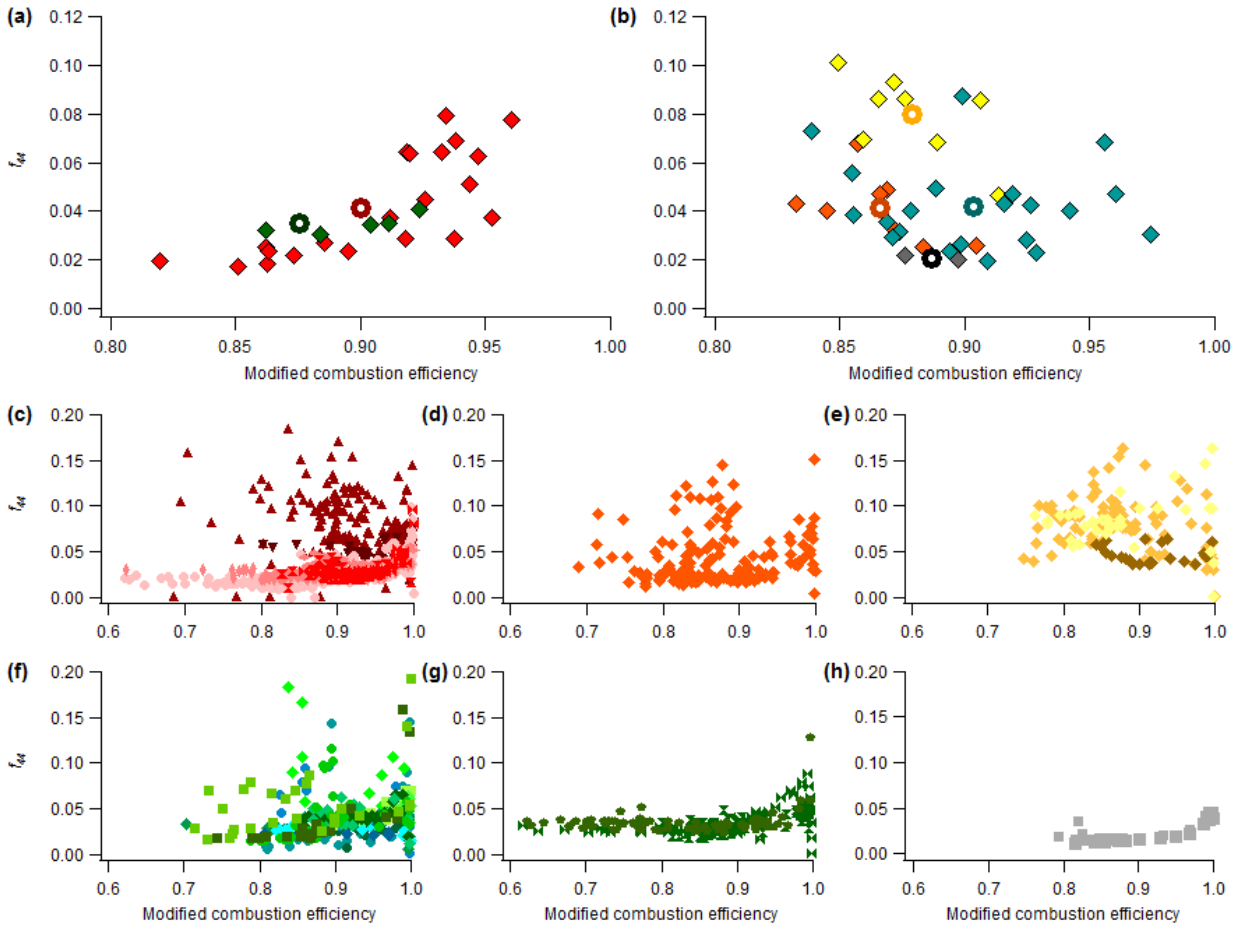

Figure 6: Burn-averaged f_{44} versus MCE, separating (a) coniferous and (b) non-coniferous fuels to emphasise the contrasting trends between each group. Shown below are instantaneous f_{44} versus MCE for fires involving (c) montane forest, (d) rangeland, (e) chaparral, (f) coastal plain, (g) boreal forest and (h) rice straw fuels. Fuel types are sub-divided into constituent species and fuel components, as for Figure 4.

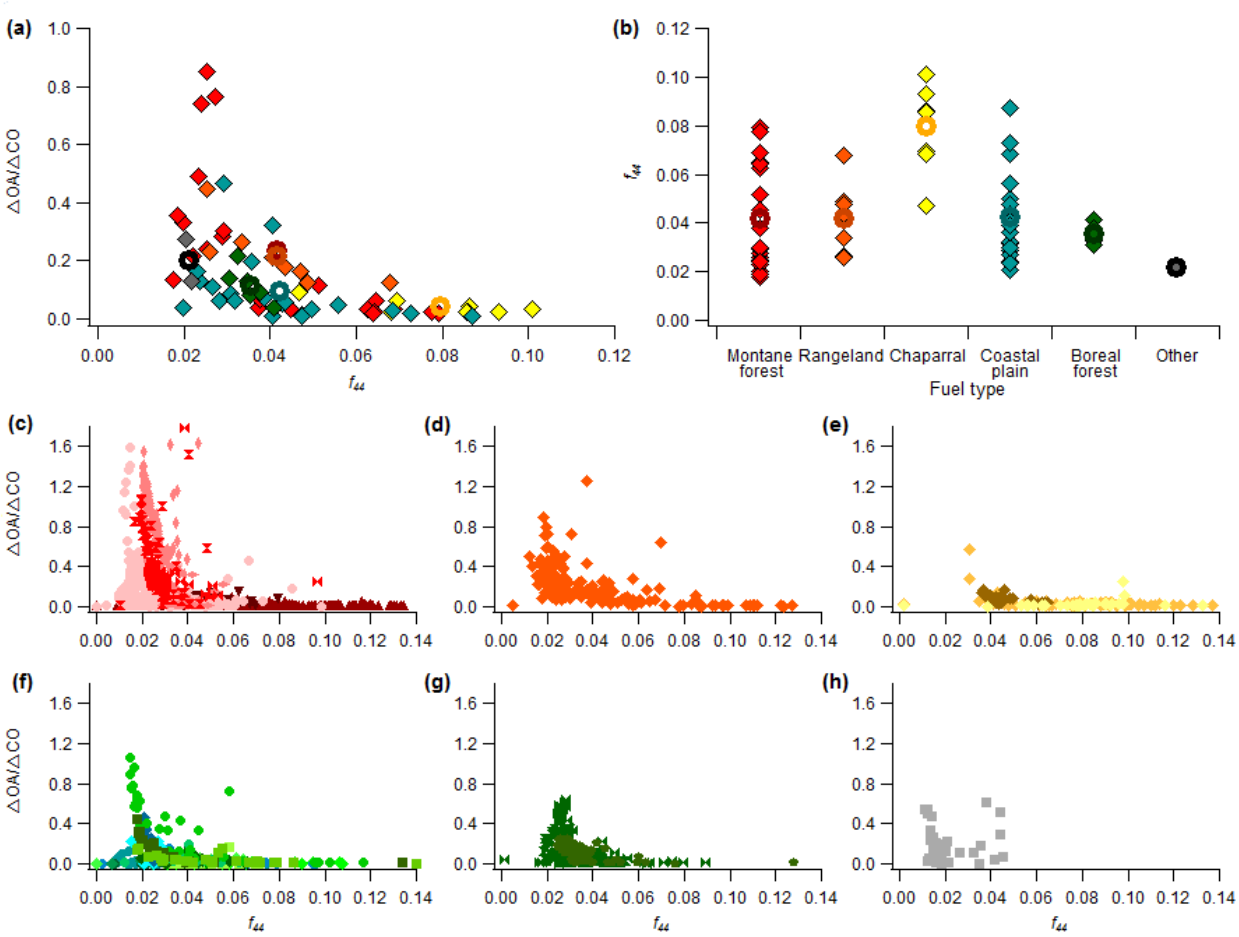

Figure 7: (a) Burn-averaged △OA/△CO versus f_{44} versus MCE and (b) Distributions of burn-averaged f_{44} for different fuel types during FLAME II. Shown below are instantaneous △OA/△CO versus f_{44} for fires involving (c) montane forest, (d) rangeland, (e) chaparral, (f) coastal plain, (g) boreal forest and (h) rice straw fuels.

Figure 8: Average △OA/△CO across all burns segregated into prescribed bins for (a) fire duration, (b) fuel mass consumed, (c) mass consumption rate, (d) moisture content, (e) f_{44} and (f) MCE. Average values from single burns were used when multiple burns were not available for given criteria. Markers below x-axes indicate an absence of corresponding burns.

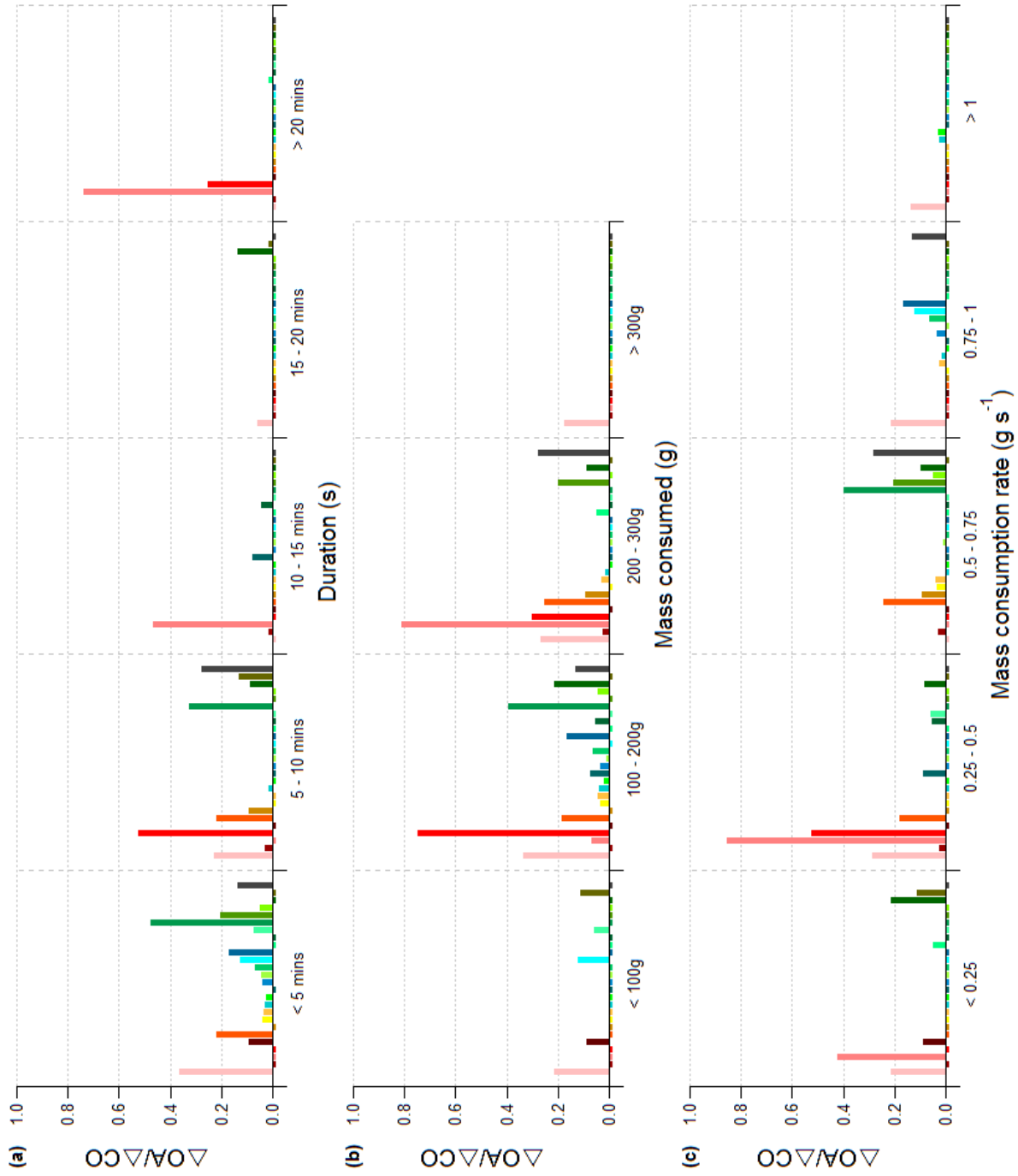

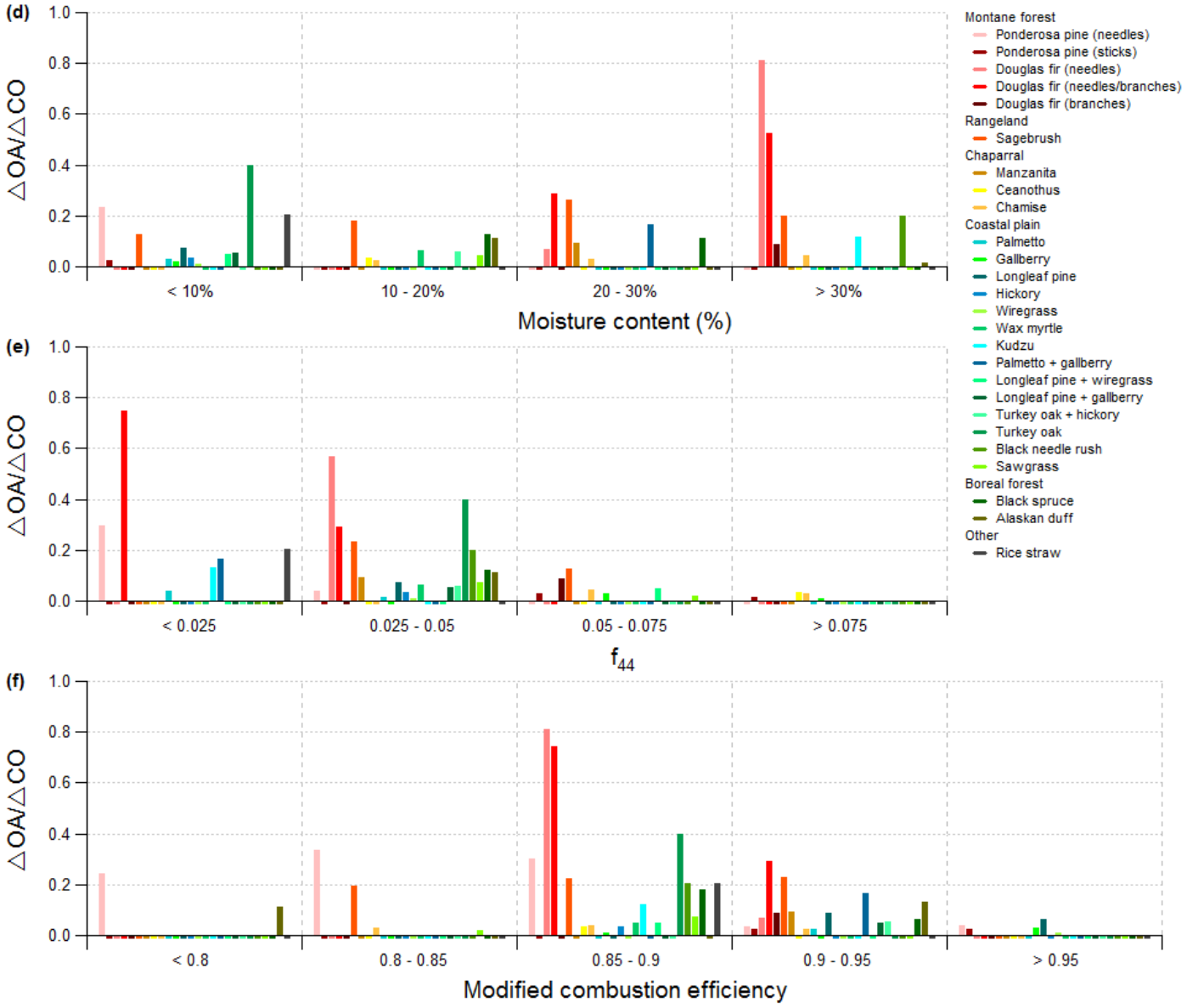
(d)
△OA/△CO
1.0
0.8
0.6
0.4
0.2
0.0
< 10%
10 - 20%
20 - 30%
> 30%
Moisture content (%)
(e)
△OA/△CO
1.0
0.8
0.6
0.4
0.2
0.0
< 0.025
0.025 - 0.05
0.05 - 0.075
> 0.075
f44
(f)
△OA/△CO
1.0
0.8
0.6
0.4
0.2
0.0
< 0.8
0.8 - 0.85
0.85 - 0.9
0.9 - 0.95
> 0.95
Modified combustion efficiency
Montane forest
Ponderosa pine (needles)
Ponderosa pine (sticks)
Douglas fir (needles)
Douglas fir (needles/branches)
Douglas fir (branches)
Rangeland
Sagebrush
Chaparral
Manzanita
Ceanothus
Chamise
Coastal plain
Palmetto
Gallberry
Longleaf pine
Hickory
Wiregrass
Wax myrtle
Kudzu
Palmetto + gallberry
Longleaf pine + wiregrass
Longleaf pine + gallberry
Turkey oak + hickory
Turkey oak
Black needle rush
Sawgrass
Boreal forest
Black spruce
Alaskan duff
Other
Rice straw

3.6 Paper 3: Properties and evolution of biomass burning organic aerosol from Canadian boreal forest fires

Status:

To be submitted to Atmospheric Chemistry & Physics (BORTAS Special Issue)

Overview:

This paper evaluates emissions of BBOA from boreal forest fires in eastern Canada during the BORTAS campaign in 2011. BB plumes of varying ages were sampled by the FAAM BAe-146 research aircraft, providing measurements at a range of scales from directly at source to thousands of kilometres downwind. Properties of these emissions ensembles were compared in order to characterise differences in vertical distribution, composition and mass enhancements. While overall OA concentrations were typically higher in aged plumes, increased lofting of plumes to higher altitudes and elevated contributions of BC relative to fresh plumes are indicative of a significant change in combustion conditions. Compositional changes were assessed using the prominent f_{44} and f_{60} tracers as indicators for oxygenated OA and primary BB emissions respectively, revealing higher levels of oxidation in transported plumes than those sampled close to source. Primary BBOA constituents were also shown to be more effectively conserved in more heavily aged emissions, following advection to higher altitudes. Profiles of f_{44} and f_{60} from BORTAS were also compared with examples from wider studies, showing broad consistency for the evolution of BBOA with aging, with increasing oxygenation again coinciding with an overall reduction in $\triangle$OA/$\triangle$CO.

Contributions from co-authors:

J. Taylor, S. O'Shea, M. Le Breton, S. Bauguitte, S. Moller, P. Di Carlo, E. Aruffo and J. Lee participated in fieldwork and performed initial data processing. P. Palmer initiated the project. H. Coe and G. McFiggans assisted with preparation of the manuscript.

Properties and evolution of biomass burning organic aerosol from Canadian boreal forest fires

Matthew D. Jolleys[*1], *Hugh Coe*[1], *Gordon McFiggans*[1], *Jonathan W. Taylor*[1], *Sebastian J. O'Shea*[1], *Michael Le Breton*[1], *Stephan J.-B. Bauguitte*[2], *Sarah Moller*[3], *Piero Di Carlo*[4,5], *Eleonora Aruffo*[5], *Paul I. Palmer*[6], *James D. Lee*[3]

* Corresponding author email: matthew.jolleys@postgrad.manchester.ac.uk

[1] Centre for Atmospheric Science, School of Earth, Atmospheric and Environmental Science, University of Manchester, Manchester, UK

[2] Facility for Airborne Atmospheric Measurements, Bedford, UK

[3] National Centre for Atmospheric Science (NCAS), Department of Chemistry, University of York, York, UK

[4] Centre of Excellence CETEMPS, University of L'Aquila, L'Aquila, Italy

[5] Department of Physical and Chemical Sciences, University of L'Aquila, L'Aquila, Italy

[6] School of Geosciences, University of Edinburgh, Edinburgh, UK

Abstract

Airborne measurements of biomass burning organic aerosol (BBOA) from boreal forest fires reveal highly contrasting properties for plumes of different ages. These measurements, performed using an Aerodyne Research Inc. compact time-of-flight aerosol mass spectrometer (C-ToF-AMS) during the BORTAS (quantifying the impact of BOReal forest fires on Tropospheric oxidants over the Atlantic using Aircraft and Satellites) experiment in the summer of 2011, have been used to derive normalised excess organic aerosol (OA) mass concentrations ($\triangle$OA/$\triangle$CO), with higher average ratios observed closer to source (0.190 ± 0.010) than in the far-field (0.097 ± 0.002). The difference in $\triangle$OA/$\triangle$CO between fresh and aged plumes is influenced by a change in dominant combustion conditions throughout the campaign. Measurements at source sampled largely smouldering fires, while plumes encountered in the near field originated from fires occurring earlier in the campaign when fire activity had been more intense. Changing combustion conditions also affect the vertical distribution of biomass burning emissions, as aged plumes from more flaming-dominated fires are injected to higher altitudes of up to 6000 m. Proportional contributions of the *m*/*z* 44 and 60 peaks in the AMS mass spectra to the total OA mass (denoted f_{44} and f_{60}) are used as respective tracers for primary and oxidized BBOA. Given the shorter aging times associated with near-field plumes, f_{44} is lower on average than in more aged, transported plumes. However, high levels of $\triangle O_3/\triangle CO$ and $-\log(NO_x/NO_y)$ close to source indicate that emissions can be subject to very rapid oxidation over short timescales. Conversely, the lofting of plumes into the upper troposphere can lead to the retention of source profiles after transportation over extensive temporal and spatial scales, with f_{60} higher on average in aged plumes. Evolution of OA composition with aging is comparable to observations of BB tracers in previous studies, revealing a consistent progression from f_{44} to f_{60}. The elevated levels of oxygenation in aged plumes, and their association with lower average $\triangle$OA/$\triangle$CO, highlight the influence of OA losses during aging, although there remain considerable uncertainties regarding the role of combustion processes on BBOA production and composition.

1. Introduction

The BORTAS (quantifying the impact of BOReal forest fires on Tropospheric oxidants over the Atlantic using Aircraft and Satellites) campaign was a major international research effort to improve understanding of the properties and evolution of biomass burning (BB) plumes. BB emissions form a major source of atmospheric particulate matter on a global scale, contributing around 90% of the total primary organic aerosol (OA) (*Bond et al., 2004*). The radiative effects of atmospheric aerosols represent one of the major sources of uncertainty with regard to influences on climate change (*Textor et al., 2006; Forster et al., 2007*). Given the prominence of OA in global aerosol budgets (*Zhang et al., 2007; Jimenez et al., 2009*), limited understanding of BB emissions, and more specifically biomass burning organic aerosol (BBOA), forms an important component of this uncertainty. Improved projection of climate change impacts through global climate model simulation is dependent on more robust parameterisation of the constituent drivers, constrained by direct measurements. Several fundamental aspects of the BBOA lifecycle remain poorly characterised, including the conditions and processes controlling formation, and the effects of transformations occurring during aging (*Hallquist et al., 2009*). Variability at source has been shown to be extensive, in response to changes in both fuel properties and combustion conditions (*McMeeking et al., 2009; Jolleys et al., 2012; 2013*). The influence of secondary organic aerosol (SOA) in aging plumes is also particularly unclear. Substantial SOA formation as a result of photochemical processing has been demonstrated in laboratory experiments, increasing concentrations by up to a factor of 4 over several hours (*Grieshop et al., 2009; Hennigan et al., 2011; Heringa et al., 2011*). However, under ambient conditions the importance of SOA addition relative to primary (POA) emissions is more disputable. Despite widespread evidence for the increasing oxygenation of BBOA with aging (*Capes et al., 2008; DeCarlo et al., 2008; Cubison et al., 2011; Jolleys et al., 2012*), net mass enhancements are not observed consistently. The underlying causes of this variable SOA contribution, including the implications of initial OA composition, also remain ambiguous and require further refinement.

The BORTAS campaign is described in detail by *Palmer et al.* (*2013*), with an overview of measurements used within this analysis given here. BORTAS took place across several regions of Canada between the 12th July and 3rd August in both 2010 and 2011, although activity during the 2010 deployment (BORTAS-A) was limited to ground-based measurements at a main ground station located at Dalhousie University in Halifax, Nova Scotia, along with ozonesonde launches from a network of seven sites across central and eastern Canada and supporting satellite observations (*Parrington et al., 2012*). Airborne measurements were carried out during BORTAS-B in 2011, providing all data contributing towards this study. The UK Facility for Airborne Atmospheric Measurements (FAAM) BAe-146 Atmospheric Research Aircraft (ARA) performed a total of 15 flights, including 11 dedicated science flights between the 15-31st July. Research flights primarily originated from Halifax and largely involved surveying areas adjacent to the Gulf of St. Lawrence and the North Atlantic. A predominant source region in northwestern Ontario (approximately 52.5° N, 93.5° W) has been identified for the majority of plumes sampled throughout BORTAS, although more disperse fires were also active in northern Alberta and the Northwest Territories (*Palmer et al., 2013; Parrington et al., 2013*). As the majority of plumes from fires in this region were encountered at a distance of several thousand kilometres downwind, emissions would have undergone substantial processing prior to sampling, with estimated photochemical ages between 1-11 days. A single flight to the Ontario source region also sampled active fires directly at source, providing a valuable inventory of fresh plume measurements and enabling comparison of emissions in the near and far-field. However, such comparison is subject to potential contrasts in fire behaviour, given that each set of measurements were obtained at different stages of the campaign. Fire activity within the region peaked between the 17-19th July, with emissions from these fires intercepted far downwind. Plumes from fires within the same region were also sampled at source on the 26th July (flight B626), representing the only measurements of fresh plumes from BORTAS. However, by this time fire activity had significantly abated, bringing about a change in combustion conditions to yield smaller, less intense fires more typically

dominated by smouldering combustion (*O'Shea et al., 2013a*). The more intense period of fires earlier in the campaign is expected to involve larger events with a more prominent flaming combustion phase, as indicated by the detection of pronounced smoke plumes at altitudes of up to approximately 7000 m over the North Atlantic (*Palmer et al., 2013*). As a result, any comparison of fresh and aged plumes during BORTAS must also account for this disparity in source conditions. While such a scenario would reduce the potential to evaluate the continuous evolution of smoke plumes from source into the ambient atmosphere, and prevent direct comparison of near and far-field plumes derived from similar combustion conditions, it also provides a baseline for conditions at source.

2. Background

2.1 Instrumentation and measurements

A wide array of instrumentation performing particulate and gas phase measurements were deployed throughout BORTAS. This study focuses primarily on the analysis of OA mass and composition data obtained from an Aerodyne Research Inc. compact time-of-flight aerosol mass spectrometer (C-ToF-AMS; *Drewnick et al., 2005; Canagaratna et al., 2007*). The AMS provides highly time-resolved mass concentrations of sub-micron, non-refractory aerosol, and full chemical speciation across a complete range of constituent ion mass-to-charge ratios (*m*/*z*). Operation of the AMS, including calibration and necessary correction factors, during aircraft deployment (*Bahreini et al., 2003*) and specifically onboard the BAe-146 (*Crosier et al., 2007; Morgan et al., 2009*) have been described in detail. Refractory black carbon (BC) was measured using a Droplet Measurement Technologies single particle soot photometer (SP-2; *Schwarz et al., 2006*). Although analysis of the chemical and optical properties of single BC particles was not performed as part of this study, mass concentrations in smoke plumes, particularly in relation to OA concentrations, were used as a means of evaluating the proportional contributions of different combustion phases. A range of gas phase

measurements were undertaken on the BAe-146, including species used as tracers for both primary emissions and photochemical processing. CO mixing ratios were measured with an Aerolaser AL5002 UV fluorescence analyser and O_3 by a Thermo Scientific TEi49C UV photometric analyser as part of the standard complement of instrumentation for BAe-146 science flights. Additional instrumentation included a chemical ionisation mass spectrometer (CIMS; *Nowak et al., 2007*) providing real-time measurements of HCN, which is widely used as a tracer for BB emissions given that vegetation fires constitute its primary global source (*Li et al., 2000; Sinha et al., 2003; Yokelson et al., 2007*). NO_x ($NO + NO_2$) and NO_y (NO_x oxidation products, including HNO_3 and N_2O_5) act as important tracers for oxidation in aging plumes, and were measured respectively by an Air Quality Design Inc. chemiluminescence NO_x analyser and by thermal dissociation-laser induced fluorescence (TD-LIF; *Di Carlo et al., 2013*). The assembly of gas phase measurements used within this analysis was completed by CO_2 mixing ratios from a Los Gatos Research Inc. cavity enhanced absorption spectrometer-based fast greenhouse gas analyser (FGGA; *O'Shea et al., 2013$_b$*). Aerosol size distributions in the range 20-350 nm were obtained from a scanning mobility particle sizer (SMPS), with integrated distributions over the full size range used as an approximation of particle number concentration, given the lack of dedicated measurements due to failure of a condensation particle counter preventing its use in all BORTAS flights.

2.2 Data selection

Data from BORTAS were screened in order to isolate emissions with a biomass burning influence. This was performed using the guidelines proposed by *Capes et al.* (*2008*) and *Jolleys et al.* (*2012*) based upon minimum $\triangle$CO (the excess CO concentration above background levels) and number concentrations. A threshold of 0.003 was used for f_{60}, representing the ratio of levoglucosan-like species, which correspond to the *m/z* 60 peak in the AMS mass spectra (*Schneider et al., 2006; Alfarra et al., 2007*), to the total OA mass. This threshold is based upon observed background levels of f_{60} in OA emissions from urban and

biogenic sources where BB influences are absent (*Cubison et al., 2011; Aiken et al., 2009; DeCarlo et al., 2008*). Levoglucosan and other anhydrous sugars such as mannosan and galactosan have been shown to be strongly associated with primary BB emissions (*Simoneit et al., 1999; Iinuma et al., 2007; Sullivan et al., 2008; Lee et al., 2010*). Respective thresholds of 20 ppb and 2000 cm^{-3} were applied for △CO and number concentration. Background CO concentrations were calculated for each flight according to the minimum observed concentrations. All data were also averaged to the temporal resolution of the AMS (~8 second time step on average) to enable direct comparison of different species. Alternative screening procedures for BB influences have been applied throughout separate analyses of BORTAS data (*Palmer et al., 2013*). Concentrations of trace gases primarily produced by fire sources, including HCN and CH_3CN, are commonly used as indicators for BB plumes (*Li et al., 2000; Yokelson et al., 2007; Crounse et al., 2009; Yokelson et al., 2009; Akagi et al., 2011*). A scheme using a HCN concentration threshold of six times the standard deviation (6σ) has been proposed for BORTAS (*Le Breton et al., 2013*). However, to ensure consistency with previous assessments of BBOA and facilitate intercomparison of different datasets, a simplified scheme using only OA, CO and number concentration data has been applied here. This approach performs well when compared to other methods, producing similarly strong correlations between HCN and CO for flights B621, B622, B624 and B626 (R^2 = 0.64, 0.52, 0.84 and 0.93) as the 6σ technique (R^2 = 0.83, 0.46, 0.82 and 0.81). These four flights, in addition to B623, were the only flights from which data was used in this analysis. Several flights carried out later in the campaign (B628-B630) also measured highly aged plumes with a photochemical age of up to 10 days (*Palmer et al., 2013*). However, correlations between △OA and △CO throughout these flights were exceptionally weak, yielding R^2 values consistently well below 0.1, contrasting with values in the range 0.39-0.74 for flights B621-B624 and B626. These weak correlations from later flights suggest that sampled air masses lack a common emission source and instead represent extensive mixtures of different plumes following dispersion, or that emissions have been differentially processed to the extent that

representative properties can no longer be distinguished. As a result, data from these flights were omitted from this analysis.

3. Results and discussion

3.1 Spatial and temporal variability in BB emissions properties

Measurements of OA in BB plumes during BORTAS encompassed a wide range of ages, from directly at source to up to 5 days of aging. The extent of this diversity contributed to a high level of variability in plume properties, both across separate research flights and between individual plumes encountered in different periods of the same flight. Excess OA concentrations measured in-plume ranged from close to zero to around 180 μg m^{-3}, with maximum △CO concentrations approaching 1000 ppb. Vertical profiles of both species are shown in Figure 1, revealing an overall increase in concentrations throughout the boundary layer to a peak at around 2000 m, before declining to background levels through the free troposphere. Significant elevations in both △OA and △CO occurred close to ground level, most likely as a result of influence from local sources. The observed decrease in concentration with altitude is more marked for △OA, which returns to background levels by 6000 m. Variability in △CO out of plume is much greater at higher altitudes. Concentrations of up to 800 ppb were observed between 5000–8000 m, indicating a potential influence of non-BB sources in aged plumes, following mixing with different air masses. However, the presence of BB plumes above 5000 m was limited. As such, the effect of mixing on background concentrations applied throughout this analysis should be minimal, with little evidence for substantially elevated △CO away from BB plumes at lower altitudes.

The change in combustion conditions between different periods of BORTAS is reflected in the contrast between loadings of particulate and gas-phase species. Concentrations in aged plumes sampled during flights B621-B624 consistently exceeded those at source from B626, irrespective of the effect of dilution as plumes dispersed into the ambient

atmosphere. During flight B626, △OA peaked at around 50 μg m^{-3}, with concentrations in more aged plumes exceeding this level by a factor of four. △CO concentrations were also significantly elevated in aged plumes relative to fresh emissions. The contrast in properties between plumes of different ages is likely to be primarily affected by a change in the size and intensity of fires, rather than combustion phase alone, given the stronger association of OA production with predominantly smouldering combustion in the latter stages of fire evolution (*Reid et al., 2005*). While the higher concentrations identified in aged plumes may be influenced to some extent by contributions from SOA, initial indications from calculated △OA/△CO ratios suggest this contribution did not provide any net increase in OA loadings. Normalising to a co-emitted, non-reactive tracer such as △CO provides an emission ratio (ER) when calculated at source, also denoted as a normalised excess mixing ratio (NEMR) for any other point in a plume away from source, and accounts for the effects of dispersion. These ratios can also be used as a marker for potential SOA formation, as the longer atmospheric lifetime of CO (~1 month) relative to that of OA (on the order of several weeks to months) makes it likely that any enhancement of the ratio between the two species will be a result of the addition of OA, rather than increased removal of CO in isolation. Figure 2 shows △OA/△CO for all 5 relevant BORTAS flights, with average values determined from the gradient of linear least squares regressions. Using this approach reveals that the average △OA/△CO close to source (0.190 ± 0.010) exceeds that for aged plumes (0.097 ± 0.002) by around 50%, with an overall campaign average of 0.092 ± 0.002. Average ratios for individual flights sampling aged emissions range from 0.056 ± 0.003 (B624) to 0.114 ± 0.003 (B622), giving an overall range of 0.058. The level of average △OA/△CO for fresh emissions from boreal forest fires during BORTAS falls between the upper extent derived from the eucalypt forests of northern Australia during ACTIVE (0.329), and lower ratios from several other campaigns where OA enhancements were comparatively reduced (0.019-0.065; *Jolleys et al., 2012*). Average △OA/△CO from aged plumes during BORTAS was again within the range identified from previous field observations, although with closer proximity to ratios from the

lower extent of the observed range, including aged boreal forest fire plumes sampled during the Arctic Research of the Composition of the Troposphere from Aircraft and Satellites (ARCTAS) campaign (*Hecobian et al., 2011*). The extent of variability amongst aged emissions during ACTIVE also exceeded that observed during BORTAS, with flights throughout the former campaign sampling plumes from fires in a number of different source regions. However, analysis of ERs from vegetation fires performed under laboratory conditions during the second Fire Lab At Missoula Experiment (FLAME II) also revealed extensive variability in △OA/△CO directly at source, even amongst single plant species (*Jolleys et al., 2013*). The single source region from which BORTAS plumes originated could therefore still be expected to give rise to significantly contrasting △OA/△CO, while the effects of atmospheric processing during transportation provide further perturbation of initial ERs. Aged BORTAS plumes had been transported over extensive geographical and temporal scales, and provide an indication of the potential implications of OA losses during long-range transport. Average △OA/△CO decreased progressively as the distance from source at which plumes were intercepted increased, with B622 performing a transit between Halifax and Quebec City, and B624 primarily sampling plumes over the North Atlantic off the eastern coast of Nova Scotia and Newfoundland. Unexpectedly low △OA concentrations during sections of flight B622 where △CO was significantly elevated provide further evidence for the removal of BB aerosol from aged plumes. This relationship has also been identified in BC concentrations, and attributed to wet removal of particulates following advection through clouds, as corroborated by meteorological observations and back trajectory models (*Taylor et al., 2013*).

3.2 Tracers for combustion conditions

While the evolution of △OA/△CO in aging plumes would appear to be strongly influenced by the effects of atmospheric processing, source conditions remain a critical factor in controlling OA production. Contrasts in △OA/△CO between fresh and aged OA are accompanied by varying properties with respect to the location and composition of plumes.

Proportional contributions of OA mass fragment marker species differ between near and far-field measurements. f_{60} represents the prevalence of primary combustion products such as levoglucosan and is used as an indicator for fresh BB emissions (*Schneider et al., 2006; Alfarra et al., 2007*). Conversely, f_{44} is associated with the CO_2^+ ion derived from more aged OA as hydrocarbon fragments are oxidised to form organic acids (*Zhang et al., 2005; Aiken et al., 2008*), although *m*/*z* 44 has also been shown to be significantly elevated at source, dependent on combustion conditions (*Weimer et al., 2008; Jolleys et al., 2013*). While strongly associated with saturated hydrocarbon fragments, *m*/*z* 43 can also originate from oxidised compounds such as aldehydes and ketones (*Alfarra et al., 2004*). Large contributions of *m*/*z* 43 have been observed within the mass spectra of OA during the laboratory combustion of a range of biomass fuels, typically accounting for a greater proportion of total OA mass than any other detected fragments (*Schneider et al., 2006*). This dominance of *m*/*z* 43 above *m*/*z* 44 amongst even compounds with high oxygen contents suggests the former can be produced preferentially during the fragmentation of oxygenated molecules, and as such f_{43} may prove to be an appropriate indictor of OA oxygenation at source.

Variations in the average proportions of *m*/*z* 43, 44 and 60 in OA between fresh and aged plumes are widely observed throughout BORTAS, emphasising the contrasting properties of aerosol of different ages. Mean f_{44} for B626, which comprised the only measurements of fresh OA during BORTAS, was lower than all other flights at 0.086 ± 0.014, with mean values for B621-B624 ranging from 0.104 to 0.139. This trend between the near and far-field is consistent with observations of boreal forest fire plumes during ARCTAS, where f_{44} was shown to increase as a function of plume transport time (*Cubison et al., 2011; Hecobian et al., 2011*). f_{60} was also shown to decrease concurrently with increasing f_{44} during ARCTAS, as a result of the oxidation of primary levoglucosan-type species with aging. However, mean f_{60} for BORTAS flight B626 was also amongst the lowest throughout the campaign at 0.007 ± 0.004. Averages were higher for B621-B623 (0.010-0.017), although B624 provided the lowest f_{60} with a mean of 0.005 ± 0.001.

While the higher mean f_{44} observed in the far-field is likely to primarily result from more extensive oxidation of OA after longer periods of aging, the transition to more smouldering-dominated combustion prior to sampling of near-field plumes could also have influenced observed changes in composition. Elevated levels of f_{60} in aged plumes are indicative of such an effect, as *m*/*z* 60 would be expected to constitute a greater proportion of fresh OA, given its typical progressive depletion through oxidation (*Cubison et al., 2011*). However, the relationships between f_{44}, f_{60} and combustion phase are known to be complex and subject to considerable uncertainty. *Weimer et al.* (*2008*) showed f_{60} to be more strongly associated with the initial flaming phase of combustion in wood burners used for domestic heating, while f_{44} was higher during the later stages of the burning process when smouldering combustion dominated. These trends are attributed to changes in combustion behaviour and the consumption of different fuel components at each stage of the fire. In contrast, *Gao et al.* (*2003*) reported significantly elevated levoglucosan concentrations from smouldering fires in southern Africa, and severe depletion in emissions from flaming fires. Furthermore, *Lee et al.* (*2010*) reported overall similarity in f_{60} across flaming and smouldering phases for open biomass fires carried out in a laboratory setting as part of FLAME II, while the ratio of levoglucosan to total organic carbon in filter samples from the same experiment shows a dependence on the fuel component burned (*Sullivan et al., 2008*). Although both f_{44} and f_{60} were more frequently at a maximum during flaming combustion in FLAME II burns (*Jolleys et al., 2013*), differences between phases were more pronounced for f_{44}, with less variation amongst f_{60}. This behaviour is expected to result from greater fire intensity during flaming combustion, although the specific effects of increased intensity on OA composition through changing oxygen availability remain unclear.

Further indication of a shift in combustion phase is provided by the differences in f_{43} between fresh and aged plumes, for which respective mean values were 0.123 ± 0.013 and 0.088 ± 0.012. The low f_{44} and f_{60} for fresh OA suggest a dominance of smouldering fires, in agreement with the trends identified by *Jolleys et al.* (*2013*). Additional variations in plume

properties appear to substantiate an association between f_{43} and smouldering combustion, including the correlation between periods of high f_{43} (>0.1) and low △BC /△OA (<0.02) in both fresh and aged plumes, with production of BC expected to be at a maximum during flaming combustion (*Reid & Hobbs, 1998*). Absence of a prominent flaming phase close to source is also corroborated by very low BC mass loadings, and reduced △BC /△OA relative to aged emissions, while the elevated △OA/△CO from these fires is consistent with the enhanced OA production typical of smouldering combustion (*Yokelson et al., 1997*). The lower △OA/△CO and f_{43}, but higher f_{44} and f_{60}, for aged OA would therefore be expected to derive from more intense, flaming-dominated combustion, which would also account for the significantly higher concentrations observed for many species despite plumes being progressively diluted over several days.

3.3 Effects of combustion conditions on vertical distributions

Altitudinal variations in plume composition further emphasise the importance of combustion conditions as a control on BB emissions and their propagation within the atmosphere. Using the △BC/△OA ratio as an indicator for the comparative contributions from flaming and smouldering combustion phases to the overall BB particulate loading (*Grieshop et al., 2009*) reveals a clear shift between the properties of aged plumes sampled in the upper and lower troposphere, with higher altitude plumes more typical of flaming combustion (Figure 3). With the exception of a few isolated points, △BC/△OA only rises above 0.02 when f_{43} is below 0.09, and remains consistently low when f_{43} is above this level. This trend is in part due to the reduced production of BC under smouldering conditions, as reflected by corresponding distributions of low BC mass concentration, CO_2 and f_{60}. Conversely, plumes sampled at lower altitudes exhibit characteristics associated with smouldering combustion, and are comparable to fresh plumes with regards to △BC/△OA, f_{43} and f_{60} levels, with all measurements during flight B626 taking place below 2000 m. Weaker convection resulting from smouldering fires limits vertical transportation, retaining plumes

within the boundary layer (*Andreae et al., 1996; Warneke et al., 2006; Burling et al., 2011*). The presence of flaming-derived emissions at higher altitudes alludes to an elevated injection height resulting from increased buoyancy and pyroconvection (*Fromm et al., 2005; Damoah et al., 2006*) driven by more intense fires earlier in the BORTAS campaign period. A similar dependence on combustion phase has previously been observed for the altitudinal distribution of different combustion products from boreal forest fires during ARCTAS (*Kondo et al., 2011*).

Altitudinal profiles for a number of properties shown in Figure 4 highlight the apparent influence of combustion phase on the vertical distribution aged plumes during BORTAS. The vertical decrease in △OA/△CO and increase in △BC/△OA through successive 500 m bins highlights the changing composition of plumes at different altitudes and the apparent influence of fire properties at source. Mean △OA/△CO stands at 0.155 ± 0.061 and 0.196 ± 0.103 for the two bins closest to the surface, declining to 0.038 ± 0.015 at 6000 m. The interquartile range also decreases from 0.147 to 0.044 between 1500 and 5500 m, reflecting an overall reduction in variability with altitude. In contrast, mean △BC/△OA rises from 0.015 ± 0.003 at 500 m to 0.110 ± 0.055 at 6000 m, with the interquartile range increasing from 0.006 (2000 m) to 0.068 (5500 m). The altitudinal trends identified for △OA/△CO and △BC/△OA also show broad agreement with those of f_{43} and f_{60}, with mean values for the former decreasing from 0.078 ± 0.003 to 0.128 ± 0.006 and latter increasing from 0.005 ± 0.001 to 0.015 ± 0.002. The directly opposing profiles of f_{43} and CO_2, along with the agreement between increased f_{60} and BC mass at high altitudes (Figure 5), further underline the importance of initial combustion conditions for aged emissions. Minimum CO_2 concentrations within aged plumes were around 375 ppm, representing a minimal elevation above typical background levels for boreal Canadian forest environments (*Vay et al., 2011, Higuchi et al., 2003*). Although the distribution of CO_2 clearly reflects the influence of the biosphere closer to the surface through uptake in photosynthesis, expected source profiles also appear to be largely conserved, further corroborated by the sustained correlation between periods of high f_{43} and low CO_2 and vice versa.

3.4 Aging as a driver for plume variability

Despite the apparent influence of combustion conditions on the vertical distribution and composition of aged emissions, the effects of transformations associated with atmospheric processing cannot be entirely discounted. Certain contrasting properties between emissions of different ages could also be less dependent on source conditions and more strongly influenced by processing throughout plume evolution. Differences between fresh and aged plumes in the respective relationships of total △OA loadings, and those normalised to △CO, with a number of tracers highlight the combined effects of source conditions and processing, and their changing influence with aging. Both △OA and △CO concentrations show a positive correlation with f_{60} and negative correlation with f_{44}. These overriding trends remain consistent for emissions of all ages, although the nature of the relationship changes in each case. Linear relationships appear consistently for △OA (R^2 = 0.51 and 0.80 with f_{44} and f_{60} respectively) and △CO (R^2 = 0.23 and 0.49) in fresh emissions. The same relationships also persist to an extent for △OA/△CO in fresh plumes (R^2 = 0.42 and 0.47). However, at a greater distance from source, correlations for △OA and △CO are consistently below 0.3, while there is no relationship between △OA/△CO and either f_{44} or f_{60}. This disparity suggests that NEMRs in the far-field are less solely dependent on source conditions than ERs in the near-field, and are more strongly affected by further influences during aging.

In addition to providing a tracer for source profiles in aged BB emissions, △BC/△OA can also be used as an indicator for OA processing. Observations of increasing △BC/△OA with aging have previously been attributed to the loss of OA mass through evaporation (*Liousse et al., 1995*). Similar behaviour has also been proposed as a possible cause of the overall reduction in △OA/△CO between BB plumes in the near and far-field throughout several campaigns across different global regions (*Jolleys et al., 2012*). Any decrease in △BC/△OA could therefore be considered a product, to a certain degree, of the addition of secondary organic mass from either the processing of BBOA or external sources. Measurements performed at lower altitudes (<2000 m) during flights B621 and B622 provide possible

evidence to support such an effect. Both BC mass and f_{60} remain low during these periods, at less than 0.5 μg m^{-3} and 0.01 respectively, consistent with wider observations of smouldering fire emissions at low altitude during BORTAS. However, △CO concentrations are also diminished and consistently below 100 ppb, relative to an average of 200 ppb for aged plumes, while △OA concentrations are comparable to levels in higher altitude, flaming-type plumes (~20 μg m^{-3}). These trends, which diverge from the expected characteristics for emissions of this origin, are further compounded by high $\triangle O_3/\triangle CO$ (>0.2), indicative of an elevated level of oxygenation and photochemical activity (*Mason et al., 2001*). Formation of SOA from biogenic precursors has previously been observed in the forests of Ontario (*Slowik et al., 2010*). These SOA events were also characterised by △OA/△CO levels far in excess of those derived for BB emissions during the same study. In accordance with this trend, △OA/△CO within the low altitude plumes in B621 and B622 were consistently above the average for aged emissions (0.097), reaching as high as ~0.4. There is subsequently considerable evidence to support biogenic SOA as a potential contributor to the OA burden during BORTAS, which could provide further enhancement of △OA/△CO as demonstrated by the *Slowik et al.* (*2010*) Ontario study. Whilst the further properties of aged plumes discussed here would suggest this effect is isolated and limited in its overall impact, it presents a further source of uncertainty for any attempts to develop parameterisations for the contribution of forest fires to regional and global OA budgets.

Although f_{60} displays a level of consistency with flaming combustion products in upper troposphere plumes, and increases on average with increasing altitude, further trends oppose the expected relationships for different combustion phases. Maximum concentrations of △OA, △BC, △CO and CO_2 all coincide with high f_{60} (0.025-0.300) and show a reduction as f_{60} decreases (Figure 5). Overall correlations between each species and f_{60} are all positive, albeit with varying fit coefficients. R^2 values were highest for CO_2 and △BC (0.52 and 0.47), reflecting their stronger associations with flaming combustion (*Crutzen & Andreae, 1990; Reid et al., 2005*). Correlations with △OA and △CO were weaker (R^2 = 0.28 and 0.23), as would be

expected given production of each is greatest during the smouldering phase (*Ferek et al., 1998; Andreae & Merlet; 2001; Gao et al., 2003*). However, the underlying relationships identified for each species with f_{60} suggest this factor may prove to be a more resilient tracer for overall plume intensity at long aging times. *Petzold et al.* (*2007*) demonstrated export efficiencies of up to 90% for BC following intercontinental transport of boreal forest fire plumes. In the absence of significant removal through wet deposition, BC/△CO remained consistent with typical source values in plumes encountered at altitudes above 4km, indicating that mixing of emissions can be suppressed where fire intensity is sufficient to generate elevated injection heights. Conversely, the weaker convection associated with smouldering combustion may lead to emissions being retained within the boundary layer, contributing to the observed enhancements in △OA/△CO and f_{43} at low altitudes.

3.5 Tracer evolution during BORTAS

The progression from f_{60} to f_{44} can provide a useful metric to assess the evolution of OA composition with aging. Figure 6 shows the nature of this progression for both fresh and aged OA, together with further trends with several additional parameters. A strong linear relationship (R^2 = 0.72) is identified for emissions close to source. However, these observations comprised measurements of three separate periods of flight B626, and reveal a clear discrepancy for one of these periods. Measurements performed further to the east of the source region, on a transect from approximately 52.3° N, 90.0° W to 52.8° N, 91.3° W (a 'downwind' plume) yielded higher f_{44} than any other fresh plumes, with f_{60} not exceeding 0.045. The two remaining sets of plumes ('source' plumes) were both encountered within a region where active fires were present at around 52.4-52.8° N, 93.0-93.7° W. Despite sampling taking place roughly two hours apart, and over a slightly different geographical extent, the f_{44}/f_{60} relationship remains highly consistent across all 'source' plumes, with an R^2 of 0.82. The higher levels of f_{44} and absence of a trend with f_{60} in the 'downwind' plume indicate OA is more heavily oxidised than in the fresher 'source' plumes. This contrast in oxygenation is

linked to other changes between plumes, including apparent photochemical age, which in this instance is represented by the $-\log(NO_x/NO_y)$ ratio (*Kleinman et al., 2008; DeCarlo et al., 2008*). Levels of the ratio are significantly elevated in the 'downwind' plume from B626, with an average of 1.45 ± 0.43, exceeding the mean value of 1.09 ± 0.29 for highly aged plumes sampled during flights B621-B624. CO_2 concentrations during this period are also higher than for the remainder of B626, with an average of 378.6 ± 0.6 ppm compared to 375.0 ± 1.3 ppm closer to source. The $-\log(NO_x/NO_y)$ photochemical clock is also shown to increase throughout 'source' plumes with f_{44} and f_{60} changing in a manner consistent with the increasing oxidation of OA, and is further corroborated by a trend of increasing $\triangle O_3/\triangle CO$. However, these changes also coincide with a trend of decreasing $\triangle OA/\triangle CO$, belying the expected addition of OA mass resulting from increasing oxygenation. Average $\triangle OA/\triangle CO$ is similar for the two 'source' plumes (0.165 ± 0.042 and 0.180 ± 0.045), but is lower in the more photochemically aged 'downwind' plume (0.114 ± 0.015). It is difficult to speculate on the significance of any link between a higher rate of oxidation and an overall reduction in $\triangle OA/\triangle CO$ given the continuing uncertainty regarding the processes affecting OA in aging BB plumes. *Yokelson et al.* (*2009*) reported that $\triangle OA/\triangle CO$ increased by a factor of 2.3 over a period of 1.4 hours for plumes from fires in the Yucatan region of Mexico, coinciding with a comparably high f_{44}/f_{60} gradient to that in the 'downwind' section of B626. Conversely, an increase in f_{44} has also been shown in conjunction with stable or even decreasing levels of $\triangle OA/\triangle CO$ (*Capes et al., 2008; Cubison et al., 2011; Akagi et al., 2012; Jolleys et al., 2012*), suggesting OA loss through evaporation has an equally important effect throughout plume evolution.

Linear relationships between f_{44} and f_{60} are weaker for more aged plumes sampled at a greater distance downwind, with an overall R^2 value for all plumes of 0.44 and individual flights ranging from 0.01 (B624) to 0.32 (B622). The overall decline of f_{60} again appears to be strongly influenced by distance from the source region, decreasing from a maximum of ~0.027 in B622 to a minimum of ~0.004 in B624. An effect of dilution is evident, given the concurrent

reduction in both △CO and CO_2 with decreasing f_{60} and increasing f_{44}. $\triangle O_3/\triangle CO$ shows the reverse progression, increasing with the oxygenation of OA, while $-\log(NO_x/NO_y)$ does not exhibit the strong trend observed for near-field measurements but is typically higher and reflects longer aging times. However, $-\log(NO_x/NO_y)$ ratios were highest on average for the 'downwind' plume in B626, which did not provide any significant indication of net addition of OA mass. While the highest average △OA/△CO ratio for an individual plume throughout the entirety of BORTAS was derived for one of the 'source' plumes during B626, two aged plumes from B622 exhibited average △OA/△CO of a similar magnitude (0.120 ± 0.080 and 0.119 ± 0.042), with each plume representing a different region of f_{44}/f_{60} space. Together with the overall lack of consistency between △OA/△CO and f_{44}/f_{60} throughout aged plumes, and the subsequent contrast with plumes at source, this inconsistency further highlights the need for improved characterisation of the processes contributing towards aging of BBOA during long range transport.

The contrasting behaviours of various tracers throughout fresh and plumes highlights the different ways in which these properties can be used to evaluate influences on BBOA evolution. With regards to f_{44}, the consistently higher values observed in aged plumes, and the strong trends identified with indicators of photochemical aging such as $-\log(NO_x/NO_y)$ and $\triangle O_3/\triangle CO$ close to source (Figure 6), substantiate its use as a tracer for OA aging. Although f_{60} exhibits the same clear relationship with $-\log(NO_x/NO_y)$ and $\triangle O_3/\triangle CO$ in fresh plumes, albeit reversed and decreasing with aging, values are higher on average amongst aged plumes. Given the overall trend of increasing f_{44} with decreasing f_{60} remains for aged OA, the longer periods of aging to which these plumes have been exposed would be expected to bring about a more extensive reduction in the latter tracer. The elevation in f_{60} relative to fresh plumes would therefore seem to stem from the contrasting combustion phases associated with plumes of different ages, and the persistence of high levels in flaming-derived OA at greater altitudes. In contrast, f_{43} shows an overall reduction with aging, with mean values of 0.123 ± 0.013 and 0.088 ± 0.012 for near and far-field plumes respectively, consistent with the

oxidation of primary OA components over time. However, overall trends with $-\log(NO_x/NO_y)$ and $\triangle O_3/\triangle CO$ in fresh plumes are generally positive, albeit with fairly weak correlation coefficients (R^2 = 0.12 and 0.34), resulting in f_{43} peaking at greater photochemical ages. This relationship contradicts that which would be expected in aging OA (Ng et al., 2010; Morgan et al., 2010), and suggests additional factors may be contributing to the observed variability in f_{43}. Values of f_{43} in fresh OA are almost entirely greater than 0.1, while this threshold is most frequently exceeded amongst aged OA in plumes below around 3000 m (Figure 4). These lower altitude plumes exhibit the same low $\triangle BC/\triangle OA$ levels as identified close to source (< 0.02), in contrast to the greater range in $\triangle BC/\triangle OA$ (up to 0.15) coinciding with lower f_{43} (Figure 3). Differing distributions of f_{43} in aged plumes, and the prescribed similarities with near-field observations, may reflect an influence of changing combustion conditions, with f_{43} seemingly more prominent in OA from smouldering fires. As a result, f_{43} may prove to be a more suitable tracer for source conditions rather than the effects of aging, although comparison between different combustion phases at source would be required in order to fully constrain any such relationship.

3.6 Campaign intercomparison and evaluation of f_{44} and f_{60} tracers

The progression of f_{44} and f_{60} throughout BORTAS shows a number of similarities with observations from other field campaigns and laboratory experiments. Distributions for fresh and aged emissions from BORTAS and montane forest fires during the Megacities Initiative: Local and Global Research Observations (MILAGRO) campaign are presented in Figure 7, along with data from numerous plumes measured during ARCTAS-B. Data are also shown for the combustion of boreal forest plant species under laboratory conditions as part of FLAME II. Similar trends in f_{44}/f_{60} for fresh and aged emissions are identified for BORTAS and MILAGRO, with average f_{44} increasing with aging in both cases. A significant contrast is also evident in the distributions of f_{60}, which is higher on average for fresh plumes in MILAGRO and aged plumes in BORTAS, possibly as a result of the reduced intensity of fires sampled close to source.

Average △OA/△CO is again lower for the aged fraction in MILAGRO, decreasing from 0.051 ± 0.001 to 0.041 ± 0.001 (*Jolleys et al., 2012*), consistent with a loss of OA. The lower magnitude of these ratios is likely to be a consequence of different fuel properties and resulting combustion conditions, as strongly-flaming grass fires are expected to have made a significant contribution to smoke plumes sampled at the Paso de Cortes measurement site (*Jolleys et al., 2013*). Figure 7 also emphasises the differences in emissions from boreal forest fires during ARCTAS-B and BORTAS. Plumes encountered close to source in each campaign exhibit contrasting levels of f_{60}, reflecting the dominance of different combustion phases in each set of measurements. Unlike the heavily smouldering fires sampled in flight B626, the plume from a fire at Lake McKay in northwestern Saskatchewan was produced by highly intense, flaming fires (*Cubison et al., 2011*). The Lake McKay fires subsequently yielded higher f_{60} than was observed for any BORTAS plumes, peaking at around 0.05. As the Lake McKay plume was tracked downwind, f_{44} increased to ~0.12, comparable to the upper extent for fresh plumes in BORTAS. Although f_{60} decreased to ~0.015, this level remained above the majority of the distribution from BORTAS. Similarly high levels of f_{60} were observed for black spruce fires during FLAME II. However, f_{44} from these burns was generally exceptionally low, as would be expected given the direct measurement at source and lack of aging. Higher f_{44} comparable to the range identified in ambient emissions did occur in chamber fires for plant species representing environments other than boreal forests, with average values particularly high for chaparral fuels. Montane forest fuels, which like the boreal equivalent comprised samples of coniferous species, also yielded f_{44} up to ~0.15, although such fires largely involved drier, woody plant material leading to more flaming-dominated combustion (*Jolleys et al., 2013*).

The different f_{44} and f_{60} regimes in ambient and chamber fires, and their conflicting relationships with combustion phases, suggest their use as tracers for processing of BBOA is highly dependent on both fire properties and experimental conditions. Throughout FLAME II, f_{44} was shown to be more strongly associated with flaming combustion, as increased intensity and turbulent mixing enhanced the supply of oxygen to fires. In contrast, the rapid increase in

f_{44} in fresh OA from smouldering firesduring BORTAS, to levels comparable to more extensively aged plumes, indicate that f_{44} is strongly influenced by post-emission processing under ambient conditions. Relationships with f_{60} are more consistent, being higher on average more frequently for flaming-dominated fires under laboratory conditions, and showing a stronger association with seemingly flaming-derived aged emissions during BORTAS. Probability density functions (PDFs) for f_{44} and f_{60} in fresh and aged emissions from BORTAS, along with source emissions from fires involving boreal and montane forest fuels during FLAME II, are shown in Figure 8. The clear separation in f_{44} distributions between chamber and ambient measurements reflects the role of aging in determining the level of oxidation in BBOA, as further evidenced by the enhancement in plumes in the far-field above those at source. However, the trend of increasing f_{44} in fresh plumes suggests that this processing can occur over very short timescales under certain atmospheric conditions. Rapid oxidation of BB smoke plumes has previously been inferred from the addition of secondary OA mass within ~1 hour of emission (*Gao et al., 2003; Yokelson et al., 2009*), corroborating the BORTAS trend. Values of f_{44} coinciding with peak concentrations for a number of combustion products are also shown in Figure 8. These peak concentrations show a good agreement with prescribed combustion phase relationships for FLAME II data, with $\triangle CO_2$ reaching a maximum when f_{44} is higher, and hence combustion more flaming-dominated, while $\triangle$OA and $\triangle$CO peak at a lower f_{44}. The same trends are also observed throughout BORTAS, with peak concentrations for $\triangle CO_2$ and $\triangle$BC coinciding with higher levels of f_{44} than those of $\triangle$CO or $\triangle$OA. PDFs for f_{60} exhibit the same trend amongst ambient plumes, shifting to higher values with aging. Distributions are also broadened for emissions from chamber burns, for which levoglucosan-type species constitute a larger proportion of the total OA mass. The very low peak for near-field BORTAS plumes could be influenced by both the absence of a significant flaming phase and subsequent oxidation of primary OA (*Cubison et al., 2011*), contributing to the increase in f_{44}. The variable gradients for f_{44}/f_{60} regressions (Figure 7) indicate a slower rate of decay for levoglucosan-type OA in aged BORTAS plumes compared to their equivalents from

MILAGRO. Furthermore, mean f_{60} in aged MILAGRO plumes (0.006 ± 0.003) was lower than in fresh plumes (0.018 ± 0.006), while the opposite was true for BORTAS plumes (0.012 ± 0.005 and 0.007 ± 0.004 respectively). As such, the slower decline of f_{60} and potential influences from more strongly flaming combustion may contribute towards the observed enhancement in aged BORTAS plumes, while a faster rate of oxidation and largely smouldering fires reduce levels closer to source.

4. Conclusions

Smoke plumes from Canadian boreal forest fires have been shown to exhibit highly variable properties over a range of ages. Average △OA/△CO in plumes sampled close to source (0.190 ± 0.010) exceed ratios in the far-field (0.056 ± 0.003 to 0.114 ± 0.003), reaffirming an absence of significant net SOA formation for aging BB emissions, at least to an extent that provides an elevation above initial OA production at source. A lack of increasing △OA/△CO has been widely observed in previous BB assessments, with a similar trend in BORTAS further emphasising the importance of source conditions. High levels of typical flaming combustion products were identified in highly aged plumes following transportation over a period of several days. Enhancements in △BC/△OA and f_{60} were most prominent within the free troposphere, typically displaying an overall increase with altitude, while aged OA sampled within the boundary layer showed stronger evidence for production by smouldering combustion. Plume injection height, as determined by combustion conditions at source, may therefore have a pivotal influence on the long-range retention of initial plume properties.

Aging of BBOA during BORTAS has been extensively evaluated using the key tracers f_{44} and f_{60} from the AMS mass spectrum. An enhancement in f_{44} was determined for far-field plumes, where the mean value of 0.121 ± 0.016 significantly exceeded that in the near-field (0.086 ± 0.014). Similarly, f_{60} remained higher in aged plumes (0.012 ± 0.005) than those close

to source (0.007 ± 0.004), in spite of the concurrent increase in oxygenation and expected processing of primary OA components. These trends highlight the importance of both source conditions and processing for OA composition in BB plumes. While the influence of combustion phase on f_{44} remains highly uncertain given contrasting relationships with smouldering and flaming combustion reported in different studies, increases observed close to source suggest oxidation can occur over very short timescales after emission. This rapid processing is further corroborated by concurrent increases in photochemical tracers such as $\triangle O_3/\triangle CO$ and $-\log(NO_x/NO_y)$ ratios in plumes sampled at source. The increasing oxygenation of BBOA is not accompanied by an increase in $\triangle OA/\triangle CO$, which shows no significant change with $\triangle O_3/\triangle CO$ and decreases on average with $-\log(NO_x/NO_y)$. A lack of $\triangle OA/\triangle CO$ enhancement irrespective of evidence for wider transformations therefore further substantiates the impact of OA losses in aging BB plumes.

Presenting the changing composition of BBOA in f_{44}/f_{60} space reveals a consistent progression from high f_{60} to high f_{44} as primary levoglucosan-like species are lost through oxidation. Similar transitions occur across multiple datasets encompassing smoke plumes of varying origins and ages, although the gradients and extents of distributions show some variability between campaigns. Levels of f_{44} are also comparatively depleted in chamber burns of boreal forest fuels. The absence of aging and a strong association with flaming combustion, and hence oxygen supply through entrainment, in these experiments denote alternative tracer functions under laboratory and ambient conditions. While f_{44} can act as an indicator for oxygenation through combustion processes in chamber experiments, the influence of aging is likely to limit such application for ambient emissions. However, f_{60} has been shown to act as a long-lived tracer for BB emissions, despite evidence for an overall reduction with increasing f_{44}.

Analysis of measurements performed during the BORTAS campaign has provided further insight to the variability associated with BB emissions and the processes affecting changes in BBOA loadings and composition over time. However, there remains considerable uncertainty regarding the main drivers of OA processing. While data from BORTAS provide

evidence for the influence of a range of source and aging processes, the extents of any effects on aging BBOA are unclear, particularly with regard to their consistency across different environments and fire types. Key trends identified in this analysis, such as the comparatively lower levels of f_{60} close to source, contradict previous findings and highlight the lack of consistency prevalent amongst many aspects of investigations focusing on BB emissions. Further research specifically targeting these areas of uncertainty is therefore essential in order to understand the cause of these disparities and provide more reliable parameterisations of BB contributions to the atmospheric aerosol burden.

Acknowledgments

The authors would like to acknowledge financial support from the United Kingdom Natural Environment Research Council (NERC), and thank all those involved in the BORTAS project. Airborne data was obtained using the FAAM BAe-146 Atmospheric Research Aircraft (ARA) operated by Directflight Ltd (DFL) and managed by the Facility for Airborne Atmospheric Measurements (FAAM), which is a joint entity of NERC and the UK Meteorological Office. M. D. Jolleys was supported by a NERC studentship NE/H525162/1.

References

Aiken, A. C., et al. (2008), O/C and OM/OC ratios of primary, secondary, and ambient organic aerosols with high-resolution time-of-flight aerosol mass spectrometry, *Environmental Science & Technology*, *42*(12), 4478-4485, doi:10.1021/es703009q.

Aiken, A. C., et al. (2009), Mexico City aerosol analysis during MILAGRO using high resolution aerosol mass spectrometry at the urban supersite (T0) - Part 1: Fine particle composition and organic source apportionment, *Atmospheric Chemistry and Physics*, *9*(17), 6633-6653.

Akagi, S. K., R. J. Yokelson, C. Wiedinmyer, M. J. Alvarado, J. S. Reid, T. Karl, J. D. Crounse, and P. O. Wennberg (2011), Emission factors for open and domestic biomass burning for use in atmospheric models, *Atmospheric Chemistry and Physics*, *11*(9), 4039-4072, doi:10.5194/acp-11-4039-2011.

Akagi, S. K., et al. (2012), Evolution of trace gases and particles emitted by a chaparral fire in California, *Atmospheric Chemistry and Physics*, *12*(3), 1397-1421, doi:10.5194/acp-12-1397-2012.

Alfarra, M. R., H. Coe, J.D. Allan, K.N. Bower, H. Boudries, M.R. Canagaratna, J.L. Jimenez, J.T. Jayne, A.A. Garforth, S.M. Li, and D.R. Worsnop (2004), Characterization of urban and rural organic particulate in the Lower Fraser Valley using two Aerodyne Aerosol Mass Spectrometers, *Atmospheric Environment*, *38* (34), 5745-5758, doi: 10.1016/ j.atmosenv.2004.01.054.

Alfarra, M. R., A. S. H. Prevot, S. Szidat, J. Sandradewi, S. Weimer, V. A. Lanz, D. Schreiber, M. Mohr, and U. Baltensperger (2007), Identification of the mass spectral signature of organic aerosols from wood burning emissions, *Environmental Science & Technology*, *41*(16), 5770-5777, doi:10.1021/es062289b.

Andreae, M. O., E. Atlas, H. Cachier, W. R. Cofer III, G. W. Harris, G. Helas, R. Koppmann, J.-P. Lacaux and D. E. Ward (1996), Trace gas and aerosol emissions from savanna fires, in *Biomass Burning and Global Change*, edited by S. Levine, pp. 278-295, MIT Press, Cambridge, Mass.

Andreae, M. O., and P. Merlet (2001), Emission of trace gases and aerosols from biomass burning, *Global Biogeochemical Cycles*, *15*(4), 955-966.

Bahreini, R., J. L. Jimenez, J. Wang, R. C. Flagan, J. H. Seinfeld, J. T. Jayne, and D. R. Worsnop (2003), Aircraft-based aerosol size and composition measurements during ACE-Asia using an Aerodyne aerosol mass spectrometer, *Journal of Geophysical Research-Atmospheres*, *108*(D23), doi:10.1029/2002jd003226.

Bond, T. C., D. G. Streets, K. F. Yarber, S. M. Nelson, J. H. Woo, and Z. Klimont (2004), A technology-based global inventory of black and organic carbon emissions from combustion, *Journal of Geophysical Research-Atmospheres*, *109*(D14), doi:10.1029/2003jd003697.

Burling, I. R., R. J. Yokelson, S. K. Akagi, S. P. Urbanski, C. E. Wold, D. W. T. Griffith, T. J. Johnson, J. Reardon, and D. R. Weise (2011), Airborne and ground-based measurements of the trace gases and particles emitted by prescribed fires in the United States, *Atmospheric Chemistry and Physics*, *11*(23), 12197-12216, doi:10.5194/acp-11-12197-2011.

Canagaratna, M. R., et al. (2007), Chemical and microphysical characterization of ambient aerosols with the aerodyne aerosol mass spectrometer, *Mass Spectrometry Reviews*, *26*(2), 185-222, doi:10.1002/mas.20115.

Capes, G., B. Johnson, G. McFiggans, P. I. Williams, J. Haywood, and H. Coe (2008), Aging of biomass burning aerosols over West Africa: Aircraft measurements of chemical composition, microphysical properties, and emission ratios, *Journal of Geophysical Research-Atmospheres*, *113*(D20), doi:10.1029/2008jd009845.

Crosier, J., J. D. Allan, H. Coe, K. N. Bower, P. Formenti, and P. I. Williams (2007), Chemical composition of summertime aerosol in the Po Valley (Italy), northern Adriatic and Black Sea, *Quarterly Journal of the Royal Meteorological Society*, *133*, 61-75, doi:10.1002/qj.88.

Crounse, J. D., et al. (2009), Biomass burning and urban air pollution over the Central Mexican Plateau, *Atmospheric Chemistry and Physics*, *9*(14), 4929-4944.

Crutzen, P. J., and M. O. Andreae (1990), Biomass Burning in the Tropics - Impact on Atmospheric Chemistry and Biogeochemical Cycles, *Science*, *250*(4988), 1669-1678, doi:10.1126/science.250.4988.1669.

Cubison, M. J., et al. (2011), Effects of aging on organic aerosol from open biomass burning smoke in aircraft and laboratory studies, *Atmospheric Chemistry and Physics*, *11*(23), 12049-12064, doi:10.5194/acp-11-12049-2011.

Damoah, R., N. Spichtinger, R. Servranckx, M. Fromm, E. W. Eloranta, I. A. Razenkov, P. James, M. Shulski, C. Forster, and A. Stohl (2006), A case study of pyro-convection using transport model and remote sensing data, *Atmospheric Chemistry and Physics*, *6*, 173-185.

DeCarlo, P. F., et al. (2008), Fast airborne aerosol size and chemistry measurements above Mexico City and Central Mexico during the MILAGRO campaign, *Atmospheric Chemistry and Physics*, *8*(14), 4027-4048.

Di Carlo, P., et al. (2013), Aircraft based four-channel thermal dissociation laser induced fluorescence instrument for simultaneous measurements of NO2, total peroxy nitrate, total alkyl nitrate, and HNO3, *Atmospheric Measurement Techniques*, *6*(4), 971-980, doi:10.5194/amt-6-971-2013.

Drewnick, F., et al. (2005), A new time-of-flight aerosol mass spectrometer (TOF-AMS) - Instrument description and first field deployment, *Aerosol Science and Technology*, *39*(7), 637-658, doi:10.1080/02786820500182040.

Ferek, R. J., J. S. Reid, P. V. Hobbs, D. R. Blake, and C. Liousse (1998), Emission factors of hydrocarbons, halocarbons, trace gases and particles from biomass burning in Brazil, *Journal of Geophysical Research-Atmospheres*, *103*(D24), 32107-32118.

Forster, P., et al. (2007), Changes in Atmospheric Constituents and in Radiative Forcing, in: *Climate Change 2007: The Physical Science Basis, contribution of Working Group I to the Fourth Assessment Report of the Intergovernmental Panel on Climate Change*, edited by: Solomon, S. D., Qin, M., Manning, Z., Chen, M., Marquis, K. B., Averyt, M. T., and Miller, H. L., p. 129–234, Cambridge University Press, Cambridge, United Kingdom and New York, NY, USA.

Fromm, M., R. Bevilacqua, R. Servranckx, J. Rosen, J. P. Thayer, J. Herman, and D. Larko (2005), Pyro-cumulonimbus injection of smoke to the stratosphere: Observations and impact

of a super blowup in northwestern Canada on 3-4 August 1998, *Journal of Geophysical Research-Atmospheres*, *110*(D8), doi:10.1029/2004jd005350.

Gao, S., D. A. Hegg, P. V. Hobbs, T. W. Kirchstetter, B. I. Magi, and M. Sadilek (2003), Water-soluble organic components in aerosols associated with savanna fires in southern Africa: Identification, evolution, and distribution, *Journal of Geophysical Research-Atmospheres*, *108*(D13), doi:10.1029/2002jd002324.

Grieshop, A. P., J. M. Logue, N. M. Donahue, and A. L. Robinson (2009), Laboratory investigation of photochemical oxidation of organic aerosol from wood fires 1: measurement and simulation of organic aerosol evolution, *Atmospheric Chemistry and Physics*, *9*(4), 1263-1277.

Hallquist, M., et al. (2009), The formation, properties and impact of secondary organic aerosol: current and emerging issues, *Atmospheric Chemistry and Physics*, *9*(14), 5155-5236.

Hecobian, A., et al. (2011), Comparison of chemical characteristics of 495 biomass burning plumes intercepted by the NASA DC-8 aircraft during the ARCTAS/CARB-2008 field campaign, *Atmospheric Chemistry and Physics*, *11*(24), 13325-13337, doi:10.5194/acp-11-13325-2011.

Hennigan, C. J., et al. (2011), Chemical and physical transformations of organic aerosol from the photo-oxidation of open biomass burning emissions in an environmental chamber, *Atmospheric Chemistry and Physics*, *11*(15), 7669-7686, doi:10.5194/acp-11-7669-2011.

Heringa, M. F., P. F. DeCarlo, R. Chirico, T. Tritscher, J. Dommen, E. Weingartner, R. Richter, G. Wehrle, A. S. H. Prevot, and U. Baltensperger (2011), Investigations of primary and secondary particulate matter of different wood combustion appliances with a high-resolution time-of-flight aerosol mass spectrometer, *Atmospheric Chemistry and Physics*, *11*(12), 5945-5957, doi:10.5194/acp-11-5945-2011.

Higuchi, K., D. Worthy, D. Chan, and A. Shashkov (2003), Regional source/sink impact on the diurnal, seasonal and inter-annual variations in atmospheric CO2 at a boreal forest site in Canada, *Tellus Series B-Chemical and Physical Meteorology*, *55*(2), 115-125, doi:10.1034/j.1600-0889.2003.00062.x.

Iinuma, Y., E. Bruggemann, T. Gnauk, K. Muller, M. O. Andreae, G. Helas, R. Parmar, and H. Herrmann (2007), Source characterization of biomass burning particles: The combustion of selected European conifers, African hardwood, savanna grass, and German and Indonesian peat, *Journal of Geophysical Research-Atmospheres*, *112*(D8), doi:10.1029/2006jd007120.

Jimenez, J. L., et al. (2009), Evolution of Organic Aerosols in the Atmosphere, *Science*, *326*(5959), 1525-1529, doi:10.1126/science.1180353.

Jolleys, M. D., et al. (2012), Characterizing the Aging of Biomass Burning Organic Aerosol by Use of Mixing Ratios: A Meta-analysis of Four Regions, *Environmental Science & Technology*, *46*(24), 13093-13102, doi:10.1021/es302386v.

Jolleys, M. D., et al. (2013), Organic Aerosol Emission Ratios from the Laboratory Combustion of Biomass Fuels, in preparation.

Kleinman, L. I., et al. (2008), The time evolution of aerosol composition over the Mexico City plateau, *Atmospheric Chemistry and Physics*, *8*(6), 1559-1575.

Kondo, Y., et al. (2011), Emissions of black carbon, organic, and inorganic aerosols from biomass burning in North America and Asia in 2008, *Journal of Geophysical Research-Atmospheres*, *116*, doi:10.1029/2010jd015152.

Le Breton, M., et al. (2013), Airborne hydrogen cyanide measurements using a chemical ionisation mass spectrometer for the plume identification of biomass burning forest fires, *Atmospheric Chemistry and Physics Discussions*, *13*, 5649-5685, doi:10.5194/acpd-13-5649-2013.

Lee, T., et al. (2010), Chemical Smoke Marker Emissions During Flaming and Smoldering Phases of Laboratory Open Burning of Wildland Fuels, *Aerosol Science and Technology*, *44*(9), I-V, doi:10.1080/02786826.2010.499884.

Li, Q. B., D. J. Jacob, I. Bey, R. M. Yantosca, Y. J. Zhao, Y. Kondo, and J. Notholt (2000), Atmospheric hydrogen cyanide (HCN): Biomass burning source, ocean sink?, *Geophysical Research Letters*, *27*(3), 357-360, doi:10.1029/1999gl010935.

Liousse, C., C. Devaux, F. Dulac, and H. Cachier (1995), Aging of Savanna Biomass Burning Aerosols - Consequences on their Optical Properties, *Journal of Atmospheric Chemistry*, *22*(1-2), 1-17, doi:10.1007/bf00708178.

Mason, S. A., R. J. Field, R. J. Yokelson, M. A. Kochivar, M. R. Tinsley, D. E. Ward, and W. M. Hao (2001), Complex effects arising in smoke plume simulations due to inclusion of direct emissions of oxygenated organic species from biomass combustion, *Journal of Geophysical Research-Atmospheres*, *106*(D12), 12527-12539.

McMeeking, G. R., et al. (2009), Emissions of trace gases and aerosols during the open combustion of biomass in the laboratory, *Journal of Geophysical Research-Atmospheres*, *114*, doi:10.1029/2009jd011836.

Morgan, W. T., J. D. Allan, K. N. Bower, G. Capes, J. Crosier, P. I. Williams, and H. Coe (2009), Vertical distribution of sub-micron aerosol chemical composition from North-Western Europe and the North-East Atlantic, *Atmospheric Chemistry and Physics*, *9*(15), 5389-5401, doi:10.5194/acp-9-5389-2009.

Morgan, W. T., J. D. Allan, K. N. Bower, E. J. Highwood, D. Liu, G. R. McMeeking, M. J. Northway, P. I. Williams, R. Krejci and H. Coe (2010), Airborne measurements of the spatial distribution of aerosol chemical composition across Europe and evolution of the organic fraction, *Atmospheric Chemistry and Physics*, *10*(8), 4065-4083, doi: 10.5194/acp-10-4065-2010.

Ng, N. L., et al. (2010), Organic aerosol components observed in Northern Hemispheric datasets from Aerosol Mass Spectrometry, *Atmospheric Chemistry and Physics*, *10*(10), 4625-4641, doi:10.5194/acp-10-4625-2010.

Nowak, J. B., J. A. Neuman, K. Kozai, L. G. Huey, D. J. Tanner, J. S. Holloway, T. B. Ryerson, G. J. Frost, S. A. McKeen, and F. C. Fehsenfeld (2007), A chemical ionization mass spectrometry technique for airborne measurements of ammonia, *Journal of Geophysical Research-Atmospheres*, *112*(D10), doi:10.1029/2006jd007589.

O'Shea, S. J., et al. (2013_a), Airborne observations of trace gases over boreal Canada during BORTAS: campaign climatology, airmass analysis and enhancement ratios, *Atmospheric Chemistry and Physics Discussions*, *13*, 14069-14114, doi:10.5194/acpd-13-14069-2013.

O'Shea, S. J., S. J. B. Bauguitte, M. W. Gallagher, D. Lowry, and C. J. Perciyal (2013$_b$), Development of a cavity-enhanced absorption spectrometer for airborne measurements of CH4 and CO2, *Atmospheric Measurement Techniques*, *6*(5), 1095-1109, doi:10.5194/amt-6-1095-2013.

Palmer, P. I., et al. (2013), Quantifying the impact of BOReal forest fires on Tropospheric oxidants over the Atlantic using Aircraft and Satellites (BORTAS) experiment: design, execution and science overview, *Atmospheric Chemistry and Physics*, *13*(13), 6239-6261, doi:10.5194/acp-13-6239-2013.

Parrington, M., et al. (2012), The influence of boreal biomass burning emissions on the distribution of tropospheric ozone over North America and the North Atlantic during 2010, *Atmospheric Chemistry and Physics*, *12*(4), 2077-2098, doi:10.5194/acp-12-2077-2012.

Parrington, M., et al. (2013), Ozone photochemistry in boreal biomass burning plumes, *Atmospheric Chemistry and Physics*, *13*(15), 7321-7341, doi:10.5194/acp-13-7321-2013.

Petzold, A., et al. (2007), Perturbation of the European free troposphere aerosol by North American forest fire plumes during the ICARTT-ITOP experiment in summer 2004, *Atmospheric Chemistry and Physics*, *7*(19), 5105-5127.

Reid, J. S., and P. V. Hobbs (1998), Physical and optical properties of young smoke from individual biomass fires in Brazil, *Journal of Geophysical Research-Atmospheres*, 103(D24), 32013-32030.

Reid, J. S., R. Koppmann, T. F. Eck, and D. P. Eleuterio (2005), A review of biomass burning emissions part II: intensive physical properties of biomass burning particles, *Atmospheric Chemistry and Physics*, *5*, 799-825.

Schneider, J., S. Weimer, F. Drewnick, S. Borrmann, G. Helas, P. Gwaze, O. Schmid, M. O. Andreae, and U. Kirchner (2006), Mass spectrometric analysis and aerodynamic properties of various types of combustion-related aerosol particles, *International Journal of Mass Spectrometry*, *258*(1-3), 37-49, doi:10.1016/j.ijms.2006.07.008.

Schwarz, J. P., et al. (2006), Single-particle measurements of midlatitude black carbon and light-scattering aerosols from the boundary layer to the lower stratosphere, *Journal of Geophysical Research-Atmospheres*, *111*(D16), doi:10.1029/2006jd007076.

Simoneit, B. R. T., J. J. Schauer, C. G. Nolte, D. R. Oros, V. O. Elias, M. P. Fraser, W. F. Rogge, and G. R. Cass (1999), Levoglucosan, a tracer for cellulose in biomass burning and atmospheric particles, *Atmospheric Environment*, *33*(2), 173-182, doi:10.1016/s1352-2310(98)00145-9.

Sinha, P., P. V. Hobbs, R. J. Yokelson, I. T. Bertschi, D. R. Blake, I. J. Simpson, S. Gao, T. W. Kirchstetter, and T. Novakov (2003), Emissions of trace gases and particles from savanna fires in southern Africa, *Journal of Geophysical Research-Atmospheres*, *108*(D13), 32, doi:10.1029/2002jd002325.

Slowik, J. G., et al. (2010), Characterization of a large biogenic secondary organic aerosol event from eastern Canadian forests, *Atmospheric Chemistry and Physics*, *10*(6), 2825-2845.

Sullivan, A. P., A. S. Holden, L. A. Patterson, G. R. McMeeking, S. M. Kreidenweis, W. C. Malm, W. M. Hao, C. E. Wold, and J. L. Collett, Jr. (2008), A method for smoke marker measurements and its potential application for determining the contribution of biomass

burning from wildfires and prescribed fires to ambient PM2.5 organic carbon, *Journal of Geophysical Research-Atmospheres*, *113*, doi:10.1029/2008jd010216.

Taylor, J. W., et al. (2013), Black carbon wet removal in Canadian biomass burning plumes, in preparation.

Textor, C., et al. (2006), Analysis and quantification of the diversities of aerosol life cycles within AeroCom, *Atmospheric Chemistry and Physics*, *6*, 1777-1813.

Vay, S. A., et al. (2011), Patterns of CO2 and radiocarbon across high northern latitudes during International Polar Year 2008, *Journal of Geophysical Research-Atmospheres*, *116*, doi:10.1029/2011jd015643.

Warneke, C., et al. (2006), Biomass burning and anthropogenic sources of CO over New England in the summer 2004, *Journal of Geophysical Research-Atmospheres*, *111*(D23), doi:10.1029/2005jd006878.

Weimer, S., M. R. Alfarra, D. Schreiber, M. Mohr, A. S. H. Prevot, and U. Baltensperger (2008), Organic aerosol mass spectral signatures from wood-burning emissions: Influence of burning conditions and wood type, *Journal of Geophysical Research-Atmospheres*, *113*(D10), doi:10.1029/2007jd009309.

Yokelson, R. J., R. Susott, D. E. Ward, J. Reardon, and D. W. T. Griffith (1997), Emissions from smoldering combustion of biomass measured by open-path Fourier transform infrared spectroscopy, *Journal of Geophysical Research-Atmospheres*, *102*(D15), 18865-18877, doi:10.1029/97jd00852.

Yokelson, R. J., et al. (2007), Emissions from forest fires near Mexico City, *Atmospheric Chemistry and Physics*, *7*(21), 5569-5584.

Yokelson, R. J., et al. (2009), Emissions from biomass burning in the Yucatan, *Atmospheric Chemistry and Physics*, *9*(15), 5785-5812.

Zhang, Q., D. R. Worsnop, M. R. Canagaratna, and J. L. Jimenez (2005), Hydrocarbon-like and oxygenated organic aerosols in Pittsburgh: insights into sources and processes of organic aerosols, *Atmospheric Chemistry and Physics*, *5*, 3289-3311.

Zhang, Q., et al. (2007), Ubiquity and dominance of oxygenated species in organic aerosols in anthropogenically-influenced Northern Hemisphere midlatitudes, *Geophysical Research Letters*, *34*(13), doi:10.1029/2007gl029979.

Figures

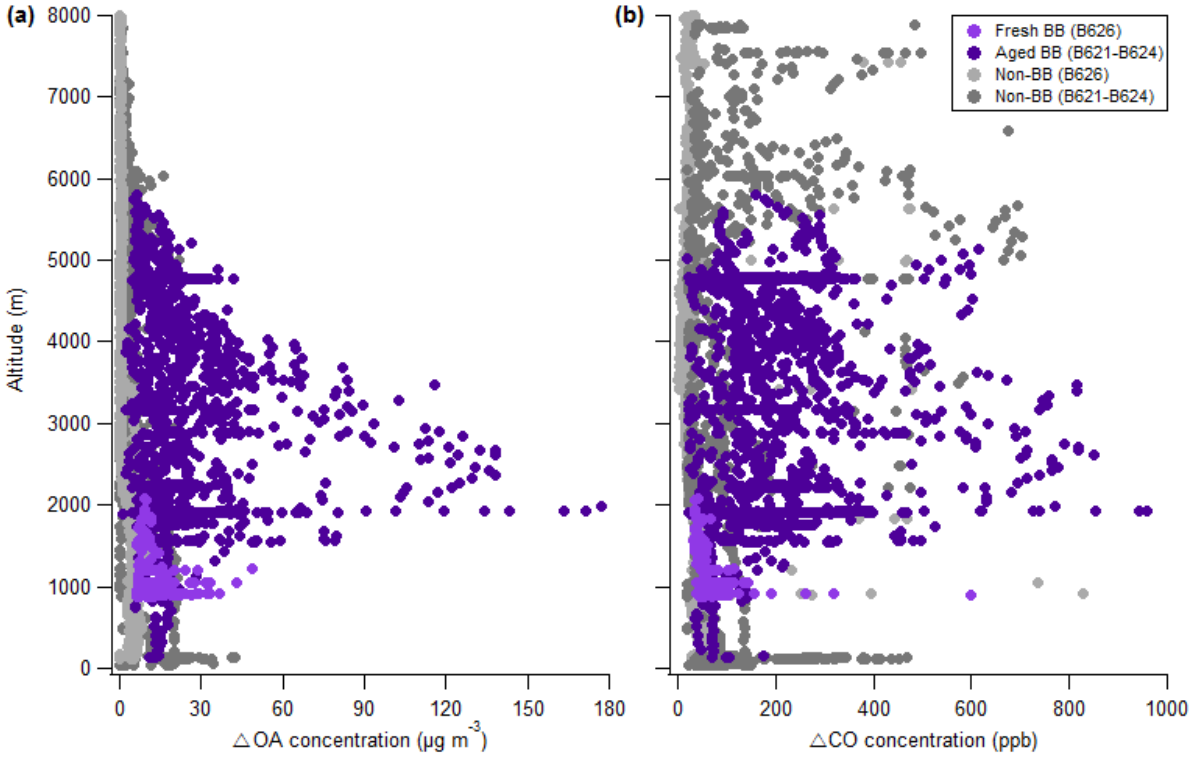

Figure 1: Vertical profiles of (a) △OA and (b) △CO in fresh and aged plumes, together with concentrations in air masses free from the influence of biomass burning.

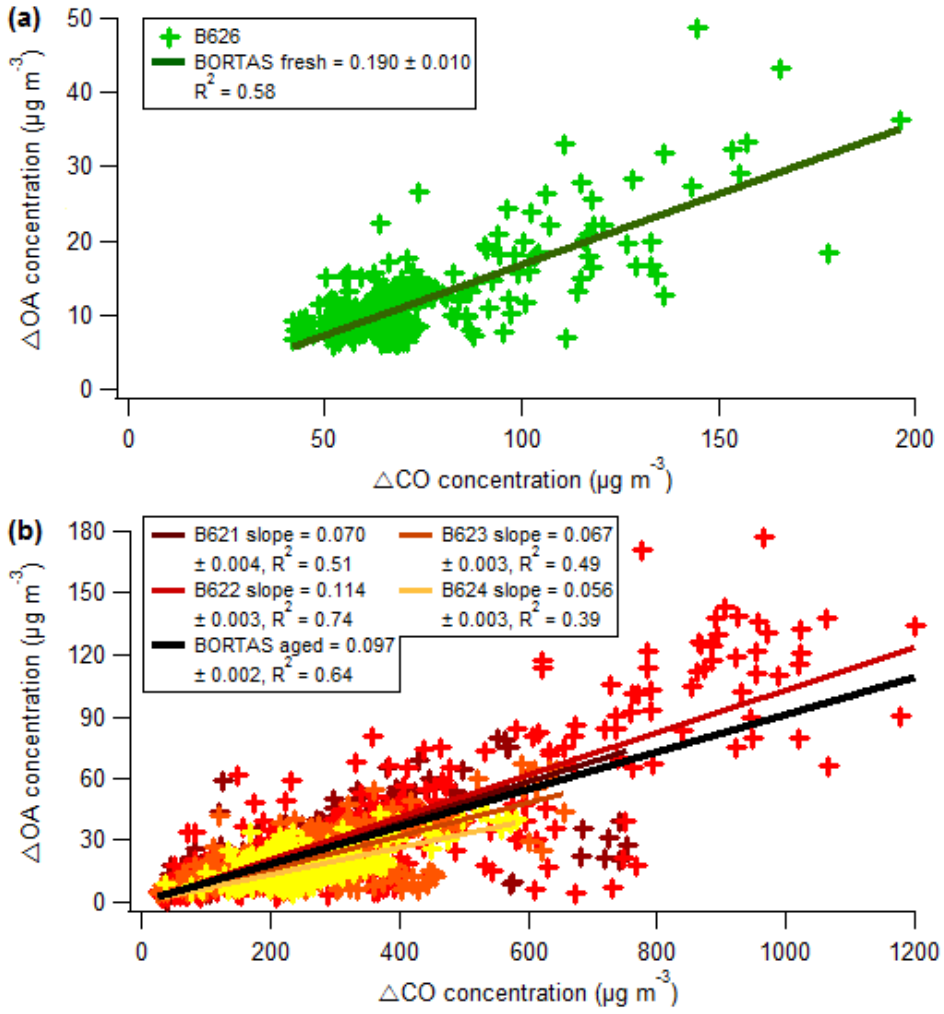

Figure 2: △OA versus △CO for (a) fresh and (b) aged plumes. Coefficients are for linear regressions, from which average △OA/△CO ratios are derived, with uncertainties of ± 1σ.

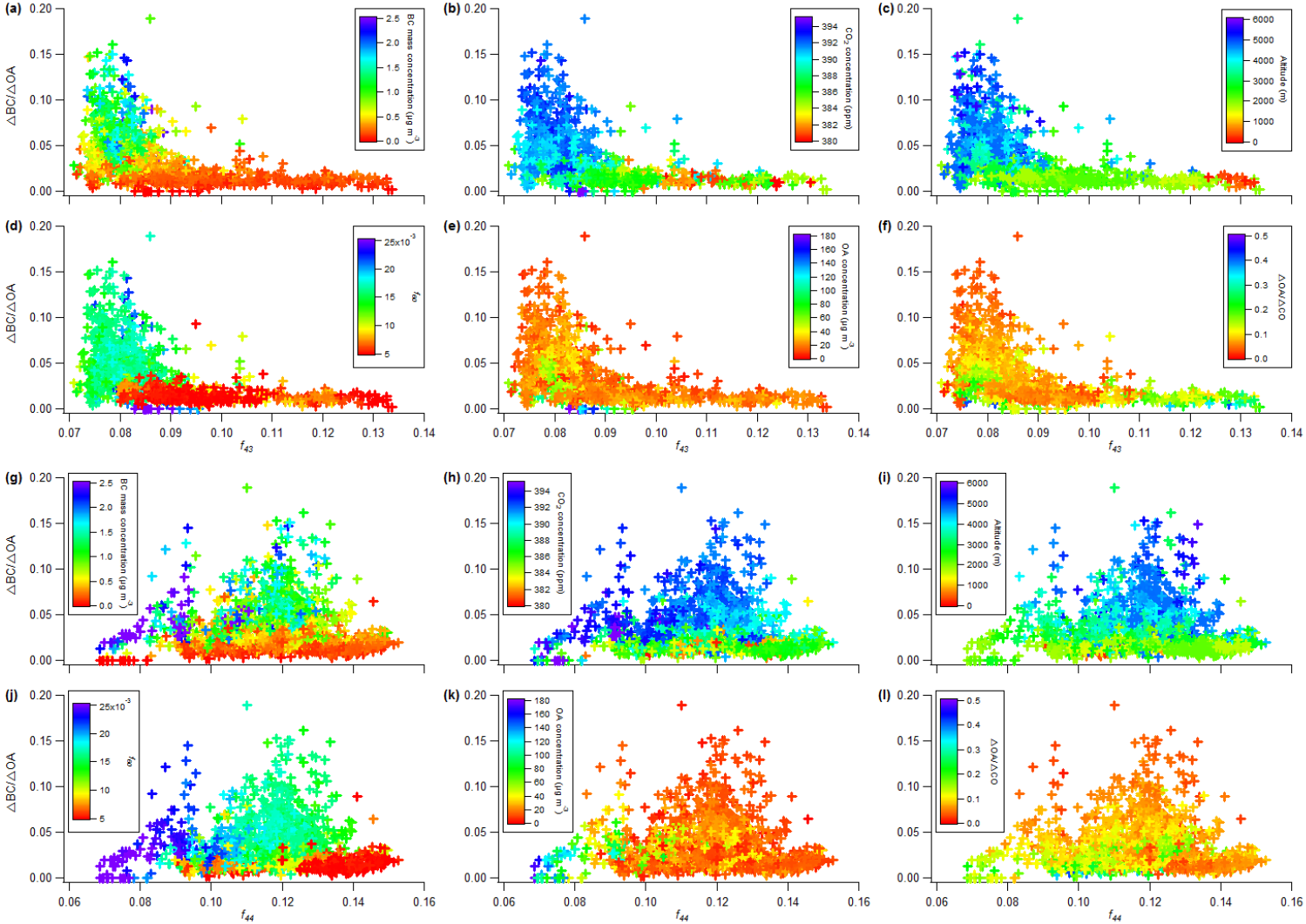

Figure 3: △BC/△OA versus (a-f) f_{43} and (g-l) f_{44} for aged emissions. Datapoints are coloured to show relationships with a number of different parameters.

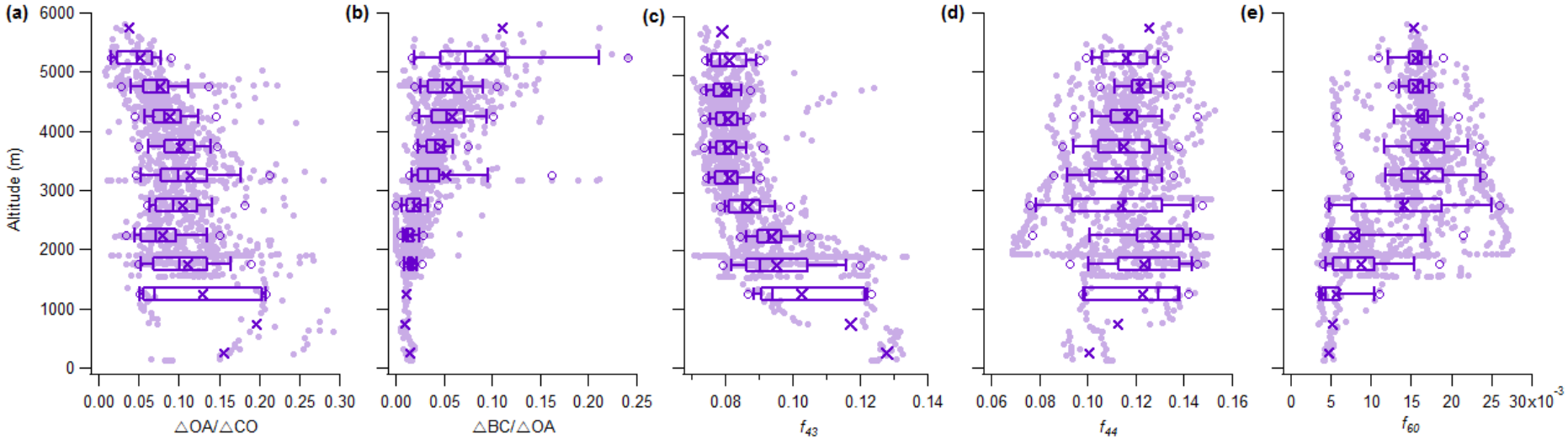

Figure 4: Vertical profiles of (a) △OA/△CO, (b) △BC/△OA, (c) f_{43}, (d) f_{44} and (e) f_{60} in aged plumes. Circles represent the 5th and 95th percentiles, vertical lines the 10th, 25th, 50th, 75th and 90th percentile, with crosses denoting mean values in each 500 m altitudinal bin.

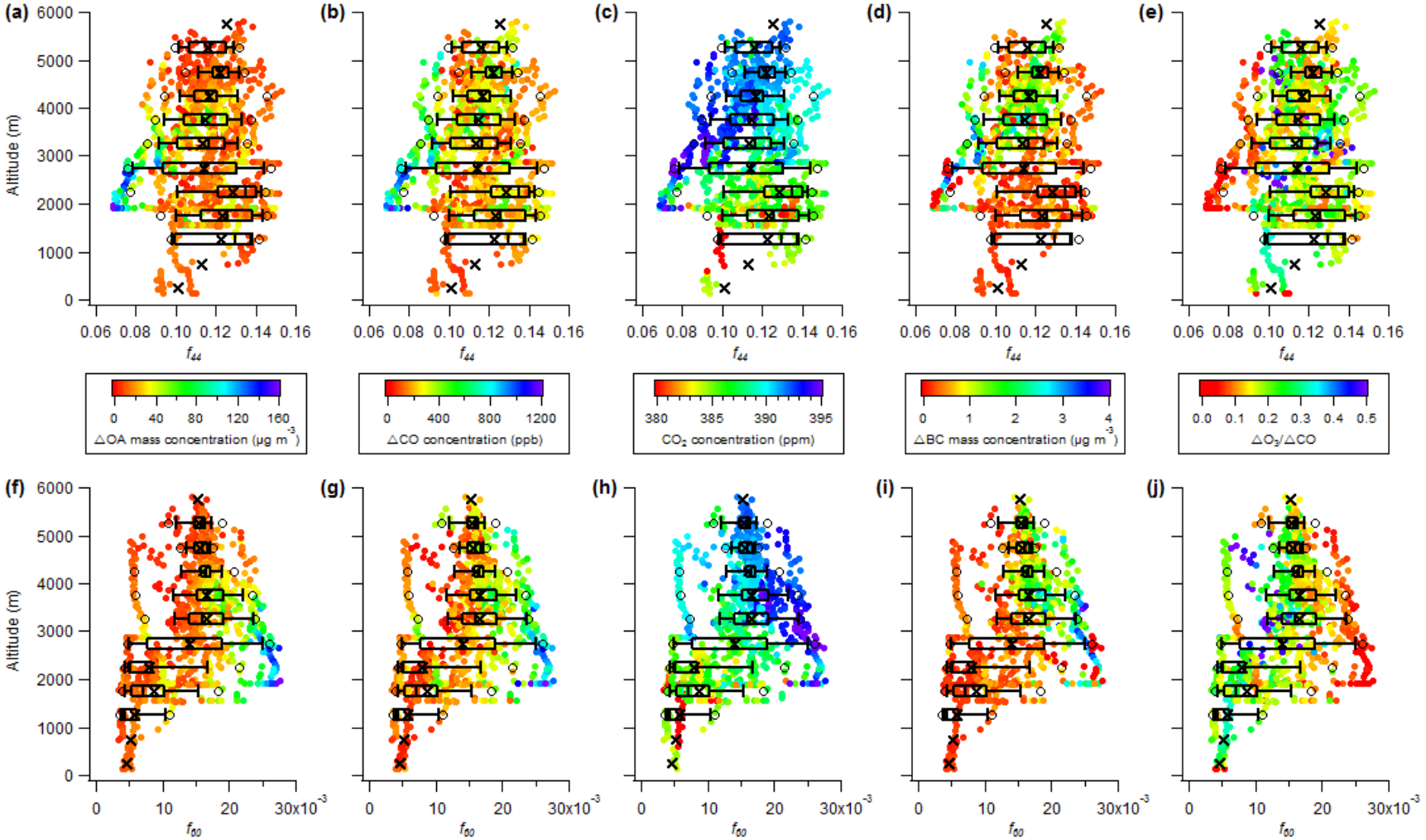

Figure 5: Vertical profiles of (a-e) f_{44} and (f-j) f_{60} in aged plumes. Datapoints are coloured by (a+f) △OA, (b+g) △CO, (c+h) CO_2, (d+i) △BC and (e+j) △O_3/△CO. Circles represent the 5th and 95th percentiles, vertical lines the 10th, 25th, 50th, 75th and 90th percentile, with crosses denoting mean values in each 500 m altitudinal bin.

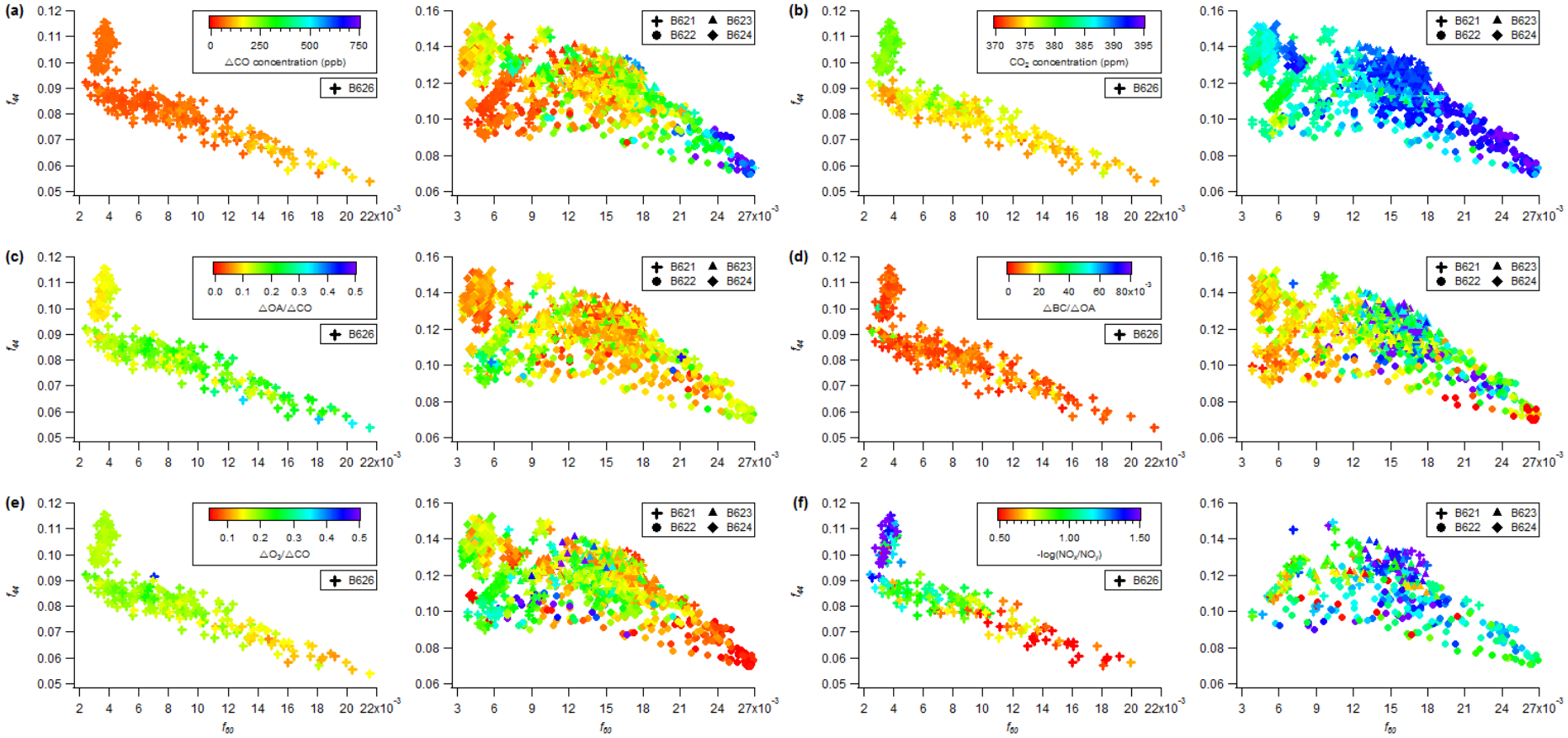

Figure 6: f_{44} versus f_{60} with datapoints coloured by (a) △CO, (b) CO_2, (c) △OA/△CO, (d) △BC/△OA, (e) $\triangle O_3/\triangle CO$ and (f) $-\log(NO_x/NO_y)$. Data from fresh and aged plumes are shown on the left and right hand side of each panel, respectively.

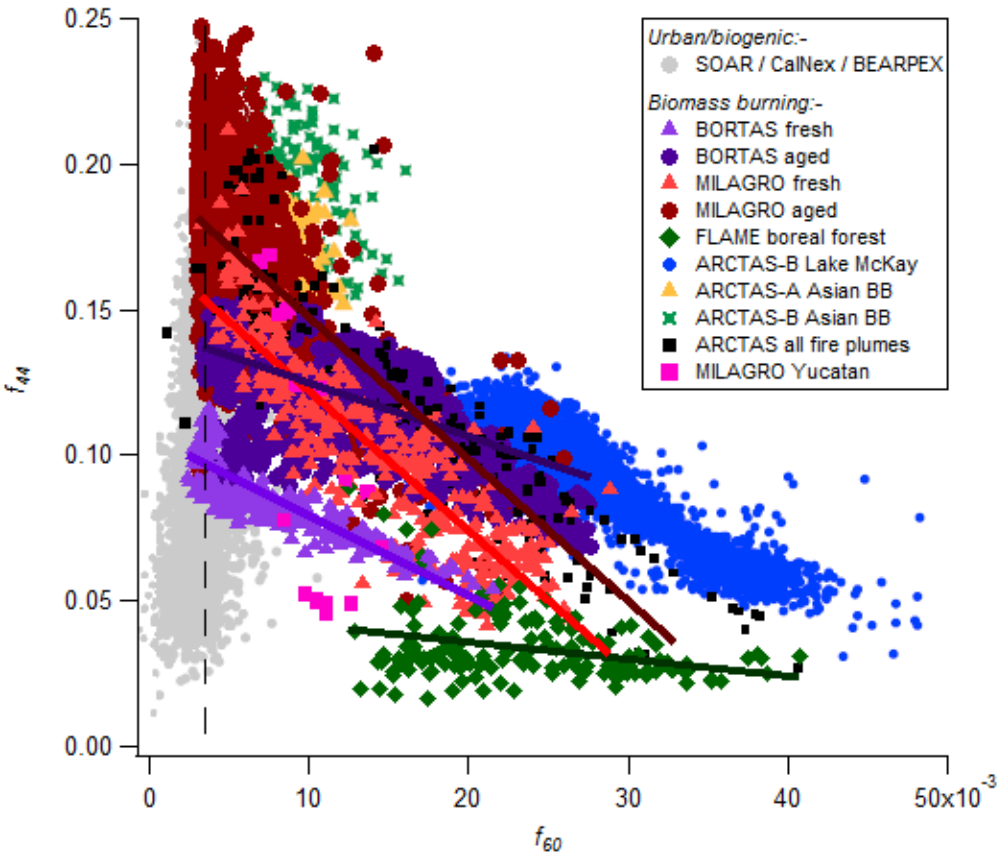

Figure 7: Synthesis of f_{44} versus f_{60} from a range of ambient and laboratory measurements of BBOA, along with data from non-BB sources. The specified background f_{60} value of 0.003 used to identify BB influences is shown as the dashed vertical line. Coloured lines denote linear regressions for corresponding datasets. Adapted from *Cubison et al.* (*2011*).

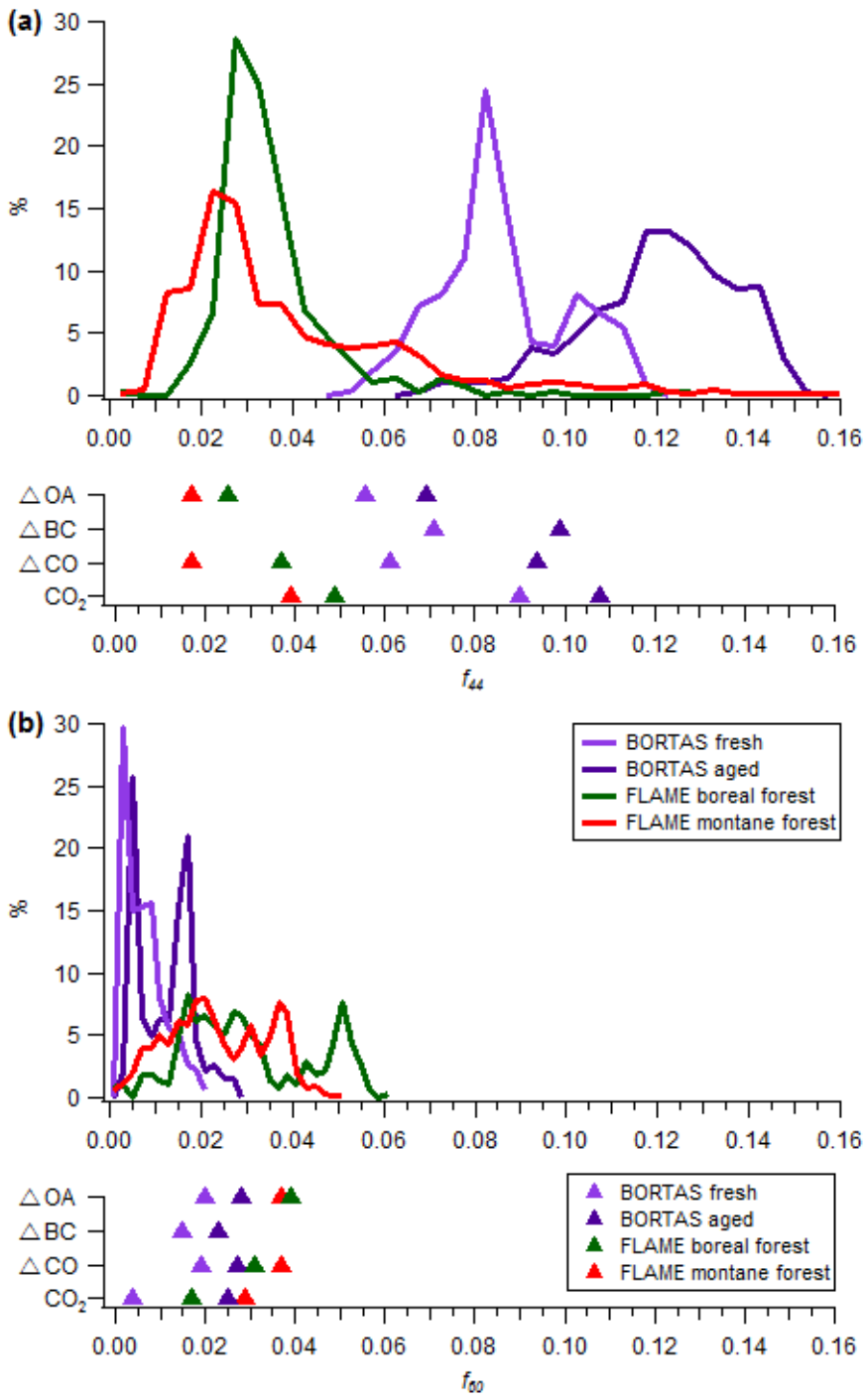

Figure 8: Probability density functions for (a) f_{44} and (b) f_{60} from a range of ambient and laboratory BB measurements. Also shown in the lower sections of each panel are the f_{44} and f_{60} values corresponding to maximum concentrations of △OA, △BC, △CO and CO_2.

Chapter 4

Conclusions and further work

This thesis provides an assessment of a wide range of BBOA properties, with the aim of addressing a number a number of key uncertainties regarding BB emissions and their evolution in the atmosphere. Data acquired from several field campaigns with a broad geographical coverage, together with comprehensive measurements from laboratory studies, form the basis for these attempts to develop more extensive parameterisations for regional and global modelling. The availability of measurements from different regions has enabled comparison of emissions regimes to determine variations between a range of environments and ecosystems. ΔOA/ΔCO ratios were used as a means of normalising ΔOA concentrations, accounting for the effects of dilution and differences in the overall size and intensity of fires to give a representative measure of BBOA production. While average ΔOA/ΔCO for fires in Mexican montane forests and grasslands (0.049), West African savannas (0.056) and Alaskan boreal forests (0.019) are broadly comparable, measurements from eucalypt forests in northern Australia yielded an average ratio around an order of magnitude higher (0.293), while ΔOA/ΔCO was also elevated for Canadian boreal forest fires (0.092). These contrasting mixing ratios indicate a fundamental difference in OA emissions between regions and highlight the pressing need for wider characterisation of BB emissions.

Based upon contrasting observations from previous studies (*Gao et al., 2003; Capes et al., 2008; DeCarlo et al., 2008; Yokelson et al., 2009; Cubison et al., 2011; Akagi et al., 2012*), formation of SOA in aging BB plumes represents one of the major uncertainties relating to BBOA and its contributions to global aerosol budgets. Measurement of both fresh and aged emissions at a range of distances from source provided a means of determining changes in ΔOA/ΔCO in response to physical and chemical transformations over time. Average

ΔOA/ΔCO was shown to consistently decrease between the near and far-field, showing an absence of net SOA formation with aging, and greater loss of OA through evaporation or deposition. However, the extent of any change in ΔOA/ΔCO between fresh and aged emissions remained well below initial variability close to source. These high levels of variability between different fresh plumes within single regions suggest that source conditions form a more significant control on the production of OA from BB sources than additions from secondary formation.

The overriding effects of different source conditions on BBOA emissions and their properties are subject to considerable uncertainty. While ambient measurements highlight the implications of changing fire behaviour through ΔOA/ΔCO variability, observations of fuels being burned, their properties and combustion phase transitions are typically limited. Laboratory experiments were therefore used to provide a more rigorous assessment of controls on BB emissions, revealing a series of highly complex relationships between source conditions and ΔOA/ΔCO. Overall variability in burn-averaged ΔOA/ΔCO for chamber experiments is exceptionally high, far exceeding corresponding ranges from field campaigns, even amongst samples of the same plant species. It is possible that this extensive variability obscures relationships with drivers to some degree, as no uniform trends are observed consistently across all fuel types, although indications of potential influences on ΔOA/ΔCO are evident for certain fuel types and components. Coniferous species, and in particular samples of needles from both montane and boreal forests, show an inverse correlation with MCE, which appears to be exacerbated by increasing fuel moisture content. However, these trends are based on a limited number of observations, and would require further support from additional experiments to be fully elucidated.

Greater uniformity is apparent in the relationship with f_{44} across all fuel types. ΔOA/ΔCO is consistently higher when emissions are less heavily oxidised, and decreases accordingly as the fraction of oxygenated OA increases. As f_{44} also shows a positive correlation with MCE, albeit for a limited number of fuel types, the level of oxygenation in

BBOA is seemingly influenced by the proportion of flaming combustion, as a result of effects on oxygen availability through turbulent mixing. However, the limited extent of this dependency restricts wider scale parameterisation of combustion conditions as a driver for ΔOA/ΔCO variability. These results also contradict observations from previous studies (e.g. *Weimer et al., 2008*), where f_{44} was found to be more strongly associated with the smouldering phase, emphasising the current level of uncertainty associated with BB emissions, even for fires under controlled conditions.

While clearly exhibiting a relationship with combustion conditions in laboratory studies, f_{44} can also be used as a tracer for processing of BB plumes. Observations of ambient emissions consistently show the oxygenated content of BBOA to increase with aging. For campaigns where measurements were performed both close to and at greater distances from source, average f_{44} was higher for the aged OA fraction in all cases. These repeated compositional changes coincided with an absence of ΔOA/ΔCO enhancements in aged plumes, further emphasising that SOA formation does not represent a dominant process throughout the evolution of BBOA in the atmosphere. Although measurements of Canadian boreal forest fires during BORTAS conform to the typical f_{44} trends from all other campaigns, the contrast between age fractions appears to also be influenced by wider differences in emissions properties determined by changes in combustion conditions during the campaign. Plumes were only sampled at source later in the main period of fire activity, by which time smouldering combustion had begun to dominate. This change in fire behaviour is reflected by the contrasting vertical distributions of fresh and aged emissions, and concurrent differences in aerosol composition. Plumes in the far-field were frequently located at considerably higher altitudes than those close to source, with this increased elevation likely driven by enhanced lofting resulting from more intense fires. Proportional contributions of BC increase with altitude, consistent with the injection of flaming combustion products into the upper troposphere.

The variable injection heights of emissions from smouldering and flaming combustion phases appear to provide further indication of the origins of BB aerosols. The observed increase in ΔBC/ΔOA with increasing altitude coincided with a similar trend for f_{60}, indicating that a higher proportion of primary levoglucosan-type BBOA constituents are retained in high altitude plumes. In contrast, ΔOA/ΔCO and f_{43} were shown to decrease with altitude, reflecting a greater proportional level of OA within boundary layer plumes. These trends are further corroborated by low altitude measurements of smouldering emissions close to source, which provided the highest average values of ΔOA/ΔCO and f_{43} throughout BORTAS. As such, it would appear that less buoyant plumes from smouldering fires are more likely to remain within the boundary layer, where they can be subject to rapid chemical transformation on timescales of less than one day, while injection of strongly convective plumes from more intense, flaming combustion leads to greater retention of source emission profiles, even after transportation and aging over several days. Observations of rapid photochemical processing of BBOA are consistent with findings from previous assessments of both ambient (*Gao et al., 2003; DeCarlo et al., 2008; Yokelson et al., 2009)* and laboratory fires (*Grieshop et al., 2009a; Hennigan et al., 2011; Heringa et al., 2011*). The overall evolution of OA composition across all BORTAS measurements is also comparable to the typical pathway described by *Cubison et al.* (*2011*), with f_{44} increasing with decreasing f_{60} as a result of the progressive oxidation of primary BBOA components.

The potential to develop model parameterisations for the emission and evolution of BBOA is curtailed by the extensive uncertainties highlighted throughout this analysis. Factors contributing to observed variability in ΔOA/ΔCO have been examined, and while source conditions such as fuel properties and combustion conditions have been shown to have an appreciable influence on resulting emissions, the pervasiveness and uniformity of such effects remain unclear. Similarly, the implications of changes in plume injection height for atmospheric processing have been demonstrated, but understanding of specific mechanisms and the variability of their effects is limited. It is therefore necessary to deliver far more widespread

quantification of all aspects of the BBOA lifecycle, encompassing the various processes involved in emission, aging and eventual removal. Such progress is dependent on continued utilisation of ambient and laboratory measurements, but with greater scope and coverage than provided to date. Uncertainties emerging from the FLAME II experiment highlight the need for more comprehensive examination of sources of variability in emissions relating to initial fire conditions. Introducing stricter controls on the these conditions, for example by processing fuels to give specific, selected properties, or through regulating the combustion process to maintain consistent fire behaviour, would facilitate more robust characterisation of these effects and help to reconcile observed attributes of emissions from real fires with those from chamber burns. Greater integration of ambient and laboratory studies could also improve constraint of the drivers of variability in BBOA production and properties. Collecting samples of specific fuels involved in fires studied during field campaigns would enable comparison of any changes between different experimental settings, providing a means of evaluating the impacts of various source conditions on emissions, within the wider context of in-situ observations. Structuring research flights to follow plumes from source to considerable distances downwind, performing continuous measurements throughout the aging process, would also enable complete characterisation of BBOA evolution. Such approaches may prove highly beneficial for the development of more reliable model parameterisations, contributing towards improved understanding of BBOA, its role in atmospheric processes and implications for climate change.

Chapter 5

References

Abel, S. J., J. M. Haywood, E. J. Highwood, J. Li, and P. R. Buseck (2003), Evolution of biomass burning aerosol properties from an agricultural fire in southern Africa, *Geophysical Research Letters*, 30(15).

Ackerman, A. S., O. B. Toon, D. E. Stevens, A. J. Heymsfield, V. Ramanathan, and E. J. Welton (2000), Reduction of tropical cloudiness by soot, *Science*, 288(5468), 1042-1047.

Akagi, S. K., et al. (2012), Evolution of trace gases and particles emitted by a chaparral fire in California, *Atmospheric Chemistry and Physics*, *12*(3), 1397-1421, doi:10.5194/acp-12-1397-2012.

Albrecht, B., (1989), Aerosols, cloud microphysics and fractional cloudiness, *Science*, 245(4923), 1227−1230.

Allan, J. D., et al. (2004), A generalised method for the extraction of chemically resolved mass spectra from aerodyne aerosol mass spectrometer data, *Journal of Aerosol Science*, *35*(7), 909-922, doi:10.1016/j.jaerosci.2004.02.007.

Allan, J. D., J. L. Jimenez, P. I. Williams, M. R. Alfarra, K. N. Bower, J. T. Jayne, H. Coe, and D. R. Worsnop (2003), Quantitative sampling using an Aerodyne aerosol mass spectrometer - 1. Techniques of data interpretation and error analysis, *Journal of Geophysical Research-Atmospheres*, *108*(D3), doi:10.1029/2002jd002358.

Allen, G., et al. (2008), Aerosol and trace-gas measurements in the Darwin area during the wet season, *Journal of Geophysical Research-Atmospheres*, 113(D6).

Andreae, M. O., and P. Merlet (2001), Emission of trace gases and aerosols from biomass burning, *Global Biogeochemical Cycles*, 15(4), 955-966.

Andreae, M. O., and D. Rosenfeld (2008), Aerosol-cloud-precipitation interactions. Part 1. The nature and sources of cloud-active aerosols, *Earth-Science Reviews*, 89(1-2), 13-41.

Bahreini, R., J. L. Jimenez, J. Wang, R. C. Flagan, J. H. Seinfeld, J. T. Jayne, and D. R. Worsnop (2003), Aircraft-based aerosol size and composition measurements during ACE-Asia using an Aerodyne aerosol mass spectrometer, *Journal of Geophysical Research-Atmospheres*, *108*(D23), doi:10.1029/2002jd003226.

Baumgardner, D., M. Grutter, J. Allan, C. Ochoa, B. Rappenglueck, L. M. Russell, and P. Arnott (2009), Physical and chemical properties of the regional mixed layer of Mexico's Megapolis, *Atmospheric Chemistry and Physics*, *9*(15), 5711-5727.

Bellouin, N., O. Boucher, J. Haywood, and M. S. Reddy (2005), Global estimate of aerosol direct radiative forcing from satellite measurements, *Nature*, 438(7071), 1138-1141.

Bond, T. C., D. G. Streets, K. F. Yarber, S. M. Nelson, J. H. Woo, and Z. Klimont (2004), A technology-based global inventory of black and organic carbon emissions from combustion, *Journal of Geophysical Research-Atmospheres*, 109(D14).

Canagaratna, M. R., et al. (2007), Chemical and microphysical characterization of ambient aerosols with the aerodyne aerosol mass spectrometer, *Mass Spectrometry Reviews*, *26*(2), 185-222, doi:10.1002/mas.20115.

Capes, G., B. Johnson, G. McFiggans, P. I. Williams, J. Haywood, and H. Coe (2008), Aging of biomass burning aerosols over West Africa: Aircraft measurements of chemical composition, microphysical properties, and emission ratios, *Journal of Geophysical Research-Atmospheres*, 113(D20).

Capes, G. (2009), Aging of biomass burning aerosols, and formation of secondary organics aerosols over West Africa, PhD Thesis, School of Earth, Atmospheric and Environmental Sciences, University of Manchester.

Cappa, C. D., and J. L. Jimenez (2010), Quantitative estimates of the volatility of ambient organic aerosol, *Atmospheric Chemistry and Physics*, 10(12), 5409-5424.

Chen, L. W. A., H. Moosmuller, W. P. Arnott, J. C. Chow, J. G. Watson, R. A. Susott, R. E. Babbitt, C. E. Wold, E. N. Lincoln, and W. M. Hao (2007), Emissions from laboratory combustion of wildland fuels: Emission factors and source profiles, *Environmental Science & Technology*, *41*(12), 4317-4325, doi:10.1021/es062364i.

Christian, T. J., B. Kleiss, R. J. Yokelson, R. Holzinger, P. J. Crutzen, W. M. Hao, B. H. Saharjo, and D. E. Ward (2003), Comprehensive laboratory measurements of biomass-burning emissions: 1. Emissions from Indonesian, African, and other fuels, *Journal of Geophysical Research-Atmospheres*, *108*(D23), doi:10.1029/2003jd003704.

Christopher, S. A., J. L. Zhang, Y. J. Kaufman, and L. A. Remer (2006), Satellite-based assessment of top of atmosphere anthropogenic aerosol radiative forcing over cloud-free oceans, *Geophysical Research Letters*, 33(15).

Chung, S. H., and J. H. Seinfeld (2002), Global distribution and climate forcing of carbonaceous aerosols, *Journal of Geophysical Research-Atmospheres*, 107(D19), 33.

Chylek, P., and J. Wong (1995), Effect of absorbing aerosols on global radiation budget, *Geophysical Research Letters*, 22(8), 929-931.

Clarke, A. D., et al. (2002), INDOEX aerosol: A comparison and summary of chemical, microphysical, and optical properties observed from land, ship, and aircraft, *Journal of Geophysical Research*, 107(D19), 8033.

Crosier, J., J. D. Allan, H. Coe, K. N. Bower, P. Formenti, and P. I. Williams (2007), Chemical composition of summertime aerosol in the Po Valley (Italy), northern Adriatic and Black Sea, *Quarterly Journal of the Royal Meteorological Society*, *133*, 61-75, doi:10.1002/qj.88.

Cubison, M. J., et al. (2011), Effects of aging on organic aerosol from open biomass burning smoke in aircraft and laboratory studies, *Atmospheric Chemistry and Physics*, *11*(23), 12049-12064, doi:10.5194/acp-11-12049-2011.

DeCarlo, P. F., et al. (2006), Field-deployable, high-resolution, time-of-flight aerosol mass spectrometer, *Analytical Chemistry*, *78*(24), 8281-8289, doi:10.1021/ac061249n.

DeCarlo, P. F., et al. (2008), Fast airborne aerosol size and chemistry measurements above Mexico City and Central Mexico during the MILAGRO campaign, *Atmospheric Chemistry and Physics*, *8*(14), 4027-4048.

De Gouw, J., and J. L. Jimenez (2009), Organic Aerosols in the Earth's Atmosphere, *Environmental Science & Technology*, 43(20), 7614-7618.

Dockery, D. W. and C. A. Pope (1994), Acute respiratory effects of particulate air-pollution, *Annual Review of Public Health*, 15, 107-132.

Donahue, N. M., A. L. Robinson, C. O. Stanier, and S. N. Pandis (2006), Coupled partitioning, dilution, and chemical aging of semivolatile organics, *Environmental Science & Technology*, 40(8), 02635-02643.

Drewnick, F., S. S. Hings, M. R. Alfarra, A. S. H. Prevot, and S. Borrmann (2009), Aerosol quantification with the Aerodyne Aerosol Mass Spectrometer: detection limits and ionizer background effects, *Atmospheric Measurement Techniques*, *2*(1), 33-46.

Drewnick, F., et al. (2005), A new time-of-flight aerosol mass spectrometer (TOF-AMS) - Instrument description and first field deployment, *Aerosol Science and Technology*, *39*(7), 637-658, doi:10.1080/02786820500182040.

Fehsenfeld, F. C., et al. (2006), International Consortium for Atmospheric Research on Transport and Transformation (ICARTT): North America to Europe - Overview of the 2004 summer field study, *Journal of Geophysical Research-Atmospheres*, 111(D23).

Feng, Y., and J. E. Penner (2007), Global modeling of nitrate and ammonium: Interaction of aerosols and tropospheric chemistry, *Journal of Geophysical Research-Atmospheres*, 112(D1).

Ferek, R. J., J. S. Reid, P. V. Hobbs, D. R. Blake, and C. Liousse (1998), Emission factors of hydrocarbons, halocarbons, trace gases and particles from biomass burning in Brazil, *Journal of Geophysical Research-Atmospheres*, 103(D24), 32107-32118.

Foltescu, V. L., E. Selin, and M. Below (1995), Corrections for particle losses and sizing errors during aircraft aerosol sampling using a Rosemount inlet and the PMS LAS-X, *Atmospheric Environment*, *29*(3), 449-453, doi:10.1016/1352-2310(94)00258-m.

Forster, P., et al. (2007), Changes in Atmospheric Constituents and in Radiative Forcing, in: *Climate Change 2007: The Physical Science Basis, contribution of Working Group I to the Fourth Assessment Report of the Intergovernmental Panel on Climate Change* [Solomon, S. D., et al. (eds.)], p. 129–234. Cambridge University Press, Cambridge, United Kingdom and New York, NY, USA.

Fowler, D., et al. (2009), Atmospheric composition change: Ecosystems-Atmosphere interactions, *Atmospheric Environment*, 43(33), 5193-5267.

Freeborn, P. H., M. J. Wooster, W. M. Hao, C. A. Ryan, B. L. Nordgren, S. P. Baker, and C. Ichoku (2008), Relationships between energy release, fuel mass loss, and trace gas and aerosol emissions during laboratory biomass fires, *Journal of Geophysical Research-Atmospheres*, *113*(D1), doi:10.1029/2007jd008679.

Fuzzi, S., et al. (2006), Critical assessment of the current state of scientific knowledge, terminology, and research needs concerning the role of organic aerosols in the atmosphere, climate, and global change, *Atmospheric Chemistry and Physics*, 6, 2017-2038.

Gao, S., D. A. Hegg, P. V. Hobbs, T. W. Kirchstetter, B. I. Magi, and M. Sadilek (2003), Water-soluble organic components in aerosols associated with savanna fires in southern Africa: Identification, evolution, and distribution, *Journal of Geophysical Research-Atmospheres*, 108(D13).

Goldstein, A. H., and I. E. Galbally (2007), Known and unexplored organic constituents in the earth's atmosphere, *Environmental Science & Technology*, 41(5), 1514-1521.

Grieshop, A. P., J. M. Logue, N. M. Donahue, and A. L. Robinson (2009a), Laboratory investigation of photochemical oxidation of organic aerosol from wood fires 1: measurement and simulation of organic aerosol evolution, *Atmospheric Chemistry and Physics*, 9(4), 1263-1277.

Grieshop, A. P., N. M. Donahue, and A. L. Robinson (2009b), Laboratory investigation of photochemical oxidation of organic aerosol from wood fires 2: analysis of aerosol mass spectrometer data, *Atmospheric Chemistry and Physics*, 9(6), 2227-2240.

Guelle, W., Y. J. Balkanski, M. Schulz, F. Dulac, and P. Monfray (1998), Wet deposition in a global size-dependent aerosol transport model - 1. Comparison of a 1 year Pb-210 simulation with ground measurements, *Journal of Geophysical Research-Atmospheres*, 103(D10), 11429-11445.

Hallquist, M., et al. (2009), The formation, properties and impact of secondary organic aerosol: current and emerging issues, *Atmospheric Chemistry and Physics*, 9(14), 5155-5236.

Hansen, J., and L. Nazarenko (2004), Soot climate forcing via snow and ice albedos, *Proceedings of the National Academy of Sciences of the United States of America*, 101(2), 423-428.

Hansen, J., M. Sato, and R. Ruedy (1997), Radiative forcing and climate response, *Journal of Geophysical Research-Atmospheres*, 102(D6), 6831-6864.

Haywood, J., and O. Boucher (2000), Estimates of the direct and indirect radiative forcing due to tropospheric aerosols: A review, *Reviews of Geophysics*, 38(4), 513-543.

Haywood, J. M., and K. P. Shine (1997), Multi-spectral calculations of the direct radiative forcing of tropospheric sulphate and soot aerosols using a column model, *Quarterly Journal of the Royal Meteorological Society*, 123(543), 1907-1930.

Haywood, J., P. Francis, S. Osborne, M. Glew, N. Loeb, E. Highwood, D. Tanre, G. Myhre, P. Formenti, and E. Hirst (2003), Radiative properties and direct radiative effect of Saharan dust measured by the C-130 aircraft during SHADE: 1. Solar spectrum, *Journal of Geophysical Research-Atmospheres*, *108*(D18), doi:10.1029/2002jd002687.

Haywood, J. M., et al. (2008), Overview of the Dust and Biomass-burning Experiment and African Monsoon Multidisciplinary Analysis Special Observing Period-0, *Journal of Geophysical Research-Atmospheres*, 113.

Heintzenberg, J., et al. (2003), Tropospheric aerosols. In: *Atmospheric Chemistry in a Changing World* [Brasseur, G., et al.], Springer, 125-156.

Hennigan, C. J., et al. (2011), Chemical and physical transformations of organic aerosol from the photo-oxidation of open biomass burning emissions in an environmental chamber, *Atmospheric Chemistry and Physics*, *11*(15), 7669-7686, doi:10.5194/acp-11-7669-2011.

Heringa, M. F., P. F. DeCarlo, R. Chirico, T. Tritscher, J. Dommen, E. Weingartner, R. Richter, G. Wehrle, A. S. H. Prevot, and U. Baltensperger (2011), Investigations of primary and secondary particulate matter of different wood combustion appliances with a high-resolution time-of-flight aerosol mass spectrometer, *Atmospheric Chemistry and Physics*, *11*(12), 5945-5957, doi:10.5194/acp-11-5945-2011.

Hobbs, P. V., J. S. Reid, R. A. Kotchenruther, R. J. Ferek, and R. Weiss (1997), Direct radiative forcing by smoke from biomass burning, Science, 275(5307), 1776-1778.
Hobbs, P. V., P. Sinha, R. J. Yokelson, T. J. Christian, D. R. Blake, S. Gao, T. W. Kirchstetter, T. Novakov, and P. Pilewskie (2003), Evolution of gases and particles from a savanna fire in South Africa, *Journal of Geophysical Research-Atmospheres*, 108(D13).

Iinuma, Y., E. Bruggemann, T. Gnauk, K. Muller, M. O. Andreae, G. Helas, R. Parmar, and H. Herrmann (2007), Source characterization of biomass burning particles: The combustion of selected European conifers, African hardwood, savanna grass, and German and Indonesian peat, *Journal of Geophysical Research-Atmospheres*, 112(D8).

Jacobson, M. C., H. C. Hansson, K. J. Noone, and R. J. Charlson (2000), Organic atmospheric aerosols: Review and state of the science, *Reviews of Geophysics*, 38(2), 267-294.

Janhall, S., M. O. Andreae, and U. Poschl (2010), Biomass burning aerosol emissions from vegetation fires: particle number and mass emission factors and size distributions, *Atmospheric Chemistry and Physics*, 10(3), 1427-1439.

Jayne, J. T., D. C. Leard, X. F. Zhang, P. Davidovits, K. A. Smith, C. E. Kolb, and D. R. Worsnop (2000), Development of an aerosol mass spectrometer for size and composition analysis of submicron particles, *Aerosol Science and Technology*, *33*(1-2), 49-70, doi:10.1080/027868200410840.

Jimenez, J. L., et al. (2003), Ambient aerosol sampling using the Aerodyne Aerosol Mass Spectrometer, *Journal of Geophysical Research-Atmospheres*, *108*(D7), doi:10.1029/2001jd001213.

Johnson, B. T., S. R. Osborne, J. M. Haywood, and M. A. J. Harrison (2008), Aircraft measurements of biomass burning aerosol over West Africa during DABEX, *Journal of Geophysical Research-Atmospheres*, *113*, doi:10.1029/2007jd009451.

Jurado, E., J. Dachs, C. M. Duarte, and R. Simo (2008), Atmospheric deposition of organic and black carbon to the global oceans, *Atmospheric Environment*, 42(34), 7931-7939.

Kanakidou, M., et al. (2005), Organic aerosol and global climate modelling: a review, *Atmospheric Chemistry and Physics*, 5, 1053-1123.

Kaufman, Y. J., O. Boucher, D. Tanre, M. Chin, L. A. Remer, and T. Takemura (2005), Aerosol anthropogenic component estimated from satellite data, *Geophysical Research Letters*, 32(17).

Koch, D., Jacob, D., Tegen, I., Rind, D. and Chin, M. (1999), Tropospheric sulphur simulation and sulphate direct radiative forcing in the Goddard Institute for Space Studies general circulation model, *Journal of Geophysical Research*, 104, 2239-2251.

Koch, D., et al. (2009), Evaluation of black carbon estimations in global aerosol models, *Atmospheric Chemistry and Physics*, 9(22), 9001-9026.

Köhler, H. (1936), The nucleus in and the growth of hygroscopic droplets, Transactions of the *Faraday Society*, 32, 1152–1161.

Kroll, J. H., and J. H. Seinfeld (2008), Chemistry of secondary organic aerosol: Formation and evolution of low-volatility organics in the atmosphere, *Atmospheric Environment*, 42(16), 3593-3624.

Langmann, B., B. Duncan, C. Textor, J. Trentmann, and G. R. van der Werf (2009), Vegetation fire emissions and their impact on air pollution and climate, *Atmospheric Environment*, 43(1), 107-116.

Lewis, A. C., et al. (2007), Chemical composition observed over the mid-Atlantic and the detection of pollution signatures far from source regions, *Journal of Geophysical Research-Atmospheres*, *112*(D10), doi:10.1029/2006jd007584.

Liousse, C., J. E. Penner, C. Chuang, J. J. Walton, H. Eddleman, and H. Cachier (1996), A global three-dimensional model study of carbonaceous aerosols, *Journal of Geophysical Research-Atmospheres*, 101(D14), 19411-19432.

Lohmann, U., and J. Feichter (2001), Can the direct and semi-direct aerosol effect compete with the indirect effect on a global scale?, *Geophysical Research Letters*, 28(1), 159-161.

Lohmann, U., and J. Feichter (2005), Global indirect aerosol effects: a review, *Atmospheric Chemistry and Physics*, 5, 715-737.

Mason, S. A., R. J. Field, R. J. Yokelson, M. A. Kochivar, M. R. Tinsley, D. E. Ward, and W. M. Hao (2001), Complex effects arising in smoke plume simulations due to inclusion of direct emissions of oxygenated organic species from biomass combustion, *Journal of Geophysical Research-Atmospheres*, 106(D12), 12527-12539.

Massling, A., M. Stock, and A. Wiedensohler (2005), Diurnal, weekly, and seasonal variation of hygroscopic properties of submicrometer urban aerosol particles, *Atmospheric Environment*, 39(21), 3911-3922.

Massling, A., A. Wiedensohler, B. Busch, C. Neususs, P. Quinn, T. Bates, and D. Covert (2003), Hygroscopic properties of different aerosol types over the Atlantic and Indian Oceans, *Atmospheric Chemistry and Physics*, 3, 1377-1397.

McFiggans, G., et al. (2005), Simplification of the representation of the organic component of atmospheric particulates, *Faraday Discussions*, 130, 341-362.

McFiggans, G., et al. (2006), The effect of physical and chemical aerosol properties on warm cloud droplet activation, *Atmospheric Chemistry and Physics*, 6, 2593-2649.

McMeeking, G. R. (2008), The optical, chemical and physical properties of aerosols and gases emitted by the laboratory combustion of wildland fuels, PhD Thesis, Department of Atmospheric Science, Colorado State University.

McMeeking, G. R., et al. (2009), Emissions of trace gases and aerosols during the open combustion of biomass in the laboratory, *Journal of Geophysical Research-Atmospheres*, *114*, doi:10.1029/2009jd011836.

Mochida, M., M. Kuwata, T. Miyakawa, N. Takegawa, K. Kawamura, and Y. Kondo (2006), Relationship between hygroscopicity and cloud condensation nuclei activity for urban aerosols in Tokyo, *Journal of Geophysical Research-Atmospheres*, 111.

Molina, L. T., et al. (2007), Air quality in North America's most populous city - overview of the MCMA-2003 campaign, *Atmospheric Chemistry and Physics*, *7*(10), 2447-2473.

Molina, L. T., et al. (2010), An overview of the MILAGRO 2006 Campaign: Mexico City emissions and their transport and transformation, *Atmospheric Chemistry and Physics*, *10*(18), 8697-8760, doi:10.5194/acp-10-8697-2010.

Morgan, W. T., J. D. Allan, K. N. Bower, G. Capes, J. Crosier, P. I. Williams, and H. Coe (2009), Vertical distribution of sub-micron aerosol chemical composition from North-Western Europe and the North-East Atlantic, *Atmospheric Chemistry and Physics*, *9*(15), 5389-5401, doi:10.5194/acp-9-5389-2009.

Ng, N. L., J. H. Kroll, A. W. H. Chan, P. S. Chhabra, R. C. Flagan, and J. H. Seinfeld (2007), Secondary organic aerosol formation from m-xylene, toluene, and benzene, *Atmospheric Chemistry and Physics*, 7(14), 3909-3922.

Palmer, P. I., et al. (2013), Quantifying the impact of BOReal forest fires on Tropospheric oxidants over the Atlantic using Aircraft and Satellites (BORTAS) experiment: design, execution and science overview, *Atmospheric Chemistry and Physics*, *13*(13), 6239-6261, doi:10.5194/acp-13-6239-2013.

Penner, J.E., et al., 2001: Aerosols, their direct and indirect effects. In: *Climate Change 2001: The Scientific Basis. Contribution of Working Group I to the Third Assessment Report of the Intergovernmental Panel on Climate Change* [Houghton, J.T., et al. (eds.)], p. 289–348. Cambridge University Press, Cambridge, United Kingdom and New York, NY, USA.

Petters, M. D., and S. M. Kreidenweis (2007), A single parameter representation of hygroscopic growth and cloud condensation nucleus activity, *Atmospheric Chemistry and Physics*, 7(8), 1961-1971.

Poschl, U. (2005), Atmospheric aerosols: Composition, transformation, climate and health effects, *Angewandte Chemie-International Edition*, 44(46), 7520-7540.

Posfai, M., R. Simonics, J. Li, P. V. Hobbs, and P. R. Buseck (2003), Individual aerosol particles from biomass burning in southern Africa: 1. Compositions and size distributions of carbonaceous particles, *Journal of Geophysical Research-Atmospheres*, 108(D13).

Quinn, P. K., et al. (2006), Impacts of sources and aging on submicrometer aerosol properties in the marine boundary layer across the Gulf of Maine, *Journal of Geophysical Research-Atmospheres*, *111*(D23), doi:10.1029/2006jd007582.

Raes, F., R. Van Dingenen, E. Vignati, J. Wilson, J. P. Putaud, J. H. Seinfeld, and P. Adams (2000), Formation and cycling of aerosols in the global troposphere, *Atmospheric Environment*, 34(25), 4215-4240.

Ramaswamy, V., et al., 2001: Radiative forcing of climate change. In: *Climate Change 2001: The Scientific Basis. Contribution of Working Group I to the Third Assessment Report of the Intergovernmental Panel on Climate Change* [Houghton, J.T., et al. (eds.)], p. 349–
416. Cambridge University Press, Cambridge, United Kingdom and New York, NY, USA.

Real, E., et al. (2007), Processes influencing ozone levels in Alaskan forest fire plumes during long-range transport over the North Atlantic, *Journal of Geophysical Research-Atmospheres*, *112*(D10), doi:10.1029/2006jd007576.

Redelsperger, J. L., C. D. Thorncroft, A. Diedhiou, T. Lebel, D. J. Parker, and J. Polcher (2006), African monsoon multidisciplinary analysis - An international research project and field campaign, *Bulletin of the American Meteorological Society*, 87(12), 1739.

Reid, J. S., and P. V. Hobbs (1998), Physical and optical properties of young smoke from individual biomass fires in Brazil, *Journal of Geophysical Research-Atmospheres*, 103(D24), 32013-32030.

Reid, J. S., R. Koppmann, T. F. Eck, and D. P. Eleuterio (2005), A review of biomass burning emissions part II: intensive physical properties of biomass burning particles, *Atmospheric Chemistry and Physics*, 5, 799-825.

Richter, H., and J. B. Howard (2000), Formation of polycyclic aromatic hydrocarbons and their growth to soot - a review of chemical reaction pathways, *Progress in Energy and Combustion Science*, 26(4-6), 565-608.

Robinson, A. L., N. M. Donahue, M. K. Shrivastava, E. A. Weitkamp, A. M. Sage, A. P. Grieshop, T. E. Lane, J. R. Pierce, and S. N. Pandis (2007), Rethinking organic aerosols: Semivolatile emissions and photochemical aging, *Science*, 315(5816), 1259-1262.

Rodriguez, M. A., and D. Dabdub (2004), A modeling study of size- and chemically resolved aerosol thermodynamics in a global chemical transport model, *Journal of Geophysical Research-Atmospheres*, 109(D2).

Rosenfeld, D., U. Lohmann, G. B. Raga, C. D. O'Dowd, M. Kulmala, S. Fuzzi, A. Reissell, and M. O. Andreae (2008), Flood or drought: How do aerosols affect precipitation?, *Science*, 321(5894), 1309-1313.

Schult, I., J. Feichter, and W. F. Cooke (1997), Effect of black carbon and sulfate aerosols on the Global Radiation Budget, *Journal of Geophysical Research-Atmospheres*, 102(D25), 30107-30117.

Seinfeld, J.H., and S. N. Pandis (2006), *Atmospheric chemistry and Physics: From air pollution to climate change*, Wiley-Interscience, New York, NY, USA.

Seinfeld, J. H., and J. F. Pankow (2003), Organic atmospheric particulate material, *Annual Review of Physical Chemistry*, 54, 121-140.
Spracklen, D. V., S. R. Arnold, J. Sciare, K. S. Carslaw, and C. Pio (2008), Globally significant oceanic source of organic carbon aerosol, *Geophysical Research Letters*, 35(12).

Sun, J. M., and P. A. Ariya (2006), Atmospheric organic and bio-aerosols as cloud condensation nuclei (CCN): A review, *Atmospheric Environment*, 40(5), 795-820.

Swietlicki, E., et al. (2008), Hygroscopic properties of submicrometer atmospheric aerosol particles measured with H-TDMA instruments in various environments - a review, *Tellus Series B-Chemical and Physical Meteorology*, 60(3), 432-469.

Textor, C., et al. (2006), Analysis and quantification of the diversities of aerosol life cycles within AeroCom, *Atmospheric Chemistry and Physics*, 6, 1777-1813.

Trentmann, J., R. J. Yokelson, P. V. Hobbs, T. Winterrath, T. J. Christian, M. O. Andreae, and S. A. Mason (2005), An analysis of the chemical processes in the smoke plume from a savanna fire, *Journal of Geophysical Research-Atmospheres*, 110(D12).

Twomey, S. (1977), Influence of pollution on the short-wave albedo of clouds, *Journal of the Atmospheric Sciences*, 34, 1149−1152.

van der Werf, G. R., J. T. Randerson, L. Giglio, G. J. Collatz, P. S. Kasibhatla, and A. F. Arellano, Jr. (2006), Interannual variability in global biomass burning emissions from 1997 to 2004, *Atmospheric Chemistry and Physics*, *6*, 3423-3441.

Vaughan, G., C. Schiller, A. R. MacKenzie, K. Bower, T. Peter, H. Schlager, N. R. P. Harris, and P. T. May (2008), SCOUT-03/ACTIVE - High-altitude aircraft measurements around deep tropical convection, *Bulletin of the American Meteorological Society*, 89(5), 647.

Weimer, S., M. R. Alfarra, D. Schreiber, M. Mohr, A. S. H. Prevot, and U. Baltensperger (2008), Organic aerosol mass spectral signatures from wood-burning emissions: Influence of burning conditions and wood type, *Journal of Geophysical Research-Atmospheres*, 113(D10).

Wong, J., and Z. Q. Li (2002), Retrieval of optical depth for heavy smoke aerosol plumes: Uncertainties and sensitivities to the optical properties, *Journal of the Atmospheric Sciences*, 59(3), 250-261.

Yokelson, R. J., D. W. T. Griffith, and D. E. Ward (1996), Open-path Fourier transform infrared studies of large-scale laboratory biomass fires, *Journal of Geophysical Research-Atmospheres*, *101*(D15), 21067-21080, doi:10.1029/96jd01800.

Yokelson, R. J., et al. (2007), Emissions from forest fires near Mexico City, *Atmospheric Chemistry and Physics*, *7*(21), 5569-5584.

Yokelson, R. J., T. J. Christian, T. G. Karl, and A. Guenther (2008), The tropical forest and fire emissions experiment: laboratory fire measurements and synthesis of campaign data, *Atmospheric Chemistry and Physics*, 8(13), 3509-3527.

Yokelson, R. J., et al. (2009), Emissions from biomass burning in the Yucatan, *Atmospheric Chemistry and Physics*, *9*(15), 5785-5812.

Yokelson, R. J., I. R. Burling, S. P. Urbanski, E. L. Atlas, K. Adachi, P. R. Buseck, C. Wiedinmyer, S. K. Akagi, D. W. Toohey, and C. E. Wold (2011), Trace gas and particle emissions from open biomass burning in Mexico, *Atmospheric Chemistry and Physics*, *11*(14), 6787-6808, doi:10.5194/acp-11-6787-2011.

Yu, H., et al. (2006), A review of measurement-based assessments of the aerosol direct radiative effect and forcing, *Atmospheric Chemistry and Physics*, 6, 613-666.

Zhang, Q., D. R. Worsnop, M. R. Canagaratna, and J. L. Jimenez (2005), Hydrocarbon-like and oxygenated organic aerosols in Pittsburgh: insights into sources and processes of organic aerosols, *Atmospheric Chemistry and Physics*, 5, 3289-3311.

Zhu, Y. F., W. C. Hinds, S. Kim, S. Shen, and C. Sioutas (2002), Study of ultrafine particles near a major highway with heavy-duty diesel traffic, *Atmospheric Environment*, 36(27), 4323-4335.